Faculty of Science and Engineering
Department of Imaging and Applied Physics

Haemodynamic Evaluation of Coronary Artery Plaques: Prediction of Coronary Atherosclerosis and Disease Progression

Thanapong Chaichana

This thesis is presented for the Degree of
Doctor of Philosophy
of
Curtin University

June 2012

Declaration

"To the best of my knowledge and belief this thesis contains no material previously published by any other person except where due acknowledgement has been made."

"This thesis contains no material which has been accepted for the award of any other degree or diploma in any university."

.....

Thanapong Chaichana

9th August 2012

To my mother, my father, and persons who always support me.

Kitsana Chaichana
Prasert Chaichana
Zhonghua Sun

Abstract

Coronary artery disease is the leading cause of death in advanced countries. Coronary artery disease tends to develop at locations where disturbed flow patterns occur, such as the left coronary artery. Haemodynamic change is believed to play an important role in the pathogenesis of coronary artery disease. This study was conducted to analyse the haemodynamic variations in the left coronary artery, with normal and diseased conditions, based on idealised human left coronary artery models and realistic reconstructed left coronary geometries. Computational fluid dynamics analysis was performed, to replicate the actual physiological conditions that reflect the *in vivo* cardiac haemodynamics with high resolution CT images. The wall shear stress, wall shear stress gradient, velocity flow patterns, pressure gradient, wall pressure, wall pressure gradient, wall pressure stress gradient, were calculated though in idealised but near realistic left coronary geometries during the cardiac pulsatile cycles. This novel research was performed in four stages, with Stage 1 studying the correlation between bifurcation angle and subsequent haemodynamic effects; Stage 2 focused on the position of plaques in the left coronary artery and corresponding haemodynamic variations based on realistic models; Stage 3 investigated the impact of plaques on coronary side branches based on realistic models. Stage 4 analysed individual patients with the bifurcation stenosis based on CT images.

Normal coronary artery geometries were generated to investigate the haemodynamic variations of various angulations of the left coronary artery, based on idealised and actual coronary artery models. Eight idealised left coronary artery models were generated, with inclusion of different coronary angulations, namely, 120°, 105°, 90°, 75°, 60°, 45°, 30° and 15°. Four realistic left coronary artery geometries were reconstructed, based on selected patient's data, with angulations ranging from wide angulations of 110° and 120° to narrow angulations of 73° and 58°. There were twelve left coronary artery models in total which consisted of left main stem, left anterior descending and left circumflex branches. Haemodynamic analysis showed

that disturbed flow patterns were observed in both idealised and realistic left coronary geometries with wider angles. Wall pressure was found to reduce when the flow changed from the left main stem to the bifurcated locations. A low wall shear stress gradient was revealed at left main bifurcations in models with wide angulations. There is a direct correlation between coronary angulations and subsequent haemodynamic changes, based on realistic and idealised geometries.

Diseased coronary geometry was used to study the haemodynamic changes surrounding the bifurcation plaques based on patient's data. High resolution CT images of the coronary plaques were used to locate and generate the position of actual plaques, which was combined with the reconstructed left coronary disease geometry. Coronary plaques were replicated and located at the left main stem and the left anterior descending to produce at least 60% coronary stenosis. Computational fluid dynamic analysis was used to investigate the haemodynamic effects with and without the presence of coronary plaques. Our results revealed that the highest pressure gradients were observed in stenotic locations caused by the coronary plaques. Low flow velocity regions were found at post-stenotic locations in the left bifurcation, left anterior descending, and left circumflex. Wall shear stress at the plaque locations was similar between the non-Newtonian and Newtonian models, although more details were observed with non-Newtonian model. There is a direct correlation between coronary plaques and subsequent haemodynamic changes, based on the simulation of plaques in the realistic left coronary geometries.

Coronary artery disease with their side branches was used to analyse the change of haemodynamic factors surrounding bifurcation plaques to characterise the effect of disturbed flow to their side branches. Coronary plaques were located at the left main bifurcation, which is composed of the left main stem and the left anterior descending to generate >50% narrowing of the coronary lumen. Haemodynamic parameters were compared in the left coronary artery models, with and without the presence of plaques. The analysis demonstrated that wall shear stress decreased while wall pressure stress gradient was increased in coronary side branches due to the presence of plaques. There is a direct relationship between coronary plaques and subsequent haemodynamic changes based on the bifurcation plaques located in the realistic coronary geometries.

Patient-specific models with coronary disease were used to analyse the haemodynamic variations surrounding the stenotic locations. Three sample patients with left coronary artery disease were chosen based on CT data. Coronary plaques were shown at the left anterior descending and left circumflex branches with more than 50% lumen narrowing. Wall shear stress and blood flow changes in the left coronary artery disease were calculated during cardiac pulsatile cycles. Our results showed that wall shear stress was found to increase at the stenotic regions and decrease at pre- and post-plaque regions, while the disturbed flow regions was found at post-plaque location. There is a direct effect bifurcation plaque on the changes of blood flow and wall shear stress, based on the realistic coronary disease geometries.

In summary, the results of this project show that coronary angulation is directly related to haemodynamic changes, resulting in the formation of atherosclerosis, leading to coronary artery disease. Presence of coronary plaques impacts the haemodynamic changes to both the left main coronary artery, and side branches. Computational fluid dynamic analysis of realistic normal and diseased coronary models improves our understanding of the pathogenesis of coronary artery disease. Further studies are needed to correlate the haemodynamic changes in the presence of plaques with clinical outcomes in patients with suspected coronary artery disease.

Acknowledgements

First of all, I would like to deeply express my gratitude to my supervisor, Prof Zhonghua Sun, for encouragement, patience, guidance, constructive advice, and scientific expertise which assisted me to produce quality research. Special thanks for providing an opportunity to work with you, and I could not finish PhD without you.

Secondly, I would like to express my sincere appreciation and thank to my assistant supervisor, Dr James Jewkes, for patience, guidance, advice, wisdom and kindness.

Particularly, I would like to thank Curtin University for offering me the Curtin International Postgraduate Research Scholarships (CIPRS).

Additionally, I would like to thank Dr Wei-Yong Yan for providing a good chance to be the sessional academic to teach the subject of Control System 301 for undergraduate and postgraduate course at the Department of Electrical & Computer Engineering, Curtin University.

I would like to thank the Department of Imaging and Applied Physics and the Office of Research and Development, especially the administrative and technical staff.

I would like to thank my parents for providing the financial support during my PhD.

Finally, I would like to thank everyone and my good friends I have seen in Australia who bring the happiness to my life.

List of publications included as part of the thesis

Refereed journal publications (Impact Factor (IF) based on ISI 2010).

In order to list the following journals as found in this thesis.

Chaichana, T., Sun, Z., Jewkes, J., 2011. Computation of hemodynamics in the left coronary artery with variable angulations. Journal of Biomechanics 44 (10), 1869–1878. (IF= 2.463)

Chaichana, T., Sun, Z., Jewkes, J., 2012. Computational fluid dynamics analysis of the effect of plaques in the left coronary artery. Computational and Mathematical Methods in Medicine 2012, 504367:1–9. (IF= 0.814)

Chaichana, T., Sun, Z., Jewkes, J., 2012. Impact of plaques in the left coronary artery on wall shear stress and pressure gradient in coronary side branches. Computer Methods in Biomechanics and Biomedical Engineering, Epub a head of print, 1–11. doi:10.1080/10255842.2012.671308. (IF= 1.573)

Chaichana, T., Sun, Z., Jewkes, J., 2012. Investigation of the haemodynamic environment of bifurcation plaques within the left coronary artery in realistic patient models based on CT images. Australasian Physical & Engineering Sciences in Medicine 35 (2), 231–236. (IF= 0.561)

Statement of Contribution of Others

Thanapong Chaichana's input into this research and all journals consisted of the performance of scientific works, and a lead author of research articles to the intellectual property implicated in this thesis. As is almost always the cases in the biomedical engineering, and the other specialists made assistant to the research that were significantly sufficient to warrant co-authorship on the appearing journals, described as:

Zhonghua Sun provided overall project supervision and technical advice and manuscript editing.

James Jewkes provided technical support and manuscript editing.

.....	.....
Thanapong Chaichana	Prof Zhonghua Sun
5th August 2012	5th August 2012

List of additional publications by the candidate relevant to the thesis but not forming part of it

Chaichana, T., Sun Z., 2010. Identification and characterization of coronary plaques with CT virtual intravascular endoscopy: A pictorial review. Atherosclerosis Supplements 11 (2), 18–18. (IF= 2.064)

Chaichana, T., Sun Z., Jewkes, J., 2012. Hemodynamic analysis of the effect of different types of plaque in the left coronary artery. Computerized Medical Imaging and Graphics, submitted for publication, accepted in revision. (IF= 1.467)

Chaichana, T., Sun Z., Jewkes, J., 2012. Hemodynamic impacts of various types of stenosis in the left coronary bifurcation: A patient-specific analysis. Computer Methods and Programs in Biomedicine, submitted for publication. (IF= 1.516)

Chaichana, T., Sun Z., Jewkes, J., 2012. Hemodynamic impacts of left coronary stenosis: A patient-specific analysis. Acta of Bioengineering and Biomechanics, submitted for publication. (IF= 0.449)

Chaichana, T., Sun Z., Jewkes, J., 2012. Hemodynamic analysis of the effect of different types of plaque at the left coronary artery. The 2012 China Hangzhou International Medical Imaging Forum, 13–15 April 2012, Hangzhou, Zhejiang, China. (Invited Talk)

Chaichana, T., Sun Z., Jewkes, J., 2011. Investigation of hemodynamic effect of plaques at the left coronary bifurcation. The 9th International Congress on Coronary Artery Disease, 23–26 October 2011, Venice, Italy. (Poster Presentation)

Chaichana, T., Sun Z., Jewkes, J., 2011. Computational fluid dynamics analysis of the effect of simulated plaques in the left coronary: A preliminary study. The 2011 International Congress on Modelling and Simulation, 12–16 December 2011, Perth Convention Exhibition Centre, Western Australia, Australia, pp. 51–515.

Chaichana, T., Sun, Z., Tungjitkusolmun, S., Sangworasil, M., 2010. Flow simulation in coronary artery models: An investigation of the effect of variable angulations at left coronary. The 23rd IEEE International Symposium on Computer-Based Medical Systems, 12-15 October, Curtin University, Perth, Western Australia, pp. 279–284.

Chaichana, T., Jewkes, J., King, A., Sun Z., 2010. An investigation of hemodynamic function in realistic coronary arteries: A study representing the actualpsychodynamic. The 6th Australasian Congress on Applied Mechanics, 12–15 December 2010, Perth Convention Exhibition Centre, Western Australia, Australia, pp. 1-6.

Chaichana, T., Sun, Z., Wong, K., Tu, J., 2010. Plaque formation at the left coronary artery: Analysis of the relationship between arterial angulations and hemodynamics. The 30th IASTED Conference on Modelling, Identification, and Control, 24-26 November, Phuket, Thailand, pp. 283–287.

Chaichana, T., Sun Z., Jewkes, J., 2010. Haemodynamic effect of coronary angulations on subsequent development of coronary artery disease: A preliminary study. The 6th IEEE e-science 2010 Computational Science and Engineering workshop, 7–10 December 2010, Brisbane, Queensland, Australia, pp. 39–43.

Lists of Figures

Lists of Tables

Lists of Abbreviations, Acronyms and Symbols

2D	Two-dimensional
3D	Three-dimensional
CAD	Coronary Artery Disease
CCTA	Coronary Computed Tomography Angiography
CFD	Computational Fluid Dynamics
CT	Computed Tomography
DICOM	Digital Imaging and Communications in Medicine
EPL	Effective Plaque Location
FFR	Fractional Flow Reserve
GTM format	ANSYS CFX mesh file
in vivo	Occurrence within a living organism
IVUS	IntraVascular UntraSound
LCA	Left Coronary Artery
LCX/LCx	Left Circumflex
LAD	Left Anterior Descending
LMS	Left Main Stem
OSI	Oscillatory Shear Index
PSG	PresSure Gradient
RRT	Relative Resistance Time

SB	Side Branch after left main coronary bifurcation
STL format	STereoLithography file
TAWSS	Time-Averaged Wall Shear Stress
VIE	Virtual Intravascular Endoscopy
WPD	Wall Particular Density
WPSG	Wall Pressure Stress Gradient
WSS	Wall Shear Stress
WSSG	Wall Shear Stress Gradient
Kg/m^3	Kilogram per cubic metre
m/s	Metre per second
ml/min	Millilitres per minute
Pa s	Pascal-second
Q_{LMS}	Flow rate in parent branch
Q_{LAD}	Flow rate in daughter branch
Q_{LCX}	Flow rate in daughter branch
$\vec{V}_{LMS}$	Velocity in left main stem
$\vec{V}_{LAD}$	Velocity in left anterior descending
$\vec{V}_{LCX}$	Velocity in left circumflex
μ	Blood viscosity

m	Temporal mean wall shear stress direction
n	Tangential to surface and normal to m
τ	Shear stress
$\vec{V}_t$	Velocity near wall perpendicular to surface
p	Pressure in the area of interest
x, y, z	Cartesian coordinates in direction of blood velocity
$\dot{\gamma}$	Stress strain
π	Mathematical constant of Pi
R_s	Splitting ratio of flow rate
r^2	Square Radius of coronary lumen diameter
T	Pulsatile period
d_0	Inlet diameter at left main stem branch
dt	Time derivative
∂y	Distance to wall surface
U	Flow velocity
ρ	Density of fluid
τ_w	Instantaneous wall shear stress vector
90^o	A 90 degree angle of left main coronary bifurcation

Lists of Contents

Chapter 1

General Introduction

1.1 Research Overviews

Biomechanics is a study of mechanics, applied to biology, which provides an understanding of the mechanics of life and living organisms (Fung 1993). In general, biomechanics is focused upon natural life sciences, particularly the analysis of heat and mass transfer, thermodynamics, and dynamic systems. The majority of recent research in biomechanics has been focused on physiological and medical applications. The latest computer technologies have had an increasing influence upon medical health care, professional engineers have become closely involved in many medical enterprises (Enderle and Bronzino 2011; Tu et al. 2008). Thus, the discipline of biomedical engineering has been established to bridge the gap between medicine and engineering. Biomedical engineers have aided the fight against disease by developing medical tools such as image processing and analysis, artificial intelligence, biomaterials and biosensors. They serve as a relatively new member of the medical health care community, who provide new solutions for research, diagnosis and treatment of various kinds of disease.

This thesis presents research which is emerging in the field of biomedical engineering, concerned with the application of biomechanics to the cardiovascular system. Coronary artery disease is the leading cause of death in Australia, and other developed countries and it has become a serious issue for the health care system (Australian Institute of Health and Welfare 2006).

Over the last decade, clinicians have been searching for effective and accurate methods for early detection and diagnosis of coronary artery disease. The established technique is invasive coronary angiography. Coronary angiography has a high diagnostic value owing to its superior spatial and temporal resolution. However, it is not only an invasive procedure, but also is associated with procedure-related morbidity (1.5%) and mortality (0.2%) (Noto et al. 1991). Less-invasive cardiac imaging has experienced rapid growth in recent years. Several techniques have been developed for diagnostic and prognostic workup of patients with proven or suspected coronary artery disease.

These modalities include computed tomography (CT), magnetic resonance imaging (MRI) and nuclear medicine imaging (Nieman et al. 2001; Sommer et al. 2005; Hachamovitch et al. 1998). Although there is no less-invasive imaging modality that can replace invasive coronary angiography, the development of new modalities provides unique opportunities to detect and diagnose coronary artery disease less invasively, when compared with coronary angiography (Sun et al. 2011). Despite rapid developments in cardiac CT and MRI imaging, these imaging techniques are still limited to the visualisation of anatomical details, and no information is available on the haemodynamic changes, directly related to the development of coronary artery disease.

Biomechanics using computational fluid dynamics represents a fast emerging area which is increasingly used in the diagnostic management of cardiovascular disease. This is the main motivation for performing this study with the aim of improving our understanding of haemodynamics in patients with suspected coronary artery disease, with a focus on the left coronary arteries. The flow diagram of this study is shown in Figure 1.

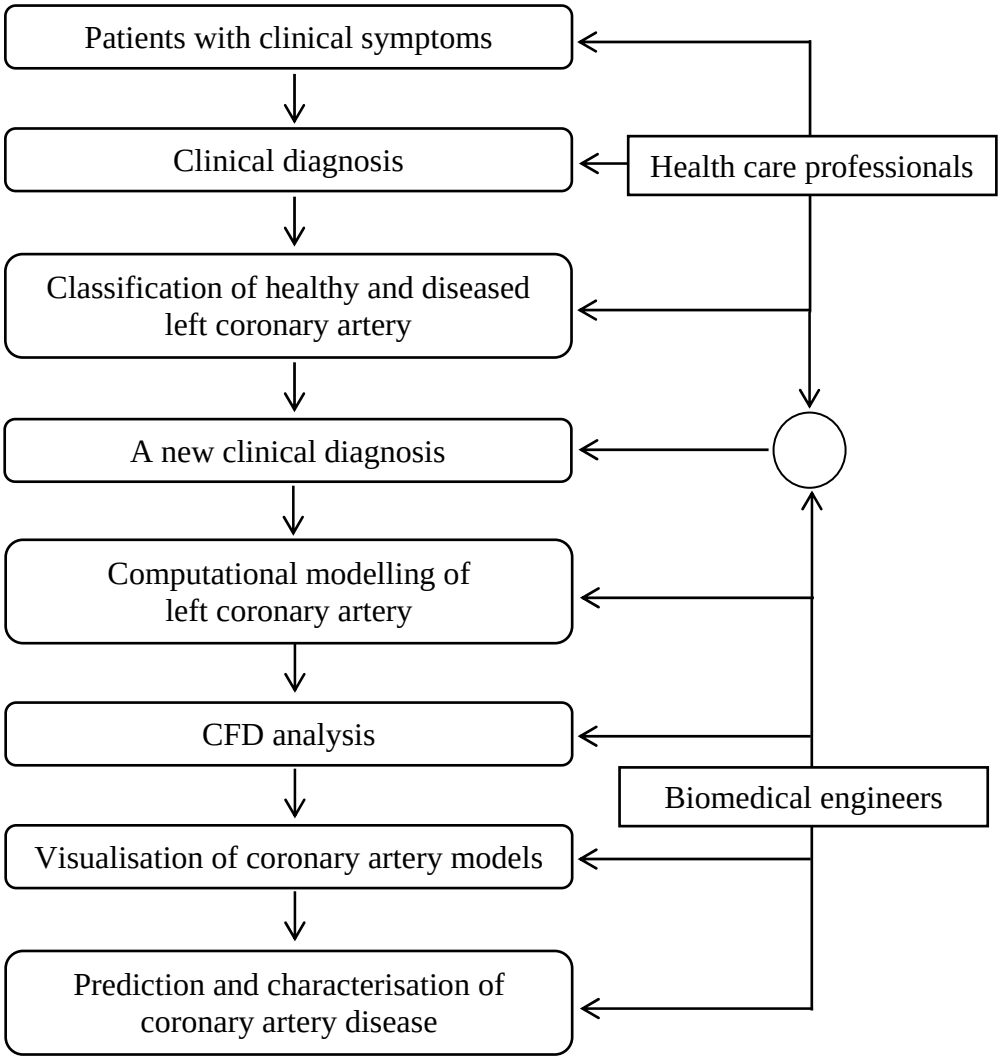

Figure 1. Flow chart demonstrates the summary of the research plan

1.2 Aims and Significance

This research is to evaluate the haemodynamics of the coronary artery, and to predict plaque progression and blood flow in coronary artery disease. Therefore, the objectives of this study are as follows:

1. To provide haemodynamic analysis of both healthy and diseased coronary arteries at various cardiac pulsatile cycles;

2. To improve understanding of the effect of coronary plaques on coronary haemodynamics;
3. To assist cardiologists in identifying patients at risk of developing coronary disease;

The purpose of this study is to investigate the haemodynamic environment in human coronary arteries in both normal and abnormal conditions. The healthy coronary arteries are analysed to characterise the possible development of atherosclerosis, and enable the prediction of the actual plaque locations. The diseased coronary arties are analysed to demonstrate disease progression, and blood flow change surrounding the plaque positions. Since coronary artery disease is one of the leading causes of death in Australia and developed countries, the patients who suffer from coronary artery disease will continue to increase in the future. Thus our proposed study will play an important role in both the diagnosis and the prevention of cardiac disease events. The detailed objectives of the study are as follows:

1. To perform computational fluid dynamic analysis of normal and diseased coronary arteries;
2. To simulate the main bifurcation in healthy left coronary arteries with various angulations, and analyse the corresponding blood flow changes;
3. To characterise plaques in the diseased left coronary arteries with different configurations and corresponding haemodynamic variations;
4. To perform computational fluid dynamic analysis in specific patients with suspected coronary artery disease, with the intention of identifying the risk of developing coronary disease;
5. To apply research results in specific patients for risk stratification, and prediction of disease progression.

1.3 Research Schemes

The research schemes are divided into four stages;

1. Computational analysis of a healthy left coronary artery to predict atherosclerotic progression;
    - An initial study of the left coronary artery, with variable angulations at the left main bifurcation to investigate the influence of the degree of bifurcation angle upon atherosclerotic progression.
2. Computational fluid dynamic analysis of the diseased left coronary artery bifurcation is conducted to characterise the haemodynamic environment at the plaque location;
    - In this stage, coronary artery disease with realistic plaques is simulated at the left main coronary bifurcation. The haemodynamic parameters are calculated and visualisations of the blood flow environment surrounding the plaque locations are produced.

3. Haemodynamic analysis of the plaques at the main bifurcation in the left coronary artery;
    - In this third stage, the actual plaques are reconstructed at the main bifurcation in the left coronary artery. Then haemodynamic variations are analysed to predict the impact of flow velocity effects at the main bifurcation to coronary side branches.

4. Computational analysis of specific patients with left coronary artery disease, to characterise the haemodynamic factors surrounding the plaque regions.
    - In this final stage, patients suspected of coronary artery disease are selected to provide realistic coronary artery anatomy and side branches. The analysis is used to characterise the flow environment near to the plaque locations.

1.4 Background of Coronary Artery Disease

The heart is the centre of human circulatory system, pumping the blood through vascular channels to the whole body for maintaining normal physiological functions. Cardiac function requires the supply of nutrition and oxygen which is carried by the blood through coronary arteries, to supply the heart muscles. Left and right coronary arteries originate at the root of the aorta behind the left and right cusps of the aortic valve (Berne and Levy 2001). The left coronary artery (LCA) arises from the left coronary sinus, and it is divided into the left anterior descending (LAD), left circumflex (LCx) and their side branches. The LCA and its side branches principally supply the blood to the left ventricle and atrium. The right coronary artery (RCA) originates from the right coronary sinus, with descending branches. The RCA primarily supplies the blood to the right ventricle and atrium (Rushmer 1976). In coronary circulation, LCA is present in 30% of the human heart, RCA is dominant of the aorta branch in another 50%, and the flow balanced by each main coronary artery is approximately 20% (Berne and Levy 2001). The left and right coronary arteries and their branches are shown in Figure 2.

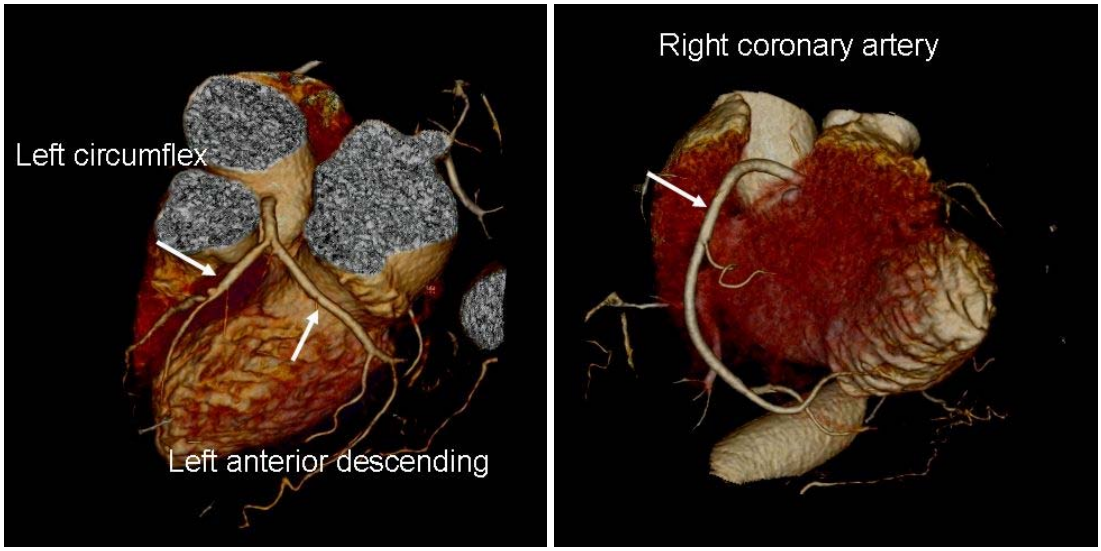

Figure 2. 3D CT images of the heart present the left coronary artery and their side branches (left image), and the right coronary artery (right image).

The blood flows through the lumen of the coronary artery, and has direct effect upon the coronary wall mechanism. The wall of the coronary artery has three layers, which are as follows: the adventitia (outer), the media (middle), and the intima (inner). These three layers bordering the vascular channel are shown in Figure 3.

- **Outer layer of coronary wall**

  The adventitia is the external layer of the coronary artery and is composed of the cells that generate collagen and elastin (fibroblasts and fibrocytes), thick bundles of collagen fibrils forming a fibrous tissue. The thickness of adventitia layer is strongly dependent on the type of elastic or muscular, physiological function of the blood vessels and its topographical vessel location, for example, the walls of cerebral vessels practically have no adventitia layer (Holzapfel et al. 2000).

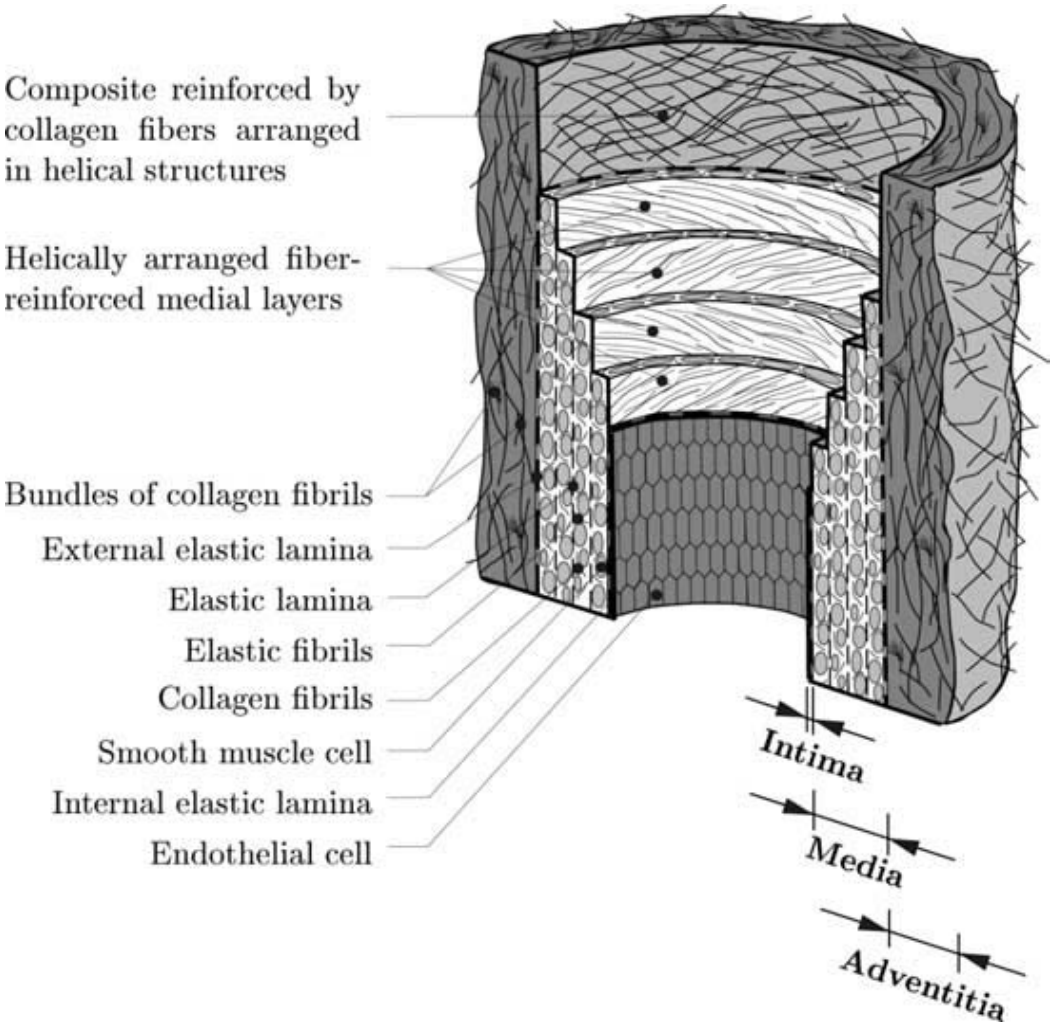

Figure 3. Healthy coronary artery demonstrates the three layers of mechanical wall components surrounding the vessel lumen (adopted from Holzapfel et al. 2000), reprinted with permission from Springer Publishing Company, New York, NY.

- **Middle layer of coronary wall**

  The media layer of the coronary artery is composed of smooth muscles, elastin, and collagen fibrils. This layer is distinctly separated from the adventitia and intima layers. The structure of the media layer provides high strength to resist the loads in circumferential and longitudinal directions (Holzapfel et al. 2000).

- **Inner layer of coronary wall**

  The intima layer is the inner level of the coronary wall mechanism, composed of a single layer of endothelial cells. The thickness of the intima layer varies, depending strongly on the age of the human, and the topography at the vessel location, specifically the diseased section. In a young human specimen, healthy coronary vessel has a very thin intima layer, and is insignificantly associated with the mechanical properties of the blood vessels. However, it should be noticed that the diseased condition is associated with age (arteriosclerosis), which contributes to vessel properties and may have a significant effect upon intima thickness and stiffness (Holzapfel et al. 2000).

It is also known that pathological changes are significantly related to changes in the intimal layer. These changes may be associated with atherosclerosis progression. The intimal components are formed by the deposition of fatty substances, calcium, collagen fibres, cellular waste products, and fibrin (a clotting material in blood). The consequential development is called “atherosclerotic plaques”, the most common disease in the arterial walls. In later stages, the media layer is also affected after the endothelial cells are damaged. In addition, the blood flows through the coronary artery lumen in certain locations where changes of vessel geometries (tortuous or bending sections) affect blood flow behaviour. These changes may generate different forces to affect the intima layer, specifically the vessel walls. The resulting blood flow changes create a region of “Disturbed flow” that may be associated with the alignment of endothelial cells, and is linked to the changes of arterial wall shear stress. Consequently, the blood flow velocity changes in vascular lumen and the aging of the population are related to coronary artery disease, and both parameters may have a direct effect upon endothelial cell damage at the intimal layer, thus, affecting the intimal thickness.

Atherosclerotic plaque is associated with lipid deposition in the subendothelial domain, intimal thickening, and arterial wall injury resulting from local blood flow effects (Chandran et al. 2006). These general features are located at bifurcation, curvature, and branching points. These arterial sections are haemodynamic complications which lead to the formation of atherosclerotic lesions (DeBakey et al. 1985). In the last four decades, theories have been proposed for the initiation and development of atherosclerotic plaques (Chandran et al. 2006). The postulation is that the arterial regions of low wall shear stress are involved in the deposition of endothelial cells to the intimal layer by the blood flow moving slowly in an area with excessive lipids (Caro et al. 1971a, 1971b). On the other hand, the arterial locations of high wall shear stress are susceptible to endothelial cell damage, formation of atherosclerotic lesions, and possible rupture (Fry 1968, 1969). The example of coronary artery lesions shows the atherosclerotic plaque occurring at common bifurcation locations, as shown in Figure 4.

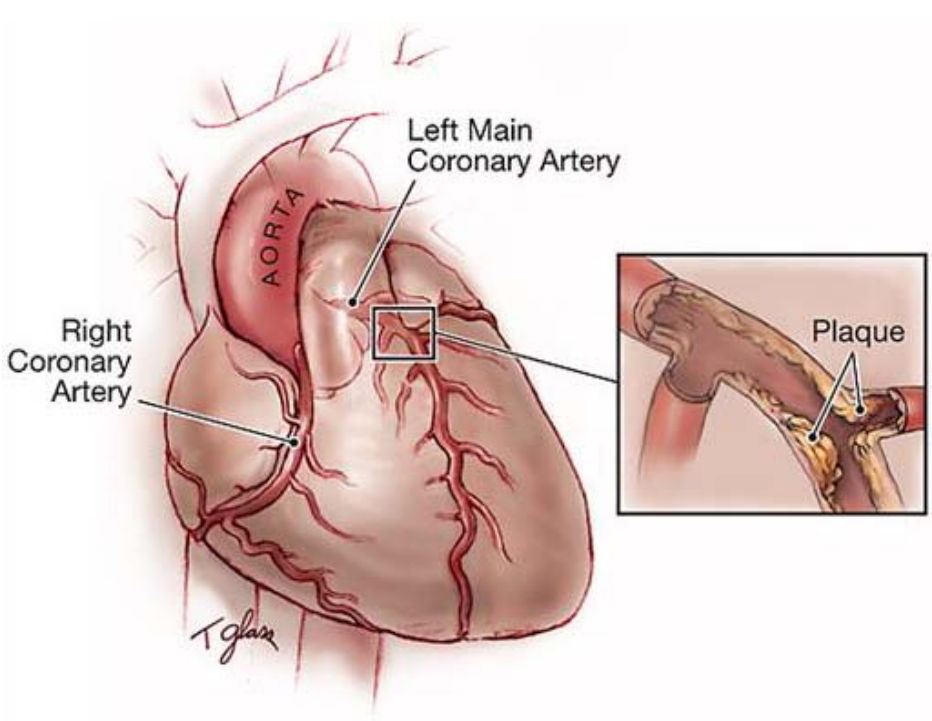

Figure 4. Locations of atherosclerotic lesions associated changes in intimal wall thickness (adopted from Parmet 2004), reprinted with permission from American Medical Association, United States.

Coronary artery disease is the main cause of death, worldwide. In Australia, specifically, it is responsible for the death of approximately 47,637 Australians per year, accounting for 36% of total deaths in Australia. It is also a leading cause of disability, for approximately 1.4 million Australians, 6.9% of the total population in 2004 (Australian Institute of Health and Welfare 2006, 2011). Moreover, in 2006, the Australian Institute of Health and Welfare produced a National Health Survey, showing that about 1.7% of the respondents had coronary artery disease. In April 2010, the Australian Institute of Health and Welfare stated that Australian people at different ages tend to be affected with cardiovascular disease and showed that Australian deaths due to coronary artery disease were about 50.3% of total cardiovascular disease, accounting for 22,983 Australians in 2006 (Australian Institute of Health and Welfare 2010). Most significantly, the mortality rate due to coronary artery disease has increased by 70% since the late 1960s. Therefore, early detection and diagnosis of coronary disease is particularly important for the reduction of mortality and subsequent complications (Australian Institute of Health and Welfare 2006, 2011).

1.4.1 Review of coronary artery disease

The most common cause of coronary artery disease is atherosclerosis, which is caused by the presence of plaques in the artery wall, resulting in lumen stenosis. Plaques are a particular cause of blood clots, and block blood flow to the heart muscle. This event occurs when coronary plaques suddenly rupture, and if a clot cannot be treated in a timely manner then the heart muscle will be impaired due to ischemic changes, leading to ischemia or myocardial infarction or necrosis (Australian Institute of Health and Welfare 2006, 2011).

The natural history of coronary plaque is dependent not only on the formation and progression of atherosclerosis, but also on the vascular remodelling response. If the local WSS is low, a proliferative plaque will form (Samady et al. 2011). Local inflammatory response will stimulate the formation of so-called “vulnerable plaque” which is prone to rupture with superimposed thrombus formation. The vast majority of these inflamed, high-risk vulnerable plaques cannot be detected by anatomic imaging and myocardial perfusion imaging. Since the progression and development of vulnerable plaques is associated with low WSS and the presence of expansive remodelling, measurement of these characteristics *in vivo* will enable risk stratification for the entire coronary circulation (Rybicki et al. 2009).

Furthermore, some preliminary studies have been done in the development of mathematical models of calcified plaques (Sun et al. 2009). Plaques were simulated in the main bifurcation with the assumption of a concentrated calcium property, and they studied the effects of blood flow variations surrounding the bifurcations. The proposed progression of the plaque may have potential risk factors in the provision of stenotic locations with high WSS. This study also reflected potential clinical applications in providing visualisation of haemodynamic parameters in actual situations where practical experimental measurement of blood flow velocity changes are unavailable.

The wall shear stress, wall pressure and blood flow changes in a human body cannot be measured directly in blood vessels, but CFD can provide an alternative ways to predict coronary artery disease (Samady et al. 2011; Shanmugavelayudam et al. 2010). The WSS factor in the coronary artery is known as playing a significant role in the initiation of coronary disease (Johnston et al. 2004).

In addition, previous studies investigated the prediction of atherosclerotic lesions within the normal coronary artery and WSS, as the local vessel wall demonstrates anatomical sections predisposed for the development of atherosclerosis (Soulis et al. 2006). Their findings focused upon the early detection of atherosclerotic progression but their studies did not compare the analysis of normal artery with that of coronary disease conditions. Furthermore, primary research studied specifically, the abnormal cardiac condition based on an in vivo model of the left coronary artery bifurcation, with the aim of describing the relationship between WSS, wall thickness and remodelling of the specific patient (Gijsen et al. 2007). The limitation of their study was that only one site of coronary disease was analysed, and no comparison was performed with normal cardiac conditions. Therefore, a more in-depth study under normal condition is required. CFD analysis provides a reliable means to estimate blood flow within the coronary artery, but it needs realistic geometries that are rendered precisely, to simulate *in vivo* conditions (Samady et al. 2011).

CFD simulation requires the solution of the Navier-Stokes equations to calculate the WSS, wall pressure, flow patterns and other haemodynamic parameters. This calculation can be performed with either idealised, or realistic geometries at different cardiac cycles. For the realistic models, computational simulation can be performed with three-dimensional volume rendered CT data of the coronary artery with normal and diseased environments. In addition, the fluid mechanics of the computational study are based on the laws of mass conservation and motion, to compute small elements of volume data of coronary geometries. CFD has proven accurate in the prediction of accelerated atherosclerosis and inflammation enlargement (Samady et al. 2011; Shanmugavelayudam et al. 2010; Rybicki et al. 2009).

So far, a few studies have been done in the analysis of coronary artery disease, particularly where coronary plaques rupture, causing ischemia or myocardial infarction or necrosis. At the early stage, the cross-sectional models of plaques were generated with 86% stenosis (Versluis et al. 2006). In their analysis it was assumed that the plaque condition represented a chronic injury process, and multiple pulsatile cycles were applied to calculate the two-dimensional (plane strain) stress distributions of three-dimensional stress models. The baseline anatomy of a two-dimensional model is composed of artery wall, lumen, lipid, fibrous cap and plaque areas. Then, their study varied a circular baseline (radius of lumen) into five patterns of two-dimensional models of this analysis, grouped as follows: the first group consisting of three models of fibrous cap with its shape changed and the second group consisting of two models with lumen change (Versluis et al. 2006).

The results showed that variant blood pressure had no effect on initiative areas and rupture directions. The biomechanics within the lumen of the internally pressurized artery predicted “highest stress” and suggested that rupture is unlikely to be caused by the lipids and sturts at the lumen. Later they concluded that these experimental results are reconciled in clinical evidence of acute plaque rupture and it could create a framework for developing strategies for biomechanically benign conditions that are least conductive to plaque rupture (Versluis et al. 2006). Consequently, it seems that the analysis of two-dimensional models of stress distributions needs more explanation. Three-dimensional analysis using timely computational analysis framework can be used to understand the haemodynamic effects of plaque progression and potential risk-factors.

In addition, a simulation of blood flow in the coronary artery showed that fatal vulnerable-plaques influenced micro-calcifications in eccentric stenosis models. Furthermore, this study compared two cases with, and without micro-calcification (including a fibrous cap). The analytical results showed that the embedded calcification model displayed “higher WSS” regions in the fibrous cap, upstream of the calcification location, with stress disseminating to the deformable areas of structure around calcification location (Speelman et al. 2011; Bluestein et al. 2008). Additionally, they argued that the results of their study were supported by findings that micro-calcification increased plaque weakness (Speelman et al. 2011; Bluestein et al. 2008). Nevertheless, their study was limited to include only one pattern of calcification model, and further studies are needed to investigate the effect of different calcification patterns and plaque mechanisms on potential risk factors. Therefore, computational analyses of healthy and diseased coronary arteries are required to explain the causes of heart attacks.

In summary, vulnerable plaque conditions in coronary artery disease lead to sudden heart attacks or myocardial infarction. Many studies have been conducted in normal coronary analysis (Torii et al. 2008; Soulis et al. 2006; Johnston et al. 2004, 2006; Jung et al. 2006) to predict plaque development and progression. Whereas, a few studies have been performed in analysing coronary disease conditions with simulation of coronary plaques (Katritsis et al. 2010; Shanmugavelayudam et al. 2010; Bluestein et al. 2008; Versluis et al. 2006) and currently these studies need more investigation for various plaque patterns. CFD analysis may be able to demonstrate to some extent the actual physiological haemodynamics in the presence of cardiovascular disease, thus, providing valuable information about pathological changes at an early stage. Furthermore, three-dimensional computational analysis allows for efficient and accurate computations that enable *in vivo* simulation of coronary artery geometries. Therefore, from a numerical point of view CFD analysis contributes to providing information which could assist clinical diagnosis and treatment of patients suspected of coronary disease, and can be used as the baseline datasets for medical treatments.

1.5 Review of Coronary Imaging

Invasive coronary angiography is widely recognised as the standard technique for the diagnosis of coronary artery disease, and is routinely performed in an angiography suite. This invasive procedure involves the insertion of a flexible catheter into the femoral artery, which is then moved upwards along the abdominal aorta to the thoracic aorta, and then into the coronary arteries. It is performed under the guidance of x-ray fluoroscopy, with the aid of an injected contrast medium (Phillips 2002). Conventional coronary angiography is not only invasive, but also has an associated morbidity rate of 1.5% and mortality rate of 0.2% (Fishman 2005). In addition, coronary angiography is not able to predict the physiologic information about a coronary artery stenosis (Townsend 2008). Therefore, clinicians are looking for non-invasive or less invasive imaging modalities with an acceptable diagnostic accuracy (Mahesh 2002).

Cardiac imaging has experienced rapid growth in recent years. Several techniques have been investigated for the diagnosis and prognosis of patients with proven or suspected coronary artery disease. Although currently, there is no less-invasive imaging modality that can replace conventional coronary angiography, the development of CT, MRI contributes to the less-invasive detection and diagnosis of coronary artery disease, when compared with coronary angiography (Takuro et al. 2007; Hingorani et al. 2007).

Despite promising results having been achieved with these less-invasive modalities, the application is still limited to the visualisation of anatomical details such as stenosis or occlusion. Haemodynamic interference due to the presence of coronary plaques and subsequent flow variations cannot be assessed by traditional imaging techniques. Therefore, identification of coronary plaques that may induce cardiac events is of paramount importance for reducing the mortality and improving healthcare in patients suspected of coronary artery disease.

1.6 Brief Analysis of Flow in Coronary Artery

Computational fluid dynamics (CFD) is a numerical method used to solve and analyse problems involving fluid flows. CFD is a widely developed numerical technique for solving complex problems in many fields of modern engineering. However, in biomedical engineering, medical imaging data can be used to generate a realistic geometry of interest, and CFD is principally used to investigate blood flow behaviour in this geometry.

Recently, attempts have been made to use CFD to study the flow in biomedical applications, for example, haemodynamic flow in the cardiovascular system, and the airflow in the human upper airway. With rapid advances in hardware and software in recent years, CFD has increasingly been used in biomedical research to improving our pathophysiological understanding of the progression and development of human disease (Lee 2011; Tu et al. 2008).

Previous research has indicated that CFD models of flow in the human coronary artery can provide information which is comparable with invasive clinical investigation. There is clinical evidence that recirculation regions play an important role in the initiation and progression of atherosclerosis (Kleinstreuer et al. 2001). Key haemodynamic wall parameters were analysed to indicate vulnerable locations of intimal thickening, constructive to the development of thrombi (Kleinstreuer et al. 2001). These primary parameters include wall shear stress and wall pressure, which are commonly used to interpret clinical and experimental observations. These parameters can be used as the indicator for the locations of potential stenosis development, and the prediction of further disease developments and vessel remodelling. Currently, a key focus is on using CFD for the prediction of vulnerable regions and disease progression in the subsequently remodelled coronary arteries. There are generally four parameters of interest: wall shear stress, wall pressure, wall pressure stress gradient, and velocity. These four parameters will be discussed briefly in the following sections.

1.6.1 Wall Shear Stress

Wall shear stress is defined as (Ku 1997; Katritsis et al. 2007a, 2007b; Pantos et al. 2007):

$$\tau_W = \mu \cdot \dot{\gamma}_W \tag{1.1}$$

where μ is dynamic viscosity of liquid, $\dot{\gamma}_W = \frac{du}{dy}$ is shear rate; u is flow velocity is along the wall, and y is the coordinate in a direction perpendicular to the wall.
Wall shear stress is the tangential force per unit area, exerted by a liquid. Shear stress is dependent on the velocity gradient in the near-wall region.

Steady laminar flow in a cylindrical tube provides a reasonable estimate of the mean wall shear stress in arteries, and can be expressed as:

$$\tau_{Wall} = \frac{32\mu Q}{\pi D^3} \tag{1.2}$$

where Q is volume flow rate, μ is dynamic viscosity of liquid, D is mean diameter of conducted cylindrical tube (Ku 1997; Katritsis et al. 2007a, 2007b; Pantos et al. 2007).

Circulatory blood flow induces a drag-force between the vessel wall, and it is implied that variations in this force affects the structural and functional integrity of endothelium cells in the inner level (intima layer) of the vessel wall, (shown in Figure 3) (Milnor 1982; Pantos et al. 2007).

Disturbed flow patterns are caused by the various geometric features of blood vessels, for example, sudden expansions, branches and bifurcations. These features directly influence changes in wall shear stress (WSS). In general, WSS variations are accompanied by the changes to endothelial cell morphology. Although endothelial cell morphology is affected by laminar flow in steady conditions, it can nevertheless still take several hours to modify its cell alignment. WSS changes are not suddenly accommodated by the movement of the transient blood flow. In addition, the responses are shown inside the nucleus of cells almost instantaneously. This means that WSS variations may modify the endothelial cell morphology (Kleinstreuer et al. 2001). Smooth laminar blood flow influences WSS alterations under normal conditions, as shown in Figure 5, while WSS changes adjust the endothelial cell alignments, which are likely linked to the progression of atherogenesis, as shown in Figure 6.

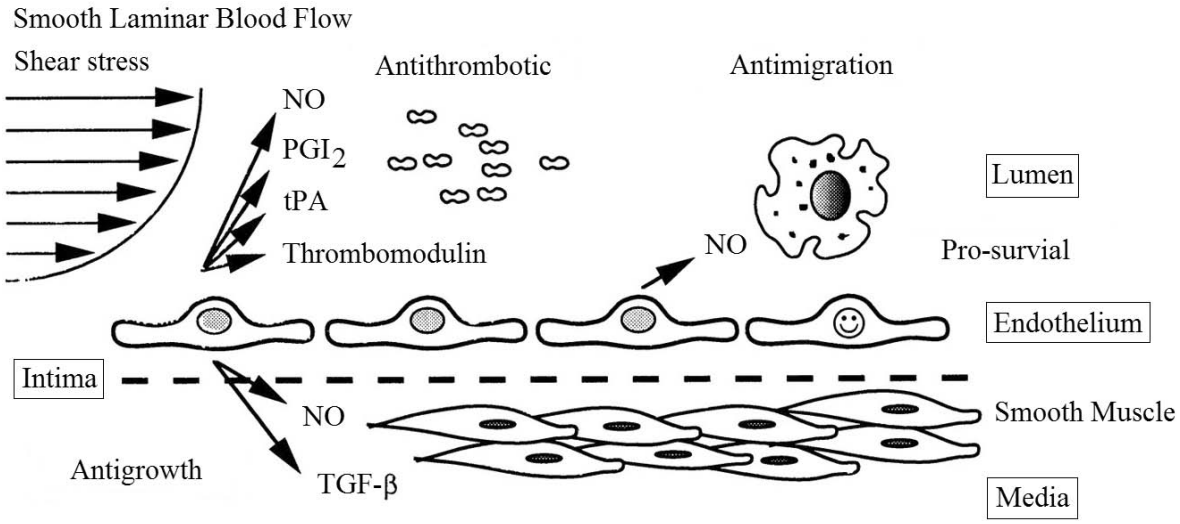

Figure 5. Laminar flow passes the artery walls (adopted from Traub and Berk 1998), reprinted with permission from Wolters Kluwer Health, the Netherlands.

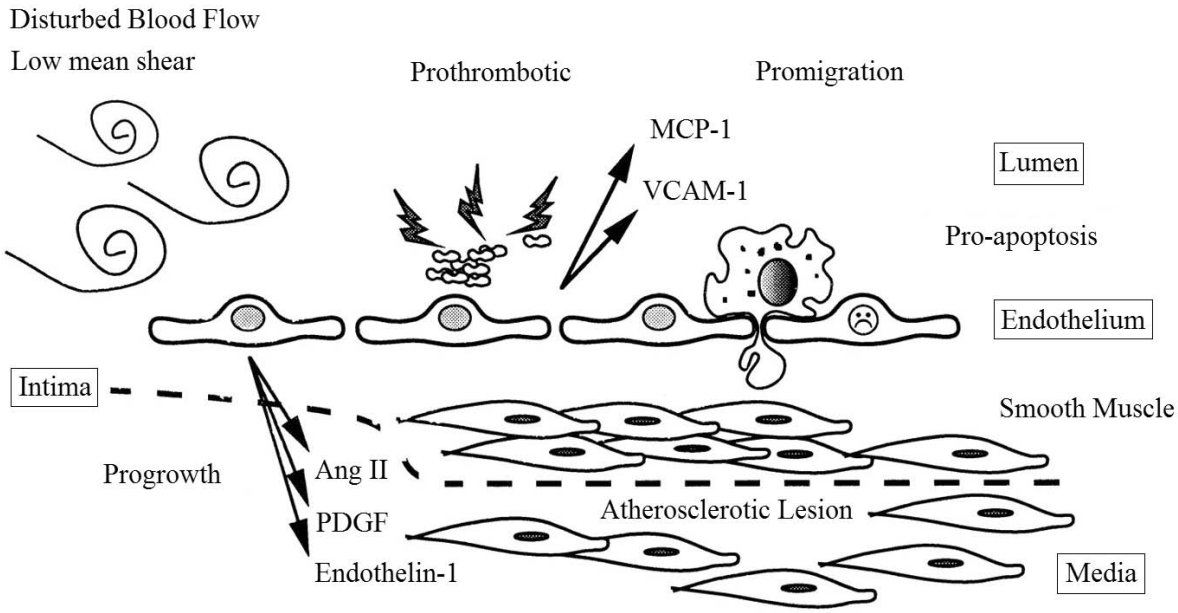

Figure 6. Disturbed flow passes the artery walls (adopted from Traub and Berk 1998), reprinted with permission from Wolters Kluwer Health, the Netherlands.

The WSS is a commonly used parameter in haemodynamic analysis. The endothelial cells have been shown to align themselves with the flow direction that corresponds to the local WSS. Thus, this parameter provides information about potential damage to the endothelial cells which could induce atherosclerotic progression (Kleinstreuer et al. 2001). The WSS is defined as:

$$\mathrm{WSS} = \frac{1}{T}\int_0^T \left| \mu \frac{\partial v_t}{\partial_n} \right| dt \tag{1.3}$$

where μ is blood viscosity, v_t is velocity vector near wall perpendicular to the surface and n is distance to the wall surface, T is pulsatile period, dt is the time derivative of the local shear stress. A recent study has shown that high WSS regions were caused by a sudden increase of flow velocity in the stenotic section of blood vessels. These regions of high WSS may lead to plaque rupture (Samady et al. 2011). Furthermore, studies have revealed that the low WSS regions were caused by disturbed flow, which passes the artery walls, and low WSS may induce plaque formation (Samady et al. 2011; Koskinas et al. 2012).

1.6.2 Wall Pressure

The blood flow in the coronary artery induces variations in the pressure field (Giannoglou et al. 2005, 2002; Ku 1997). Blood pressure within the coronary artery is unsteady and pulsatile, and varies according to the systolic and diastolic phases of the cardiac cycle. The pulsatile pressure in the left coronary artery during the cardiac cycle, represents a unique local pressure field that suddenly increases in the transition from the systolic to the diastolic phase, furthermore this corresponds with a short period of reverse flow (Nichols and O'Rourke 2005).

The normal blood pressure fluctuates between (approximately) 80 mmHg and 120 mmHg (Nichols and O'Rourke 2005). It has been shown that the local wall pressure is strongly correlated with the development and progression of atherosclerotic plaque (Giannoglou et al. 2005, 2002). Therefore investigation of wall pressure in coronary artery enables the evaluation of the arterial wall condition.

The velocity flow-field interacts with the vessel walls of the venous conduits in a number of ways, including pressure induced circumferential stress (Kleinstreuer et al. 2001). It has been stated that if pressure is approximately 200 mmHg, it can lead to endothelial cell damage, and changes to the mechanical properties of the coronary blood vessels (Chervu and Moore 1990). Therefore, haemodynamic parameters such as the wall pressure are used to characterise pressure variations throughout sections of vessel walls. Nevertheless, detail is restricted in certain locations, such as the coronary trees. Hence the characterisation of the local effect of the pressure distributions in coronary artery disease could be considered by using a wall pressure stress gradient parameter.

1.6.3 Wall Pressure Stress Gradient

The parameter used to characterise the impact of plaques on coronary side branches is the local wall pressure stress gradient (WPSG). WPSG is dependent upon the local pressure field (Kleinstreuer et al. 2001). As a result, the WPSG is chosen to determine the impact of bifurcation plaques on the side branches. The WPSG indicates changing pressure loads on vessel walls leading to wall stress and strain problems (Kleinstreuer et al. 2001; Thubrikar and Robicsek 1995). The value of WPSG oscillates in relation to the percentage of plaques in the coronary lumen (Anderson et al. 1986). The WPSG is defined as:

$$\text{WPSG} = \frac{1}{T}\frac{2d_0}{\rho U^2}\int_0^T \frac{\partial_p}{\partial_n}\,dt \tag{1.4}$$

where p is local wall static pressure in the area of interest, d_0, U, and ρ are the inlet diameter, the flow velocity and the density of the fluid, respectively (Kleinstreuer et al. 2001; Garcia et al. 2006; Cheng et al. 1973).

WPSG indicates regions of high flow acceleration, which are associated with the development of atherosclerosis and coronary disease progression (Giannoglou et al. 2005). The static WPSG or spatial WPSG values identify possible sites where atherosclerotic plaque can form due to the high WPSG value. In other words, the WPSG value is strongly linked to the stenosis location, and consequently to plaque rupture (Kleinstreuer et al. 2001; Garcia et al. 2006; Cheng et al. 1973). Therefore, the distributions of WPSG values in the normal and diseased coronary artery are important.

1.6.4 Velocity

The cardiovascular system is an internal flow with multiple, tortuous branches, and unsteadiness characterises the flow-field. The Womersley number that governs the correlation between blood flow condition and fluid viscous forces, is a non-dimensional frequency parameter (Ku 1997). Normal blood flow in arteries is laminar with secondary flow conditions generated at curves and branches. Arterial vessels are a living organ that can change and adapt its shapes, and coupled moving haemodynamic conditions. In certain positions, unusual blood flow can create an abnormal biological response at the arterial wall. Velocity profiles are skewed by the sudden change of native vascular sites. Atherosclerosis tends to be localised in the section of skewed blood flow (Ku 1997). Hence the study of arterial blood flow can have an effect upon the treatment and prediction of individual patients with unusual haemodynamic circumstances.

As previously detailed in section 1.6.1, the velocity is a vector, which has direction and magnitude. The velocity in blood flow is dependent on the particular geometric features of the blood vessels. The geometry can cause disturbed flow, e.g. flow separation, recirculation region, complex vertical flows, the secondary flow velocities, stagnation point region. Previous studies have stated that the velocity was low in the location of disturbed flow patterns and this can cause low WSS (Kleinstreuer et al. 2001; Asakura and Karino 1990). Thus, the blood flow velocity will reveal the regions of interest. In addition, the flow performance indicators, such as, the time-averaged wall shear stress (TAWSS), oscillatory shear index (OSI), flow relative resistance time (RRT) are adopted by flow velocity indicator in blood flow research. Furthermore, in clinical trials, the fractional flow reserve (FFR) normally measured by using intravascular approaches such as intravascular ultrasound or invasive coronary angiography can also be predicted by CFD method. Thus, the stenosis lesions can also be classified easily by CFD approach with demonstration of FFR parameter.

1.7 Review of Arterial Flow Simulation

According to the general CFD introduction in section 1.6, CFD was used to analyse human left coronary artery and characterise the haemodynamic parameters. An explanation of the application of CFD in the context of haemodynamic flow modelling, and its broad methodologies, is described as below.

Among other factors, the flexible vessel wall of the LCA, the non-Newtonian behaviour of blood, and the tortuous geometry of arteries, cause the behaviour of the real LCA to be highly non-linear. In order for simulations of the LCA to be tractable, a number of assumptions must be made. Some of the basic assumptions are discussed below:

- **Arterial wall model**

  A multitude of early studies have explored blood flow in the human artery based on the assumption that the arterial wall is rigid. Authors that used this approach include Sun et al. (2009) who investigated blood flow changes in the carotid artery. Katritsis et al. (2007a, 2007b) used a rigid coronary wall assumption in their investigation of WSS changes in a healthy coronary artery. Giannoglou et al. (2005, 2002) assumed that the LCA wall was rigid, to simulate blood flow variations in the LCA. He and Ku (1996) studied WSS effects in the LCA bifurcation using a rigid wall assumption.

Other studies have examined haemodynamic changes in large blood vessels and aortic valve using a moving wall assumption. Frauenfelder et al. (2006) studied blood flow changes to an abdominal aortic aneurysm based on an assumption of a deformable artery wall. Their study was performed by using two-way fluid structure interaction to characterise velocity alteration. Gao et al. (2009, 2008, 2011) have explored blood flow effects in the carotid artery based on a moving wall assumption by using fluid structure interaction. Their investigation used magnetic resonance images of four selected patients to characterise haemodynamic variations. Previous researchers (Morbiducci et al. 2009; De Hart 2003a, 2003b) assumed the aorta wall to be a deformable arterial wall, damage to which can lead to sudden heart attacks. Their studies, characterised blood flow in the heart valve and aortic vessels using fluid structure interaction simulation. Hence, the assumption of moving arterial wall is generally suited to the modelling of large blood vessels, such as, the abdominal aorta and aortic valve.

The same cannot be said for small blood vessels, the comparison of the impact of rigid wall and moving wall assumptions upon the accuracy of human LCA models (small blood vessel) has not yet been performed. However, Siogkas et al. (2011) studied the impact of rigid wall versus deformable wall assumptions upon WSS variations. Their study showed that a rigid wall model provided similar WSS values to a moving wall model. Their results demonstrated that blood flow simulations with a rigid wall assumption can provide accurate WSS values regarding WSS alterations. Accordingly, given Siogkas' work, and the precedent set by previous researchers in small blood vessel simulation, we believe that it is reasonable to assume that the coronary wall is rigid in the context of the human LCA.

In this study, we emphasise that the rigid wall is reasonable as having shorter computational cost when the plaque composition is not being taken into consideration. The walls of the LCA were assumed to be rigid, and we would argue that this is a reasonable representation of the LCA geometry and of the pathology of coronary disease.

- **Blood**

  Blood is a suspension of particles in plasma. The various particles are comprised of erythrocytes (red blood cells), leukocytes (white blood cells), and platelets (cell fragments for clotting). These normally occupy approximately 45% of the blood volume (a proportion that is lightly dependent on sex and species). Blood function is mainly to transport and distribute the oxygen and nutrients to cells, within the body, and to remove carbon dioxide. Various approaches for the simulation of blood, flowing in the human artery are briefly described as below:

  Newtonian fluid blood

  Pedley (1980) stated that blood plasma can be treated as Newtonian in arterial vessels. Authors that have utilised a Newtonian approach include Sun and Chaichana (2010, 2009), who investigated blood flow effects upon stent placement in abdominal aorta aneurysm based on an assumption of Newtonian viscosity. Sun et al. (2009) also used the assumption of Newtonian viscosity to characterise haemodynamic impacts in carotid artery bifurcation. He and Ku (1996) assumed that blood is Newtonian in the simulation of blood flow in LCA bifurcation. Katritsis et al. (2010, 2007a, 2007b) used an assumption of a Newtonian model for their primary studies to characterise WSS variation in coronary arteries.

Rheological parameters utilised by previous researchers have generally been derived from parametric studies of clinical data. Milnor (1989) reported that blood in the human body had a density of 1,060 kg/m^3, and a viscosity of 0.0035 Pa s.

Various rheological values utilised are shown in Table 1.

Studies	Viscosity (Pa s)	Density (kg/m^3)
Sun et al. (2009)	0.00270	1,060
Shanmugavelayudam et al. (2011)	0.00350	1,050
Lantz et al. (2011)	0.00256	1,080
Tse et al. (2011)	0.00371	1,060
Katritsis et al. (2010)	0.00040	1,067
Fukumoto et al. (2008)	0.00300	1,050

Table 1. Various assumptions of blood parameters

Several non-Newtonian blood viscosity models have been proposed, based upon an evaluation of the stress strain relationship (Ballyk et al. 1994, Fung 1993; Cho and Kensey 1991; Walburn and Schneck 1976). However, none of these assumptions are presently accepted as a reasonable reflection of blood behaviour. Furthermore, Johnston et al. (2004, 2006) have investigated the effect of Newtonian and non-Newtonian blood viscosity models upon the WSS in the right coronary artery, and they concluded that a Newtonian model provided similar WSS values to the non-Newtonian model. In addition, Johnston et al. (2004) stated that the magnitude of WSS for Newtonian and Non-Newtonian models was significantly different, especially for low inlet velocities. Other studies have stated that both Newtonian and non-Newtonian viscosity models have produced similar results upon WSS changes (Jeong and Rhee 2009).

We would argue that in this context, it is reasonable to assume that blood is a Newtonian fluid, in the modelling of haemodynamic changes to human LCA.

Single phase flow

Various authors have assumed blood flow in the LCA to be single phase. He and Ku (1996), Giannoglou et al. (2005, 2002), and Johnston et al. (2004, 2006) have investigated haemodynamic changes in the right coronary artery with the assumption of single phase flow. Katritsis et al. (2010, 2007a, 2007b) have observed coronary flow changes based on the assumption of fluid blood as a single phase flow in the artery, to show WSS distributions. Sun and Chaichana (2010, 2009) also made the same assumption in their study of blood flow in the abdominal aorta. In addition, Sun et al. (2009) reported haemodynamic changes in the carotid artery with the assumption of single phase flow, to characterise pressure and velocity changes.

In contrast, there are few authors who have modelled blood as a multiphase flow. So far, these studies are restricted to simple, idealised geometries, for example, Sharan and Popel (2001) have simulated a tube section as an idealised arterial geometry. Their study attempted to divide the properties of blood into two parts: i) red blood cells, and ii) white blood cells and platelets. Their study focused upon the behaviour of blood flow in narrowed arteries, to characterise velocity changes. However, their study did not model pathological changes in blood vessels.

Therefore, we would argue that our assumption that blood is a single phase flow is reasonable in the context of the study blood flow variations in the human LCA.

Laminar flow model

Many authors have assumed Laminar flow for the modelling of the haemodynamics of the LCA. He and Ku (1996) stated that the flow in the LCA was laminar, based on the nature of blood behaviour in small arterial sections (eg. the coronary artery). Their studies used a laminar model to simulate haemodynamic changes in the LCA. Johnston et al. (2004, 2006) studied blood flow variations in the right coronary artery, and their investigations used a laminar assumption to reflect coronary flow changes. Katritsis et al. (2010, 2007a, 2007b) explored flow variations in the coronary artery, and their simulations have assumed laminar flow. Sun et al. (2009) assumed a laminar model for blood flow in the carotid artery bifurcation. The Reynolds number of <500 revealed laminar flow condition, based on inflow conditions at left main stem branch (He and Ku, 1996; Sun and Chaichana 2009, 2010). Sun and Chaichana (2010, 2009) studied blood flow in an abdominal aorta aneurysm, and their studies used the assumption of transitional and turbulent flow to investigate the haemodynamic effects in a large artery (abdominal aorta diameter >3 cm).

A laminar assumption is not always appropriate, however. Blood flow in large arteries can be transitional and turbulent. Generally speaking, previous researchers assumed flow to be laminar as an inflow boundary condition, since mean flow velocity is low, resulting in a relatively low Reynolds number (Tse 2011; Frauenfelder et al. 2006; Fung 1993, 1997; Hart 1997). Tse et al. (2011) investigated haemodynamic changes due to aorta aneurism in clinical data. Their results showed that laminar flow can become transitional and turbulent due to cross-sectional area changes induced by aortic aneurism. Furthermore, mean Reynolds number may refer to a factor that can be used to identify person to person variations which have similar lesions at the same arterial locations.

In addition, Frauenfelder et al. (2006) investigated haemodynamics variations to abdominal aortic aneurysms based on a group of eleven patients. Their study showed that only a small eddy is visible during the systolic phase, and these eddies are mostly apparent at the concavity area of aortic aneurysm (a maximum cross-sectional aorta). Hence, it is clear that a laminar blood flow becomes a turbulent flow model in the area of aortic aneurysm.

Apparently the LCA can be classified as a fairly small blood vessel, and in this environment flow is usually laminar. We would argue that in this context it is reasonable to follow the precedent of previous researchers, and assume the blood flow to be laminar in our primary investigations of WSS variation.

Cardiac phase flow

Clearly, flow in the LCA is unsteady, blood flow varying with the cardiac cycle. Johnston et al. (2004, 2006) used steady velocity values (centre-line velocity) compared Newtonian and non-Newtonian models. Other authors that used the cardiac cycle as an inflow condition include He and Ku (1996), Katritsis et al. (2010, 2007a, 2007b), and Sun et al. (2009). Sun and Chaichana (2010, 2009) applied the cardiac cycle at the main aorta to provide both the inflow and outflow conditions to observe haemodynamic change in abdominal aorta aneurysm.

Hence, many researchers have used the cardiac cycle as the basis for time-varying boundary conditions applied at inlets and outlets. Accordingly, our LCA simulation utilised cardiac cycle inflow and outflow conditions in this study.

1.8 Research Summary

This thesis has presented the idea of using CFD in the field of biomedical engineering with the aim of investigating the biomechanics of the coronary artery, in relation to the pathogenesis of atherosclerosis. The left coronary artery is considered, since it represents a realistic coronary geometry, consisting of an angulation at the main bifurcation which is formed between left circumflex, and left anterior descending. Clinical statistics have also reported that the left coronary artery is the most common location where plaques usually occur and induce myocardial ischaemic changes (Topol 2008; Cho et al. 2001). In addition, CFD analysis is performed to investigate the haemodynamic variations in both healthy and diseased coronary arteries, including simulation of different types of plaques. The results provide an insight into the biomechanics of coronary artery disease. Therefore, this research has delivered information which will help to improve our understanding of haemodynamic behaviour during the cardiac cycles under normal and diseased conditions. Future research will focus upon the investigation of haemodynamic effects due to different type of plaques and subsequent follow-up of clinical outcomes in terms of development of major adverse cardiac events. Therefore, it is expected that prevention of adverse cardiac events can be achieved through a combination of computed tomography imaging and computational haemodynamic analysis.

1.9 List of References

Anderson, H.V., Roubin, G.S., Leimgruber, P.P., Cox, W.R., Douglas, J.S., Jr, King, S.B., 3rd, Gruentzig, A.R., 1986. Measurement of transstenotic pressure gradient during percutaneous transluminal coronary angioplasty. Circulation 73 (6), 1223–1230.

Asakura, T., Karino, T., 1990. Flow patterns and spatial distribution of atherosclerotic lesions in human coronary arteries. Circulation Research 66, 1045–1066.

Australian Institute of Health and Welfare, 2011. Cardiovascular disease: Australian facts 2011, Cat. no. CVD 53. Canberra: AIHW.

Australian Institute of Health and Welfare, 2010. Cardiovascular disease mortality Trends at different ages, Cat. no. CVD 47. Canberra: AIHW.

Australian Institute of Health and Welfare, 2006. The tenth biennial health report of the Australian Institute of Health and Welfare, Cat. no. AUS 73. Canberra: AIHW.

Berne, R.M., Levy, M.N., 2001. Cardiovascular physiology. Mosby, St Louis (MI), 230–231.

Bluestein, D., Alemu, Y., Avrahami, I., Gharib, M., Dumont, K., Ricotta, J.J., Einav, S., 2008. Influence of microcalcifications on vulnerable plaque mechanics using FSI modelling. Journal of Biomechanics 41 (5), 1111–1118.

Caro, C.G., Fitz-Gerald, J.M., Schroter, R.C., 1971a. Proposal of a shear dependent mass transfer mechanism for atherogenesis. Clinical Science 40 (2), 5P.

Caro, C.G., Fitz-Gerald, J.M., Schroter, R.C., 1971b. Atheroma and arterial wall shear: Observation, correlation and proposal of a shear dependent mass transfer mechanism for atherogenesis. Proceedings of the Royal Society B: Biological Sciences 177 (46), 109–159.

Chandran, K.B., Wahle, A., Vigmostad, S.C., Olszewski, M.E., Rossen, J.D., Sonka, M., 2006. Coronary arteries: imaging, reconstruction, and fluid dynamic analysis. Critical Reviews in Biomedical Engineering 34 (1), 23–103.

Cheng, L.C., Robertson, J.M., Clark, M.E., 1973. Numerical Calculations of plane oscillatory non-uniform flow – II. Parametric study of pressure gradient and frequency with square wall obstacles. Journal of Biomechanics 6 (5), 521–538.

Chervu, A., Moore, W.S., 1990. An overview of intimal hyperplasia, Surg Gynecol Obstet 171 (5), 433–447.

Cho, G.Y., Lee, C.W., Hong, M.K., Kim, J.J., Park, S.W., Park, S.J., 2001. Effects of stent desing on side branch occlusion after coronary stent placement. Catheterization and Cardiovascular Interventions 52 (1), 18–23.

DeBakey, M.E., Lawrie, G.M., Glaeser, D.H., 1985. Patterns of atherosclerosis and their surgical significance. Annals of Surgery 201 (2), 115–131.

De Hart, J., Baaijens, F.P., Peters, G.W., Schreurs, P.J., 2003a. A computational fluid-structure interaction analysis of a fiber-reinforced stentless aortic valve. Journal of Biomechanics 36 (5), 699–712.

De Hart, J., Peters, G.W., Schreurs, P.J., Baaijens, F.P., 2003b. A three-dimensional computational analysis of fluid–structure interaction in the aortic valve. Journal of Biomechanics 36 (1), 103–112.

Enderle, J.D., Bronzino, J.D. 2011. Introduction to biomedical engineering, third. Academic Press, London 1–5.

Fishman, E.K., 2005. Multidetector-row computed tomography to detect coronary artery disease: the importance of heart rate. European Heart Journal Supplements 7 (suppl G): G4–G12.

Frauenfelder, T., Lotfey, M., Boehm, T., Wildermuth, S., 2006. Computational fluid dynamics: Hemodynamic changes in abdominal aortic aneurysm after stent-graft implantation. CardioVascular and Interventional Radiology 29 (4), 613–623.

Fry, D.L., 1969. Certain histological and chemical responses of the vascular interface to acutely induced mechanical stress in the aorta of the dog. Circulation Research 24 (1), 93–108.

Fry, D.L., 1968. Acute vascular endothelial changes associated with increased blood velocity gradients. Circulation Research 22 (2), 165–197.

Fukumoto, Y., Hiro, T., Fujii, T., Hashimoto, G., Fujimura, T., Yamada, J., Okamura, T., Matsuzaki, M., 2008. Localized elevation of shear stress is related to coronary plaque rupture: a 3-dimensional intravascular ultrasound study with in-vivo color mapping of shear stress distribution. Journal of the American College of Cardiology 51 (6), 645-650.

Fung, Y.C., 1997. Biomechanics: circulation, 2nd ed. Springer-Verlag, New York.

Fung, Y.C., 1993. Biomechanics: mechanical properties of living tissues, second. Springer-Verlag, New York 1–5.

Gao, H., Long, Q., Das, S.K., Sadat, U., Graves, M., Gillard, J.H., Li, Z. 2011. Stress analysis of carotid atheroma in transient ischemic attack patient: Evidence for extreme stress-induced plaque rupture. Annals of Biomedical Engineering 39 (8), 2203–2212.

Gao, H., Long, Q., Graves, M., Gillard, J.H., Li, Z. 2009. Carotid arterial plaque stress analysis using fluid-structure interactive simulation based on *in-vivo* magnetic resonance images of four patients. Journal of Biomechanics 42 (10), 1416–1423.

Gao, H., Long, Q., 2008. Effects of varied lipid core volume and fibrous cap thickness on stress distribution in carotid arterial plaques. Journal of Biomechanics 41 (14), 3053–3059.

Garcia, D., Kadem, L., Savéry, D., Pibarot, P., Durand, L.G., 2006. Analytical modeling of the instantaneous maximal transvalvular pressure gradient in aortic stenosis. Journal of Biomechanics 39 (16), 3036–3044.

Giannoglou, G.D., Soulis, J.V., Farmakis, T.M., Giannakoulas, G.A., Parcharidis, G.E., Louridas, G.E., 2005. Wall pressure gradient in normal left coronary artery tree. Medical Engineering & Physics 27 (6), 455–564.

Giannoglou, G.D., Soulis, J.V., Farmakis, T.M., Farmakis, D.M., Louridas, G.E., 2002. Haemodynamic factors and the important role of local low static pressure in coronary wall thickening. International Journal of Cardiology 86 (1), 27–40.

Gijsen, F.J., Wentzel, J.J., Thury, A., Lamers, B., Schuurbiers, J.C., Serruys, P.W., van der Steen, A.F., 2007. A new imaging technique to study 3-D plaque and shear stress distribution in human coronary artery bifurcations in vivo. Journal of Biomechanics 40 (11), 2349–2357.

Hachamovitch, R., Berman D.S., Shaw L.J., Kiat H., Cohen I., Cabico J.A., Friedman J., Diamond G.A., 1998. Incremental prognostic value of myocardial perfusion single photon emission computed tomography for the prediction of cardiac death: differential stratification for risk of cardiac death and myocardial infarction. Circulation 97 (6), 535–543.

Hart, J.D., 1997. Nonparametic smoothing and lack-of-fit tests, 1st ed. Springer-Verlag, New York.

He, X., Ku, N.D., 1996. Pulsatile flow in the human left coronary artery bifurcation: average conditions. Journal of Biomechanical Engineering 118 (1), 74–82.

Hingorani, A., Ascher, E., Marks, N., 2007. Preprocedural imaging: New options to reduce need for contrast angiography. Seminars in vascular surgery 20 (1), 15–28.

Holzapfel, G.A., Gasser, T.C., Ogden, R.W., 2000. A new constitutive framework for arterial wall mechanics and comparative study of material models. Journal of Elasticity 61 (1-3), 1–48.

Jeong, W.W., Rhee, K., 2009. Effects of surface geometry and non-newtonian viscosity on the flow field in arterial stenoses. Journal of Mechanical Science and Technology 23 (9), 2424–2433.

Johnston, B.M., Johnston, P.R., Corney, S., Kilpatrick, D., 2006. Non-Newtonian blood flow in human right coronary arteries: Transient simulations. Journal of Biomechanics 39 (1), 1116–1128.

Johnston, B.M., Johnston, P.R., Corney, S., Kilpatrick, D., 2004. Non-Newtonian blood flow in human right coronary arteries: steady state simulations. Journal of Biomechanics 37 (5), 709–720.

Jung, J., Lyczkowski, R.W., Panchal, C.B., Hassanein, A., 2006. Multiphase hemodynamic simulation of pulsatile flow in a coronary artery. Journal of Biomechanics 39 (11), 2064–2073.

Katritsis, D.G., Theodorakakos, A., Pantos, I., Andriotis, A., Efstathopoulos, E.P., Siontis, G., Karcanias, N., Redwood, S., Gavaises, M., 2010. Vortex formation and recirculation zones in left anterior descending artery stenosis: computational fluid dynamics analysis. Physics in Medicine and Biology 55 (5), 1395–1411.

Katritsis, D., Kaiktsis, L., Chaniotis, A., Pantos, J., Efstathopoulos, E.P., Marmarelis, V., 2007a. Wall shear stress: theoretical considerations and methods of measurement. Progress in Cardiovascular Diseases 49 (5), 307–329.

Katritsis, D.G., Pantos, J., Efstathopoulos, E., 2007b. Hemodynamic factors and atheromatic plaque rupture in the coronary arteries: from vulnerable plaque to vulnerable coronary segment. Coronary Artery Disease 18, 229–237.

Kleinstreuer, C., Hyun, S., Buchanan, J.R., Longest, P.W., Archie, J.P., Truskey, J.P., 2001. Hemodynamic parameters and early intimal thickening in branching blood vessels. Critical Reviews in Biomedical Engineering 29 (1), 1–64.

Ku, D.N., 1997. Blood flow in arteries. Annual Review of Fluid Mechanics 29, 399–434.

Koskinas, K.C., Chatzizisis, Y.S., Antoniadis, A.P., Giannoglou, G.D., 2012. Role of Endothelial Shear Stress in Stent Restenosis and Thrombosis: Pathophysiologic Mechanisms and Implications for Clinical Translation. Journal of the American College of Cardiology 59 (15), 1337–1349.

Lantz, J., Renner, J., Karlsson, M., 2011. Wall shear stress in a subject specific human aorta – Influence of fluid-structure interaction. International Journal of Applied Mechanics 3 (4), 759–778.

Lee, B., 2011. Computational fluid dyanamics in cardiovascular disease. Korea Circulation Journal 41 (8), 423–430.

Mahesh, M., 2002. Search for isotropic resolution in CT from conventional through multiple-row detector. Radiographics 22 (4), 949–962.

Milnor, W., 1989. Hemodynamics. Williams & Wilkins, Baltimore.

Morbiducci, U., Ponzini, R., Nobili, M., Massai, D., Montevecchi, F.M., Bluestein, D., Redaelli, A., 2009. Blood damage safety of prosthetic heart valves. Shear-induced platelet activation and local flow dynamics: A fluid–structure interaction approach. Journal of Biomechanics 42 (12), 1952–1960.

Nichols, W., O'Rourke, M., 2005. McDonald's blood flow in arteries. Hodder Arnold, London, 326–327.

Nieman, K., Oudkerk M., Rensing B.J., van Ooijen P., Munne A., van Geuns R.J., de Feyter P.J., 2001. Coronary angiography with multi-slice computed tomography. Lancet 357 (9256), 599–603.

Noto, T.J. Jr, Johnson L.W., Krone R., Weaver W.F., Clark D.A., Kramer J.R. Jr, Vetrovec G.W., 1991. Cardiac catheterization 1990: a report of the registry of the Society for Cardiac Angiography and Interventions. (SCA&I). Catheterization and Cardiovascular Diagnosis 24 (2), 75–83.

Pantos, J., Efstathopoulos, E., Katritsis, D.G., 2007. Vascula wall shear stress in clinical practice. Current Vascular Pharmacology 5, 113–119.

Parmet, S., 2004. Coronary Artery Disease. Journal of the American Medical Association 292 (20), 2540.

Pedley, T.J., 1980. The Fluid Mechanics of Large Blood Vessels. Cambridge university press, Cambridge, 30–31.

Phillips, T.L., 2002. 50 years of radiation research: Medicine. Radiation research 158 (4), 389–417.

Rushmer, R.F., 1976. Cardiovascular dynamics. WB Saunders, Philadelphia.

Rybicki, F., Melchionna, S., Mitsouras, D., Coskun, A., Whitmore, A., Steigner, M., Nallamshetty, L., Welt, F., Bernaschi, M., Borkin, M., Sircar, J., Kaxiras, E., Succi, S., Stone, P., Feldman, C., 2009. Prediction of coronary artery plaque progression and potential rupture from 320-detector row prospectively ECG-gated single heart beat CT angiography: Lattice Boltzmann evaluation of endothelial shear stress. International Journal of Cardiovascular Imaging 25, 289–299.

Samady, H., Eshtehardi, P., McDaniel, M.C., Suo, J., Dhawan, S.S., Maynard, C., Timmins, L.H., Quyyumi, A.A., Giddens, D.P., 2011. Coronary artery wall shear stress is associated with progression and transformation of atherosclerotic plaque and arterial remodeling in patients with coronary artery disease. Circulation 124, 779–788.

Shanmugavelayudam, S.K., Rubenstein, D.A., Yin, W., 2010. Effect of geometrical assumptions on numerical modelling of coronary blood flow under normal and disease conditions. Journal of Biomechanical Engineering 132, 061004.

Sharan, M., Popel, A.S., 2001. A two-phase model for flow of blood in narrow tubes with increased effective viscosity near the wall. Biorheology 38, 415–428.

Speelman, L., Akyildiz, A.C., den Adel, B., Wentzel, J.J., van der Steen, A.F.W., Virmani, R., vander Weerd, L., Jukema, J.W., Poelmann, R.E., van Brummelen, E.H., Gijsen, F.J.H., 2011. Initial stress in biomechanical models of atherosclerotic plaques. Journal of Biomechanics 44 (13), 2376–82.

Sommer T., Hackenbroch M., Hofer U., Schmiedel A., Willinek W.A., Flacke S., Gieseke J., Träber F., Fimmers R., Litt H., Schild H., 2005. Coronary MR angiography at 3.0 T versus that at 1.5 T: initial results in patients suspected of having coronary artery disease. Radiology 234 (3), 718–25.

Soulis, J.V., Farmakis, T.M., Giannoglou, G.D., Louridas, G.E., 2006. Wall shear stress in normal left coronary artery tree. Journal of Biomechanics 39 (4), 742–749.

Sun, Z., Cao Y., Li H., 2011. Multislice CT angiography in the diagnosis of coronary artery disease. Journal of Geriatric Cardiology 8 (2), 104–113.

Sun, Z., Chaichana, T., 2010. Fenestrated stent graft repair of abdominal aortic aneurysm: hemodynamic analysis of the effect of fenestrated stents on the renal arteries. Korean Journal of Radiology 11 (1), 95–106.

Sun, Z., Chaichana, T., 2009. Investigation of the hemodynamic effect of stent wires on renal arteries in patients with abdominal aortic aneurysms treated with suprarenal stentgrafts. CardioVascular and Intervention al Radiology 32 (4), 647–657.

Sun, Z., Mwilpatayi B., Chaichana T., Ng C., 2009. Hemodynamic effect of calcified plaque on blood flow in carotid artery disease: a preliminary study. Proc IEEE Bioinformat Biomed Eng 1, 1–4.

Takuro, T., Souki, L., Shuichi, H., Kouichi, T., Daisuke, K., Keisuke, K., Hitoshi, T., Toshihiro, T., Masaaki, M., Ryuichiro, A., Yutaka, O., Chuwa, T., 2007. Limitation of angiography to identify the culprit plaque in acute myocardial infarction with coronary total occlusion: Utility of coronary plaque temperature measurement to identify the culprit plaque. Journal of the American College of Cardiology 50 (23), 2197–2203.

Torii, R., Keegan, J., Dowsey, A., Wood, N., Yang, G.Z., Firmin, D., Hughes, A., Thom, S., Xu. X.Y., 2008. A CFD study on coronary artery haemodynamics with dynamic vessel motion based on MR images. Journal of Biomechanics 41 (Suppl 1), S212.

Tse, K.M., Chiu, P., Lee, H.P., Ho, P., 2011. Investigation of hemodynamics in the development of dissecting aneurysm within patient-specific dissecting aneurismal aortas using computational fluid dynamics (CFD) simulations. Journal of Biomechanics 44 (5), 827–836.

Thubrikar, M.J., Robicsek, F., 1995. Pressure-induced arterial wall stress and atherosclerosis. Annals of Thoracic Surgery 59 (6), 1594–1603.

Topol, E.J., 2008. Textbook of interventional cardiology, fifth. Saunders Elsevier, Philadelphia, 1075.

Townsend, D.W., 2008. Dual-modality imaging: Combining anatomy and function. Journal of nuclear medicine 49 (6), 938–955.

Traub, O., Berk, B.C., 1998. Laminar Shear Stress: Mechanisms by Which Endothelial Cells Transduce an Atheroprotective Force. Arteriosclerosis, Thrombosis, and Vascular Biology 18 (5), 677–685.

Tu, J., Yeoh, G.H., Liu, C., 2008. Computational fluid dynamics: A practical approach. Butterworth-Heinemann: Elsevier, Burlington (MA).

Versluis, A., Bank, A.J., Douglas, W.H., 2006. Fatigue and plaque rupture in myocardial infarction. Journal of Biomechanics 39 (2), 339–347.

Chapter 2

Computation of hemodynamics in the left coronary artery with variable angulations. Journal of Biomechanics 44 (10), 1869–1878.

Thanapong Chaichana, Zhonghua Sun and James Jewkes

Journal of Biomechanics 44 (2011) 1869–1878

Contents lists available at ScienceDirect

Journal of Biomechanics

journal homepage: www.elsevier.com/locate/jbiomech
www.JBiomech.com

Computation of hemodynamics in the left coronary artery with variable angulations

Thanapong Chaichana [a], Zhonghua Sun [a,*], James Jewkes [b]

[a] Discipline of Medical Imaging, Department of Imaging and Applied Physics, Curtin University, G.P.O Box U1987, Perth, Western Australia 6845, Australia
[b] Fluid Dynamics Research Group, Department of Mechanical Engineering, Curtin University, Perth, Western Australia 6845, Australia

ARTICLE INFO

Article history:
Accepted 16 April 2011

Keywords:
Coronary artery disease
Angulation
Computational fluid dynamics
Wall shear stress
Wall shear stress gradient

ABSTRACT

The purpose of this study was to investigate the hemodynamic effect of variations in the angulations of the left coronary artery, based on simulated and realistic coronary artery models. Twelve models consisting of four realistic and eight simulated coronary artery geometries were generated with the inclusion of left main stem, left anterior descending and left circumflex branches. The simulated models included various coronary artery angulations, namely, 15°, 30°, 45°, 60°, 75°, 90°, 105° and 120°. The realistic coronary angulations were based on selected patient's data with angles ranging from narrow angles of 58° and 73° to wide angles of 110° and 120°. Computational fluid dynamics analysis was performed to simulate realistic physiological conditions that reflect the *in vivo* cardiac hemodynamics. The wall shear stress, wall shear stress gradient, velocity flow patterns and wall pressure were measured in simulated and realistic models during the cardiac cycle. Our results showed that a disturbed flow pattern was observed in models with wider angulations, and wall pressure was found to reduce when the flow changed from the left main stem to the bifurcated regions, based on simulated and realistic models. A low wall shear stress gradient was demonstrated at left bifurcations with wide angles. There is a direct correlation between coronary angulations and subsequent hemodynamic changes, based on realistic and simulated models. Further studies based on patients with different severities of coronary artery disease are required to verify our results.

1. Introduction

Atherosclerosis is the leading cause of morbidity and mortality in the advanced countries. The causes of atherosclerosis are multifactorial and identification of these factors could allow earlier detection and prevention of the disease. Hemodynamics and vessel geometry may play an important role in the cause of plaque formation, since atherosclerotic plaques occur frequently in well-recognized arterial regions of curvature, bifurcated area and vessel branches (Zarins et al., 1983; Asakura and Karino, 1990; Conner, 1994). Blood flow variations, particularly those related to the rate of change of stream-wise velocity perpendicular to the blood vessel wall (known as the wall shear stress), have been reported to be related to the pathogenesis of atherosclerosis (Lehoux, 2006; Sabbah et al., 1986).

Early hemodynamic analysis of coronary artery disease performed using computational fluid dynamic (CFD) techniques has been typically performed using one of two approaches, they were based on either simulated models or realistic coronary artery geometry simulations (Lim and Kern, 2005; Katritsis et al., 2007; Shanmugavelayudam et al., 2010; Wellnhofer et al., 2010; Nordgaard et al., 2010). As far as we know, no systematic studies have been performed hitherto that relate bifurcation angles to flow instabilities predisposing to the formation of atherosclerotic lesions. The left coronary artery differs from the right coronary artery in terms of geometric appearance as the left side has a very short main stem, which quickly divides into left anterior descending and left circumflex with an angle formed between these two branches. Thus the angulation between these two coronary branches induces local hemodynamic changes, which may pose a potential risk for development of atherosclerosis. The aim of this study was to investigate the relationship between hemodynamics and angulations at the left coronary artery, based on simulated models and realistic patients' data. Various angles were simulated at the left coronary artery with the aim of identifying the effect of angulation on the subsequent hemodynamic changes to the left coronary artery.

2. Materials and Methods

2.1. Measurement of left coronary artery anatomical details

Four patients suspected of coronary artery disease underwent multislice CT angiography and were included in the patient datasets. This original DICOM

* Corresponding author. Tel.: +61 8 9266 7509; fax: +61 8 9266 2377.
E-mail address: z.sun@curtin.edu.au (Z. Sun).

0021-9290/$ - see front matter © 2011 Elsevier Ltd. All rights reserved.
doi:10.1016/j.jbiomech.2011.04.033

(digital imaging and communication in medicine) data was transferred to a separate workstation equipped with Analyze version 7.0 (Analyze Direct, Inc., Lexana, KS, USA) for image post-processing and segmentation. Three-dimensional (3D) volume data was post-processed and segmented using a semi-automatic method with a CT number thresholding technique (Sun et al., 2003, 2004) and manual editing was performed in some slices to remove soft tissues and artifacts. Four models were produced with a special focus on the left coronary artery (LCA) and its branches. The 3D LCA models were saved in 'STL' stereolithography CAD format for further reconstruction purposes. Anatomic measurements were performed at the LCA location and its branches in the volumetric models so that these measurements could be used to provide suitable dimensions for the simulated LCA models, as shown in Table 1. Fig. 1 shows anatomical details of the LCA with an angle formed between the left anterior descending (LAD) and left circumflex (LCx) branches.

This investigation conforms to the principles outlined in the declaration of Helsinki for use of human subjects (World Medical Association declaration of Helsinki, 1997). Since patients underwent routine CT scanning for clinical diagnosis of coronary artery disease, and only the DICOM images were used for generation of 3D coronary artery images, with patient's details being de-identified, there is no ethical issue involved in this study.

2.2. Generation of simulated left coronary artery models

The geometry of a simulated, perpendicular (90°) model was generated based on the anatomical details of LCA and standard dimensions measured based on Fig. 1, using Blender version 2.48 (Blender Institute, Amsterdam, Netherlands). The surface of the 90° LCA model was used as a reference model, which was then converted into a solid model. A bifurcation angle of 80° is recommended as a cut off value to determine whether there is presence of coronary artery disease, as confirmed by previous reports studying the natural distribution of coronary bifurcation angles (Reig and Petit, 2004; Pflederer et al., 2006). Our simulation on different angles of the left coronary artery reflects the range of angulations from very small to large angles, which enables us to perform an in-depth study of the relationship between angulation and development of atherosclerosis. Based on the reference model, seven other models were generated by changing the angle between LAD and LCx these included 15°, 30°, 45°, 60°, 75°, 105° and 120°. All baseline models were saved in 'STL format' for producing mesh models. Fig. 2 shows variable angles that were simulated in the left coronary artery models. Finally the merging of side branches within left main trunk generated sharp edges at the bifurcation regions, which could potentially have an undesirable impact on local flow simulation (He and Ku, 1995). Therefore, gentle B-spline smoothing was applied at the interface between branches and the trunk to reduce any potential non-physical behavior that could be induced by sharp edges. The splitting of flow rate at a symmetric bifurcation is defined by Zheng et al. (2006) and Lou and Yang (1993). Their flow rate system of equal diameter branches can be defined as a splitting ratio (Zheng et al., 2006):

$$Q_{LMS} = Q_{LCx} + Q_{LAD} \tag{1}$$

$$R_s = \frac{Q_{LCx}}{Q_{LAD}} \tag{2}$$

where $Q_{LMS} = \pi r_{LMS}^2 \vec{V}_{LMS}$ is the flow rate in parent with r_{LMS}^2 and $\vec{V}_{LMS}$ being radius and velocity at main trunk, respectively, Q_{LCx} and Q_{LAD} are the flow rates in daughter branches. However, in this study, the two left coronary artery branches are unequal in diameter and distance in regard to the main left coronary artery, as shown in Table 1. In our case, R_s (splitting ratio) of a 90°model is calculated as $R_s = (\pi r_{LCx}^2 \vec{V}_{LCx})/(\pi r_{LAD}^2 \vec{V}_{LAD}) = 9\vec{V}_{LCx}/16\vec{V}_{LAD}$.

2.3. Generation of realistic left coronary artery models

The patient 3D LCA models consisting of the ascending aorta, and right and left coronary arteries were then imported into a computer-aided design program using Blender version 2.48. Four volume models were reconstructed into the surface models, which were then converted into solid models and saved in 'STL format' for generation of CFD mesh models. Fig. 3 shows four sample realistic patient left coronary models with variable angulations. The realistic patient bifurcation angles ranged from 58° to 73°, 110° and 120°, respectively. These patients were selected to reflect the relationship between hemodynamics and angulations in the LCA. In summary, there were a total of twelve models consisting of four patient models and eight simulated models.

Table 1
Measurements of anatomical dimensions at the left coronary model.

Diameter of LCA (mm)	Distance between bifurcation to proximal/distal segment (mm)
LMS 3.0	Proximal inlet of LMS 35
LAD 2.0	Distal outlet of LAD 25
LCx 1.5	Distal outlet of LCX 20

LMS left main stem, LAD left anterior descending, LCx left circumflex.

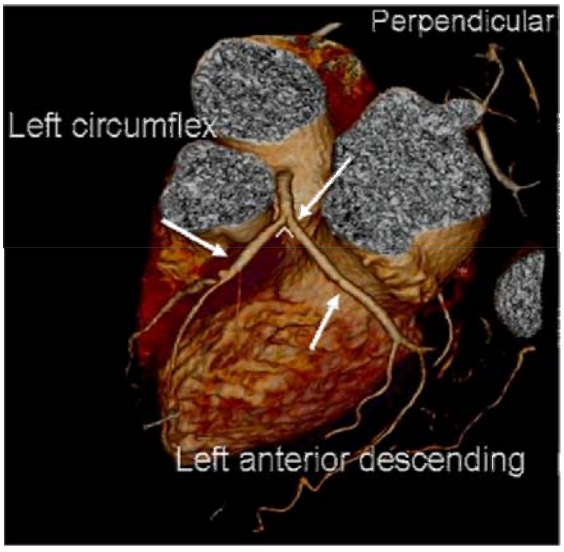

Fig. 1. 3D CT visualization of a normal left coronary artery with side branches in a patient with suspected coronary artery disease.

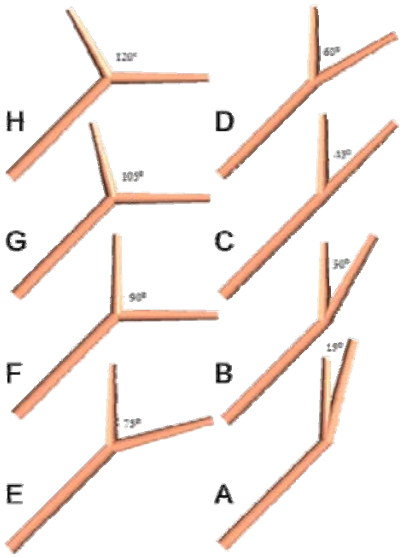

Fig. 2. Diagrams showing variable angles of the left coronary artery, including 120°, 105°, 90°, 75°, 60°, 45°, 30° and 15°.

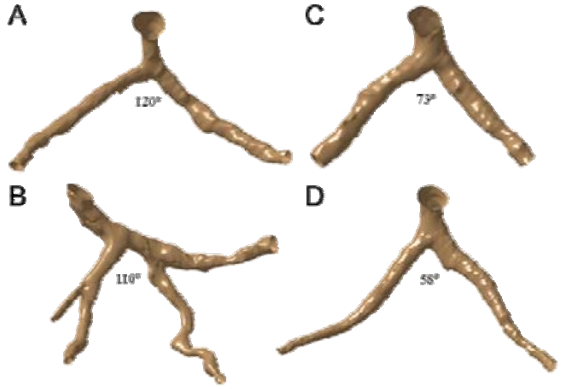

Fig. 3. Realistic coronary models in 4 selected patients with different angles at the left coronary artery including 120°, 110°, 73° and 58°.

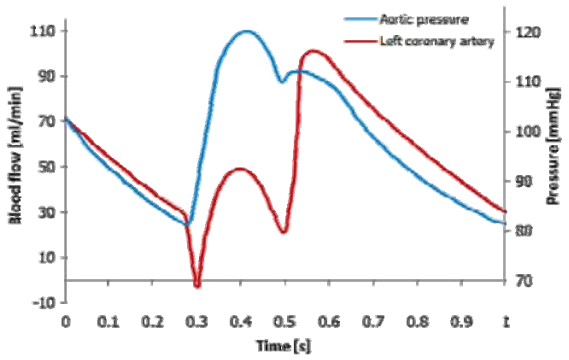

Fig. 4. Cardiac pulsatile velocity and pressure are applied for computational fluid dynamic simulation at the left coronary artery.

Table 2
Details of Hex-meshing for both simulated and realistic models.

Angulations (deg.)	No. of nodes	No. of cells
Simulated left coronary models		
120	326,325	365,517
105	353,589	369,218
90	336,807	354,827
75	343,290	357,502
60	358,395	366,925
45	343,626	364,552
30	340,923	358,038
15	320,460	330,427
Realistic left coronary models		
120	327,465	363,519
110	346,659	361,150
73	337,872	351,996
58	334,167	353,215

2.4. CFD simulation in the left coronary artery generation of meshes

All of the above models were used to create hexahedral meshes with which to perform the CFD simulations (mesh details are shown in Table 2). The meshes were generated using ANSYS ICEM CFD version 12 (ANSYS, Inc., Canonsburg, PA, USA), with details having been described in previous studies (Sun and Chaichana, 2010, 2009). Finally, the twelve 3D meshes were saved in 'GTM format' for CFD computation.

2.5. Application of physiological parameters

In order to ensure that our analysis reflects the realistic simulation of *in vivo* conditions, realistic physiological boundary conditions were applied for 3D numerical analysis. The transient simulation was performed using accurate hemodynamic rheological and material properties, as described in a previous study (Frauenfelder et al., 2006). Fig. 4 shows the pulsatile flow rates and pressure (Nichols and O'Rourke, 2005) at the aorta and LCA, reconstructed using a Fourier series (Smith, 1997) in Matlab (Math Works, Inc. Natick, MA, USA). This Fourier series was applied using ANSYS CFX Command Language (CCL) programming to define velocity and pressure boundary conditions. Pulsatile velocity was applied as an inlet boundary condition at the left main stem, and pulsatile pressure was applied at the left anterior descending and left circumflex outlet boundaries. Appropriate rheological parameters were applied with a blood density of 1060 kg/m^3 and blood viscosity of 0.0035 Pa s (Boutsianis et al., 2004; Milnor, 1989). The blood flow was assumed to be laminar and a no-slip condition was applied at the walls. Blood was assumed to be a Newtonian and incompressible fluid (Johnston et al., 2004, 2006; Borghi et al., 2008).

2.6. Performance of CFD computation

The Navier–Stokes equations were solved using the ANSYS CFX CFD package (version 12 ANSYS, Inc.), on a Microsoft Windows XP 32-bit machine, 4 MB RAM with a dual core 2.4 GHz CPU. The CFD simulation was run for 80 time-steps, representing 1.0 s of pulsatile flow (0.0125 s per time step), with each time step converged to a residual target of less than 1×10^{-4} by approximately 100 iterations. The CFD solution was fully converged by approximately 8000 time iterations per LCA model. The calculation time for each LCA model was approximately 5 h. The configuration of this simulation is similar to those in previously published simulations (Sun and Chaichana, 2010, 2009). Flow patterns, flow velocity, wall pressure, wall shear stress (WSS) and wall shear stress gradient (WSSG) were calculated and visualized using ANSYS CFD-Post version 12 (ANSYS, Inc.). The parameter used to characterize the impact of bifurcation angle on hemodynamic flow was calculated as the magnitude of local wall shear stress gradient (Kleinstreuer et al., 2001), which is defined as

$$\mathrm{WSSG} = \sqrt{\left(\frac{\partial \tau_{w,m}}{\partial n}\right)^2 + \left(\frac{\partial \tau_{w,\pi}}{\partial n}\right)^2} \tag{3}$$

where m is the temporal mean WSS direction, n is tangential to the surface and normal to m. $\tau_{w,m}$ and $\tau_{w,n}$ are WSS components along m and n directions, respectively and $\partial\tau_{w,m}/\partial m$ and $\partial\tau_{w,n}/\partial n$ are the off-diagonal components of $\nabla\tau_w$ tensor, which is obtained by computing a spatial derivative of WSS vector with respect to the Cartesian coordinates (x,y,z directions). The local WSS is calculated as $\tau_w = \mu(\partial\vec{v}_t/\partial y)$, where μ is blood viscosity, $\partial\vec{v}_t$ is velocity near wall perpendicular to surface and ∂y is distance to the wall surface. The WSSG components demonstrated that localized cellular proliferation may coincide with sudden pronounced changes in WSS (LaDisa et al., 2004; Ojha, 1993; White et al., 2001; Lei et al., 2001). Therefore the temporal WSSG is an alteration of WSS over a small period of time at the same location (White et al., 2001; Ojha, 1993), and can be obtained by taking the time derivative of the local WSSG, which is considered as $\partial\tau_w/\partial t$ and this has been described before (Lei et al., 1996). The time-dependent alterations in WSS and temporal WSSG were determined to evaluate the impact of bifurcation angles upon the flow and the ANSYS CCL language was used to develop a code to compute WSSG in ANSYS CFX-Post processing.

3. Results

The simulated and realistic left coronary artery models were successfully performed with CFD analysis under the *in vivo* physiological conditions during the systolic and diastolic phases. The analysis demonstrates a strong relationship between hemodynamics and angulations at the left coronary artery, as observed in both types of models.

3.1. Simulated left coronary artery models

Peak systolic velocity and pressure were reached at a time of 0.4 s during the cardiac cycles. Velocity patterns measured with different angulations of the simulated models are shown in Fig. 5. The CFD analysis showed that a small region of low-velocity blood flow distributed in the small-angled models gradually became a large region of flow separation when the angulations were

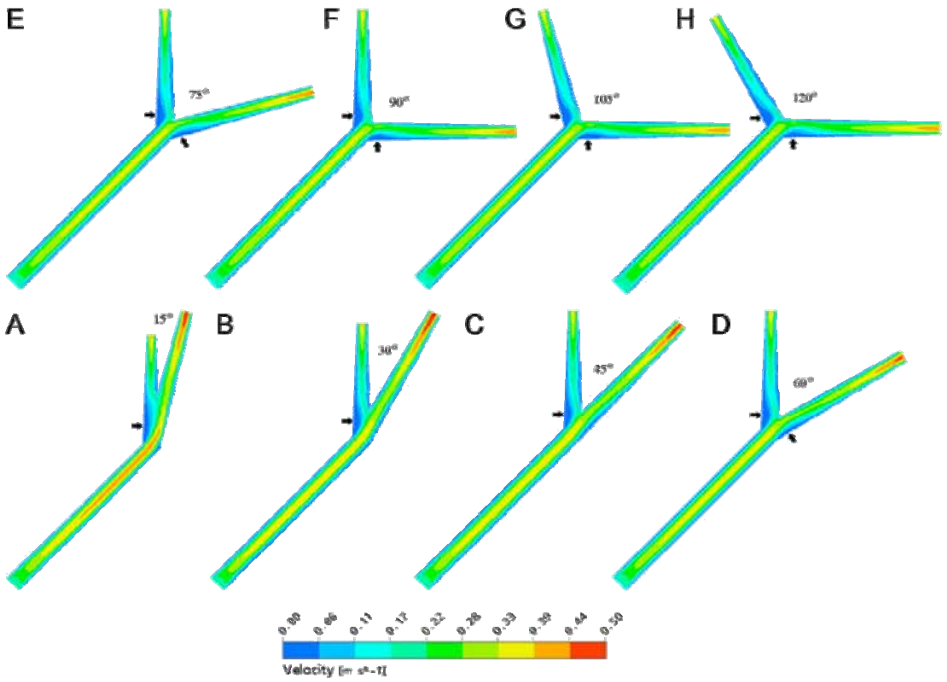

Fig. 5. Velocity observed with variable angles of the simulated left coronary artery models generated at peak systolic phase of 0.4 s. Arrows show the distribution regions of low flow and a big region of flow separation present in the wide-angled models.

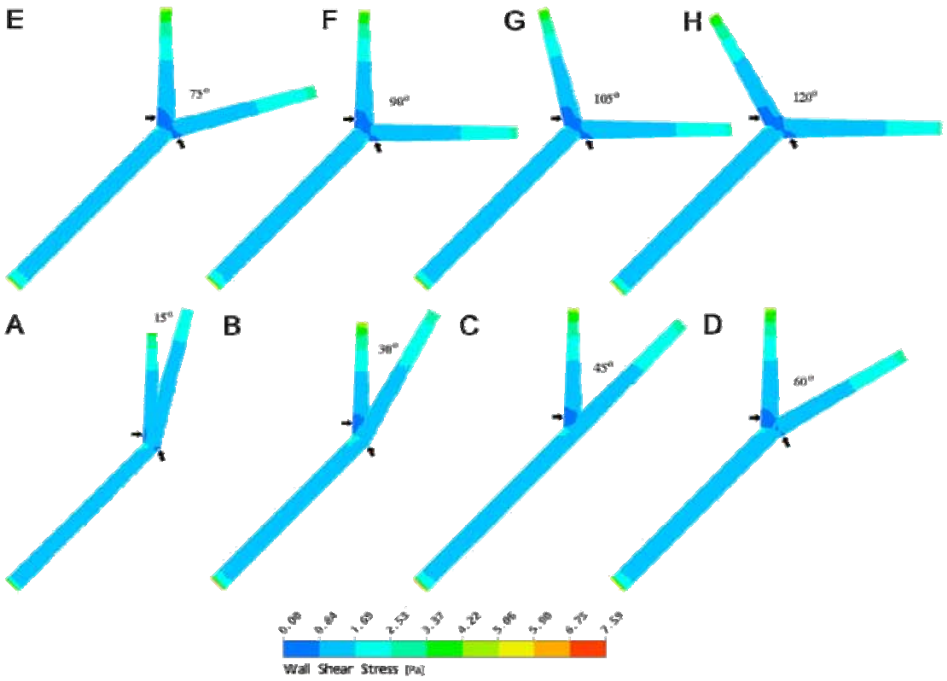

Fig. 6. Wall shear stress observed with variable angles of the simulated left coronary artery models generated at peak systolic phase of 0.4 . Arrows present the low wall shear stress distributions and a big region of low wall shear stress distributed in the wide coronary bifurcation.

increased, and this is particularly apparent at the location of the left coronary bifurcation.

Low WSS regions occurred at bifurcations where the left coronary main stem branches into left anterior descending and left circumflex. Fig. 6 demonstrates that WSS regions were found to reduce in wide-angled models when compared to the narrowed models and this phenomenon is particularly obvious in the systolic phase.

Similarly, wall pressure was affected to some extent with the change of angulations in different models. Fig. 7 displays that wall pressure increased from narrow-angled models to wide-angled models, particularly near the left coronary bifurcation. This is especially obvious in the model with a 15° angulation, as the results show significantly reduced wall pressure when the blood flows through from the left main stem to the left anterior descending and left circumflex braches.

Fig. 8 presents the magnitude of temporal WSSG and the regions of low WSSG at the left coronary bifurcations. A very low WSSG occurred in models with an angle of 120°, 105°, 90° and 75°, with the measured values ranging from 15.76 to 219.82 kg/m^2 s^2. In contrast, low temporal WSSG was not significantly apparent in small angle models such as 15° and 30° models. The temporal WSSG magnitude ranging 423.89–627.95 and 627.95–832.02 kg/m^2 s^2 was only measured in the models with an angle of 15°, 30°, 45°, 60°.

3.2. Realistic left coronary artery models

The analysis of realistic models is consistent with which was observed in the simulated models, showing a direct correlation between hemodynamic effects and the angulation of left coronary models. Fig. 9 demonstrates that flow velocity was decreased at bifurcation regions, and a small low-velocity region was observed in the small-angled models, becoming a large separated region in the wide-angled models.

WSS was found to be related to blood flow velocity at bifurcating regions. Low WSS was noticed in the bifurcated locations (angles between both left main artery branches and side branches), as shown in Fig. 10. The realistic coronary artery shapes introduced complex wall geometry that directly affected the WSS and wall pressure. However, our analysis showed that the impact on low WSS distributions at the left bifurcation was largely in wide-angled models, and this reflects our similar observations in the simulated models (shown in Fig. 6).

Similarly, wall pressure was noticed to change with different angulations of realistic left coronary models. Wall pressure decreased from wide-angled models to narrow-angled models. This is particularly apparent in the model with a 73° angulation when compared to a 120° angulation, as shown in Fig. 11. Again, this is consistent with that observed in the simulated models.

The magnitude of temporal WSSG is shown in Fig. 12. The regions of low WSSG were distributed around the left coronary bifurcations. The magnitude of low WSSG was obviously demonstrated for bifurcations with 120° and 110° angulations, with measured WSSG values ranging from 15.76 to 219.82 kg/m^2 s^2. Low WSSG also occurred at 58° angulation model due to the complex shape of the daughter branches. This indicates the difference between realistic models and simulated models as the realistic models represent the patient's actual arterial geometry, while simulated models do not reflect the complex wall geometry such as curved or tortuous appearance of the vessel wall. The temporal WSSG magnitude between 627.95 and 832.02 kg/m^2 s^2 was measured only in the 58° model.

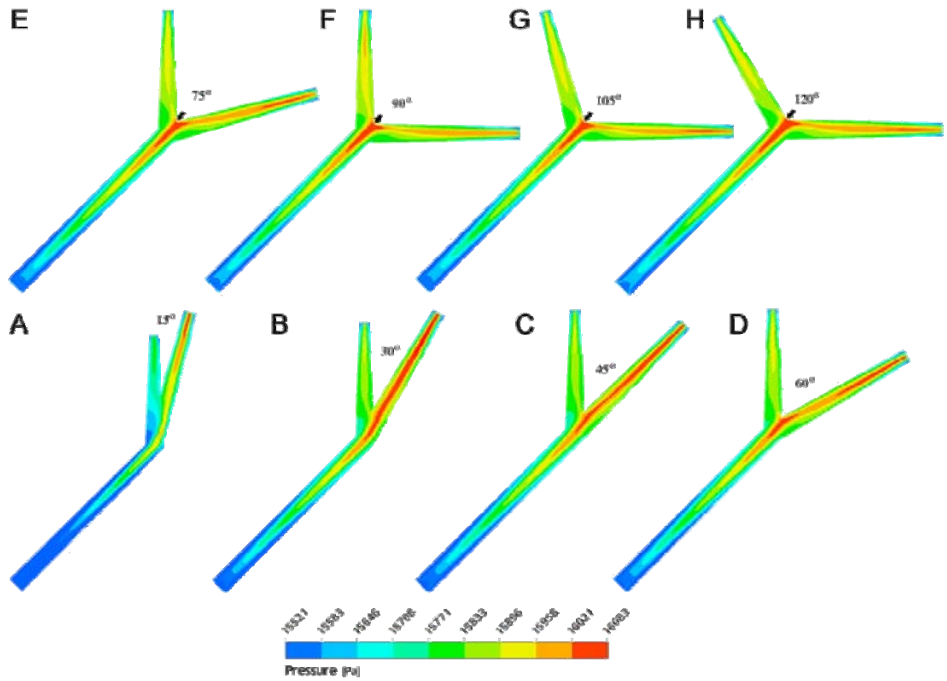

Fig. 7. Wall pressure observed with variable angles of the simulated left coronary artery models generated at peak systolic phase of 0.4 s Arrows reveal the high wall pressure distributions at wide angulations and a 15° angulation displays the low wall pressure at coronary bifurcation.

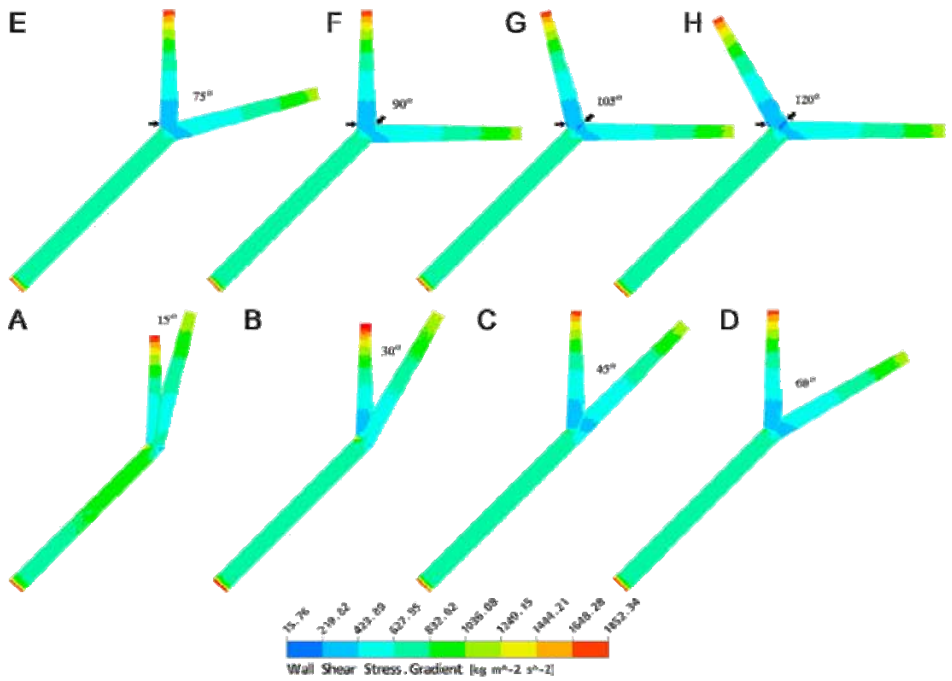

Fig. 8. Wall shear stress gradient observed with variable angles of the simulated left coronary artery models generated at peak systolic phase of 0.4 s. Arrows display the wall shear stress gradient distributions and a big region of the low magnitude present at a 120° angulation model.

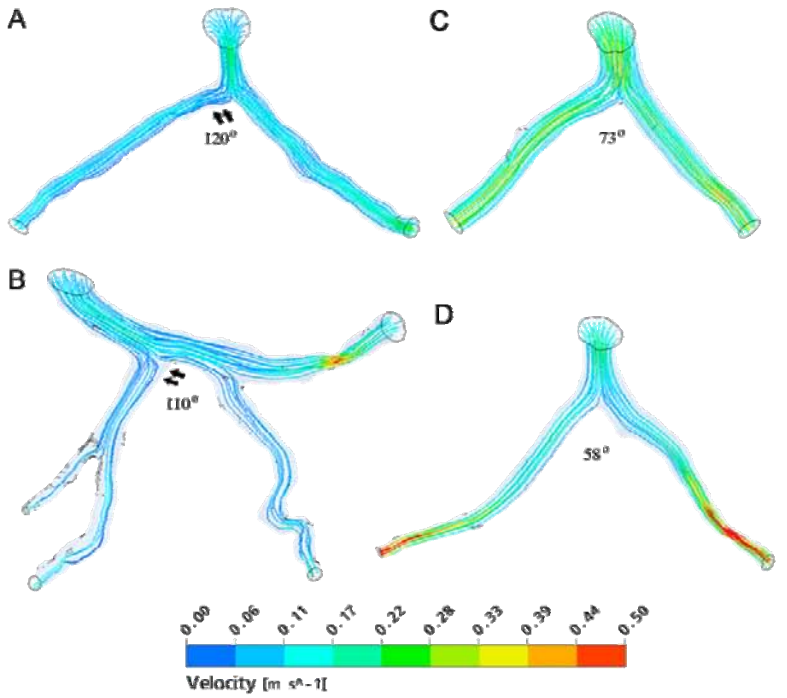

Fig. 9. Velocity observed with variable angles of the realistic left coronary artery models generated at peak systolic phase of 0.4 s. Double arrows show the big region of low flow at coronary bifurcations.

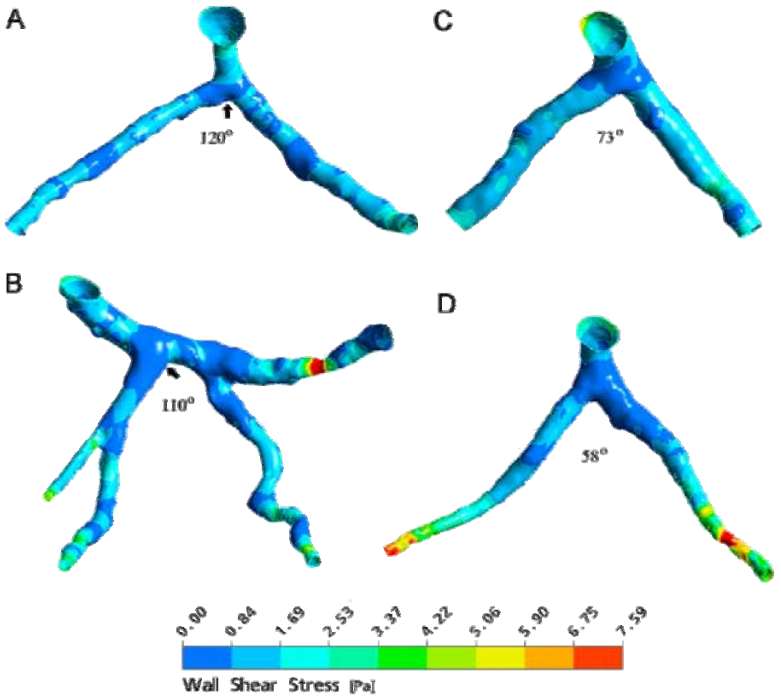

Fig. 10. Wall shear stress observed with variable angles of the realistic left coronary artery models generated at peak systolic phase of 0.4 s. Arrows refer to the low wall shear stress distributions at coronary bifurcations.

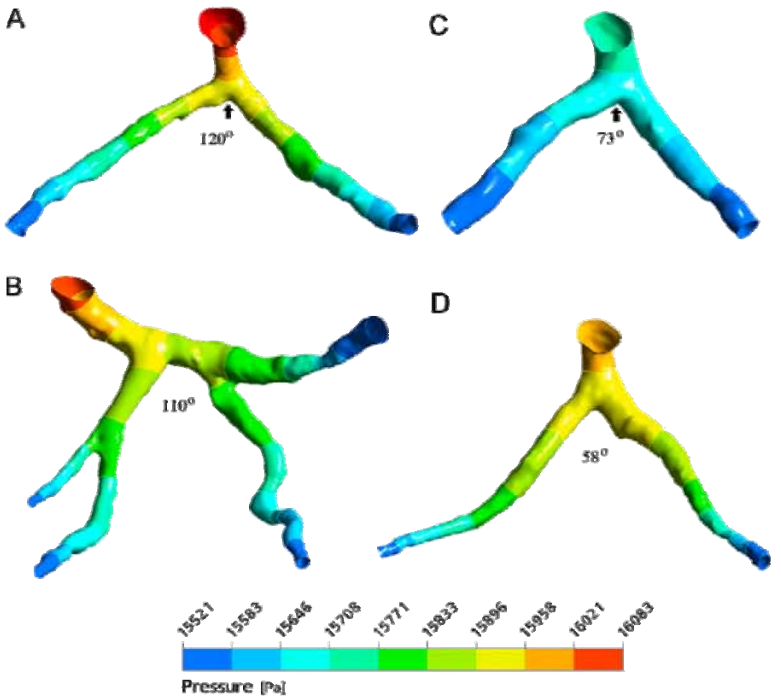

Fig. 11. Wall pressure observed with variable angles of the realistic left coronary artery models generated at peak systolic phase of 0.4 s. Arrows indicate the pressure distributions at coronary bifurcations and display higher wall pressure in a 120° angulation model than that of a 73° model.

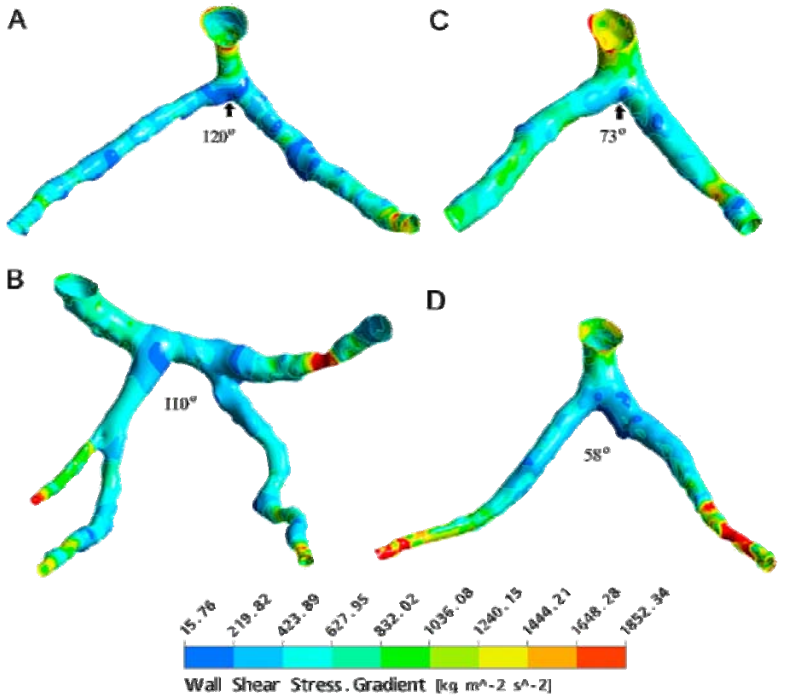

Fig. 12. Wall shear stress gradient observed with variable angles of the realistic left coronary artery models generated at peak systolic phase of 0.4 s. Arrows display the wall shear stress gradient distributions, with a large region of the low magnitude present in a 120° model and a small region in a 73° model.

4. Discussion

Our results based on simulated and realistic coronary models showed that there is a direct correlation between angulations of the left coronary artery and subsequent hemodynamic changes. Low wall shear stress and wall shear stress gradient were noticed in wide-angled models, and this indicates the potential risk of developing atherosclerosis at the left coronary bifurcation.

It is believed that local hemodynamic forces play an important role in the formation of atherosclerosis (Malek et al., 1999; Chien, 2007; Schroeder and Falk, 1995). Soulis et al. (2006) explored the change of WSS in the reconstructed left coronary artery and its branches with inclusion of coronary bifurcation. The hemodynamic analysis in their study showed that the atherosclerosis plaques frequently occurred in bifurcation regions where WSS was low. This is confirmed in our study, as a large region of low WSS was noticed at wide-angled models, indicating the tendency to induce atherosclerotic changes.

Early studies reported that atherosclerotic plaques tend to form at specific locations of the coronary artery such as the proximity branches, curvatures and bifurcations, where the flow separation occurred and WSS was low (Katritsis et al., 2007; Soulis et al., 2006; VanderLaan et al., 2004; Tarbell, 2010; Qi et al., 2008). Later reports further confirmed these early observations (Katritsis et al., 2007; Nordgaard et al., 2010). Katritsis et al. (2007) investigated the WSS oscillations based on the simulated artery bifurcation model comprising a straight tube, and their results showed that low wall shear stress occurred in the bifurcation locations. Nordgaard et al. (2010) in their recent report studied WSS in the remodeled left coronary artery and stated that low WSS was found in regions of low flow rate. Again, our analysis is consistent with these observations. Further to the simulated models we included a number of models generated from patients' data with variable left coronary bifurcation angles, which is one of the advantages of the current study. Another advantage of our study is the direct comparison between two types of model, which showed consistent results. This indicates the additional value provided by this study.

In addition to the conventional CFD analysis, quantitative analysis of the impact of bifurcation angulations on hemodynamic flow was performed in this study by analyzing WSSG. The magnitude of wall shear stresses causes elongation and alignment of endothelial cells, while WSSG has direct effects on intercellular tension. The strong correlation between averaged low WSS and the localization of atherosclerotic lesions in arterial bifurcations has been well established (Katritsis et al., 2007; Soulis et al., 2006). However, WSS analysis topographically restricts the corresponding regions of low WSS at the vicinity of the coronary artery branches (Farmakis et al., 2004). Thus, low WSS regions appear to cover smaller surface area than the corresponding regions prone to developing atherosclerosis (Montenegro and Eggen, 1968). In contrast, low WSSG has been reported to clearly describe the regions where atherosclerosis prevails (Kleinstreuer et al., 2001). Hence, WSSG analysis seems to better depict these regions than WSS analysis does. Our analysis showed that the WSSG distribution tends to form a large area of low magnitude in wide-angled models, particularly at the region of bifurcation, while this was not apparent in narrow-angled models, as shown in Figs. 8 and 12. Consequently, the wide-angled bifurcations at left coronary artery may have a higher possibility to promote the atherosclerotic formation and progression than the narrow-angled bifurcations.

There are some limitations in our study that should be addressed. Firstly, the simulated and realistic left coronary

models were assumed to have a rigid wall rather than elastic wall; therefore, the simulation does not fully reflect the realistic physiological situation as coronary wall moves during cardiac cycles. Secondly no pathological changes such as presence of plaques or coronary stenosis were simulated in this study, since our focus was simply to investigate the relationship between angulation and hemodynamic changes. Thirdly the assumption of a Newtonian blood model has limitations on the biological effects of prolonged contact of blood flow with the cells of vascular wall, for example, platelet deposition (van Zanten et al., 1994) and leukocyte rolling (Sequeira et al., 2009). Additionally, a non-Newtonian blood model becomes important especially in low flow and low wall shear stress regions. However, previous studies have showed that the assumption of a Newtonian model is reasonable in this configuration (Johnston et al., 2006; Pedley, 1980). Fourthly, although cardiac CT has been increasingly used in the diagnosis of coronary artery disease with its improved diagnostic accuracy due to technological developments (Sun and Ng, 2010; Sun et al., 2008), the real CT patient data with representation of these coronary artery branches is limited for computational fluid dynamics analysis. Only four selected CT cases were included in this study, which limits our analysis. Although no significant coronary stenosis is demonstrated on these CT images, potential atherosclerotic changes in the coronary artery tree cannot be excluded given the fact that these patients are at high risk of developing atherosclerosis. However, the representative angles in these cases reflected the ranges from normal to abnormal coronary arteries thus, this limitation can be compensated for to some extent. Finally, although the geometry of simulated coronary models were based on patient's anatomical details, there are still inadequacies in the representation of realistic geometry, as most of the coronary arteries, especially at the left bifurcation, follow a curved as opposed to a straight path. Thus, future studies will use coronary models with a more realistic idealized geometry.

In conclusion, we studied the effect of various angulations of the left coronary artery on hemodynamics, based on simulated and realistic coronary models. There is a direct relationship between wide angulation in the left coronary bifurcation and hemodynamic changes such as disturbed flow and low wall shear stress and wall shear stress gradient, indicating the possible inducement of atherosclerosis. Further studies including patients with different risk factors or severity of coronary artery disease should be performed to verify our results.

Conflict of interest statement

None.

References

Asakura, T., Karino, T., 1990. Flow patterns and spatial distribution of atherosclerotic lesions in human coronary arteries. Circulation Research 66, 1045–1066.

Borghi, A., Wood, N., Mohiaddin, R., Xu, X., 2008. Fluid–solid interaction simulation of flow and stress pattern in thoracoabdominal aneurysms: a patient-specific study. Journal of Fluids and Structures 24 (2), 270–280.

Boutsianis, E., Dave, H., Frauenfelder, T., Poulikakos, D., Wildermuth, S., Turina, M., Ventikos, Y., Zund, G., 2004. Computational simulation of intracoronary flow based on real coronary geometry. European Journal of Cardiothoracic Surgery 26, 248–256.

Chien, S., 2007. Mechanotransduction and endothelial cell homeostasis: the wisdom of the cell. American Journal of Physiology Heart and Circulatory Physiology 292 (3), H1209–H1224.

Conner, L.A., 1994. Mechanisms leading to myocardial infarction: insights from studies of vascular biology. Circulation 90, 2126–2146.

Farmakis, T.M., Soulis, J.V., Giannoglou, G.D., Zioupos, G.J., Louridas, G.E., 2004. Wall shear stress gradient topography in the normal left coronary arterial tree: possible implications for atherogenesis. Current Medical Research and Opinion 20, 587–596.

Frauenfelder, T., Lotfey, M., Boehm, T., Wildermuth, S., 2006. Computational fluid dynamics: hemodynamic changes in abdominal aortic aneurysm after stent-graft implantation. Cardiovascular and Interventional Radiology 29 (4), 613–623.

He, X., Ku, D.N., 1995. Flow in T-bifurcations: effect of the sharpness of the flow divider. Biorheology 32, 447–458.

Johnston, B., Johnston, P., Corney, S., Kilpatrick, D., 2006. Non-Newtonian blood flow in human right coronary arteries: transient simulations. Journal of Biomechanics 39 (6), 1116–1128.

Johnston, B., Johnston, P., Corney, S., Kilpatrick, D., 2004. Non-Newtonian blood flow in human right coronary arteries: steady state simulations. Journal of Biomechanics 37 (5), 709–720.

Katritsis, D., Kaiktsis, L., Chaniotis, A., Pantos, J., Efstathopoulos, E.P., Marmarelis, V., 2007. Wall shear stress: theoretical considerations and methods of measurement. Progress in Cardiovascular Diseases 49 (5), 307–329.

Kleinstreuer, C., Hyun, S., Buchanan, J.R., Longest, P.W., Archie, J.P., Truskey, J.P., 2001. Hemodynamic parameters and early intimal thickening in branching blood vessels. Critical Reviews in Biomedical Engineering 29 (1), 1–64.

LaDisa, J.F., Olsan, L.E., Guler, I., Hettrick, D.A., Kersten, J.R., Warltier, D.C., Pagel, P.S., 2004. Circumferential vascular deformation after stent implantation alters wall shear stress evaluated with time-dependent 3D computational fluid dynamics models. Journal of Applied Physiology 98, 947–957.

Lehoux, S., 2006. Redox signalling in vascular responses to shear and stretch. Cardiovascular Research 71 (2), 269–279.

Lei, M., Giddens, D.P., Jones, S.A., Loth, F., Bassiouny, H., 2001. Pulsatile flow in an end-to-side vascular graft model: comparison of computations with experimental data. Journal of Biomechanical Engineering 123, 80–87.

Lei, M., Kleinstreuer, C., Truskey, G.A., 1996. A focal stress gradient-dependent mass transfer mechanism for atherogenesis in branching arteries. Medical Engineering and Physics 18 (4), 326–332.

Lim, M.J., Kern, M.J., 2005. Utility of coronary physiologic hemodynamics for bifurcation, aorto-ostial, and ostial branch stenoses to guide treatment decisions. Catheterization and Cardiovascular Interventions 65 (4), 461–468.

Lou, Z., Yang, W.J., 1993. A computer simulation of the non-Newtonian blood flow at the aortic bifurcation. Journal of Biomechanics 26, 37–49.

Malek, A.M., Alper, S.L., Izumo, S., 1999. Hemodynamic shear stress and its role in atherosclerosis. Journal of American Medical Association 282 (21), 2035–2042.

Milnor, W.R., 1989. Hemodynamics. Williams & Wilkins, Baltimore.

Montenegro, M.R., Eggen, D.A., 1968. Topography of atherosclerosis in the coronary arteries. Laboratory Investigation 18, 586–593.

Nichols, W.W., O'Rourke, M.F., 2005. McDonald's Blood Flow in Arteries, fifth ed. Hodder Arnold, London 326–327.

Nordgaard, H., Swillens, A., Nordhaug, D., Kirkeby-Garstad, I., Loo, D., Vitale, N., Segers, P., Haaverstad, R., Lovstakken, L., 2010. Impact of competitive flow on wall shear stress in coronary surgery: computational fluid dynamics of a LIMA–LAD model. Cardiovascular Research 88 (3), 512–519.

Ojha, M., 1993. Spatial and temporal variations of wall shear stress within an end-to-side arterial anastomosis model. Journal of Biomechanics 26, 1377–1388.

Pedley, T.J., 1980. The Fluid Mechanics of Large Blood Vessels. Cambridge university press, Cambridge, pp. 30–31.

Pflederer, T., Ludwig, J., Ropers, D., Daniel, W.G., Achenbach, S., 2006. Measurement of coronary artery bifurcation angles by multidetector computed tomography. Investigative Radiology 41, 793–798.

Qi, Y.X., Qu, M.J., Long, D.K., Liu, B., Yao, Q.P., Chien, S., Jiang, Z.L., 2008. Rho-GDP dissociation inhibitor alpha down regulated by low shear stress promotes vascular smooth muscle cell migration and apoptosis: a proteomic analysis. Cardiovascular Research 80 (1), 114–122.

Reig, J., Petit, M., 2004. Main trunk of the left coronary artery: anatomic study of the parameters of clinical interest. Clinical Anatomy 17, 6–13.

Sabbah, H.N., Khaja, F., Hawkins, E.T., Brymer, J.F., McFarland, T.M., van der Bel-Kahn, J., Doerger, P.T., Stein, P.D., 1986. Relation of atherosclerosis to arterial wall shear in the left anterior descending coronary of man. American Heart Journal 112 (3), 453–458.

Schroeder, A., Falk, E., 1995. Vulnerable and dangerous coronary plaques. Atherosclerosis (Suppl.), S141–S149.

Sequeira, A., Artoli, A.M., Silva-Herdade, A.S., Saldanha, C., 2009. Leukocytes dynamics in microcirculation under shear-thinning blood flow. Computers and Mathematics with Applications 58, 1035–1044.

Shanmugavelayudam, S.K., Rubenstein, D., Yin, W., 2010. Effect of geometrical assumptions on numerical modeling of coronary blood flow under normal and disease conditions. Journal of Biomechanical Engineering 132 (6), 061004.

Smith, S.W., 1997. The scientist and engineer's guide to digital signal processing. California Technical Publishing, California, pp. 255–256.

Soulis, J.V., Farmakis, T.M., Giannoglou, G.D., Louridas, G.E., 2006. Wall shear stress in normal left coronary artery tree. Journal of Biomechanics 39 (4), 742–749.

Sun, Z., Chaichana, T., 2010. Fenestrated stent graft repair of abdominal aortic aneurysm: hemodynamic analysis of the effect of fenestrated stents on the renal arteries. Korean Journal of Radiology 11 (1), 95–106.

Sun, Z., Chaichana, T., 2009. Investigation of the hemodynamic effect of stent wires on renal arteries in patients with abdominal aortic aneurysms treated with suprarenal stent-grafts. Cardiovascular and Interventional Radiology 32 (4), 647–657.

Sun, Z., Winder, R.J., Kelly, B.E., Ellis, P.K., Kennedy, P.T., Hirst, D.G., 2004. Diagnostic value of CT virtual intravascular endoscopy in aortic stent grafting. Journal of Endovascular Therapy 11 (1), 13–25.

Sun, Z., Winder, R.J., Kelly, B.E., Ellis, P.K., Hirst, D.G., 2003. CT virtual intravascular endoscopy of abdominal aortic aneurysms treated with suprarenal endovascular stent grafting. Abdominal Imaging 28 (4), 580–587.
Sun, Z., Ng, K.H., 2010. Multislice CT angiography in cardiac imaging. Part II: clinical applications in coronary artery disease. Singapore Medical Journal 51 (4), 282–289.
Sun, Z., Lin, C.H., Davidson, R., Dong, C., Liao, Y., 2008. Diagnostic value of 64-slice CT angiography in coronary artery disease: a systematic review. European Journal of Radiology 67, 78–84.
Tarbell, J.M., 2010. Shear stress and the endothelial transport barrier. Cardiovascular Research 87 (2), 320–330.
VanderLaan, P.A., Reardon, C.A., Getz, G.S., 2004. Site specificity of atherosclerosis: site-selective responses to atherosclerotic modulators. Arteriosclerosis Thrombosis and Vascular Biology 24, 12–22.
van Zanten, G.H., de Graaf, S., Slootweg, P.J., Heijnen, H.F., Connolly, T.M., de Groot, P.G., Sixma, J.J., 1994. Increased platelet deposition on atherosclerotic coronary arteries. Journal of Clinical Investigation 93 (2), 615–632.
Wellnhofer, E., Osman, J., Kertzscher, U., Affeld, K., Fleck, E., Goubergrits, L., 2010. Flow simulation studies in coronary arteries – impact of side-branches. Atherosclerosis 213 (2), 475–481.
White, C.R., Haidekker, M., Bao, X., Frangos, J.A., 2001. Temporal gradients in shear, but not spatial gradients, stimulate endothelial cell proliferation. Circulation 103, 250–2513.
World medical association declaration of Helsinki, 1997. Recommendations guiding physicians in biomedical research involving human subjects. Cardiovascular Research 35, 2–3.
Zarins, C.K., Giddens, D.P., Bharadvaj, B.K., Sottiurai, V.S., Mabon, R.F., Glagov, S., 1983. Carotid bifurcation atherosclerosis. Quantitative correlation of plaque localization with flow velocity profiles and wall shear stress. Circulation Research 53, 502–514.
Zheng, Y., Fujioka, H., Grotberg, J.C., Grotberg, J.B., 2006. Effects of inertia and gravity on liquid plug splitting at a bifurcation. Journal of Biomechanical Engineering 128, 707–716.

Chapter 3

Computational fluid dynamics analysis of the effect of plaques in the left coronary artery. Computational and Mathematical Methods in Medicine 2012, 504367:1–9.

Thanapong Chaichana, Zhonghua Sun and James Jewkes

Hindawi Publishing Corporation
Computational and Mathematical Methods in Medicine
Volume 2012, Article ID 504367, 9 pages
doi:10.1155/2012/504367

Research Article

Computational Fluid Dynamics Analysis of the Effect of Plaques in the Left Coronary Artery

Thanapong Chaichana,[1] Zhonghua Sun,[1] and James Jewkes[2]

[1] *Discipline of Medical Imaging, Department of Imaging and Applied Physics, Curtin University, GPO Box, U1987, Perth, WA 6845, Australia*
[2] *Fluid Dynamics Research Group, Department of Mechanical Engineering, Curtin University, Perth, WA 6845, Australia*

Correspondence should be addressed to Zhonghua Sun, z.sun@curtin.edu.au

Received 30 September 2011; Revised 8 November 2011; Accepted 9 November 2011

Academic Editor: Kyehan Rhee

This study was to investigate the hemodynamic effect of simulated plaques in left coronary artery models, which were generated from a sample patient's data. Plaques were simulated and placed at the left main stem and the left anterior descending (LAD) to produce at least 60% coronary stenosis. Computational fluid dynamics analysis was performed to simulate realistic physiological conditions that reflect the *in vivo* cardiac hemodynamics, and comparison of wall shear stress (WSS) between Newtonian and non-Newtonian fluid models was performed. The pressure gradient (PSG) and flow velocities in the left coronary artery were measured and compared in the left coronary models with and without presence of plaques during cardiac cycle. Our results showed that the highest PSG was observed in stenotic regions caused by the plaques. Low flow velocity areas were found at postplaque locations in the left circumflex, LAD, and bifurcation. WSS at the stenotic locations was similar between the non-Newtonian and Newtonian models although some more details were observed with non-Newtonian model. There is a direct correlation between coronary plaques and subsequent hemodynamic changes, based on the simulation of plaques in the realistic coronary models.

1. Introduction

Coronary artery disease (CAD) is the leading cause of death in advanced countries. The most common cause of CAD is atherosclerosis which is caused by the presence of plaques on the artery wall, resulting in the lumen stenosis. Plaques have been particularly associated with blood clots and compromise blood flow to the myocardium. This occurs when the coronary plaques suddenly rupture; if a clot cannot be treated in time, then the heart muscle will be impaired due to ischemic changes, leading to myocardial ischemia or infarction or, more severely, necrosis [1]. Therefore, an early detection and diagnosis of CAD is particularly important for reduction of the mortality and subsequent complications [1].

The natural history of coronary plaque is dependent not only on the formation and progression of atherosclerosis, but also on the vascular remodelling response. If the local wall shear stress is low, a proliferative plaque will form. Local inflammatory response will stimulate the formation of so-called "vulnerable plaque" which is prone to rupture with superimposed thrombus formation. The vast majority of these inflamed high-risk plaques cannot be detected by anatomic and myocardial perfusion imaging. Since the progression and development of vulnerable plaque is associated with low wall shear stress and the presence of expansive remodelling, measurement of these characteristics *in vivo* will enable risk stratification for the entire coronary circulation [2].

The wall shear stress (WSS), wall pressure, and blood flow changes in the human body cannot be measured directly on blood vessels, whereas computational fluid dynamics (CFD) can provide alternative ways to diagnose CAD [3]. The WSS factor in the coronary artery is known to play a significant role in the early formation of CAD [4]. In addition, the WSS at the local vessel wall can demonstrate a predisposition for atherosclerosis development for various anatomical sections, thus enabling the prediction of coronary disease [5].

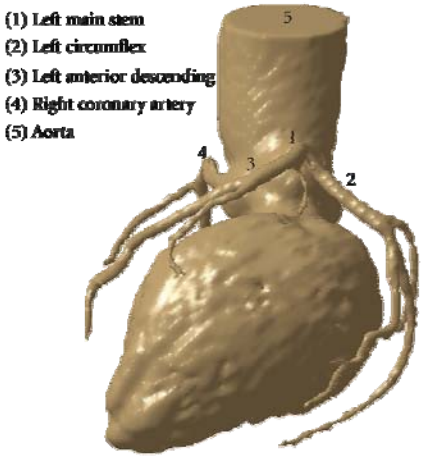

FIGURE 1: 3D CT visualisation of a normal left coronary artery with side branches in a patient with suspected coronary artery disease.

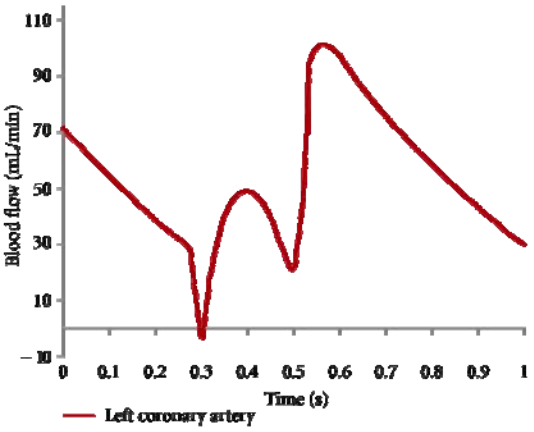

FIGURE 3: Cardiac pulsatile velocity at left main stem is applied for computational fluid dynamic simulation at the left coronary artery.

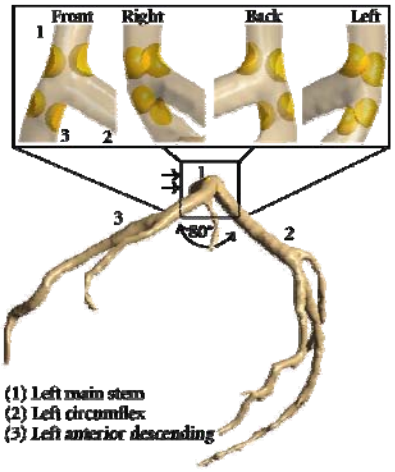

FIGURE 2: Plaque distribution in left coronary artery model is simulated at the left main stem and ostium of left anterior descending. Double arrows indicate that rectangle is an effective plaque location (EPL).

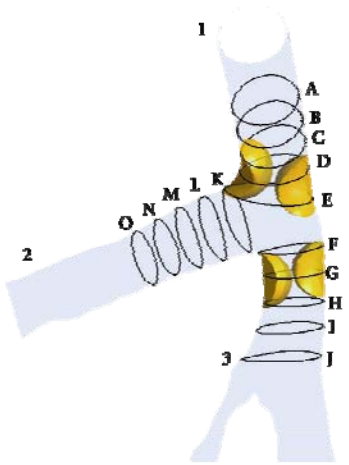

FIGURE 4: The EPL posterior view at left coronary artery model represents the cross-sectional positions of pre- and postplaque simulated models.

CFD allows for efficient and accurate computations of hemodynamic features of both normal and abnormal situations in the cardiovascular system, *in vivo* simulation of coronary artery flow changes [3–6]. CFD is different from medical imaging visualisation as medical imaging techniques such as coronary angiography or computed tomography angiography provide anatomic alterations of the coronary artery wall due to the presence of plaques, thus allowing only assessment of the degree of lumen changes such as stenosis or occlusion [7, 8]. In contrast, CFD analysis enables the identification of hemodynamic changes in the coronary artery, even before the plaques are actually formed at the artery wall or can occlude the vessels. Therefore, to some extent, CFD allows early detection of coronary artery disease and improves the understanding of the progression of plaques, which are considered of paramount importance to clinical treatment. The purpose of this study was to investigate the hemodynamic effect of plaques in the left coronary artery by using CFD analysis. Simulated plaques were inserted into the left main stem and left anterior descending coronary arteries (taken from a selected patient's data), and hemodynamic analysis was performed to correlate the effect of presence of plaques with subsequent flow changes to the coronary main and side branches.

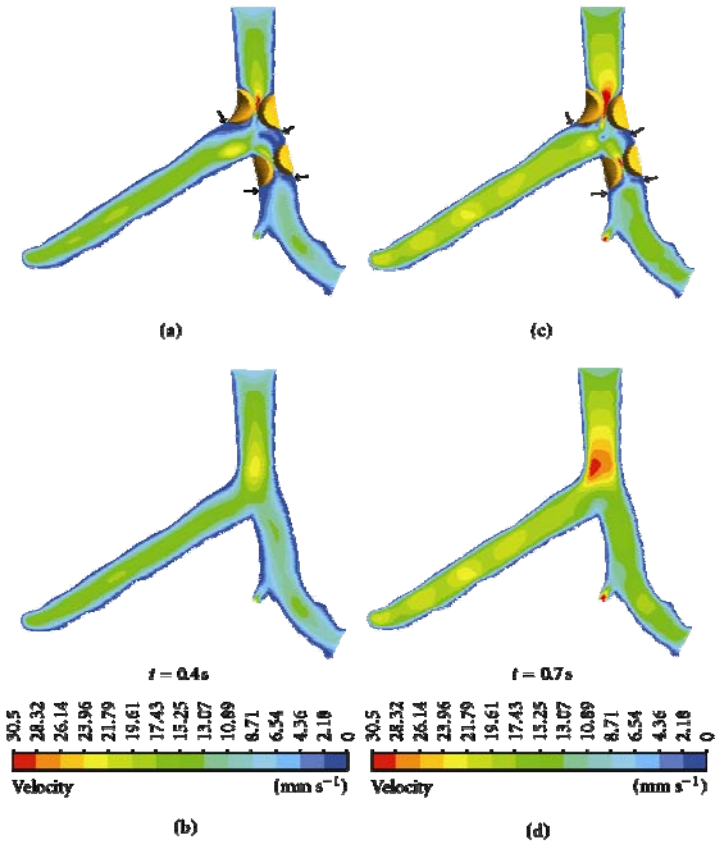

Figure 5: Flow velocity observed in pre- and postplaque simulated models during systolic peak of 0.4 s and middiastolic phase of 0.7 s. Arrows indicate the anatomic locations where plaques could spread into areas with low flow velocity.

2. Materials and Methods

2.1. Patient Data Selection for Generation of Left Coronary Artery Model. A sample patient suspected of CAD who underwent multislice CT angiography was selected, and the patient's volume CT data was used to generate a 3D coronary model. The original CT data was saved in digital imaging and communication in medicine (DICOM) format and then transferred to a workstation equipped with Analyze 7.0 (Analyze Direct, Inc., Lexana, KS, USA) for image after-processing and segmentation. Three-dimensional (3D) volume data was postprocessed and segmented using a semiautomatic method with a CT number thresholding technique [9, 10], and manual editing was performed in some slices to remove soft tissues and artefacts. The segmented model was produced with a special focus on the left coronary artery (LCA) and its branches. The 3D LCA model was saved in "STL format" for further reconstruction purposes. Figure 1 shows the anatomical details of the left coronary artery.

2.2. Realistic Plaques Modelling. The actual plaques and degree of lumen stenosis on coronary artery wall were simulated at the left main stem (LMS) and the left anterior descending (LAD), as these artery branches are the common locations where plaques tend to form and induce myocardial ischemic changes [7, 11]. The plaques produced a lumen narrowing of approximately 60% diameter at the LMS and LAD, since more than 50% lumen stenosis leads to significant hemodynamic changes to flow within the coronary artery [12]. Figure 2 is the segmented LCA model showing various views of the position of the plaques at the left coronary artery.

2.3. Generation of Computational Models. The surface of LCA model with and without plaques (Figure 2) was prepared by using Blender version 2.48 (Blender Institute, Amsterdam, Netherlands). A gentle B-spline smoothing technique was applied between the left main trunk and side branches to reduce any potential nonphysical behaviour induced by sharp edges [13]. The surface models consisting of plaques and normal coronary arteries were converted into solid models and saved in "STL format" for the additional creation of meshing elements. Both models were used to create hexahedral and tetrahedral meshes to perform the CFD simulations. The hexahedral mesh configuration for

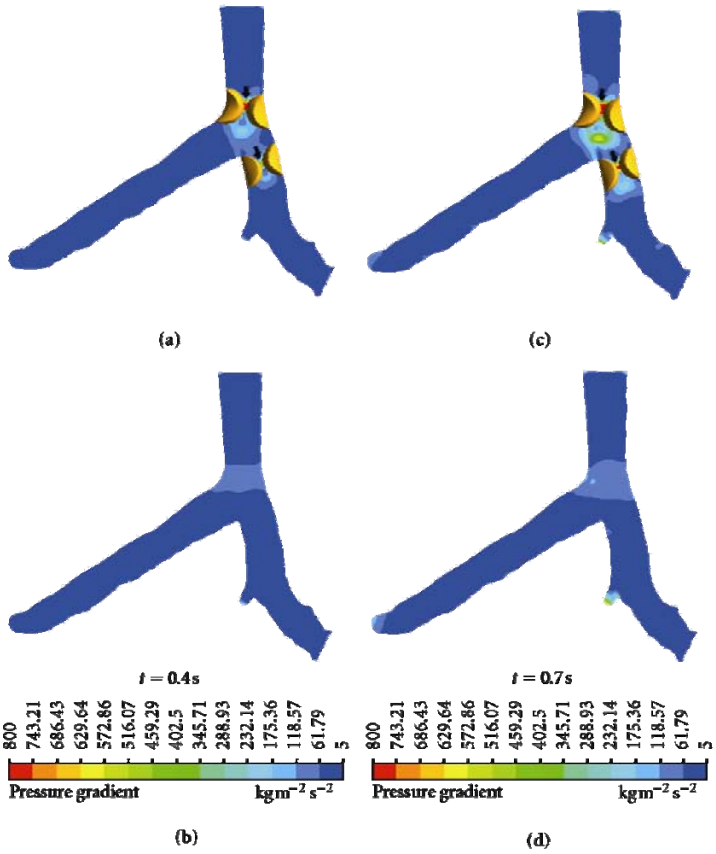

Figure 6: Pressure gradient observed in coronary models with and without plaques during systolic peak of 0.4 s and middiastolic phase of 0.7 s. Arrows indicate the high PSG locations where plaques may induce potential rupture or further atherosclerotic changes.

the LCA model without plaques was 949,289 elements and 1,062,280 nodes, while the hexahedral mesh configuration for the LCA model with plaques was 928,311 elements and 1,041,936 nodes. The tetrahedral mesh configuration was 15,519 nodes and 78,618 elements. The meshes were generated using ANSYS ICEM CFD version 12 (ANSYS, Inc., Canonsburg, PA, USA), with details having been described in previous studies [6, 14, 15]. Finally, both mesh models were saved in "GTM format" for CFD computation.

2.4. Application of Physiological Parameters. In order to ensure that our analysis reflects the realistic simulation of *in vivo* conditions, realistic physiological boundary conditions were applied for 3D numerical analysis. The transient simulation was performed using accurate hemodynamic rheological and material properties, as described in a previous study [16]. Figure 3 shows the pulsatile flow rates [17] at the aorta, reconstructed using a Fourier series [18] in Matlab (MathWorks, Inc. Natick, MA, USA). This Fourier series was applied using ANSYS CFX Command Language programming to define velocity and pressure boundary conditions. Pulsatile velocity was applied as an inlet boundary condition at the left main stem, and a zero pressure gradient was applied at the left anterior descending and left circumflex outlet boundaries [19]. Appropriate rheological parameters were applied with a blood density of 1060 kg/m^3 and blood viscosity of 0.0035 Pa s [20, 21]. The blood flow was assumed to be laminar and a no-slip condition was applied at the walls. Plaque was assumed to be a rigid body [22]. Blood was assumed to be a Newtonian and incompressible fluid [4, 23]. In addition, the comparison of WSS between Newtonian and non-Newtonian models has been considered, especially at the stenotic locations [24]. A non-Newtonian blood model was simulated using the generalized power law [4, 25] which is defined as

$$\begin{aligned} \mu &= \lambda(\dot{\gamma})\,|\dot{\gamma}|^{n(\dot{\gamma})-1}, \\ \lambda(\dot{\gamma}) &= \mu_\infty + \Delta\mu \exp\left[-\left(1+\frac{|\dot{\gamma}|}{a}\right)\exp\left(\frac{-b}{|\dot{\gamma}|}\right)\right], \\ n(\dot{\gamma}) &= n_\infty - \Delta n \exp\left[-\left(1+\frac{|\dot{\gamma}|}{c}\right)\exp\left(\frac{-d}{|\dot{\gamma}|}\right)\right], \end{aligned} \tag{1}$$

where $\mu_\infty = 0.035$, $n_\infty = 1.0$, $\Delta\mu = 0.25$, $\Delta n = 0.45$, $a = 50$, $b = 3$, $c = 50$, and $d = 4$. Generalized power law model

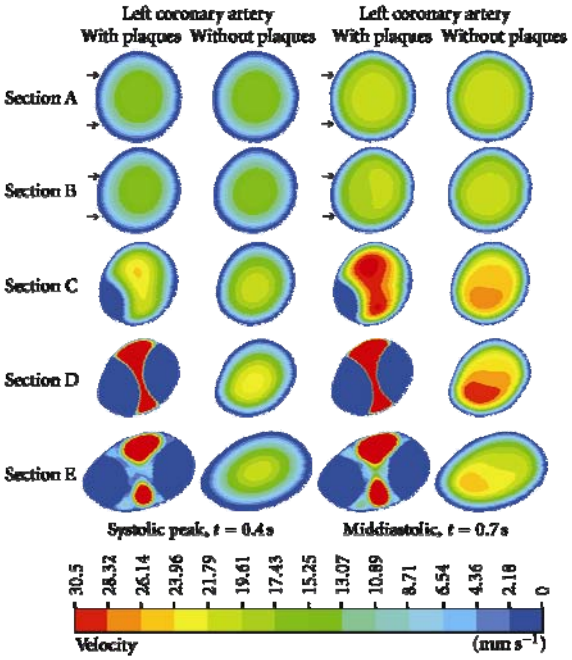

Figure 7: Cross-sectional views of A–E at the left main stem. Flow velocity observed with and without presence of plaque models during systolic peak of 0.4 s and middiastolic phase of 0.7 s. Arrows at Sections A and B refer to the normal flow pattern prior to the location of plaques, while flow pattern changes at the postplaque locations.

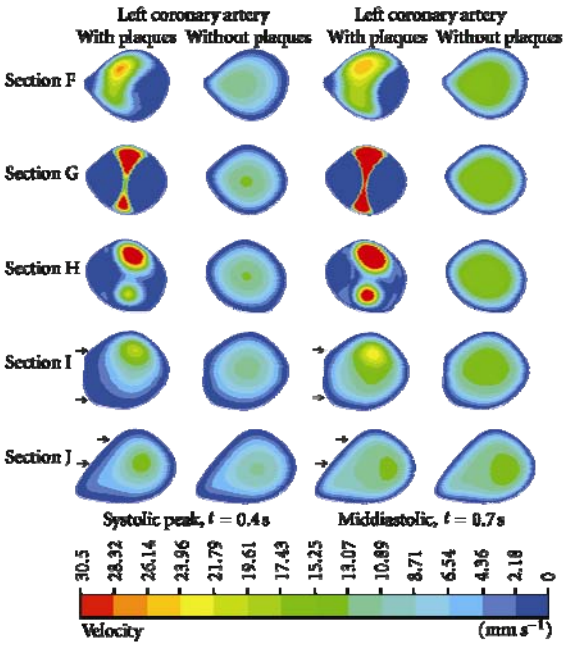

Figure 8: Cross-sectional views of F–J at the left anterior descending. Flow velocity observed with and without presence of plaque models during systolic peak of 0.4 s and middiastolic phase of 0.7 s. Arrows point to the low flow velocity areas at post-plaque locations due to interference of plaques.

fits experimental stress-strain measurements over the range of strain rates, $\dot{\gamma}$, $0.1 < \dot{\gamma} < 1000\,s^{-1}$ [25].

2.5. Performance of Computational Hemodynamic Analysis. The Navier-Stokes equations were solved using the ANSYS CFX CFD package (version 12—ANSYS, Inc.), on a Microsoft Windows 7 32-bit machine, 6 MB RAM with an Xeon W3505 2.53 GHz CPU. The CFD simulation was run for 80 timesteps, representing 1.0 second of pulsatile flow, (0.0125 seconds per timestep), with each timestep converged to a residual target of less than 1×10^{-4} by approximately 100 iterations. The CFD solution was fully converged by approximately 8,000 time iterations per LCA model. The calculation time for each LCA model was approximately 2 hours. The configuration of this simulation is similar to previously published simulations [6, 14, 15]. Flow velocity, cross-sections of velocity pattern, and pressure gradient were calculated and visualised using ANSYS CFD-Post version 12 (ANSYS, Inc.). Figure 4 represents the area of interest at the left coronary bifurcation and shows measurement positions of cross-sections of the models with and without plaques. The sectional planes were separated into 3 groups: Sections A–E, Sections F–J, and Sections K–O. The distance between sections in each group was approximately 0.5 millimetres. The parameter used to characterise the impact of plaques at the coronary bifurcation on hemodynamic flow was calculated as the magnitude of local pressure gradient [26, 27], which is defined as

$$\mathrm{PSG} = \sqrt{\left(\frac{\partial p}{\partial_u}\right)^2 + \left(\frac{\partial p}{\partial_v}\right)^2 + \left(\frac{\partial p}{\partial_w}\right)^2}, \tag{2}$$

where p is the pressure in the area of interest, u, v, and w are the Cartesian x, y, and z coordinates in the direction of blood flow velocity. The local PSG is calculated by taking the time derivative of the local pressure. Finally, the value of PSG oscillated in relation to the percentage of plaques in the coronary lumen [28].

3. Results

The realistic left coronary artery models with plaques and without plaques were successfully performed with CFD analysis under *in vivo* physiological conditions during the systolic and diastolic phases. Peak systolic velocity and pressure were reached at a time of 0.4 sec, and middiastolic phase was reached at a time of 0.7 sec during the cardiac cycles, respectively. The analysis demonstrates a strong relationship between hemodynamic change and plaques at the left coronary artery.

3.1. CFD Analysis of the Left Coronary Artery: 2D Visualisation. Flow velocity increased significantly in the presence

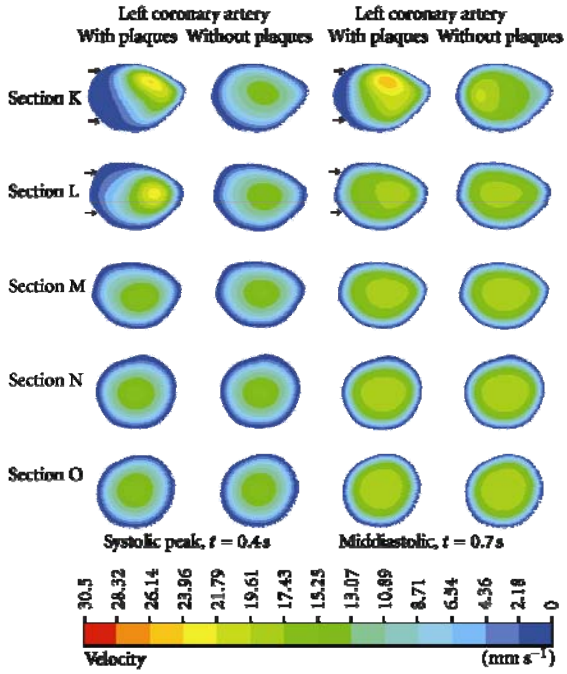

Figure 9: Cross-sectional views of K–O at the left circumflex. Flow velocity observed with and without presence of plaque models during systolic peak of 0.4 s and middiastolic phase of 0.7 s. Arrows indicate that the low flow velocity areas are present in the proximal segment of left circumflex due to the effect of plaques located at the left main stem.

of plaques due to resultant lumen stenosis. Poststenotic recirculation was observed in the LMS and LAD according to the CFD analysis, at the locations where plaques were present, as shown in Figure 5. Similarly, the pressure gradient (PSG) increased significantly at the LMS and LAD ostium, as shown in Figure 6. Measured PSG values at peak systolic and diastolic phases ranged from 459.29–800 kg/m^2 s^2 to 345.71–629.64 kg/m^2 s^2, corresponding to the LMS, LAD, and LCx in the presence of plaques. In contrast, in the absence of plaques, measured PSG values were significantly lower than those measured with presence of plaques, and these values ranged from 61.79–118.57 kg/m^2 s^2 to 5–61.79 kg/m^2 s^2.

3.2. CFD Analysis of Left Coronary Artery-Cutting Plane Visualisation. Flow velocity was visualised inside the LMS at Sections A–E, as shown in Figure 7. Flow patterns in both the pre and poststenotic cases were similar to those observed in Sections A and B (velocity ranged from 0 to 17.43 mm s^{-1}). However, the flow velocity increased in Sections C–E (velocity ranged from 23.96 to 30.50 mm s^{-1}), at the location of plaques during the systolic peak. In addition, the flow pattern was affected by the presence of plaques, which started from Sections A–E as observed in the poststenotic region, during the middiastolic phase, with velocity increasing from 28.32 to 30.50 mm s^{-1}.

Figure 8 demonstrates the hemodynamic effect of plaques inside the LAD with cutting views of Sections F–J. Poststenotic velocity reached its highest value in Sections F–H during peak systolic and middiastolic phases, with measured velocity ranging from 28.32 to 30.50 mm s^{-1}. Furthermore, a recirculation region was apparent at the postplaque locations in Sections I and J. The velocity increased slightly with measured values ranging from 17.43 to 23.96 mm s^{-1} as observed in the post-stenotic regions.

Figure 9 represents the result of flow changes observed in the LCx from where plaques were situated in the LMS. Again, the recirculation location was obviously present in Sections K and L, located at postplaque positions. Flow velocity was found to slightly increase, ranging from 17.43 to 26.14 mm s^{-1} in both systolic peak and middle diastolic phases. Furthermore, velocity changes were not observed in Sections M–O as shown in the pre and post-stenotic regions with very similar flow patterns and velocity measured ranging from 0 to 21.79 mm s^{-1}.

3.3. CFD Analysis of the Left Coronary Artery: Wall Shear Stress Comparisons. Analysis of WSS was particularly focused at the stenotic locations with comparison of non-Newtonian and Newtonian fluid models. Figure 10 compares WSS with different fluid viscosities at the left coronary model with presence of plaques. WSS contour values ranged from 0 Pa to 3.50 Pa as observed in both fluid viscosity models. WSS was different due to presence of plaques at LMS branch at peak systolic phase, ranging from 0.50 Pa to 1.75 Pa with non-Newtonian model (Figure 10(a)) and ranging from 0.50 Pa to 1.0 Pa with Newtonian model (Figure 10(b)). Similar results of WSS values ranging from 1.50 Pa to 3.50 Pa with both viscosity models (Figures 10(c) and 10(d)) were found at middiastolic phase at plaques positions in LMS branch. WSS changes at stenotic locations in LAD were compared at peak systolic phases, ranging from 0.50 Pa to 1.0 Pa with non-Newtonian model (Figure 10(a)) and from 0.50 Pa to 0.75 Pa with Newtonian model (Figure 10(b)). WSS values at plaques positions in LAD were compared at middiastolic phases, ranging from 1.50 Pa to 3.50 Pa with non-Newtonian model (Figure 10(c)) and from 1.50 Pa to 3.25 Pa with Newtonian model (Figure 10(d)).

4. Discussion

This study shows that coronary plaques produce a significant impact on the subsequent flow changes in the coronary artery, in addition to the local hemodynamic interference due to the presence of plaques. This is clinically important as further potential effects could result from the plaques' interference, leading to adverse effects on the coronary artery, such as lumen stenosis or worsening of atherosclerosis.

It is well known that plaques most commonly form in the coronary bifurcation and coronary angulation, and that this is an important factor that has been found to be related to the development of atherosclerosis, as confirmed by our and other studies [6, 12, 29–31]. Multislice CT angiography and intravascular ultrasound have been widely used to detect

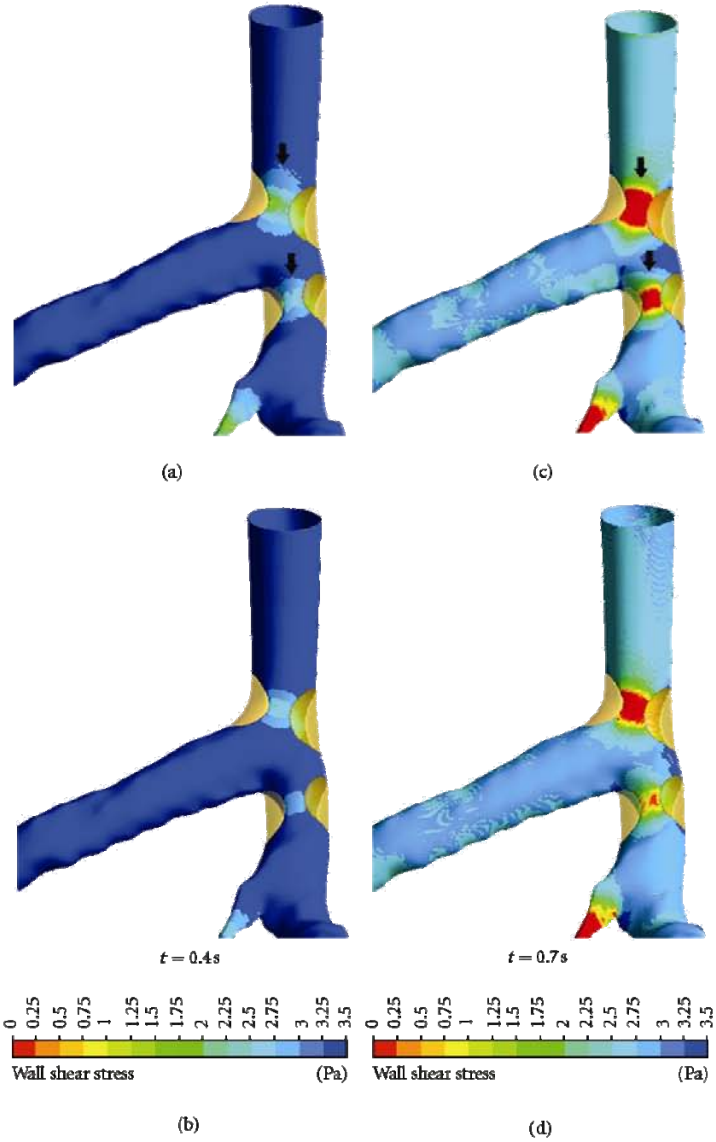

Figure 10: Comparison of WSS between non-Newtonian (a, c) and Newtonian (b, d) models observed in realistic coronary artery with presence of plaques during systolic peak of 0.4 s and middiastolic phase of 0.7 s. Arrows identify the different WSS at stenotic locations.

and characterise plaques in the coronary arteries [7, 32]. Despite promising results having been achieved with imaging modalities, the limitations of these techniques were restricted to image visualisation and identification of coronary lumen changes due to presence of plaques, and no information is available about the interference of plaques with blood flow. In contrast, CFD overcomes those limitations by enabling the analysis of coronary blood flow and rheological factors [6, 14, 15]. This study investigated two important factors: PSG and flow velocity and qualified the impact of plaques on flow changes to the coronary arteries. The static wall pressure does not reflect the velocity profile from the flow axis to the blood wall [27, 33]. In the clinical situation, the PSG magnitude has been used to judge the risk of severity of plaques [28]. The highest PSG area may be relevant to potential coronary plaque rupture. In this study, the CFD analysis of the LCA with presence of plaques showed that the highest PSG was displayed in the locations at both LMS and LAD where plaques were simulated (Figure 6), with measured PSG value ranging from 743.21 to 800 kg/m^2 s^2.

The presence of plaques in the coronary artery is responsible for obstructing blood flow to the myocardium,

consequently affecting the flow velocity [27]. Moreover, plaques influencing hemodynamic change may lead to the further distribution of plaques. Since velocity is the main component of local WSS and acts in the same direction as local WSS, which means that flow velocity is low when the WSS is low, as observed in a previous study [6], our analysis in this study has proposed explicitly hemodynamic changes inside the LCA surrounding the plaque locations (the so-called effective plaque location (EPL)) (Figure 2). In Sections A–E (Figure 7), we found that the flow velocity fluctuated in post-stenotic regions during cardiac cycles, and this could lead to abnormalities at the coronary wall, responsible for atherosclerosis. In Sections I–L (Figures 8 and 9), flow recirculation occurred, and the region of low velocity was observed within a short distance from the plaques. Consequently, plaques could generate an effect that spread into an area of low flow velocity as demonstrated in Sections I–L, matching with an area of low velocity in Figure 5, with measured low velocity value ranging from 0 to 2.18 mms^{-1}. This is confirmed by our previous analysis [6] showing that progression of plaques developed at a low-flow region. Our analysis provides insight into the effect of plaques on subsequent coronary flow changes although further studies are needed to verify our preliminary findings. WSS in non-Newtonian model was found to be similar to that observed in Newtonian model at plaques locations although more details were demonstrated in non-Newtonian model, as shown in Figure 10. The effect of plaques in left coronary is obviously shown in Newtonian model, and this is adequate for analysis of the plaque effect. The comparison of WSS between different viscosity models is confirmed by previous studies [4, 24]. A non-Newtonian model was simulated using the generalized power law as it has been reported to produce similar WSS effects to Newtonian model on coronary flow changes [4].

There are some limitations in our study that should be addressed. Firstly, realistic left coronary models, both pre and post-stenotic, were assumed to have a rigid wall rather than elastic wall; therefore, the simulation does not fully reflect the realistic physiological situation as the coronary wall moves during cardiac cycles. Secondly, the assumption of a Newtonian blood model becomes important especially in low flow and low wall shear stress regions. Nevertheless, a previous study has shown that the assumption of a Newtonian model is reasonable in this configuration [4]. Thirdly, the realistic plaques position may be affected by left coronary side branches that have not been evaluated in this study. Thus, future studies will use coronary models with a more realistic idealized geometry, extended to evaluate the effect of side branches.

In conclusion, we studied the effect of simulated plaques in the realistic left coronary artery on hemodynamic changes at the locations of plaques, as well as pre and post-stenotic regions inside the coronary artery. There is a direct effect of plaques in the left coronary artery on hemodynamic changes such as recirculation flow, low flow velocity regions, wall shear stress, and wall pressure gradient, indicating the potential for plaques to rupture, causing atherosclerosis. Further studies focusing on the realistic plaque's effect on coronary side branches should be performed to verify our results.

References

[1] Australian Institute of Health and Welfare, "The tenth biennial health report of the Australian Institute of Health and Welfare," AIHW, Canberra, Australia, 2006.

[2] F. J. Rybicki, S. Melchionna, D. Mitsouras et al., "Prediction of coronary artery plaque progression and potential rupture from 320-detector row prospectively ECG-gated single heart beat CT angiography: lattice Boltzmann evaluation of endothelial shear stress," *International Journal of Cardiovascular Imaging*, vol. 25, no. 2, pp. 289–299, 2009.

[3] S. K. Shanmugavelayudam, D. A. Rubenstein, and W. Yin, "Effect of geometrical assumptions on numerical modeling of coronary blood flow under normal and disease conditions," *Journal of Biomechanical Engineering*, vol. 132, no. 6, article 061004, 2010.

[4] B. M. Johnston, P. R. Johnston, S. Corney, and D. Kilpatrick, "Non-Newtonian blood flow in human right coronary arteries: steady state simulations," *Journal of Biomechanics*, vol. 37, no. 5, pp. 709–720, 2004.

[5] J. V. Soulis, T. M. Farmakis, G. D. Giannoglou, and G. E. Louridas, "Wall shear stress in normal left coronary artery tree," *Journal of Biomechanics*, vol. 39, no. 4, pp. 742–749, 2006.

[6] T. Chaichana, Z. Sun, and J. Jewkes, "Computation of hemodynamics in the left coronary artery with variable angulations," *Journal of Biomechanics*, vol. 44, no. 10, pp. 1869–1878, 2011.

[7] Z. Sun and Y. Cao, "Multislice CT angiography assessment of left coronary artery: correlation between bifurcation angle and dimensions and development of coronary artery disease," *European Journal of Radiology*, vol. 79, no. 2, pp. e90–e95, 2011.

[8] Z. Sun, F. J. Dimpudus, J. Nugroho, and J. D. Adipranoto, "CT virtual intravascular endoscopy assessment of coronary artery plaques: a preliminary study," *European Journal of Radiology*, vol. 75, no. 1, pp. e112–e119, 2010.

[9] Z. Sun, R. J. Winder, B. E. Kelly, P. K. Ellis, and D. G. Hirst, "CT virtual intravascular endoscopy of abdominal aortic aneurysms treated with suprarenal endovascular stent grafting," *Abdominal Imaging*, vol. 28, no. 4, pp. 580–587, 2003.

[10] Z. Sun, R. J. Winder, B. E. Kelly, P. K. Ellis, P. T. Kennedy, and D. G. Hirst, "Diagnostic Value of CT Virtual Intravascular Endoscopy in Aortic Stent-Grafting," *Journal of Endovascular Therapy*, vol. 11, no. 1, pp. 13–25, 2004.

[11] G. Y. Cho, C. W. Lee, M. K. Hong, J. J. Kim, S. W. Park, and S. J. Park, "Effects of stent design on side branch occlusion after coronary stent placement," *Catheterization and Cardiovascular Interventions*, vol. 52, no. 1, pp. 18–23, 2001.

[12] V. Fuster, "Lewis A. Conner memorial lecture: mechanisms leading to myocardial infarction: insights from studies of vascular biology," *Circulation*, vol. 90, no. 4 I, pp. 2126–2146, 1994.

[13] X. He and D. N. Ku, "Flow in T-bifurcations: effect of the sharpness of the flow divider," *Biorheology*, vol. 32, no. 4, pp. 447–458, 1995.

[14] Z. Sun and T. Chaichana, "Fenestrated stent graft repair of abdominal aortic aneurysm: hemodynamic analysis of the effect of fenestrated stents on the renal arteries," *Korean Journal of Radiology*, vol. 11, no. 1, pp. 95–106, 2010.

[15] Z. Sun and T. Chaichana, "Investigation of the hemodynamic effect of stent wires on renal arteries in patients with abdominal aortic aneurysms treated with suprarenal stent-grafts," *CardioVascular and Interventional Radiology*, vol. 32, no. 4, pp. 647–657, 2009.

[16] T. Frauenfelder, M. Lotfey, T. Boehm, and S. Wildermuth, "Computational fluid dynamics: hemodynamic changes in abdominal aortic aneurysm after stent-graft implantation," *CardioVascular and Interventional Radiology*, vol. 29, no. 4, pp. 613–623, 2006.

[17] W. Nichols and M. O'Rourke, *McDonald's Blood Flow in Arteries*, Hodder Arnold, London, UK, 2005.

[18] S. Smith, *The Scientist and Engineer's Guide to Digital Signal Processing*, Technical Publishing, Poway, Calif, USA, 1997.

[19] E. Wellnhofer, J. Osman, U. Kertzscher, K. Affeld, E. Fleck, and L. Goubergrits, "Flow simulation studies in coronary arteries-Impact of side-branches," *Atherosclerosis*, vol. 213, no. 2, pp. 475–481, 2010.

[20] E. Boutsianis, H. Dave, T. Frauenfelder et al., "Computational simulation of intracoronary flow based on real coronary geometry," *European Journal of Cardio-thoracic Surgery*, vol. 26, no. 2, pp. 248–256, 2004.

[21] W. Milnor, *Hemodynamics*, Williams & Wilkins, Baltimore, Md, USA, 1989.

[22] Z. Sun, B. Mwipatayi, T. Chaichana, and C. Ng, "Hemodynamic effect of calcifed plaque on blood flow in carotid artery disease: a preliminary study - Hemodynamic effect of calcified plaque," in *Proceedings of the 3rd International Conference on Bioinformatics and Biomedical Engineering (iCBBE '09)*, pp. 1–4, June 2009.

[23] A. Borghi, N. B. Wood, R. H. Mohiaddin, and X. Y. Xu, "Fluid-solid interaction simulation of flow and stress pattern in thoracoabdominal aneurysms: a patient-specific study," *Journal of Fluids and Structures*, vol. 24, no. 2, pp. 270–280, 2008.

[24] W. W. Jeong and K. Rhee, "Effects of surface geometry and non-newtonian viscosity on the flow field in arterial stenoses," *Journal of Mechanical Science and Technology*, vol. 23, no. 9, pp. 2424–2433, 2009.

[25] P. D. Ballyk, D. A. Steinman, and C. R. Ethier, "Simulation of non-newtonial blood flow in an end-to-side anastomosis," *Biorheology*, vol. 31, no. 5, pp. 565–586, 1994.

[26] L. C. Cheng, J. M. Robertson, and M. E. Clark, "Numerical calculations of plane oscillatory non uniform flow. II. Parametric study of pressure gradient and frequency with square wall obstacles," *Journal of Biomechanics*, vol. 6, no. 5, pp. 521–538, 1973.

[27] D. Garcia, L. Kadem, D. Savéry, P. Pibarot, and L. G. Durand, "Analytical modeling of the instantaneous maximal transvalvular pressure gradient in aortic stenosis," *Journal of Biomechanics*, vol. 39, no. 16, pp. 3036–3044, 2006.

[28] H. V. Anderson, G. S. Roubin, and P. P. Leimgruber, "Measurement of transstenotic pressure gradient during percutaneous transluminal coronary angioplasty," *Circulation*, vol. 73, no. 6, pp. 1223–1230, 1986.

[29] S. H. Han, J. Puma, H. M. Garcia-Garcia et al., "Tissue characterisation of atherosclerotic plaque in coronary artery bifurcations: an intravascular ultrasound radiofrequency data analysis in humans," *EuroIntervention*, vol. 6, no. 3, pp. 313–320, 2010.

[30] A. I. Gziut, "Comparative analysis of atherosclerotic plaque distribution in the left main coronary artery and proximal segments of left anterior descending and left circumflex arteries in patients qualified for percutaneous coronary angioplasty," *Annales Academiae Medicae Stetinensis*, vol. 52, no. 2, pp. 51–63, 2006.

[31] T. Asakura and T. Karino, "Flow patterns and spatial distributions of atherosclerotic lesions in human coronary arteries," *Circulation Research*, vol. 66, no. 4, pp. 1045–1066, 1990.

[32] F. J. H. Gijsen, J. J. Wentzel, A. Thury et al., "A new imaging technique to study 3-D plaque and shear stress distribution in human coronary artery bifurcations in vivo," *Journal of Biomechanics*, vol. 40, no. 11, pp. 2349–2357, 2007.

[33] H. W. Sung, P. S. Yu, C. H. Hsu, and J. C. Hsu, "Can cardiac catheterization accurately assess the severity of aortic stenosis? An in vitro pulsatile flow study," *Annals of Biomedical Engineering*, vol. 25, no. 5, pp. 896–905, 1997.

Chapter 4

Impact of plaques in theleft coronary artery on wall shear stress and pressure gradient in coronary side branches. Computer Methods in Biomechanics and Biomedical Engineering, Epub a head of print, 1–11. doi:10.1080/10255842.2012.671308.

Thanapong Chaichana, Zhonghua Sun and James Jewkes

Computer Methods in Biomechanics and Biomedical Engineering
iFirst article, 2012, 1–11

Taylor & Francis
Taylor & Francis Group

Impact of plaques in the left coronary artery on wall shear stress and pressure gradient in coronary side branches

Thanapong Chaichana[a], Zhonghua Sun[a]* and James Jewkes[b]

[a]*Discipline of Medical Imaging, Department of Imaging and Applied Physics, Curtin University, Perth, WA 6845, Australia;* [b]*Fluid Dynamics Research Group, Department of Mechanical Engineering, Curtin University, Perth, WA 6845, Australia*

(*Received 2 August 2011; final version received 27 February 2012*)

In this study, we investigate plaques located at the left coronary bifurcation. We focus on the effect that the resulting changes in wall shear stress (WSS) and wall pressure stress gradient (WPSG) have on atherosclerotic progress in coronary artery disease. Coronary plaques were simulated and placed at the left main stem and the left anterior descending to produce >50% narrowing of the coronary lumen. Computational fluid dynamics analysis was carried out, simulating realistic physiological conditions that show the *in vivo* cardiac haemodynamic. WSS and WPSG in the left coronary artery were calculated and compared in the left coronary models, with and without the presence of plaques during cardiac cycles. Our results showed that WSS decreased while WPSG was increased in coronary side branches due to the presence of plaques. There is a direct correlation between coronary plaques and subsequent WSS and WPSG variations based on the bifurcation plaques simulated in the realistic coronary models.

Keywords: atherosclerosis; coronary blood flow; coronary disease; wall pressure stress gradient; wall shear stress

1. Introduction

Atherosclerosis is generally regarded as the primary cause of coronary artery disease (CAD), with resultant abnormal changes to the coronary lumen (Wellnhofer et al. 2010). Plaques have been associated with intimal wall changes of the coronary artery with superimposition of blood clots, compromising blood flow to the myocardium (Australian Institute of Health and Welfare 2006). It is well known that plaques most commonly originate in the coronary bifurcation. Atherosclerosis tends to develop at locations where disturbed flow patterns occur, where a coronary angulation is formed between the left anterior descending (LAD) and left circumflex (LCx). Wide angulation leads to significant flow disturbances that are related to the formation of these plaques (Chaichana et al. 2011). This is a fundamental determinant that has been found to be associated with the development of atherosclerosis, as confirmed by previous studies (Asakura and Karino 1990; Fuser 1994; Gziut 2006; Han et al. 2010; Chaichana et al. 2011; Sun and Cao 2011). Haemodynamic variation is believed to play an important role in the pathogenesis of CAD, which is characterised by reduced local wall shear stress (WSS) and blood recirculation (Asakura and Karino 1990; Fuser 1994; Chaichana et al. 2011). Therefore, the use of realistic vascular geometry to determine the local flow field and WSS alteration in the coronary artery is of paramount importance for understanding the underlying mechanism of CAD.

Early detection and diagnosis of CAD are particularly important for the reduction in mortality and subsequent complications (Australian Institute of Health and Welfare 2006). CT virtual intravascular endoscopy (VIE) has been reported to be valuable for visualisation and assessment of coronary plaques in patients suspected of CAD (Sun et al. 2010). Despite the additional information provided by VIE with regard to the intravascular lumen changes at the coronary wall, when compared to traditional 2D or 3D visualisations (Figure 1), this technique is restricted to the anatomical details. It is unable to demonstrate the haemodynamic changes in the coronary artery due to the presence of plaques. Another imaging modality, intravascular ultrasound (IVUS), is used to measure blood flow velocity and visualise intraluminal changes in the coronary artery, but is limited to large coronary segments, and fails to assess coronary side branches and WSS variation (Grayburn et al. 1992; Gijsen et al. 2007).

Previous studies used computational fluid dynamics (CFD) to analyse coronary artery haemodynamics and implicate atherosclerosis progression (Perktold et al. 1998; Farmakis et al. 2004; Johnston et al. 2004; Giannoglou et al. 2005; Soulis et al. 2006; Katritsis et al. 2010; Shanmugavelayudam et al. 2010). These studies either involved analysis of the coronary artery remodelling under normal conditions (Perktold et al. 1998; Farmakis et al. 2004; Johnston et al. 2004; Giannoglou et al. 2005; Soulis et al. 2006) or focused on the analysis of the diseased condition (Katritsis et al. 2010; Shanmugavelayudam et al. 2010). To

*Corresponding author. Email: z.sun@curtin.edu.au

ISSN 1025-5842 print/ISSN 1476-8259 online

http://dx.doi.org/10.1080/10255842.2012.671308
http://www.tandfonline.com

the best of our knowledge, there are no publications related to the investigation of realistic coronary plaques and their influence on side branches, based on the topography of WSS and wall pressure stress gradient (WPSG). Thus, this work aims to study the haemodynamic effects of coronary plaques on side branches, and it is expected that the research findings will provide potential value for improving our understanding of the effects of coronary plaques and the pathogenesis of CAD.

2. Material and methods

2.1 Patient data selection and left coronary model

A sample patient (47-year-old male), suspected of coronary disease, was selected to represent the realistic coronary anatomy and side branches. The patient's CT volume data were used to generate a 3D luminal model, which were then saved in 'DICOM format'. The CT scan was done with a 64-slice scanner (GE Medical Systems, LightSpeed VCT, 64 × 0.625 mm, Milwaukee, WI, USA) with the following protocols: beam collimation 0.625 mm, pitch 0.2–0.26, reconstruction interval of 0.4 mm, with tube voltage of 120 kVp and tube current ranging from 300 to 650 mAs (tube current modulation). Axial images were reconstructed with a slice thickness of 0.625 mm in 0.4-mm increments, resulting in isotropic volume data with a voxel size of $0.4 \times 0.4 \times 0.4\,mm^3$. Retrospective electrocardiographic-gating protocol was used to acquire the volume data, achieving a temporal resolution of 165 ms in the centre of the gantry rotation. Volume data were reconstructed at 70–80% RR interval to minimise unwanted artefacts.

Image post-processing and segmentation of the volume data were done using a workstation equipped with Analyze 7.0 (Analyze Direct, Inc., Lexana, KS, USA). The segmentation technique used a semi-automatic procedure with CT number thresholding. Unwanted artefacts and soft tissues were manually deleted in some slices (Sun et al. 2003, 2004). The segmented luminal model was produced with a special focus on the left coronary artery (LCA), which is composed of left main stem (LMS), LAD, LCx and its side branches. Figure 2 shows the segmentation of the CT data for acquisition of the LCA model. Measurements of the LCA including major and side of branches (Figure 3) were made, and details of the measurements are shown in Table 1. In particular, special attention was paid to maintain both main and side coronary artery branches during image post-processing. Thus, this ensures that our coronary model reflects the realistic condition by including both main and side coronary branches. The 3D LCA model was saved in 'STL format' for the generation of luminal geometries.

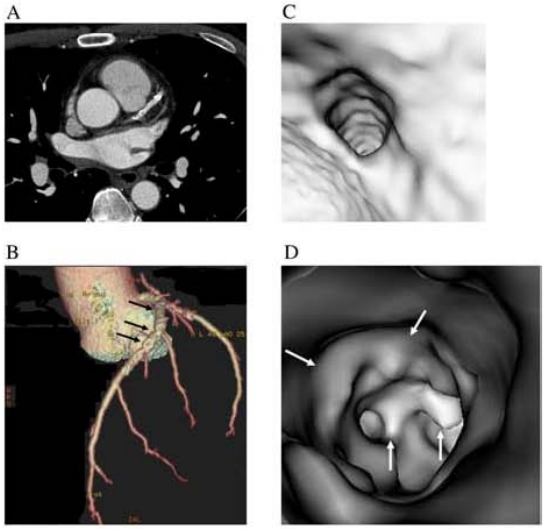

Figure 1. Significant CAD is diagnosed in a 52-year-old man with symptoms of chest pain and hypertension. (A), 2D axial image shows multiple calcified plaques in the LAD. (B), 3D volume rendering demonstrates stenotic changes in the LAD (arrows). (C) VIE shows normal right coronary ostium with smooth lumen, while irregular intraluminal changes are present in the LAD as shown in virtual endoscopy image (arrows in D).

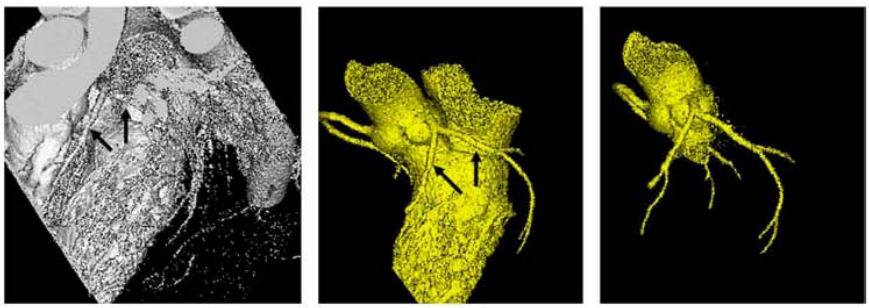

Figure 2. Steps to segment the LCA for the generation of 3D coronary models. Three-dimensional CT volume data show the visualisation of the LCA (arrows in left image). After applying image processing, the ascending aorta, coronary arteries and cardiac chambers are segmented from the volume data (middle image). Further image segmentation allows for the ascending aorta and coronary arteries to be kept while the remaining structures are removed (right image).

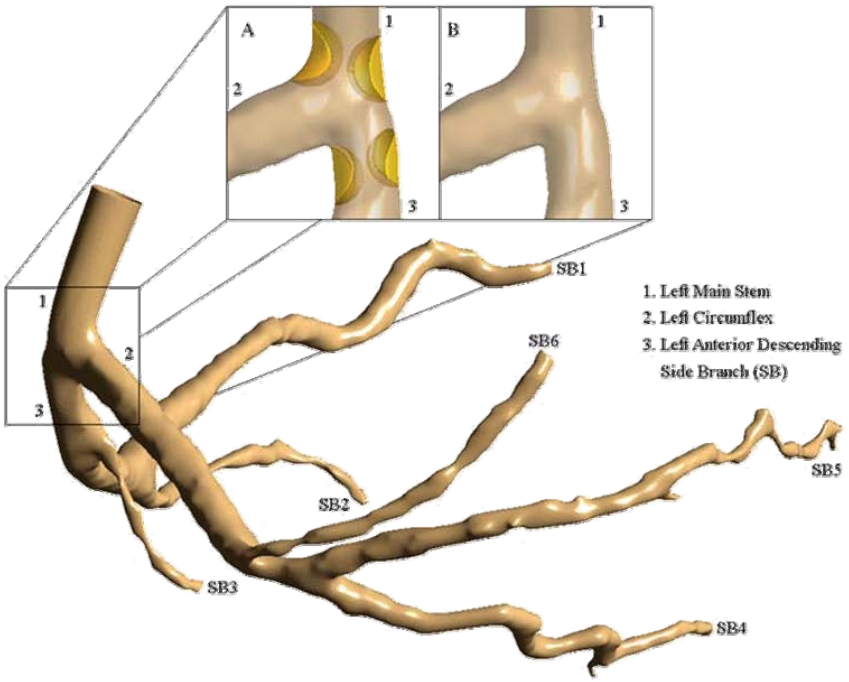

Figure 3. Plaque distribution in the LCA model is simulated at the LMS and ostium of LAD. The rectangle indicates an EPL, the LCA models (A) with plaques and (B) without plaques.

Blender version 2.48 (Blender Institute, Amsterdam, the Netherlands) was used to reconstruct the 3D luminal model. A gentle B-spline smoothing technique was applied between the left main trunk and side branches to reduce any potential non-physical behaviour induced by sharp edges (He and Ku 1995). The geometry of arteries around the LMS, LAD and LCx was obtained from the sample patient with suspected CAD, although normal anatomical structures were shown on the CT images at the LMS and LAD branches. The luminal surface models, consisting of plaques and normal coronary arteries, were converted into solid models and saved in 'STL format' for the creation of the computational mesh models.

2.2 *Plaques simulated in LCAs*

The simulated realistic plaques in the LCA were located at the ostium of LMS and LAD branches, as these artery branches are the locations where plaques usually occur and induce myocardial ischaemic changes (Cho et al. 2001). The plaque geometry at the LMS branches is composed of two sections; the dimensions of each section were 1.14 mm in height, with a mean width of 3.76 mm and a thickness of 1.46 and 1.53 mm (from left to right in Figure 3). The geometry of plaques at the LAD branches consists of two sections; dimensions were 1.17 mm in height, with a mean width of 3.59 mm and a thickness of 1.38 and 1.56 mm (from left to right in Figure 3). Although plaques contain different components depending on the concentration of calcium (Sun et al. 2010), only hard plaques (calcified plaques) were simulated in this study, as these types of plaques represent the most common form of CAD. The plaques produced a lumen narrowing of at least 50% at the LMS and LAD, since a lumen stenosis >50% leads to significant haemodynamic changes to flow within the coronary artery (Fuser 1994). Figure 3 shows the segmented LCA model and the position of the plaques at the LCA. The creation and positioning of plaque geometry were based on high-resolution CT images. The surface of the plaques was assumed to be smooth. Furthermore, the

Table 1. Mean diameters and lengths of major and side branches in LCA.

Left coronary artery			Diameters (mm)	Lengths (mm)
LMS	Main branch	Inlet	4.599	29.441
LAD	Main branch		3.763	45.982
LCx	Main branch		3.585	62.303
LAD	Side branch 1	Outlet 1	0.548	124.301
	Side branch 2	Outlet 2	0.348	64.046
	Side branch 3	Outlet 3	0.609	38.452
LCx	Side branch 4	Outlet 4	0.666	104.231
	Side branch 5	Outlet 5	0.358	151.662
	Side branch 6	Outlet 6	0.714	81.386

Note: LMS, left main stem; LAD, left anterior descending; LCx, left circumflex.

plaque models were configured to represent the true anatomy of CAD, as demonstrated by the 'Glagov phenomenon'. Glagov et al. (1987) reported that when the lesion reached about 40% lumen stenosis, the coronary artery began to throttle the flow speed and volumetric blood flow began to decrease. When the stenosis exceeds 40%, an adequate lumen area is preserved, independent of the plaque area. There are different factors (such as changing mechanical properties of plaques and changing haemodynamic behaviour as plaques enlarge) that individually affected local haemodynamic changes.

2.3 CFD analysis

The mesh was divided into the luminal LCA models (coronary artery with and without the presence of plaques) and plaque sections at the major branch (LCx and LAD). Firstly, the STL file of the LCA model was imported into ANSYS ICEM CFD version 12 (ANSYS, Inc., Canonsburg, PA, USA) and then the geometry analysis was carried out to check the geometry profiles, unconnected lines and opened surfaces were repaired. Secondly, block-mesh constructions were created to cover up the LCA geometry and its side branches (Figure 3). Then, plaque sections were added to the model in the appropriate locations. Luminal LCA models were used to create hexahedral and tetrahedral meshes to perform the CFD simulations. The LCA model with plaques was generated using a hexahedral mesh (1,041,936 nodes and 928,311 elements), and tetrahedral cells were used for the two sections of plaques at LMS and LAD (132,406 nodes and 777,817 elements, and 111,879 nodes and 656,130 elements, respectively). In addition, the LCA model without plaques was created using a hexahedral mesh (1,062,280 nodes and 949,289 elements). ANSYS ICEM CFD version 12 was used for the generation of mesh elements, with details having been described in previous studies (Sun and Chaichana 2009, 2010; Chaichana et al. 2011). Mesh convergence was established by re-running a test simulation at double the quoted grid resolution, and by looking for discrepancies in the solution. It was found that mesh convergence had been achieved, and the fairly fine meshes described above were acceptable for the purposes of this study (Myers et al. 2001; Prakash and Ethier 2001). Finally, LCA mesh models were saved in 'GTM format' for CFD computation.

This study was based on the computational simulation of *in vivo* conditions, and physiological boundary conditions were applied for the 3D numerical analysis. The transient simulation was performed using haemodynamic rheological and material properties. Figure 4 shows the pulsatile flow rate into the LCA, reconstructed using a Fourier series in Matlab (MathWorks, Inc., Natick, MA, USA), and applied using ANSYS CFX Command Language programming to define inflow boundary conditions (Tang et al. 1990; Smith

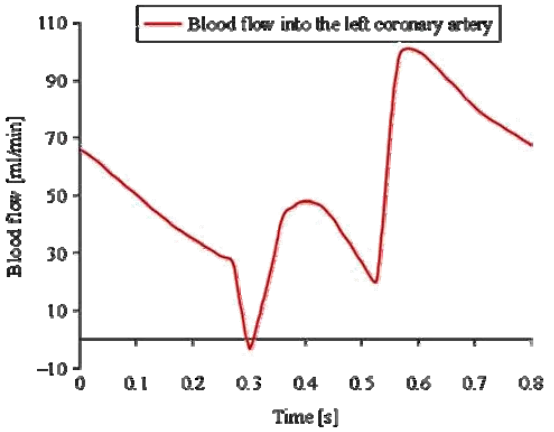

Figure 4. The blood flow into the LCA during one cardiac phase and was used as the inflow boundary condition for haemodynamic computational simulations.

1997; Berne and Levy 2001; Katritsis et al. 2010; Chaichana et al. 2011). A parabolic profile was applied for the inlet velocity boundary condition. The outlet boundary conditions were applied with the flow ratio through the six side branches at the LAD (SB1, 2 and 3) and LCx (SB4, 5 and 6) according to the diameters of the side branches (Table 1; Giannoglou et al. 2005; van der Giessen et al. 2011). The outflow relationship is also known as Murray's (1926) law and the summation of outflow conditions through the side branches is equal to the flow at inlet. Appropriate rheological parameters were applied with a blood density of 1060 kg/m^3 and a blood viscosity of 0.0035 Pa s (Milnor 1989; Boutsianis et al. 2004). Plaque was assumed to be a rigid body (Sun et al. 2009). The blood flow was assumed to be laminar. The rigid vessel walls and a no-slip condition were applied at the walls. Blood was assumed to be a Newtonian and incompressible fluid (Johnston et al. 2004; Borghi et al. 2008).

The Navier–Stokes equations were solved using the ANSYS CFX CFD package (version 12 – ANSYS, Inc.), on a Microsoft Windows 7 32-bit machine, 6 GB of RAM with a Xeon W3505 2.53 GHz CPU. The CFD simulation was converged to a residual target of less than 1×10^{-4} per LCA model. The calculation time for convergence of each LCA model was approximately 2 h. The configuration of this simulation is similar to previously published simulations (Sun and Chaichana 2009, 2010; Chaichana et al. 2011). ANSYS CFD-Post version 12 (ANSYS, Inc.) was used to calculate and visualise flow velocity, WSS and wall pressure gradient.

2.4 Computation of quantitative parameters

The haemodynamic changes in LCA surrounding the plaque locations (the so-called effective plaque location

(EPL)) are shown in Figure 3 (rectangle positions). The quantitative parameters used to characterise the impact of plaques on coronary side branches are local WSS magnitude and wall pressure stress gradient (WPSG; Kleinstreuer et al. 2001) defined as

$$\mathrm{WSS} = \frac{1}{\tau}\int_0^T \left|\mu \frac{\partial v_t}{\partial n}\right| \mathrm{d}t, \tag{1}$$

where μ is the blood viscosity, v_t is the velocity vector near the wall perpendicular to the surface, n is the distance to the wall surface, T is the pulsatile period and dt is the time derivative of the local shear stress. The WSS is a commonly used parameter in haemodynamics; endothelial cells have been shown to align themselves with the flow direction that corresponds to the local WSS. The coordinates of the wall surface elucidate the interaction of instantaneous WSS vectors and endothelial cells (Kleinstreuer et al. 2001):

$$\mathrm{WPSG} = \frac{1}{\tau}\frac{2d_0}{\rho U^2}\int_0^T \frac{\partial p}{\partial n}\mathrm{d}t, \tag{2}$$

where p is the local wall static pressure in the area of interest, d_0, U, and ρ are the inlet diameter, the flow velocity and the density of the fluid, respectively (Cheng et al. 1973; Kleinstreuer et al. 2001; Garcia et al. 2006). The local WPSG is calculated by taking the spatial derivative of the local pressure. The WPSG indicates changing pressure loads on vessel walls leading to the wall stress and strain problems (Thubrikar and Robicsek 1995; Kleinstreuer et al. 2001). The disturbed flow patterns are caused by the particular geometric features of blood vessels (e.g. sudden expansions, branches and bifurcations) and are directly related to inducing the variation in the WSS, the oscillatory shear index (OSI), the WSS gradient (WSSG), the wall particular density (WPD) and the WPSG. As a result, these haemodynamic factors include damage to endothelium cells causing the atherosclerosis progression (Thubrikar and Robicsek 1995; Kleinstreuer et al. 2001). The first three parameters (WSS, OSI and WSSG) are based on the local WSS vector, and the other two parameters (WPD and WPSG) are dependent on the particle deposition rate and local pressure field, respectively (Kleinstreuer et al. 2001). Thus, the WSS and WPSG were chosen to determine the impact of bifurcation plaques to their side branches. Finally, the value of WPSG oscillated in relation to the percentage of plaques in the coronary lumen (Anderson et al. 1986).

3. Results

CFD analysis was carried out in the 3D LCA models with and without plaques based on *in vivo* physiological conditions during cardiac phases. The systolic and diastolic pulsatile cycles were reached at a time of 0.2 and 0.7 s, respectively. Results showed that the plaques had a direct effect on haemodynamic changes at the left coronary bifurcation, which was shown by the alteration of WSS and WPSG in the coronary side branches.

3.1 Haemodynamic changes at the EPL

Figure 5 shows the flow velocity patterns visualised at the EPL (Figure 3) in both LCA models with and without plaques. The flow velocity was visualised specifically around the EPL to demonstrate the local effect of plaques at the bifurcation in terms of quantitative WSS and WPSG. Thus, no side branches were included in the models for flow analysis, as it is believed that there would not be any effect on the distal coronary branches. Velocity values were produced with 15 colour scales, which ranked from 0 to 30.50 mm/s. As shown in Figure 5, simulated plaques influenced haemodynamic changes, and flow velocity increased mainly in the presence of plaques, due to the narrowing lumen. The peak velocity ranged from 28.32 to 30.50 mm/s at the location where plaques were present. The recirculation regions were found at post-plaque locations in the LMS, LAD and LCx (Figure 5(A),(C)). In contrast, Figure 5(B),(D) showed that smooth flow patterns were observed in LCA model without the presence of plaques, and the high velocity reached at the bifurcation location ranged from 15.25 to 17.43 mm/s (0.2 s of systolic phase) and from 26.14 to 28.32 mm/s (0.7 s of diastolic phase), respectively.

3.2 WSS in the left coronary side branches

To quantify the effect of plaques on coronary side branches, WSS was calculated and compared in both LCA models with and without the presence of plaques, as shown in Figures 6 and 7. The plots were chosen to show WSS distributions from post-plaque positions to side branches by visualising right- and left-hand views. Calculated WSS values at systolic and diastolic phases ranged from 0 to 3.50 Pa, corresponding to a contour of 15 colour scales. Figures 6 and 7 show the direct effect of plaques on WSS distributions in coronary side branches, and WSS was found to decrease in the post-plaque positions in some areas of the side branches when compared to an LCA model without the presence of plaques. Figures 6(A) and 7(A) show the minor impact of plaques on WSS distribution in the coronary side branches at systolic phase of 0.2 s (indicated at points 5 and 6, respectively), while a major impact was observed in the diastolic phase of 0.7 s, shown at points of 18 (Figure 6(C)) and 15

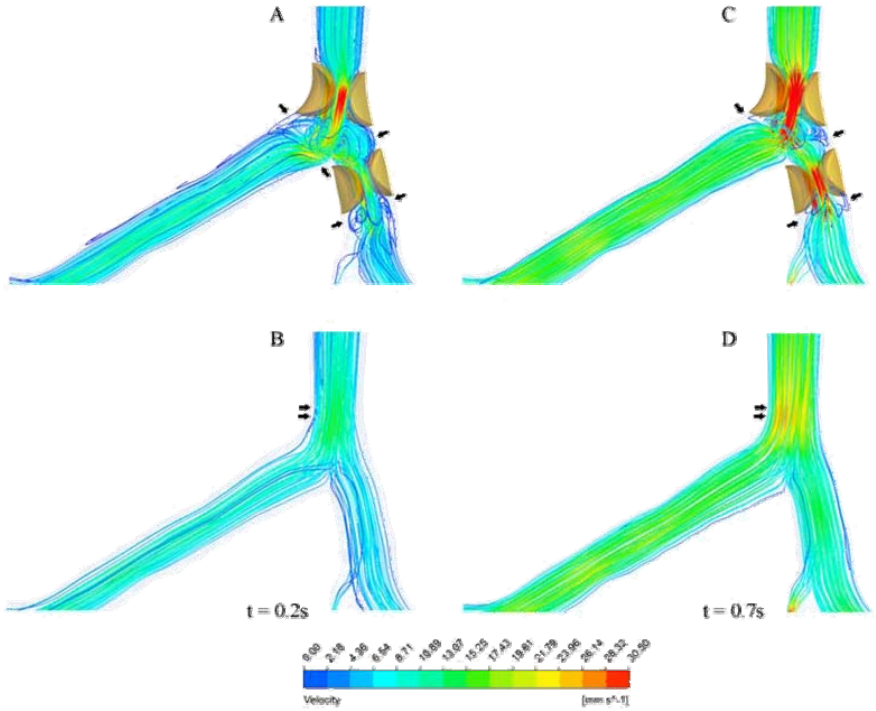

Figure 5. Local impact of flow velocity observed surrounding the EPL with and without the presence of plaque models during a systolic phase of 0.2 s and a diastolic phase of 0.7 s. Double arrows reveal high flow velocity locations at bifurcation in LCA model without plaques. Arrows indicate the recirculation regions caused by plaques.

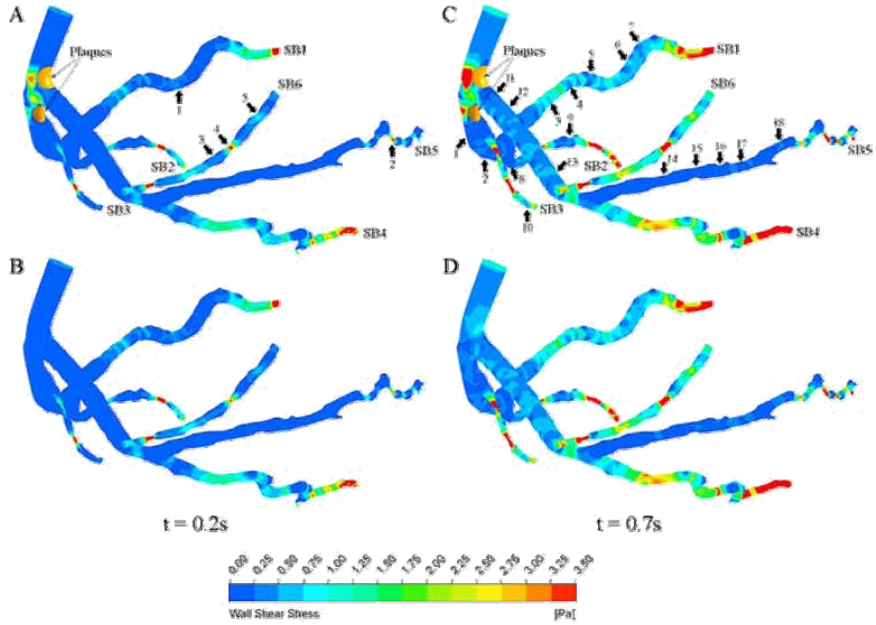

Figure 6. The right-hand perspective view of WSS observed in coronary models with and without plaques during a systolic phase of 0.2 s and a diastolic phase of 0.7 s. Arrows indicate the effect of plaques locations on WSS changes in coronary side branches in the post-plaques conditions.

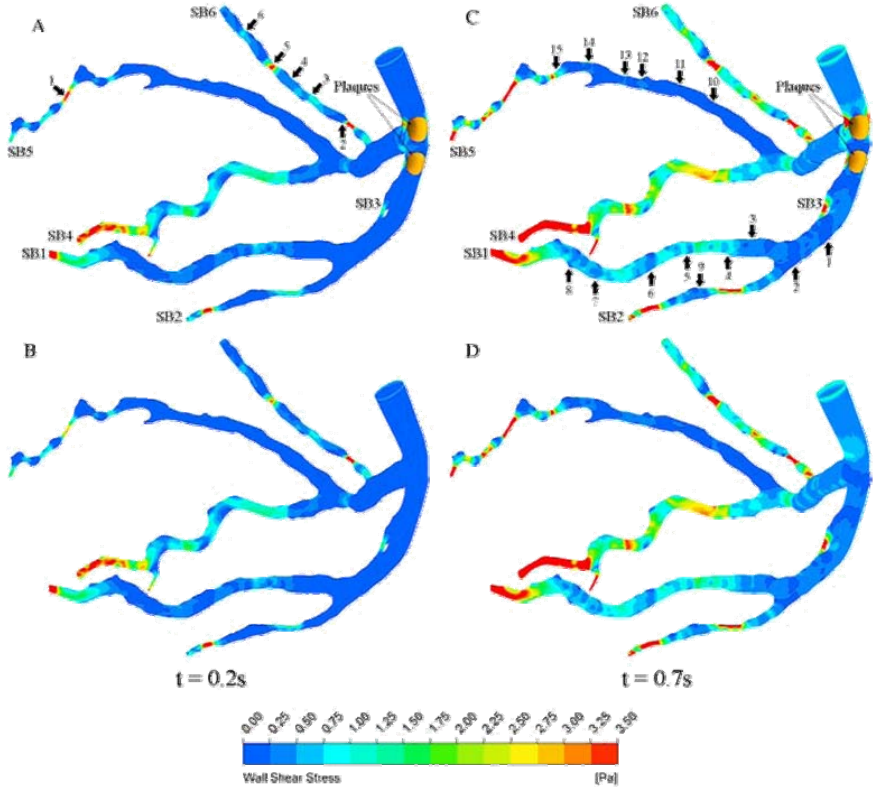

Figure 7. The left-hand perspective view of WSS observed in coronary models with and without plaques during a systolic phase of 0.2 s and a diastolic phase of 0.7 s. Arrows indicate effect of plaques locations on WSS changes in coronary side branches in the post-plaques conditions.

(Figure 7(C)). In addition, normal WSS distributions were observed in Figures 6(B),(D) and 7(B),(D).

3.3 *WPSG in the left coronary side branches*

WPSG was calculated at the systolic and diastolic phases, and displayed with both right- and left-hand views in order to compare the WPSG distribution of the LCA model with and without the presence of plaques (Figures 8 and 9, respectively). WPSG values ranged from -15 to $500\,kg/m^2s^2$, corresponding to 15 contour levels. Figures 8 and 9 demonstrated the coronary plaques influence upon WPSG distributions after EPL to coronary side branches. WPSG was found to generally increase in the post-plaque positions in some points of the side branches when compared to LCA model without plaques. Figures 8(A) and 9(A) show the large effect of plaques on WPSG distributions in the coronary side branches, at points of 28 and 23 during the systolic phase (0.2 s), while a smaller effect is observed in diastolic phase (0.7 s), shown at points 22 and 18, in Figures 8(C) and 9(C). Furthermore, normal WPSG distributions were observed in Figures 8(B),(D) and 9(B),(D).

4. Discussion

This study demonstrates that the presence of coronary plaques in the main coronary artery produces haemodynamic effects on the subsequent WSS and WPSG distributions in the coronary artery and its side branches. This is clinically significant as these haemodynamic changes will contribute to further atherosclerotic progress in the coronary artery tree, leading to potential damage to the artery wall. We assume that side branches will be affected by the plaques at major branches, as most of the studies focused on the main coronary branches with regard to plaques and disease development, while little attention is paid to the side branches. To our knowledge, no studies have been carried out to prove the assumption about the haemodynamic effect of plaques on side branches. Thus, we consider that our study has potential value for improving the understanding of the effects of coronary plaques and pathogenesis of CAD.

Coronary plaque is mostly formed in the bifurcation due to coronary angulations and low WSS, as confirmed by our and other studies (Asakura and Karino 1990; Fuser 1994; Gziut 2006; Han et al. 2010; Chaichana et al. 2011; Sun and Cao 2011). Three-dimensional image

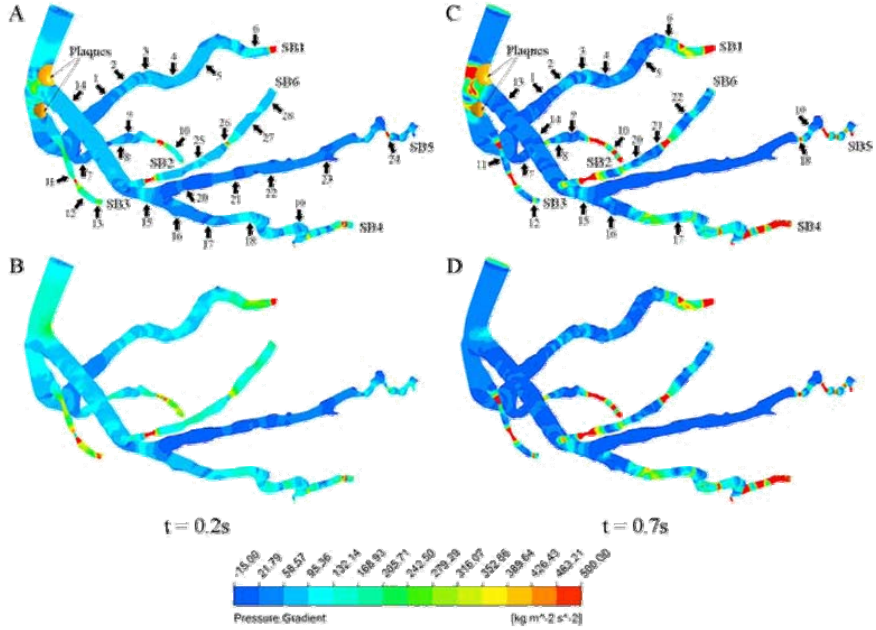

Figure 8. The right-hand perspective view of WPSG observed in coronary models with and without plaques during a systolic phase of 0.2 s and a diastolic phase of 0.7 s. Arrows indicate effect of plaques locations on WPSG changes in coronary side branches in the post-plaques conditions.

visualisation and IVUS have been used to detect and identify coronary plaques (Grayburn et al. 1992; Gijsen et al. 2007; Sun et al. 2010). Although valuable diagnostic details, including plaque assessment, are provided by these techniques, no information is available on rheological parameters. In comparison, CFD allows for haemodynamic analysis due to the presence of plaques at the coronary bifurcation (Sun and Chaichana 2009, 2010; Chaichana et al. 2011). Thus, the effects of plaques in the coronary artery can be further explored with regard to flow changes, and this is beyond the anatomical analysis of lumen stenosis or occlusion.

This study investigated two important factors: WSS and WPSG, and qualified the impact of plaques on WSS and WPSG variations to the coronary side branches. Haemodynamic changes surrounding the EPL were shown to be present, due to the local effect of plaques at the bifurcation in terms of quantitative WSS and WPSG (Figure 5). WSS is a well-known standard factor that is used to judge the point or location where atherosclerotic lesions tend to develop (Kleinstreuer et al. 2001; Chaichana et al. 2011). Recent studies suggested that high WSS was regarded as a contributor to the rupture and thrombosis of advanced coronary plaques (Samady et al. 2011; Vilahur et al. 2011). Normally, plaques that caused a large stenosis produced high WSS surrounding a jet location and this leads to a large change in WSS; thus, it would have some effect on the side branches. In this study, the CFD analysis of the LCA model with and without the presence of plaques showed that there is a direct correlation between the effect of coronary plaques at bifurcation and the WSS changes, as low WSS was observed in some side branches. The CFD analysis showed that coronary side branches (SB1 and SB5) were mostly affected in both systolic and diastolic phases (Figures 6 and 7), while more effects are in the diastolic phase (Figures 6(C) and 7(C)). The variations in WSS points were decreased approximately 0.25 Pa per point, when comparing point by point between the luminal LCA models with and without coronary plaques. Hence, the presence of plaques at the bifurcation in the LCA impacts the coronary side branch, thus this indicates that it is more likely for the plaques to lead to low WSS in tortuous side branches when compared to the straight branches.

In the clinical situation, the magnitude of the pressure gradient has been used to assess the risk of severity of plaques (Anderson et al. 1986). The highest pressure gradient region may indicate potential coronary plaque rupture. It is important to analyse the WPSG parameter, as high-pressure gradients can lead to increased locally high accelerations. This has been confirmed by a previous study that suggested that the reduction in local WPSG can decrease the likelihood of the development of plaques (Kleinstreuer et al. 2001). The role of local static pressure in coronary wall thickening has been explored, and it has been suggested that among haemodynamic parameters the

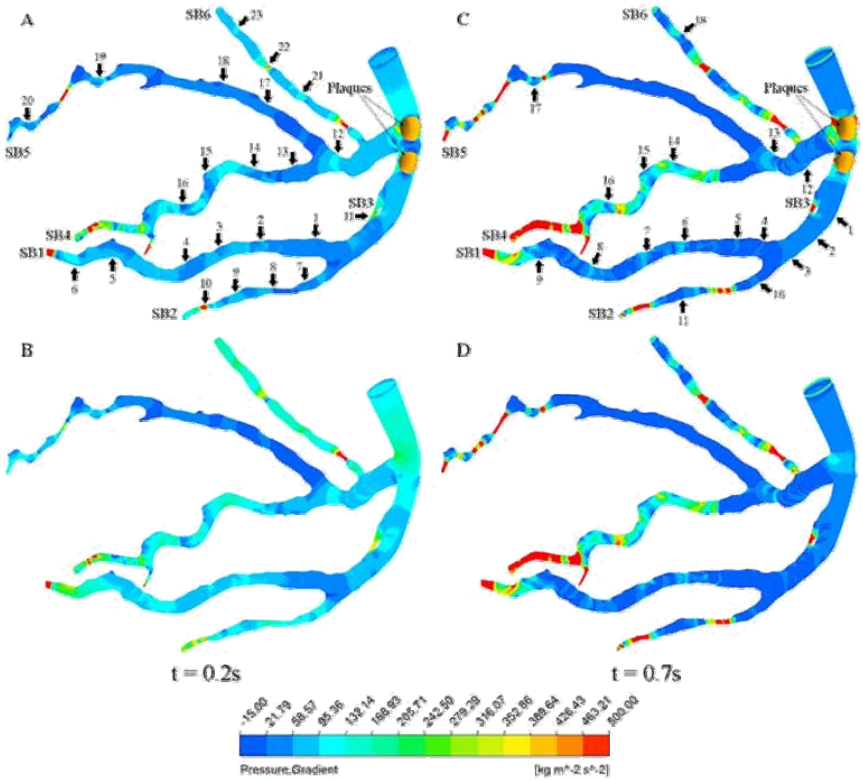

Figure 9. The left-hand perspective view of WPSG observed in coronary models with and without plaques during a systolic phase of 0.2 s and a diastolic phase of 0.7 s. Arrows indicate effect of plaques locations on WPSG changes in coronary side branches in post-plaques conditions.

static pressure (large areas in negative values) was the main factor that correlated to the wall thickening (Giannoglou et al. 2002). There is some possibility that static pressure implicated the development of atherosclerosis, which was considered a part of WPSG (Giannoglou et al. 2005). The distribution of static pressure in coronary side branches was found in this study to show large areas of positive values more than the negative values. There were a few points of pressure difference when comparing the pressure changes with and without the presence of plaques during a systolic phase of 0.2 s and a diastolic phase of 0.7 s (not shown). Thus, WPSG is the factor that can cause the great topographies to correlate between coronary bifurcation plaques influencing side branches and subsequent haemodynamic differences. Our analysis in this study has proposed explicitly haemodynamic changes inside the LCA surrounding the EPL and investigates the impact of plaques on side branches. The CFD analysis of the LCA with and without the presence of plaques showed that the WPSG parameter in the coronary side branches was directly affected by plaques at the bifurcation (Figures 8 and 9) during systolic and diastolic phases, approximately 36.78 $kg/m^2 s^2$ when comparing point by point between the LCA model with and without plaques. Our results showed that WPSG was significantly increased in SB1 and SB4 (Figures 8(A),(C) and 9(A),(C)). Thus, coronary plaques at the bifurcation in the LCA influenced WPSG variations and specifically increased in SB1 and SB4 during diastolic phase (Figures 8(C) and 9(C)).

There are some limitations in this study, which should be addressed. Firstly, the blood was assumed to have a Newtonian viscosity model. This assumption is important mostly in low flow velocity and low WSS regions, and has been shown to be reasonable in this case by a previous study (Johnston et al. 2004). Secondly, realistic LCA models, with and without the presence of plaques, were assumed to have a rigid wall rather than an elastic wall; hence, the simulation does not completely show the realistic physiological situation as the coronary wall is moving during cardiac cycles. The wall of the coronary model was rigid and this is considered to be reasonable as reported by a previous study (Moore et al. 1994). Thirdly, a single patient-specific data-set was analysed, and represented the possible direction of coronary disease and haemodynamic variations, which is another limitation

of the current study. It has been reported that studies based on a small population may not be fully representative of the whole population, thus research findings cannot be applied to other patients (Friedman and Ding 1998). Studies based on a large cohort are needed to allow a robust conclusion to be drawn. Fourthly, the different positions of realistic plaques at the bifurcation may be affected by the left coronary side branches that have not been evaluated in this study. Thus, future studies will use coronary models with a more realistic idealised geometry with various plaques at the bifurcation in a group of patients with different degrees of CAD.

5. Conclusion

This study investigates the impact of plaques in the realistic LCA on WSS and WPSG variations in coronary side branches with the use of a 3D luminal LCA model. Direct haemodynamic effects of plaques in the LCA side branches have been found to demonstrate WSS and WPSG changes, indicating the possible development of plaques in coronary side branches. Our results improve the understanding of the development of atherosclerosis by further exploring the effect of plaques on coronary artery and side branches. Further studies focusing on the various positions of realistic plaques at the bifurcation, particularly their impact on coronary side branches, should be performed to verify our results.

References

Anderson HV, Roubin GS, Leimgruber PP, Cox WR, Douglas JS, Jr, King SB, 3rd, Gruentzig AR. 1986. Measurement of transstenotic pressure gradient during percutaneous transluminal coronary angioplasty. Circulation. 73(6):1223–1230.

Asakura T, Karino T. 1990. Flow patterns and spatial distribution of atherosclerotic lesions in human coronary arteries. Circ Res. 66:1045–1066.

Australian Institute of Health and Welfare. 2006. Australia's health 2006. Canberra: AIHW.

Berne RM, Levy MN. 2001. Cardiovascular physiology. St Louis (MI): Mosby.

Borghi A, Wood NB, Mohiaddin RH, Xu XY. 2008. Fluid–solid interaction simulation of flow and stress pattern in thoracoabdominal aneurysms: a patient-specific study. J Fluid Struct. 24:270–280.

Boutsianis E, Dave H, Frauenfelder T, Poulikakos D, Wildermuth S, Turina M, Ventikos Y, Zund G. 2004. Computational simulation of intracoronary flow based on real coronary geometry. Eur J Cardiothorac Surg. 26(2):248–256.

Chaichana T, Sun Z, Jewkes J. 2011. Computation of haemodynamics in the left coronary artery with variable angulations. J Biomech. 44(10):1869–1878.

Cheng LC, Robertson JM, Clark ME. 1973. Numerical calculations of plane oscillatory non-uniform flow – II. Parametric study of pressure gradient and frequency with square wall obstacles. J Biomech. 6(5):521–538.

Cho GY, Lee CW, Hong MK, Kim JJ, Park SW, Park SJ. 2001. Effects of stent desing on side branch occlusion after coronary stent placement. Catheter Cardiovasc Interv. 52(1):18–23.

Farmakis TM, Soulis JV, Giannoglou GD, Zioupos GJ, Louridas GE. 2004. Wall shear stress gradient topography in the normal left coronary arterial tree: possible implications for atherogenesis. Curr Med Res Opin. 20(5):587–596.

Friedman MH, Ding Z. 1998. Variability of the planarity of the human aortic bifurcation. Med Eng Phys. 20(6):469–472.

Fuser V. 1994. Lewis A. Conner memorial lecture. Mechanisms leading to myocardial infarction: insights from studies of vascular biology. Circulation. 90(4):2126–2146.

Garcia D, Kadem L, Savéry D, Pibarot P, Durand LG. 2006. Analytical modeling of the instantaneous maximal transvalvular pressure gradient in aortic stenosis. J Biomech. 39(16):3036–3044.

Giannoglou GD, Soulis JV, Farmakis TM, Farmakis DM, Louridas GE. 2002. Haemodynamic factor and the important role of local static pressure in coronary wall thickening. Int J Cardiol. 86(1):27–40.

Giannoglou GD, Soulis JV, Farmakis TM, Giannakoulas GA, Parcharidis GE, Louridas GE. 2005. Wall pressure gradient in normal left coronary artery tree. Med Eng Phys. 27(6):455–564.

Gijsen FJ, Wentzel JJ, Thury A, Lamers B, Schuurbiers JC, Serruys PW, van der Steen AF. 2007. A new imaging technique to study 3-D plaque and shear stress distribution in human coronary artery bifurcations *in vivo*. J Biomech. 40(11):2349–2357.

Glagov S, Weisenberg E, Zarins CK, Stankunavicius R, Kolettis GJ. 1987. Compensatory enlargement of human atherosclerotic coronary arteries. New Engl J Med. 316(22):1372–1375.

Grayburn PA, Willard JE, Haagen DR, Brickner ME, Alvarez LG, Eichhorn EJ. 1992. Measurement of coronary flow using high-frequency intravascular ultrasound imaging and pulsed Doppler velocimetry: *in vitro* feasibility studies. J Am Soc Echocardiogr. 5(1):5–12.

Gziut AI. 2006. Comparative analysis of atherosclerotic plaque distribution in the left main coronary artery and proximal segments of left anterior descending and left circumflex arteries in patients qualified for percutaneous coronary angioplasty. Ann Acad Med Stetin. 52(2):51–62.

Han SH, Puma J, García-García HM, Nasu K, Margolis P, Leon MB, Lerman A. 2010. Tissue characterisation of atherosclerotic plaque in coronary artery bifurcations: an intravascular ultrasound radiofrequency data analysis in humans. EuroIntervention. 6(3):313–320.

He X, Ku DN. 1995. Flow in T-bifurcations: effect of the sharpness of the flow divider. Biorheology. 32(4):447–458.

Johnston BM, Johnston PR, Corney S, Kilpatrick D. 2004. Non-Newtonian blood flow in human right coronary arteries: steady state simulations. J Biomech. 37(5):709–720.

Katritsis DG, Theodorakakos A, Pantos I, Andriotis A, Efstathopoulos EP, Siontis G, Karcanias N, Redwood S, Gavaises M. 2010. Vortex formation and recirculation zones in left anterior descending artery stenosis: computational fluid dynamics analysis. Phys Med Biol. 55(5):1395–1411.

Kleinstreuer C, Hyun S, Buchanan JR, Jr, Longest PW, Archie JP, Jr, Truskey GA. 2001. Hemodynamic parameters and early intimal thickening in branching blood vessels. Crit Rev Biomed Eng. 29(1):1–64.

Milnor W. 1989. Hemodynamics. Baltimore: Williams & Wilkins.

Moore JE, Jr, Xu C, Glagov S, Zarins CK, Ku DN. 1994. Fluid wall shear stress measurements in a model of the human abdominal aorta: oscillatory behavior and relationship to atherosclerosis. Atherosclerosis. 110(2):225–240.

Murray CD. 1926. The physiological principle of minimum work: I. The vascular system and the cost of blood volume. Proc Natl Acad Sci USA. 12(3):207–214.

Myers JG, Moore JA, Ojha M, Johnston KW, Ethier CR. 2001. Factors influencing blood flow patterns in the human right coronary artery. Ann Biomed Eng. 29(2):109–120.

Perktold K, Hofer M, Rappitsch G, Loew M, Kuban BD, Friedman MH. 1998. Validated computation of physiologic flow in a realistic coronary artery branch. J Biomech. 31(3):217–228.

Prakash S, Ethier CR. 2001. Requirements for mesh resolution in 3D computational hemodynamics. J Biomech Eng. 123(2):134–144.

Samady H, Eshtehardi P, McDaniel MC, Suo J, Dhawan SS, Maynard C, Timmins LH, Quyyumi AA, Giddens DP. 2011. Coronary artery wall shear stress is associated with progression and transformation of atherosclerotic plaque and arterial remodeling in patients with coronary artery disease. Circulation. 124:779–788.

Shanmugavelayudam SK, Rubenstein DA, Yin W. 2010. Effect of geometrical assumptions on numerical modelling of coronary blood flow under normal and disease conditions. J Biomech Eng. 132:061004.

Smith S. 1997. The scientist and engineer's guide to digital signal processing. California: California Technical Publishing.

Soulis JV, Farmakis TM, Giannoglou GD, Louridas GE. 2006. Wall shear stress in normal left coronary artery tree. J Biomech. 39(4):742–749.

Sun Z, Cao Y. 2011. Multislice CT angiography assessment of left coronary artery: correlation between bifurcation angle and dimensions and development of coronary artery disease. Euro J Radiol. 79(2):e90–e95, doi:10.1016/j.ejrad.2011.04.015.

Sun Z, Chaichana T. 2009. Investigation of the hemodynamic effect of stent wires on renal arteries in patients with abdominal aortic aneurysms treated with suprarenal stent-grafts. Cardiovasc Intervent Radiol. 32(4):647–657.

Sun Z, Chaichana T. 2010. Fenestrated stent graft repair of abdominal aortic aneurysm: hemodynamic analysis of the effect of fenestrated stents on the renal arteries. Korean J Radiol. 11(1):95–106.

Sun Z, Dimpudus FJ, Nugroho J, Adipranoto JD. 2010. CT virtual intravascular endoscopy assessment of coronary artery plaques: a preliminary study. Euro J Radiol. 75(1):e112–e119.

Sun Z, Mwilpatayi B, Chaichana T, Ng C. 2009. Hemodynamic effect of calcified plaque on blood flow in carotid artery disease: a preliminary study. Proc IEEE Bioinformat Biomed Eng 1:1–4.

Sun Z, Winder RJ, Kelly BE, Ellis PK, Hirst DG. 2003. CT virtual intravascular endoscopy of abdominal aortic aneurysms treated with suprarenal endovascular stent grafting. Abdom Imaging. 28(4):580–587.

Sun Z, Winder RJ, Kelly BE, Ellis PK, Kennedy PT, Hirst DG. 2004. Diagnostic value of CT virtual intravascular endoscopy in aortic stent grafting. J Endovasc Ther. 11(1):13–25.

Tang TD, Giddens DP, Zarins CK, Glagov S. 1990. Velocity profile and wall shear measurements in a model human coronary artery. ASME Adv Biomed Eng. 17:261–263.

Thubrikar MJ, Robicsek F. 1995. Pressure-induced arterial wall stress and atherosclerosis. Ann Thorac Surg. 59(6):1594–1603.

van der Giessen AG, Groen HC, Doriot PA, de Feyter PJ, van der Steen AF, van de Vosse FN, Wentzel JJ, Gijsen FJ. 2011. The influence of boundary conditions on wall shear stress distribution in patients specific coronary trees. J Biomech. 44(6):1089–1095.

Vilahur G, Padro T, Badimon L. 2011. Atherosclerosis and thrombosis: insights from large animal models. J Biomed Biotechnol. 2011:907575.

Wellnhofer E, Osman J, Kertzscher U, Affeld K, Fleck E, Goubergrits L. 2010. Flow simulation studies in coronary arteries – impact of side-branches. Atherosclerosis. 213(2):475–481.

Chapter 5

Investigation of the haemodynamic environment of bifurcation plaques within the left coronary artery in realistic patient models based on CT images. Australasian Physical & Engineering Sciences in Medicine 35 (2), 231-236.

Thanapong Chaichana, Zhonghua Sun and James Jewkes

Australas Phys Eng Sci Med (2012) 35:231–236
DOI 10.1007/s13246-012-0135-3

TECHNICAL PAPER

Investigation of the haemodynamic environment of bifurcation plaques within the left coronary artery in realistic patient models based on CT images

Thanapong Chaichana · Zhonghua Sun · James Jewkes

Received: 17 November 2011 / Accepted: 31 March 2012 / Published online: 17 April 2012

Abstract The aim of this study was to investigate the plaques at the left coronary artery (LCA) and their effect on the haemodynamic and wall shear stress (WSS) in realistic patient models. Three sample patients with left coronary disease were selected based on CT data. The plaques were present at the left anterior descending and left circumflex branches with more than 50 % lumen narrowing. Computational fluid dynamics analysis was used to perform simulation of patient-specific models with realistic physiological conditions that demonstrate in vivo cardiac flow. WSS and blood flow in the LCA were measured during cardiac cycles. Our results showed that WSS was found to increase at the stenotic locations and decrease at pre- and post-plaque locations, whilst the recirculation location was found at post-plaque regions. There is a strong correlation between coronary bifurcation plaques and hemodynamic and WSS changes, based on the realistic coronary disease models.

Keywords Atherosclerosis · Haemodynamic · Computational fluid dynamics · Coronary artery disease · Plaques

T. Chaichana · Z. Sun (✉)
Discipline of Medical Imaging, Department of Imaging and Applied Physics, Curtin University, GPO Box U1987, Perth, WA 6845, Australia
e-mail: z.sun@curtin.edu.au

J. Jewkes
Fluid Dynamics Research Group, Department of Mechanical Engineering, Curtin University, Perth, WA 6845, Australia

Introduction

Computed tomography (CT), a non-invasive medical imaging modality, is increasingly used to diagnose coronary artery disease (CAD), in particular, the evaluation of coronary plaques with regard to their effect on a patient's prognosis [1, 2]. The emergence of multislice coronary computed tomography angiography (CCTA) and the latest CT scanners, has enabled CAD, and coronary plaque detection with high diagnostic accuracy [1, 2]. However, it is limited to the anatomical details and is unable to provide the haemodynamic changes in the coronary artery due to the presence of plaques. The CCTA has been used to characterise the different compositions of coronary plaques, with similar diagnostic value when compared to intravascular ultrasound [3]. Computational fluid dynamics (CFD) has overcome the limitations of CT imaging, and previous studies have used CFD to analyse the haemodynamic parameters in reconstructed coronary arteries, to indicate a plaque's progression [4, 5].

Haemodynamic variation is an important factor which influences the change of static pressure and wall shear stress (WSS) in the artery, thus enabling the investigation of the development of atherosclerotic plaques [6–8]. Coronary plaques are generally formed at bifurcation locations, as confirmed by previous studies [6–11]. The plaques commonly form at the left anterior descending (LAD) and left circumflex (LCX) [9, 12] and lead to the lumen narrowing with at least 50 % stenosis, inducing myocardial ischemic changes [7, 13]. Therefore, the study of the local blood flow changes due to plaques at left coronary bifurcation in realistic vascular geometry can provide an improved understanding of their effect. The purpose of this study was to investigate the corresponding influence of plaques on hemodynamic variations at coronary bifurcations, with specific patients in CAD.

Materials and methods

Patient data selection

Three patients with suspected CAD underwent multi-slice coronary CT angiography and were selected for this study, based on CT findings. CT data was processed to reconstruct the 3D left coronary artery (LCA) models. All patients had clinical symptoms of typical chest pain and a history of hypertension. Coronary CT angiography showed significant lumen stenosis caused by plaques in the LCA and its branches. The patient demographics are shown Table 1. At least 60 % lumen stenosis was noticed at the LAD and LCX, since more than 50 % lumen narrowing leads to significant blood flow variations within the CAD [7]. The original sample patient's volume CT data was collected in "DICOM format". The calcified plaque-locations were analysed with use of a 3D visualisation tool, virtual intravascular endoscopy (VIE), to visualise the stenosis lumen in the sample specific-patients as shown in Fig. 1. The commercial biomedical imaging software Analyze 7.0 (Analyze Direct, Inc., Lexana, KS, USA) was used to identify plaque locations at the bifurcations, and segment the LCA and its branches. These medical imaging techniques were applied to generate 3D LCA models with object-map creations, manual hand editing, and segmented post-processing techniques, with details having been described in previous studies [14, 15]. The 3D LCA surfaces were created, consisting of left main stem (LMS), LAD, LCX and its side-branches. The 3D LCA surfaces were saved in "Binary STL format" for generation of the computational models.

In summary, four plaques were simulated in these three selected patients, with two plaques simulated in the LAD and LCX in patient 1, one plaque in the LAD in patient 2,

Table 1 Patient characteristics in three selected patients with suspected CAD

No.	Age (years)	Sex	Degree of coronary stenosis due to plaques		Left bifurcation angle (°)
			LAD (%)	LCX (%)	
A	55	Male	>50	>50	95
B	59	Female	>70	>50	133
C	52	Male	>50	<50	140

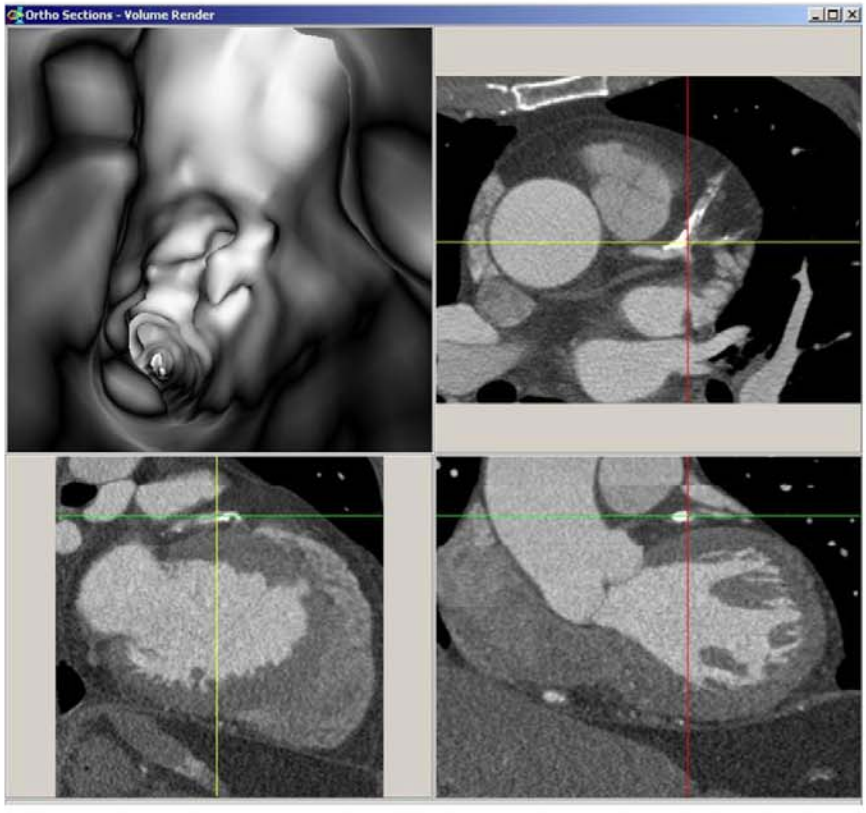

Fig. 1 CT VIE imaging was generated to identify the calcified plaque locations at the bifurcation in the LCA (*top left* image). Extensive calcified plaque is demonstrated at the LAD on 2D axial (*top right* image), and coronal and sagittal views (*bottom left* and *right* images)

and another plaque in the left bifurcation in the remaining patient.

Computational left coronary and plaques modelling

Patient's binary STL files were transferred to computer workstation, and Blender version 2.48 (Blender Institute, Amsterdam, the Netherlands) was used for reconstruction purposes. The LCA surfaces were gently smoothed to reduce any non-physical artefacts caused by sharp edges. Patient's surface models were kept to the original rough surface geometry, however unwanted anatomical structures (such as bones, soft tissues) and digital artefacts were removed. The computational LCA models that were used in this study are shown in Fig. 2. LCA models were saved into "STL format" for mesh generation. ANSYS ICEM CFD version 12 (ANSYS, Inc., Canonsburg, PA, USA) was used to generate the computational elements of the study models (details having been described in previous studies [6, 16, 17]). The LCA models were configured with a hexahedral mesh of $\sim 1 \times 10^6$ nodes and 9×10^5 elements, while the plaque-sections were configured with a tetrahedral mesh of around 1.5×10^4 nodes and 7.8×10^4 elements. Meshing models were saved in 'GTM format' for computation of haemodynamic analysis.

Computational hemodynamic analysis

A time dependent simulation was computed, using realistic physiological boundary conditions to model the actual in vivo conditions. The accurate boundary conditions of pulsatile flow velocity and pressure were calculated based on Fourier series equations, reconstructed from pulsatile graphs taken from McDonald's Blood Flow in Arteries [18] using Matlab (MathWorks, Inc. Natick, MA, USA). The velocity and pressure profiles were applied at the main inlet (LMS) and outlets (LAD and LCX), respectively, for all study LCA models [6]. Rheological properties were applied with a blood density of 1,060 kg/m^3, blood viscosity of 0.0035 Pa s [19, 20] and plaque was assumed to be a rigid body [21]. No-slip conditions were applied at the coronary walls, and blood was assumed to be Newtonian. Blood flow was assumed to be laminar and incompressible [22]. ANSYS CFX version 12 (ANSYS, Inc., Canonsburg, PA, USA) was used to solved the Navier–Stokes equations by ~ 100 iterations per time-step within 1.0 s of pulsatile flow and pressure (1 time-step is representing 0.0125 s). A converged solution was obtained for a residual target of less than 0.1×10^{-3}, and the computational time consumption was roughly 2 h for each study case. The hemodynamic profiles and WSS were calculated and visualised using ANSYS CFD-Post version 12 (ANSYS, Inc.).

Results

Effect of plaques on blood flow at the left coronary bifurcation

The current study was performed based on in vivo physiological conditions during cardiac cycles. The

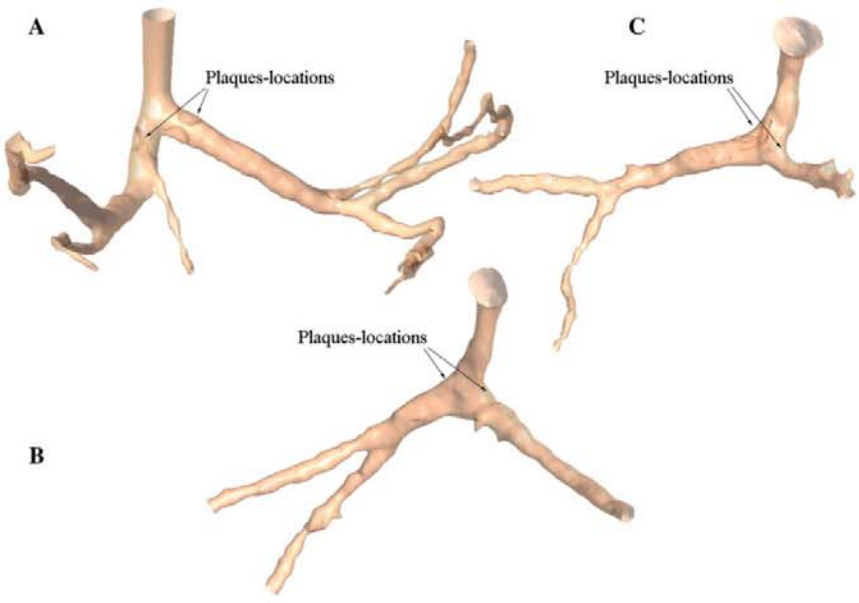

Fig. 2 The reconstructed patient-specific left coronary models have been used in this analysis and these models correspond to the patients in Table 1

peak systolic and mid diastolic phases were indicated at the time of 0.4 and 0.7 s, respectively. The results of this simulation show the influence of bifurcation plaques located at the LAD and LCX branches on hemodynamic changes. Figure 3 demonstrates the plaque's effect on flow velocity patterns at the left bifurcation. The 10 coloured levels were used to show the velocity values which ranged from 0 to 30.5 mm/s. The LCA model with patient's diseased bifurcation plaques demonstrated a significant increase of flow velocity at the plaque locations, which ranged from 27.11 to 30.5 mm/s (peak systolic) and 23.72 to 27.11 mm/s (mid diastolic, not shown). Highest velocity was reached at LAD and LCX branches where coronary plaques resulted in significant lumen narrowing. The recirculating regions were found at post-plaque locations in the LAD and LCX (Fig. 3).

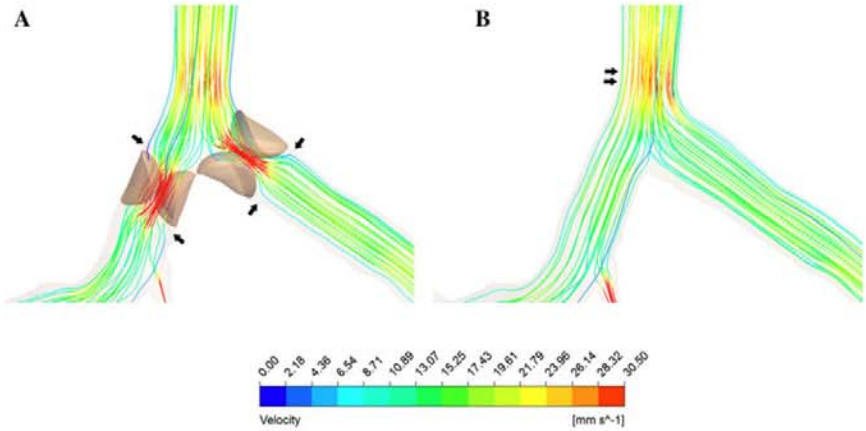

Fig. 3 Visualisation of velocity streamlines of Patient 'A' with presence of coronary plaques (**a**) and without plaques (**b**) during the systolic peak of 0.4 s. *Arrows* indicate the regions of low flow velocity which occurred at pre- and post-plaque positions. *Double arrows* reveal the regions of high flow velocity

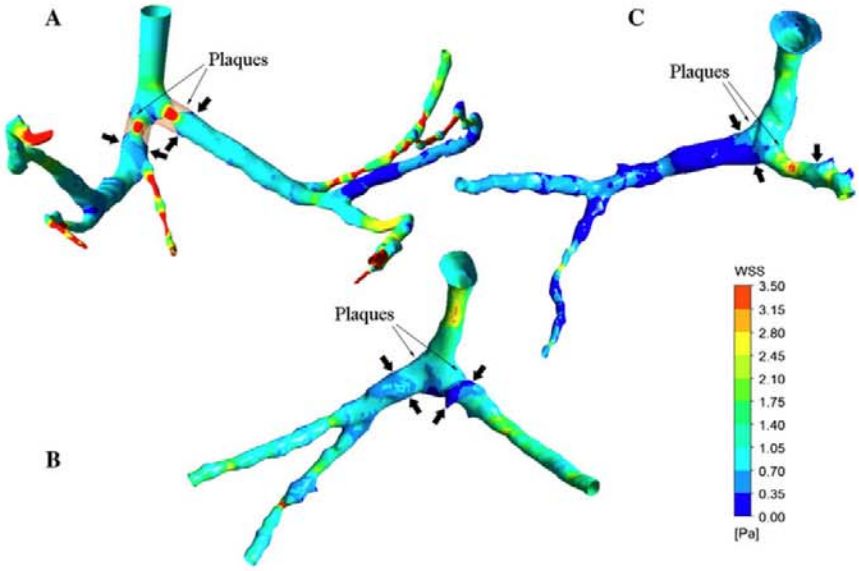

Fig. 4 Visualisation of WSS of the three patients with the coronary plaques condition during the systolic peak of 0.4 s. *Arrows* indicate the regions of low WSS which occurred at pre- and post-plaque positions

Effect of plaques on WSS at the left coronary bifurcation

Calculated WSS was visualised at the velocity peak of the systolic and diastolic phases, as shown in Fig. 4. The contour of 10 coloured scales was used to show the WSS values, which ranged from 0 to 3.50 Pa (Fig. 4). WSS distributions in all three patients were similar, with high WSS values ranging from 3.15 to 3.50 Pa at the plaque locations (Fig. 4). Low WSS was found at pre- and post-plaque locations (values ranged from 0 to 0.70 Pa).

Discussion

This study shows that bifurcation plaques can produce significant haemodynamic effects on blood flow and WSS

changes in realistic patient-specific models of the LCA. The results of this study provide a clinical understanding of coronary plaques with regard to their subsequent effect on blood flow, which could lead to the worsening of atherosclerosis. Plaques are usually located at the bifurcated regions, and early studies have shown that plaques form at the coronary bifurcation [6–12]. The current medical imaging modality of CT is limited to anatomical details, but fails to analyse the haemodynamic and WSS changes [1–3, 9]. Computational analysis of reconstructed coronary vessels is available to detect blood flow and WSS changes in the restricted conditions of modern imaging diagnosis [6, 16, 17].

This study investigated two main areas: flow velocity and WSS, and quantified the effects of bifurcation plaques on haemodynamic factors in patient-specific LCA models. Selected patient's artery geometry was reconstructed to generate the LCA models with significant lumen stenosis. High WSS regions (Fig. 4) were found at the stenotic locations and this seems to indicate that the potential plaques may rupture at high WSS locations [23]. Low WSS locations (Fig. 4) were found at pre- and post- plaque locations, these causes may lead to the progression of plaques [6–8]. Flow velocity was increased at stenotic locations, and recirculating flow was displayed at post-plaque locations (as shown in Fig. 3). According to the haemodynamic analysis, the plaques tend to develop at post-plaque locations, in low flow velocity, recirculating regions [6–8]. Our investigation provides an insight into the effect of bifurcation plaques at LAD and LCX branches on the haemodynamic parameters and demonstrates the subsequent haemodynamics surrounding plaque locations.

Recent studies have presented clinical data regarding the distribution of high-risk plaques in human coronary arties [24, 25] and focal development of atherosclerosis was related to the plaque configuration in the bifurcation regions. It has been shown that the stenoses in left coronary bifurcations may cause haemodynamic and WSS variations to the main coronary arteries and their side-branches [26, 27]. The role of WSS distribution is associated with plaque progression, and a region of high WSS has been considered contributing to the rupture and thrombosis in atherosclerotic plaques, while the location of low WSS may lead to developed progression of plaque area [28]. Our results are in line with these reports as we noticed the high WSS at the stenotic positions and low WSS at the pre- and post-plaque conditions. These findings are valuable for improving understanding of the effects of plaques, and consequently the mechanisms underlying the development of atherosclerosis.

Patient-specific LCA models of CFD analysis have some limitations that should be addressed. The simulation did not consider the elasticity of the coronary wall. The surface of the stenoses was assumed to be smooth and this assumption has been shown to be reasonable in this case [26]. Furthermore, the assumption of a non-Newtonian viscosity can be important in low flow areas. However, assumption of a rigid coronary wall is reasonable in this configuration [22]. Furthermore, patient-specific LCA models were limited as only three patients were included in this study. It is possible that plaques only occur at one side of the coronary artery, resulting in stenosis. Future studies with inclusion of more coronary models with different configurations based on a more realistic idealized geometry should be performed.

In conclusion, we performed a computational analysis of bifurcation plaques in the realistic LCA with coronary disease, at bifurcation locations between LAD and LCX. There is a direct influence of bifurcation plaques in the LCA on haemodynamic and WSS changes, such as recirculating flow, low flow velocity regions, and high WSS, indicating the potential risk for plaques to rupture. Further studies focusing on the larger populations of patient-specific left coronary disease should be performed to verify our results.

References

1. Sun Z, Dimpudus FJ, Nugroho J, Adipranoto JD (2010) CT virtual intravascular endoscopy assessment of coronary artery plaques: a preliminary study. Eur J Radiol 75:e112–e119
2. Australian Institute of Health and Welfare (2006) Australia's health 2006. AIHW, Canberra
3. Feuchtner GM, Cury RC, Jodocy D, Friedrich GJ, Blumenthal RS, Budoff MJ, Nasir K (2011) Differences in coronary plaques composition by noninvasive computed tomography in individuals with and without obstructive coronary artery disease. Atherosclerosis 215:90–95
4. Ribicki FJ, Melchionna S, Mitsouras D, Coskun AU, Whitmore AG, Steigner M, Nallamshetty L, Welt FG, Bernaschi M, Borkin M, Sircar J, Kaxiras E, Succi S, Stone PH, Feldman CL (2009) Prediction of coronary artery plaque progression and potential rupture from 320-detector row prospectively ECG-gated single heart beat CT angiography: Lattice Boltzmann evaluation of endothelial shear stress. Int J Cardiovasc Imaging 25:289–299
5. Shanmugavelayudam SK, Rubenstein DA, Yin W (2010) Effect of geometrical assumptions on numerical modelling of coronary blood flow under normal and disease conditions. ASME J Biomech Eng 132:061004
6. Chaichana T, Sun Z, Jewkes J (2011) Computation of hemodynamics in the left coronary artery with variable angulations. J Biomech 44:1869–1878
7. Fuster V (1994) Lewis A. Conner memorial lecture. Mechanisms leading to myocardial infarction: insights from studies of vascular biology. Circulation 90:2126–2146
8. Asakura T, Karino T (1990) Flow patterns and spatial distribution of atherosclerotic lesions in human coronary arteries. Circ Res 66:1045–1066
9. Sun Z, Cao Y (2011) Multislice CT angiography assessment of left coronary artery: correlation between bifurcation angle and dimensions and development of coronary artery disease. Eur J Radiol 79:e90–e95

10. Han SH, Puma J, Garcia-Garcia HM, Nasu K, Margolis P, Leon MB, Lerman A (2010) Tissue characterisation of atherosclerotic plaque in coronary artery bifurcations: an intravascular ultrasound radiofrequency data analysis in humans. EuroIntervention 6:313–320
11. Gziut AI (2006) Comparative analysis of atherosclerotic plaque distribution in the left main coronary artery and proximal segments of left anterior descending and left circumflex arteries in patients qualified for percutaneous coronary angioplasty. Ann Acad Med Stetin 52:51–62
12. Kimura BJ, Russo RJ, Bhargava V, McDaniel MB, Peterson KL, DeMaria AN (1996) Atheroma morphology and distribution in proximal left anterior descending coronary artery: in vivo observations. J Am Coll Cardiol 27:825–831
13. Cho GY, Lee CW, Hong MK, Kim JJ, Park SW, Park SJ (2001) Effects of stent design on side branch occlusion after coronary stent placement. Catheter Cardiovasc Interv 52:18–23
14. Sun Z, Winder RJ, Kelly BE, Ellis PK, Hirst DG (2003) CT virtual intravascular endoscopy of abdominal aortic aneurysms treated with suprarenal endovascular stent grafting. Abdom Imaging 28:80–587
15. Sun Z, Winder RJ, Kelly BE, Ellis PK, Kennedy PT, Hirst DG (2004) Diagnostic value of CT virtual intravascular endoscopy in aortic stent grafting. J Endovasc Ther 11:3–25
16. Sun Z, Chaichana T (2010) Fenestrated stent graft repair of abdominal aortic aneurysm: hemodynamic analysis of the effect of fenestrated stents on the renal arteries. Korean J Radiol 11:95–106
17. Sun Z, Chaichana T (2009) Investigation of the hemodynamic effect of stent wires on renal arteries in patients with abdominal aortic aneurysms treated with suprarenal stent-grafts. Cardiovasc Intervent Radiol 32:647–657
18. Nichols W, O'Rourke M (2005) McDonald's blood flow in arteries. Hodder Arnold, London, pp 326–327
19. Boutsianis E, Dave H, Frauenfelder T, Poulikakos D, Wildermuth S, Turina M, Ventikos Y, Zund G (2004) Computational simulation of intracoronary flow based on real coronary geometry. Eur J Cardiothorac Surg 26:248–256
20. Milnor W (1989) Hemodynamics. Williams & Wilkins, Baltimore
21. Sun Z, Mwilpatayi B, Chaichana T, Ng C (2009) Hemodynamic effect of calcified plaque on blood flow in carotid artery disease: a preliminary study. IEEE Proc Bio Biomed Eng 1:1–4
22. Johnston BM, Johnston PR, Corney S, Kilpatrick D (2004) Non-Newtonian blood flow in human right coronary arteries: steady state simulations. J Biomech 37:709–720
23. Slager CJ, Wentzel JJ, Gijsen FJH, Thury A, van der Wal AC, Schaar JA, Serruys PW (2004) The role of shear stress in the destabilization of vulnerable plaques and related therapeutic implications. Nat Clin Prac Cardiovasc Med 2:456–464
24. Cheruvu PK, Finn AV, Gardner C, Caplan J, Goldstein J, Stone GW, Virmani R, Muller JE (2011) Frequency and distribution of thin-cap fibroatheroma and ruptured plaques in human coronary arteries: a pathologic study. J Am Coll Cardiol 50:940–949
25. Diletti R, Onuma Y, Farooq V, Gomez-Lara J, Brugaletta S, van Geuns RJ, Regar E, de Bruyne B, Dudek D, Thuesen L, Chevalier B, McClean D, Windecker S, Whitbourn R, Smits P, Koolen J, Meredith I, Li D, Veldhof S, Rapoza R, Garcia-Garcia HM, Ormiston JA, Serruys PW (2011) 6-Month clinical outcomes following implantation of the bioresorbable everolimus-eluting vascular scaffold in vessels smaller or larger than 2.5 mm. J Am Coll Cardiol 58:258–264
26. Chaichana T, Sun Z, Jewkes J (2012) Impact of plaques in the left coronary artery on wall shear stress and pressure gradient in coronary side branches. Comput Methods Biomech Biomed Eng. doi:10.1080/10255842.2012.671308
27. Chaichana T, Sun Z, Jewkes J (2012) Computational fluid dynamics analysis of the effect of plaques in the left coronary artery. Comput Math Methods Med 2012:504367
28. Samady H, Eshtehardi P, McDaniel MC, Suo J, Dhawan SS, Maynard C, Timmins LH, Quyyumi AA, Giddens DP (2011) Coronary artery wall shear stress is associated with progression and transformation of atherosclerotic plaque and arterial remodeling in patients with coronary artery disease. Circulation 124:779–788

Chapter 6

Conclusions and Future Directions

6.1 Conclusions

In this thesis, the research has applied the idea of investigating the biomechanics of human coronary artery in relation to healthy and diseased conditions by using computational fluid dynamics. This research has used coronary artery models to reveal haemodynamic changes and predict coronary disease progression. In addition, diseased coronary artery models were generated and analysed, and have shown that further progression may lead to plaque rupture. Results from this study have shown significant clinical impact as we demonstrated the correlation between coronary angulation and development of coronary artery disease, effect of plaques on coronary flow. The research outcomes were summarised as follows:

1. Computational fluid dynamic analysis of a healthy left coronary artery to predict the atherosclerotic initiation;
    - In this section, the investigation has been performed using a healthy left coronary artery with a unique configuration, showing an angulation between left circumflex and left anterior descending branches. The study was divided into two parts: i) simulation and analysis of idealised left coronary geometries with various angulations, including 120°, 105°, 90°, 75°, 60°, 45°, 30°, 15°, ii) analysis of realistic left coronary geometries with various angulations, and comparison with to the idealised left coronary models. The research has demonstrated that the left coronary artery represented the direct effects between the unique angle and haemodynamic changes surrounding the main bifurcations. The wide angle in the left coronary bifurcation (>80°) may lead to disturbed flow patterns, low wall shear stress and a wall shear stress gradient; these are the indicators of the possible locations of the formation of atherosclerotic plaques.

2. Computation fluid dynamic analysis of the diseased left coronary artery was conducted, to characterise the haemodynamic environment at the plaque location in the left main coronary bifurcation;
    - In this section, diseased left coronary artery models were generated based on a patient's data, and haemodynamic changes were analysed to characterise the haemodynamic variations surrounding the bifurcation plaques. The realistic plaques were simulated in the left main coronary bifurcation. The research findings have indicated that these bifurcation plaques influenced the haemodynamic changes at pre- and post- stenotic. The influence of plaque is observed in the left coronary artery, through haemodynamic variations such as disturbed flow, low flow velocity regions, wall shear stress, and wall pressure gradient. Theses haemodynamic parameters are indicators of the potential for plaques to rupture. There is a direct correlation between the plaques and subsequence haemodynamic changes, based on the simulation of plaques in the realistic coronary models.
3. Haemodynamic analysis of the plaques at the main bifurcation in left coronary artery disease;
    - In this section, models of the diseased left main coronary artery were generated and analysed to characterise the possible haemodynamic changes to their side branches. This research finding demonstrated that the bifurcation plaques in the realistic left coronary artery have influenced haemodynamic variations, such as wall shear stress and wall pressure stress gradient in coronary side branches. The study was based on actual three-dimensional luminal left coronary geometry. There are changes to wall shear stress and wall pressure stress gradient, indicating the possible development of plaques in coronary trees. Our results improve our understanding of the development of atherosclerotic plaques by further exploring their impact on the left coronary artery and its side branches.

4. Computational analysis of patient-specific models with left coronary artery disease to characterise the haemodynamic factors surrounding the plaque regions.
    - In this final section, patient-specific models with the left coronary artery disease were produced and analysed to characterise haemodynamic parameters near to the stenotic regions. The bifurcation plaques were located between left anterior descending and left circumflex. The research findings showed that the bifurcation plaques have a direct effect upon haemodynamic complications such as disturbed flow, low flow velocity regions, and high wall shear stress. These parameters changes indicated the potential risk for plaques to rupture.

6.2 Future Directions

This study improves our understanding of the biomechanics of the human coronary artery under normal and diseased conditions. Moreover, these findings will assist in diagnosis and prevention of coronary artery disease. However, there are a few suggestions for the further research, which are detailed as follows:

- Studies focusing upon patients with different lengths of left main stem branches of the left coronary bifurcation should be performed to investigate the relationship between coronary length and haemodynamic changes.
- Research focusing on the different types of realistic bifurcation plaque in the left coronary artery should be performed to investigate haemodynamic changes.
- Studies based on a large population of patient-specific left coronary disease should be performed to verify our results.
- Further studies focusing on the various positions of realistic plaques at the bifurcation with patient-specific left coronary disease, particularly their local impact on haemodynamic changes, should be conducted to stratify patient risk and predict disease outcome.
- Simulation of different plaque components, especially non-calcified plaque with aim of identifying vulnerable plaques.

Appendix I

Additional publications by the candidate relevant to the thesis but not forming part of it

Appendix I-A: Hemodynamic analysis of the effect of different types of plaque in the left coronary artery.

Hemodynamic analysis of the effect of different types of plaque in the left coronary artery

Thanapong Chaichana[1], Zhonghua Sun[1], James Jewkes[2]

1. Discipline of Medical Imaging, Department of Imaging and Applied Physics, Curtin University, Perth, Western Australia, Australia, 6845

2. Fluid Dynamics Research Group, Department of Mechanical Engineering, Curtin University, Perth, Western Australia, Australia, 6845

Corresponding author:

Dr Zhonghua Sun, Ph.D.

Associate Professor

Discipline of Medical Imaging, Department of Imaging and Applied Physics, Curtin University, GPO Box, U1987, Perth, Western Australia 6845, Australia

Tel: +61-8-9266 7509

Fax: +61-8-9266 2377

Email: z.sun@curtin.edu.au

Abstract

In this study we investigate the hemodynamic effects of various types of plaque in the left coronary bifurcation. Eight types (A-H) of plaque were simulated and located in various positions in the left main stem, the left anterior descending and left circumflex to produce a >50% narrowing of the coronary lumen. We analyse and characterise hemodynamic effects caused by each type of plaque. Computational fluid dynamics was performed to simulate realistic physiological conditions that reveal the *in vivo* cardiac hemodynamics. Velocity, wall shear stress (WSS) and pressure gradient (PSG) in the left coronary artery were calculated and compared in all plaque configurations during cardiac cycles. Our results showed that the highest velocity and PSG were found at the location where all of the three left coronary branches were affected by a type D plaque configuration. Plaques located in the left circumflex (Type G) resulted in a highly significant velocity, WSS and PSG ($P < 0.001$) change when compared to the other types of plaque configuration. Our analysis provides an insight into the distribution of plaque at the left bifurcation, and corresponding hemodynamic effects, thus, improving our understanding of atherosclerosis.

Keywords: computational fluid dynamics, plaque, pressure gradient, hemodynamic, coronary bifurcation

Table of Content

1. Introduction

The angulation of the left coronary bifurcation has an affect upon blood flow that might lead to the development of atherosclerotic plaque. A recent study has shown that wide angulations can significantly increase disturbances to the flow field that are associated with the progression of coronary plaque [7]. Plaques most commonly originate in the left coronary bifurcation [30]. Various types of bifurcation plaque lesions have been classified by Topol [37], with special attention paid to the important distinction between a true bifurcation (consisting of the main branch and the side branch) and a pseudo bifurcation (which includes all of the other lesions involving a bifurcation). These distinctions are a key element in the proper planning of treatment. Cases with a lumen narrowing of >50% were considered hemodynamically significant [37], since this level of narrowing results in significant hemodynamic changes to the flow within the coronary artery [12].

Previous studies used computational fluid dynamics (CFD) to investigate the hemodynamic changes due to the severity of stenosis [22], [29]. The results of these studies confirmed that a stenosis of <50% coronary diameter due to plaque formation has a minimal effect on the flow-field inside the coronary artery. A recent study on the effect of plaque distributed in the left coronary bifurcation showed that there is a direct effect on the flow parameters at stenotic locations [8], [9], [10]. It is important for us to understand the hemodynamic patterns with the differing types of bifurcation plaque, since the different plaque positions may lead to various hemodynamic effects, although this has not been systematically studied. To the best of our knowledge, there are no publications related to the investigation of hemodynamic variations based on the plaque configuration classification. Thus, this work aims to study the hemodynamic changes due to the different types of bifurcation plaque

(Figure 1), based on realistic coronary models. It is expected that the research findings will provide potential value for improving our understanding of the flow field induced by these various bifurcation plaques, and contribute to our understanding of the pathogenesis of coronary artery disease.

2. Material and Methods

2.1. Patient information and left coronary artery geometry

A 47-year-old male with suspected coronary artery disease (CAD) was selected in this study to provide the realistic left coronary bifurcation geometry, including its side branches. The patient's CT volume data was used to create left coronary artery (LCA) geometry. Image segmentation and post-processing techniques were performed using Analyze 7.0 (Analyze Direct, Inc., Lexana, KS, USA). Scan-related artefacts and unwanted soft tissues were manually removed in 2D axial slices [35], [36]. Figure 2 demonstrates the realistic LCA model and the rectangle box refers to the effective plaque locations (EPLs). EPL represents the flow changes in the LCA surrounding the plaque-locations. LCA geometry was created for the various EPLs in the left main bifurcation, consisting of the left main stem (LMS), left anterior descending (LAD), left circumflex (LCx), and its side branches. Dimensions of the LCA geometry were measured and shown in Table 1. The geometry of the arteries around the LMS, LAD and LCx was obtained from the sample patient with suspected CAD (plaque type F as shown in Figure 1), although normal anatomical structures were shown on the CT images at the LMS and LAD branches. LCA surface geometry, comprising of plaque and normal coronary arteries, were changed into solid models and saved in 'STL format' for the computational meshing procedure.

2.2. Various plaque positions in the left coronary bifurcation

Calcified plaque was generated at different anatomical locations in the left bifurcation, as shown in Figure 1. This has been based on the bifurcation lesions reported in previous studies [37], [11]. There were 8 plaque configurations simulated altogether, with a type F plaque being the first model, based directly upon the selected patient's anatomical structures. The other 7 types were subsequently adapted from this configuration. Figure 3 shows the eight different configurations of realistic plaque, generated to study the flow effects. The geometry of the type F plaques at the LCx branches shows that the dimensions of each section were 1.14 mm in height, a mean width of 3.76 mm and a thickness of 1.46 mm and 1.53 mm (from left to right in Figure 3). In addition, the geometry of other types of plaque at the LAD branches comprised of two sections, 1.17 mm in height, a mean width of 3.59 mm and a thickness of 1.38 mm and 1.56 mm (from left to right in Figure 3). Although plaques contain different components depending on the concentration of calcium [31], only hard plaque (calcified plaque) was simulated in this study since this type of plaque is commonly seen in patients with coronary artery disease, and calcified plaque indicates the atherosclerotic changes to the coronary wall, leading to significant stenosis. The simulation of hard plaque is suitable for demonstrating the hemodynamic changes at the ELP in this case. Finally, the diseased condition was simulated with the generation of eight models with variable types of bifurcation plaque, and one baseline model without the presence of plaque is also simulated. There were nine LCA geometries in total.

2.3. Computational flow and solution

The STL models were divided into LCA geometry and plaque sections, and plaque models were merged with the LCA models in the various location combinations. These combined STLs were then used to create a volume mesh using the ANSYS

ICEM CFD hexahedral meshing tool (details having been described in previous studies [7], [32], [33]. Mesh resolution for the various models ranged from 9×10^5 to 9.8×10^5 cells. The baseline LCA geometry model (without plaques) was created using the same process, yielding 9.5×10^5 cells. A mesh independence case was produced and solved for this baseline model at approximately twice the resolution; this demonstrated agreement with the lower resolution mesh applied in this study.

Unsteady simulations were performed (similar to Chaichana et al. [7], [9]), pulsatile velocity (Figure 4a) was applied as an inflow boundary condition at the left main stem [4], [22]. The outflow boundary condition was applied with the flow ratio through the six side-branches (Figure 2) at the LAD (SB1, 2 and 3) and LCx (SB4, 5 and 6) according to side-branches diameters (Table 1) [15], [38]. The outflow relationship is also known as Murray's law and the summation of outflow conditions through the side-branches is equal to the flow at the inlet [26]. Rheological parameters were applied with a blood density of 1060 kg/m^3, blood viscosity of 0.0035 Pa s [6], [24]. Plaques and blood-vessels were assumed to be rigid [33]. Blood flow was assumed to be laminar. A no-slip condition was applied at the walls [25]. The blood was assumed to be Newtonian and incompressible [5], [21]. The Navier-Stokes equations were solved using the ANSYS CFX CFD package (version 12 - ANSYS, Inc.), on a Microsoft Windows 7 32-bit machine, 6 GB of RAM with a Xeon W3505 2.53 GHz CPU. The CFD simulation was run for 64 time-steps, representing 0.8s of phasic coronary blood flow rate (0.0125s per time-step). The CFD simulation was converged to a residual target of less than 1×10^{-4} per time-step in each LCA model. ANSYS CFD-Post version 12 (ANSYS, Inc.) was used to calculate and visualise flow velocity, pressure gradient (PSG) and wall shear stress (WSS).

The PSG is calculated from the local static pressure, to characterise the high amplitude pressure changes at the EPL. The static pressure at stenotic locations is similar to the pressure at the coronary inlet and is poorly suited to the classification of the pressure effects [14]. The PSG is defined as:

$$\mathrm{PSG} = \sqrt{\left(\frac{\partial p}{\partial x}\right) + \left(\frac{\partial p}{\partial y}\right) + \left(\frac{\partial p}{\partial z}\right)} \tag{1}$$

where p is local static pressure in the area of interest, x, y, and z are points in the Cartesian coordinates. PSG has been shown to be a significant indicator of coronary disease [13], [14].

The WSS is a commonly used parameter in hemodynamic analysis; endothelial cells have been shown to align themselves with the flow direction that corresponds to the local WSS. The coordinates of the wall surface elucidate the interaction of instantaneous WSS vectors and endothelial cells [23].

$$\mathrm{WSS} = \frac{1}{T}\int_0^T \left| \mu \frac{\partial v_t}{\partial_n} \right| dt \tag{2}$$

where μ is blood viscosity, v_t is velocity vector near wall perpendicular to surface and n is distance to the wall surface, T is pulsatile period, dt is the time derivative of the local shear stress.

2.4. Statistical analysis of hemodynamic parameters

Hemodynamic parameters were exported in “CSV format” from ANSYS CFD-Post version 12 (ANSYS, Inc.). The WSS, PSG and velocity were entered into SPSS 17.0 (SPSS, Inc., Chicago, IL, USA) for statistical analysis. A p-value of <0.05 was considered to indicate statistically significant differences. A one way Analysis of Variance (ANOVA) between groups with post-hoc comparisons was used for

analysis of hemodynamic factors to determine the differences among the eight types of bifurcation plaque.

3. Results

3.1. Statistical comparison of major hemodynamic parameters

There were significant differences in the majority of hemodynamic factors (WSS, PSG and velocity) between comparisons of the eight types of bifurcation plaque as tested with one way ANOVA ($P < 0.05$: significant; $P < 0.001$: highly significant), shown in Table 2. However, there was no significant difference in WSS and PSG parameters between type A and type B and type C ($P > 0.05$). Similarly, no significant differences were found in WSS and PSG between type F, and types A, B and C ($P > 0.05$). For the comparisons between the remaining types, most of them demonstrated significant differences.

3.2. Comparison of cross-sectional velocity

The fifteen cross-sections were defined, as shown in Figure 4b, with the type D plaque shown as an example. These cross-sections were applied to the other seven types of plaque configuration, and to the baseline. The cross-sections were divided into three groups, each group having five sectional-planes: sections A-E at the LMS, sections F-J at the LAD and sections K-O at the LCx respectively. Table 3 shows the comparisons of cross-sectional averaged velocity at the EPL for the eight types of bifurcation plaque. In the systolic phase, type A has the two sections of plaque-intersection (PIN) ( ) at sections C and E, and one section of the exclusive plaque-intersection (EPIN) ( ) at section D. In addition, a high average velocity in section D was reached, from 11.04 mm s^{-1} to 11.77 mm s^{-1} as shown in types A, C, D and F, and there is a minimal velocity change when compared to the normal velocity, which reached at 8.90 mm s^{-1}. Section G in the types B, D, E, F and H was the EPIN with

velocity ranged from 11.43 mm s^{-1} to 13.61 mm s^{-1}, showing extremely high average velocity when compared to the normal velocity, reached at 4.13 mm s^{-1}. Furthermore, section L in the types B, C, D and G was also the EPIN with velocity ranged from 17.84 mm s^{-1} to 19.82 mm s^{-1}, demonstrating extremely high average velocity when compared to the normal velocity reached at 5.18 mm s^{-1}. The type H configuration was found to have very similar average cross-sectional velocity values in both systolic and diastolic phases, to those observed during the normal flow condition. Similar results were noticed in the diastolic phase for the comparisons of average cross-sectional velocity, except for type G, showing apparently high average velocity in all sections when compared to other types of plaque.

3.3. Velocity inside the left coronary artery

To characterise the hemodynamic variations of different types of bifurcation plaque at the left coronary artery, velocity patterns were calculated and compared in all eight types of bifurcation plaque and the baseline, as shown in Figure 5 and 6. The plots were chosen to reveal the flow effects at the EPL. The velocity patterns were calculated and visualised at a systolic phase of 0.2 s (Figure 5) and the diastolic phase of 0.7 (Figure 6). The velocity values ranged from 0 mm s^{-1} to 30.50 mm s^{-1}, corresponding to fifteen contour levels, approximately 2.2 mm s^{-1} per level. Figure 5 shows high velocity in the red and yellow contour levels, which ranged from 28.23 mm s^{-1} to 30.50 mm s^{-1} at the stenotic locations (specifically in types A, C and G, as these types had the plaque at the LMS and LCx branches). In addition, the bifurcation plaque involving the LMS and LAD branches (especially for types E, F and H) show high velocity regions at LMS branch and the LAD branch (stenotic positions), ranging from 21.79 mm s^{-1} to 23.98 mm s^{-1}. Type B had the bifurcation plaque located in the LAD and LCx branches, and high velocity was observed at the

LCx, and the LAD around the stenotic regions. Type D has the bifurcation plaque positioned in LMS, LAD and LCx branches, it generated similar flow effects to the other types, with the high velocity regions near plaque locations at the LMS and LCx branches, and the LAD branch. Figure 6 shows the flow in the systolic phase, however there are more regions of high velocity in the stenotic locations at LMS, LAD and LCx branches. Thus, the recirculation regions were found downstream of plaque locations in all types of bifurcation plaque and in both systolic and diastolic phases.

3.4. Pressure gradient in the left coronary artery

PSG was calculated at the systolic phase of 0.2 s and diastolic phase of 0.7 s, and displayed within coronary at ELP in order to compare the PSG changes for all eight cases. PSG values ranged from -15 $kg/m^2\ s^2$ to 500 $kg/m^2\ s^2$, corresponding to 15 contour levels. Figure 7 reveals PSG variations with the types of bifurcation plaque and normal condition during the diastolic phase (0.7 s). The high PSG was found in all types of bifurcation plaque at the stenotic locations, with values ranging from 463.21 $kg/m^2\ s^2$ to 500.00 $kg/m^2\ s^2$. Large distribution of high PSG was found in the type D configuration. The high PSG was also found at post-plaque locations, and this was particularly apparent in types A, C, D and F. The type G was found to be different from the other types in terms of PSG changes due to only the involvement of the LCx, and this is consistent with statistical comparisons as shown in Table 3 (type G had significant differences when compared to the other types). Figure 8 reveals the comparison of PSG in all types of bifurcation plaque configurations with the baseline, during the systolic phase (0.2 s). The high PSG at stenotic locations ranged 352.86 $kg/m^2\ s^2$ to 389.64 $kg/m^2\ s^2$. Thus, PSG variations were distributed in the same pattern as that observed in the diastolic phase (Figure 7).

4. Discussion

This study reveals that the various types of bifurcation plaque influence the subsequent hemodynamic parameters in the left coronary bifurcation, resulting in flow changes. This finding provides additional information about the hemodynamic effect of coronary plaque, hence, it improves our understanding of the atherosclerotic changes due to the presence of plaque at different coronary locations.

The classification system was considered to be a practical way of dealing with the various bifurcation lesions, allowing us to make distinctions between the various bifurcation geometries [37]. In this study, we investigated the hemodynamic effects of these plaques, and determined whether there exists a statistically significant difference in variable parameters. Our results showed that types A, G and H (plaque located in each LMS, LCx and LAD branches) cause less severe hemodynamic variations around the bifurcation than the other types (B, C, D, E and F). In addition, type D causes more significant flow variations at the coronary bifurcation than the other seven types of bifurcation plaque. These findings provide an insight into the effect of plaque position upon resulting hemodynamics in the left coronary artery.

Coronary plaque generally originates in the bifurcation region due to the angulations. The angulations cause a region of low WSS, as confirmed by our study and previous reports [2], [7], [12], [18], [19], [30], [37]. Medical imaging modality such as intravascular ultrasound and mutislice CT coronary angiography has been commonly used to detect plaque locations in the left main coronary artery [16], [17], [28], [31]. These imaging techniques provide valuable diagnostic information, such as assessment of plaque components and corresponding coronary lumen changes, however, they offer no tangible insight into the resultant hemodynamics. Computational fluid dynamics provides an opportunity to predict the hemodynamic

behaviour [7], [20], [23]. Thus, the characterisation of hemodynamic variations due to the various types of bifurcation plaque in the configurations can be further explored with flow visualisations; this exceeds the classical anatomical analysis of coronary stenosis or occlusion.

This study visualised the wall shear stress, velocity and pressure gradient inside the left coronary bifurcations, and compared the hemodynamic parameters between each groups for the types of bifurcation plaque statistically. We found that plaque type G was very different compared to the other types of plaque. Types D and H were found to produce different velocity, WSS and PSG distributions compared to the other types. Types A, B, C and F were very similar in velocity, WSS and PSG, compared to the plaque types D, E, F and H. Type E was found to have PSG similar to the other types. Our results indicate that different types of plaque demonstrate various hemodynamic effects, although most of the types are statistically significantly different from the other types, as shown in tables 2 and 3. Some types of plaque caused unique effects, for example, type D causing huge velocity variations. Type A showed limited velocity variations compared to the baseline. Thus, it is clinically important to understand the different types of plaque and their corresponding hemodynamic effects.

In the clinical situation, the PSG magnitude has been used to assess the severity of plaques [1], [27]. The highest PSG region may indicate the location of a potential coronary plaque rupture. The type D configuration has shown the largest distribution of high PSG at the bifurcation and thus, this type is potentially more dangerous than the other types during diastolic phases (Figure 7). PSG inside the coronary artery was used to characterise the impacts of plaque in the left main coronary bifurcation. The hemodynamic factors were shown as velocity patterns and PSG, for the analysis of

changes inside the coronary artery at the main bifurcation. WSS was analysed in this study, however it was not shown visually and was only used for the statistical analysis, as shown in Table 2.

There are some limitations to this study that should be addressed. Firstly, the blood model was assumed to have a Newtonian viscosity. Our study focused on the hemodynamic visualisation of the coronary artery and this assumption has been shown to be reasonable by previous studies [3], [21]. Secondly, realistic LCA geometries were assumed to have a rigid wall rather than an elastic wall; hence, the simulation does not completely reflect the realistic physiological behaviour, as the coronary wall is moving during cardiac cycles. Thirdly, a single patient has been selected for the generation of various types of bifurcation plaque and coronary models. Despite this limitation, the simulated models represent realistic coronary geometry, and accordingly, our results are still valid for clinical applications. Future studies will analyse realistic plaque at the bifurcation based on different patients' data.

5. Conclusion

This study investigates the different types of bifurcation plaque in the realistic left coronary artery and visualises the velocity patterns and PSG variations within left main coronary bifurcation. Statistical analysis has been performed to compare the hemodynamic factors for characterisation of various plaque types at bifurcation regions. Plaque type G demonstrates significant differences in hemodynamic parameters when compared to the other types. Velocity and PSG are increased when the left coronary bifurcation contains more plaque, and this is especially apparent with type D. The research findings of this study indicate that extra plaque located in left coronary bifurcation may increase the risk of plaque rupture.

6. References

[1] Anderson, H.V., Roubin, G.S., Leimgruber, P.P., Cox, W.R., Douglas. JS. Jr., King, S.B. 3rd, Gruentzig, A.R., 1986. Measurement of transstenotic pressure gradient during percutaneous transluminal coronary angioplasty. Circulation 73(6), 1223-1230.

[2] Asakura, T., Karino, T., 1990. Flow patterns and spatial distribution of atherosclerotic lesions in human coronary arteries. Circulation Research 66, 1045-1066.

[3] Ballyk, P.D., Steinman, D.A., Ether, C.R., 1994. Simulation of non-Newtonian blood flow in an end-to-end anastomosis. Biorheology 31(5), 565-586.

[4] Berne, R.M., Levy, M.N., 2001. Cardiovascular physiology. Mosby, St Louis MI.

[5] Borghi, A., Wood, N.B., Mohiaddin, R.H., Xu, X.Y., 2008. Fluid-solid interaction simulation of flow and stress pattern in thoracoabdominal aneurysms: a patient-specific study. Journal of Fluids and Structures 24, 270-280.

[6] Boutsianis, E., Dave, H., Frauenfelder, T., Poulikakos, D., Wildermuth, S., Turina, M., Ventikos, Y., Zund, G., 2004. Computational simulation of intracoronary flow based on real coronary geometry. European Journal of Cardio-Thoracic Surgery 26(2), 248-256.

[7] Chaichana, T., Sun, Z., Jewkes, J., 2011. Computation of haemodynamics in the left coronary artery with variable angulations. Journal of Biomechanics 44(10), 1869-1878.

[8] Chaichana. T., Sun, Z., Jewkes, J., 2012. Computational fluid dynamics analysis of the effect of plaque in the left coronary artery. Computational and Mathematical Methods in Medicine 2012, 504367.

[9] Chaichana, T., Sun, Z., Jewkes, J., 2012. Impact of plaques in the left coronary artery on wall shear stress and pressure gradient in coronary side branches. Computer Methods in Biomechanics and Biomedical Engineering, DOI: 10.1080/10255842.2012.671308.

[10] Chaichana, T., Sun, Z., Jewkes, J., 2012. Investigation of the haemodynamic environment of bifurcation plaques within the left coronary artery in realistic

patient models based on CT images. Australasian Physical & Engineering Sciences in Medicine 35(2), 231-236.

[11] Cho, G.Y., Lee, C.W., Hong, M.K., Kim, J.J., Park, S.W., Park, S.J., 2001. Effects of stent desing on side branch occlusion after coronary stent placement. Catheterization and Cardiovascular Interventions 52(1), 18-23.

[12] Fuster, V., 1994. Lewis A. Conner memorial lecture. Mechanisms leading to myocardial infarction: insights from studies of vascular biology. Circulation. 90(4), 2126-2146.

[13] Garcia, D., Pibarot, P., Louis-Gilles, D., 2005. Analytical modeling of the instantaneous pressure gradient across the aortic valve. Journal of Biomechanics 38(6), 1303-1311.

[14] Garcia. D., Kadem. L., Savéry, D., Pibarot, P., Durand, L.G., 2006. Analytical modeling of the instantaneous maximal transvalvular pressure gradient in aortic stenosis. Journal of Biomechanics 39(16), 3036-3044.

[15] Giannoglou, G.D., Soulis, J.V., Farmakis, T.M., Giannakoulas, G.A., Parcharidis, G.E., Louridas, G.E., 2005. Wall pressure gradient in normal left coronary artery tree. Medical Engineering & Physics 27(6), 455-564.

[16] Gijsen, F.J., Wentzel, J.J., Thury, A., Lamers, B., Schuurbiers, J.C., Serruys, P.W., van der Steen, A.F., 2007. A new imaging technique to study 3-D plaque and shear stress distribution in human coronary artery bifurcations in vivo. Journal of Biomechanics 40(11), 2349-2357.

[17] Grayburn, P.A., Willard, J.E., Haagen, D.R., Brickner, M.E., Alvarez, L.G., Eichhorn, E.J., 1992. Measurement of coronary flow using high-frequency intravascular ultrasound imaging and pulsed Doppler velocimetry: in vitro feasibility studies. Journal of the American Society of Echocardiography 5(1), 5-12.

[18] Gziut, A.I., 2006. Comparative analysis of atherosclerotic plaque distribution in the left main coronary artery and proximal segments of left anterior descending and left circumflex arteries in patients qualified for percutaneous coronary angioplasty. Annales Academiae Medicae Stetinensis 52(2), 51-62.

[19] Han, S.H., Puma, J., García-García, H.M., Nasu, K., Margolis, P., Leon, M.B., Lerman, A., 2010. Tissue characterisation of atherosclerotic plaque in

coronary artery bifurcations: an intravascular ultrasound radiofrequency data analysis in humans. EuroIntervention 6(3), 313-320.

[20] He. X., Ku, D.N., 1995. Flow in T-bifurcations: effect of the sharpness of the flow divider. Biorheology 32(4), 447-458.

[21] Johnston, B.M., Johnston, P.R., Corney, S., Kilpatrick, D., 2004. Non-Newtonian blood flow in human right coronary arteries: steady state simulations. Journal of Biomechanics 37(5), 709-720.

[22] Katritsis, D.G., Theodorakakos, A., Pantos, I., Andriotis, A., Efstathopoulos, E.P., Siontis, G., Karcanias, N., Redwood, S., Gavaises, M., 2010. Vortex formation and recirculation zones in left anterior descending artery stenosis: computational fluid dynamics analysis. Physics in Medicine and Biology 55(5), 1395-1411.

[23] Kleinstreuer, C., Hyun, S., Buchanan, J.R. Jr., Longest, P.W., Archie, J.P. Jr., Truskey, G.A., 2001. Hemodynamic parameters and early intimal thickening in branching blood vessels. Critical Reviews in Biomedical Engineering 29(1), 1-64.

[24] Milnor, W., 1989. Hemodynamics. Williams & Wilkins, Baltimore.

[25] Moore, J.E.Jr, Xu, C., Glagov, S., Zarins, C.K., Ku, DN., 1994. Fluid wall shear stress measurements in a model of the human abdominal aorta: oscillatory behavior and relationship to atherosclerosis. Atherosclerosis 110(2), 225-240.

[26] Murray, C.D., 1926. The Physiological Principle of Minimum Work: I. The Vascular System and the Cost of Blood Volume. Proceeding of the National Academy of Science of the United States of America 12(3), 207-214.

[27] Rajabi-Jaghargh, E., Kolli, K.K., Back, L.H., Banerjee, R.K., 2011. Effect of guidewire on contribution of loss due to momentum change and viscous loss to the translesional pressure drop across coronary artery stenosis: an analytical approach. Biomedical Engineering Online 10, 51.

[28] Rodriguez-Granillo, G.A., Rosales, M.A., Degrossi, E., Durbano, I., Rodriguez, A.E., 2007. Multislice CT coronary angiography for the detection of burden, morphology and distribution of atherosclerotic plaque in the left main bifurcation. International Journal of Cardiovascular Imaging 23, 389-392.

[29] Shanmugavelayudam, S.K., Rubenstein, D.A., Yin, W., 2010. Effect of geometrical assumptions on numerical modelling of coronary blood flow under normal and disease conditions. Journal of Biomechanical Engineering 132(6), 061004.

[30] Sun, Z., Cao, Y., 2011. Multislice CT angiography assessment of left coronary artery: Correlation between bifurcation angle and dimensions and development of coronary artery disease. European Journal of Radiology 79(2), e90-e95.

[31] Sun, Z., Dimpudus, F.J., Nugroho, J., Adipranoto, J.D., 2010. CT virtual intravascular endoscopy assessment of coronary artery plaque: A preliminary study. European Journal of Radiology 75(1), e112-e119.

[32] Sun, Z., Chaichana, T., 2010. Fenestrated stent graft repair of abdominal aortic aneurysm: hemodynamic analysis of the effect of fenestrated stents on the renal arteries. Korean Journal of Radiology 11(1), 95-106.

[33] Sun, Z., Chaichana, T., 2009. Investigation of the hemodynamic effect of stent wires on renal arteries in patients with abdominal aortic aneurysms treated with suprarenal stent-grafts. Cardiovascular and Interventional Radiology 32(4), 647-657.

[34] Sun, Z., Mwilpatayi, B., Chaichana, T., Ng, C., 2009. Hemodynamic effect of calcified plaque on blood flow in carotid artery disease: a preliminary study. Proceeding of IEEE Bioinformatics and Biomedical Engineering, 1-4.

[35] Sun, Z., Winder, R.J., Kelly, B.E., Ellis, P.K., Kennedy, P.T., Hirst, D.G., 2004. Diagnostic value of CT virtual intravascular endoscopy in aortic stent grafting. Journal of Endovascular Therapy 11(1), 13-25.

[36] Sun, Z., Winder, R.J., Kelly, B.E., Ellis, P.K., Hirst, D.G., 2003. CT virtual intravascular endoscopy of abdominal aortic aneurysms treated with suprarenal endovascular stent grafting. Abdominal Imaging 28(4), 580-587.

[37] Topol, E.J., 2008. Textbook of interventional cardiology, 5th ed. Saunders Elsevier, Philadelphia, pp. 1075.

[39] van der Giessen, A.G., Groen, H.C., Doriot, P.A., de Feyter, P.J., van der Steen, A.F., van de Vosse, F.N., Wentzel, J.J., Gijsen, F.J., 2011. The influence of boundary conditions on wall shear stress distribution in patients specific coronary trees. Journal of Biomechanics 44(6), 1089-1095.

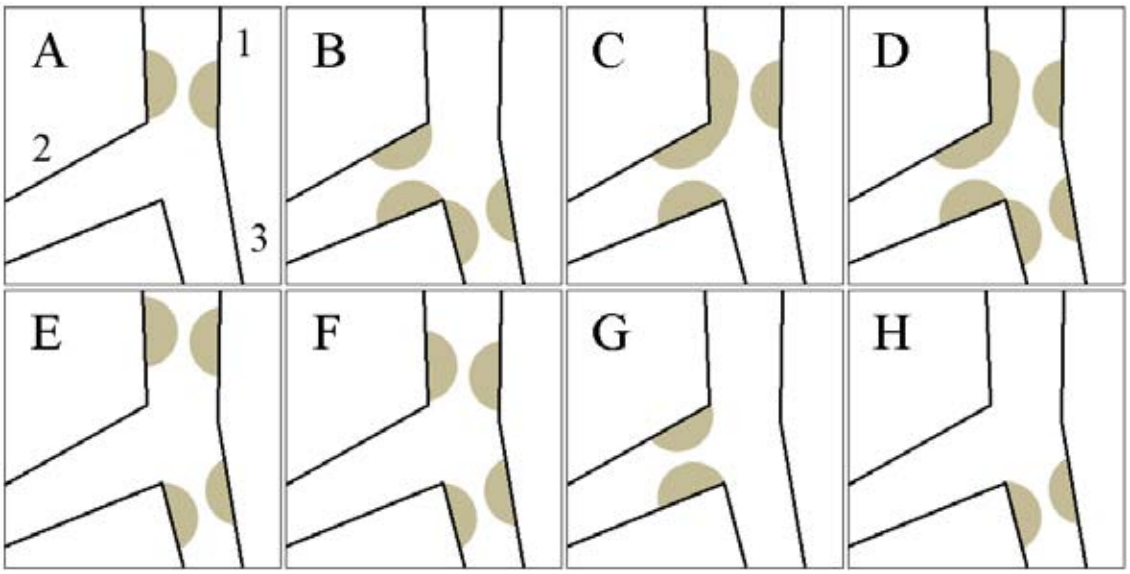

Figure 1. Diagram showing characterization of the eight types of bifurcation plaque in the left coronary artery.

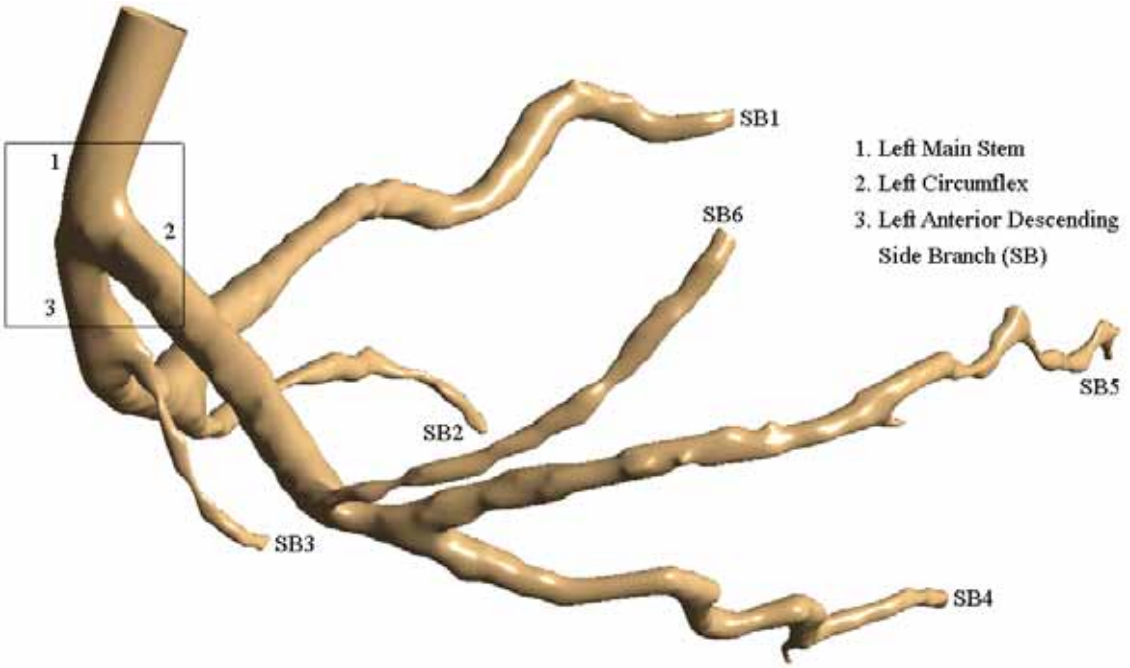

Figure 2. Realistic coronary model showing left coronary artery and its side-branches. The rectangle shows the effective plaque locations where eight types of bifurcation plaque influence hemodynamic variations.

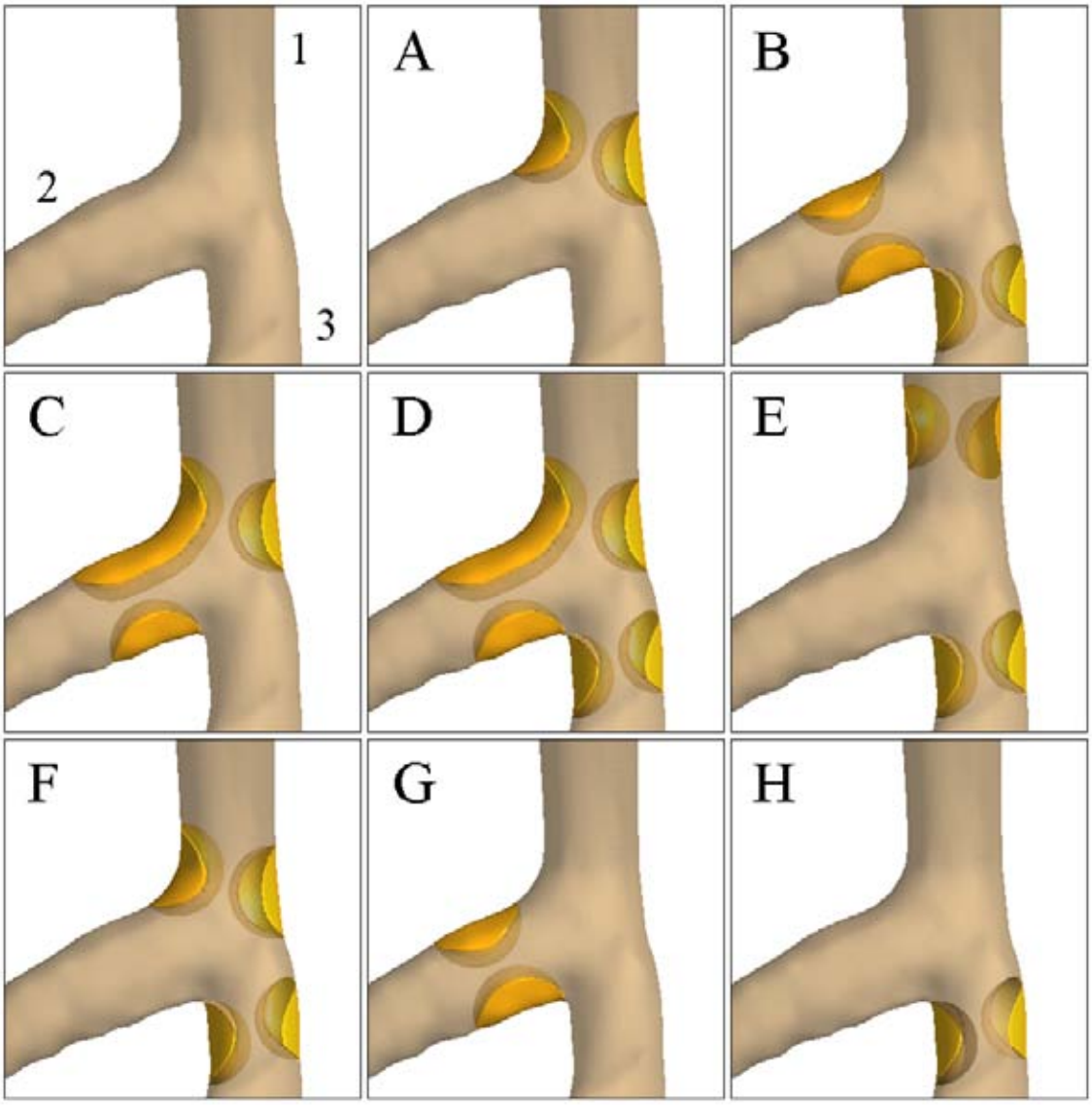

Figure 3. The realistic bifurcation plaque was simulated at different anatomical locations according to the diagram in Figure 1.

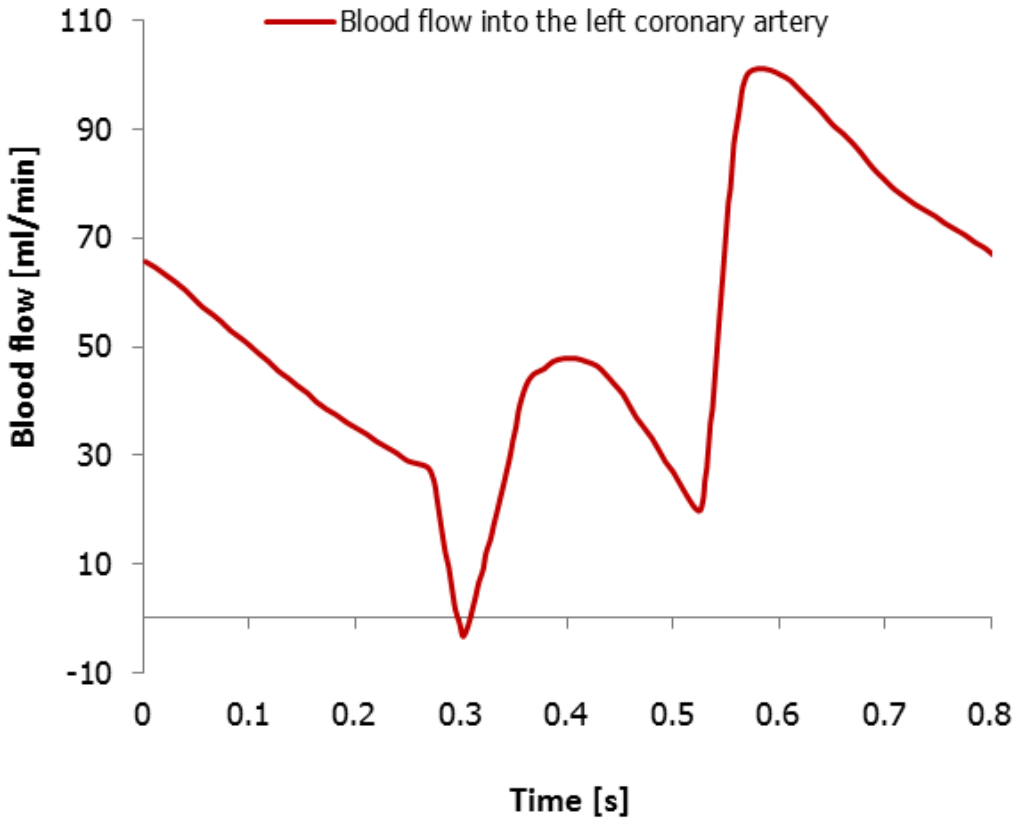

Figure 4a. Pulsatile flow cycle into the left coronary artery.

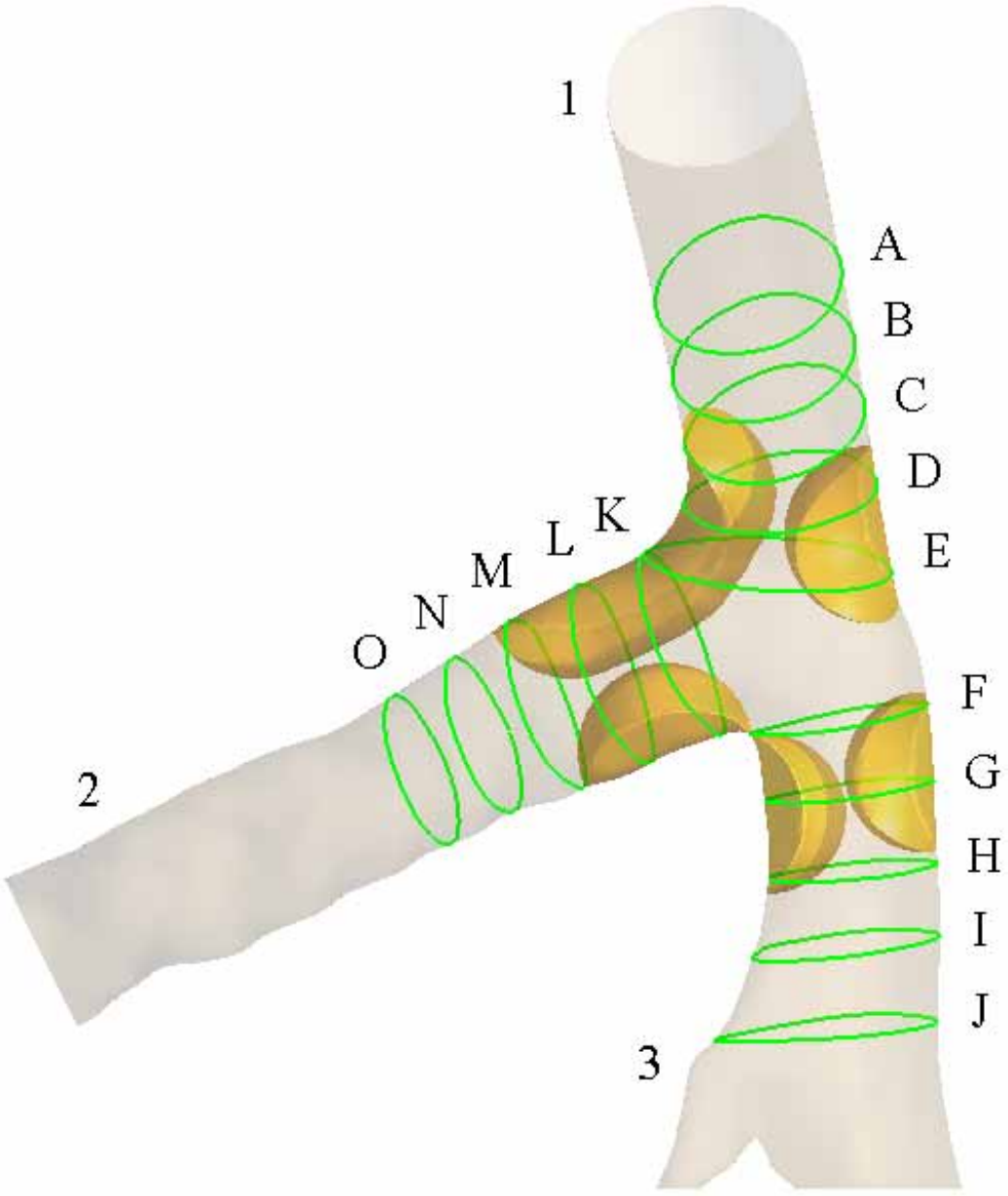

Figure 4b. The fifteen cross-sections were defined to calculate the average velocity inside coronary bifurcation at effective plaque locations.

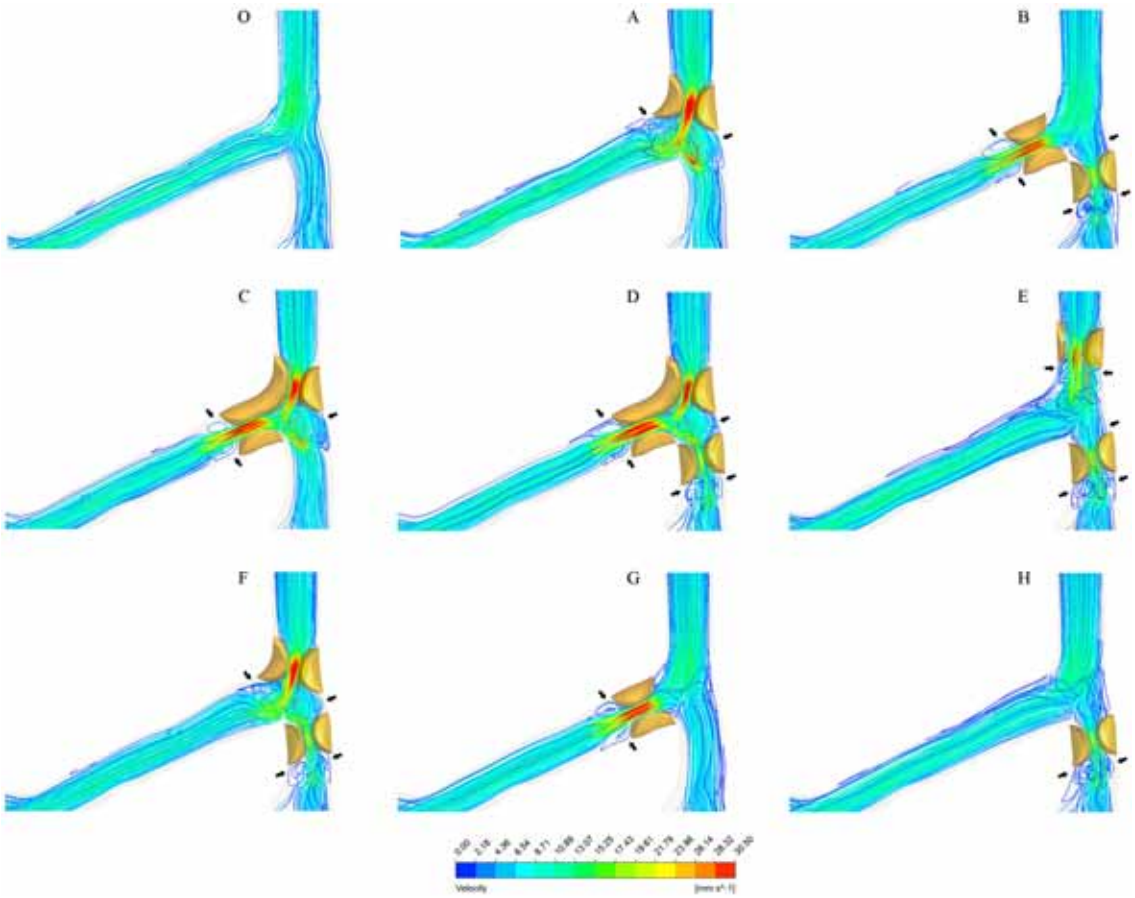

Figure 5. The velocity patterns inside left bifurcation at effective plaque locations with eight types of bifurcation plaque and normal condition during the systolic phase (0.2 s).

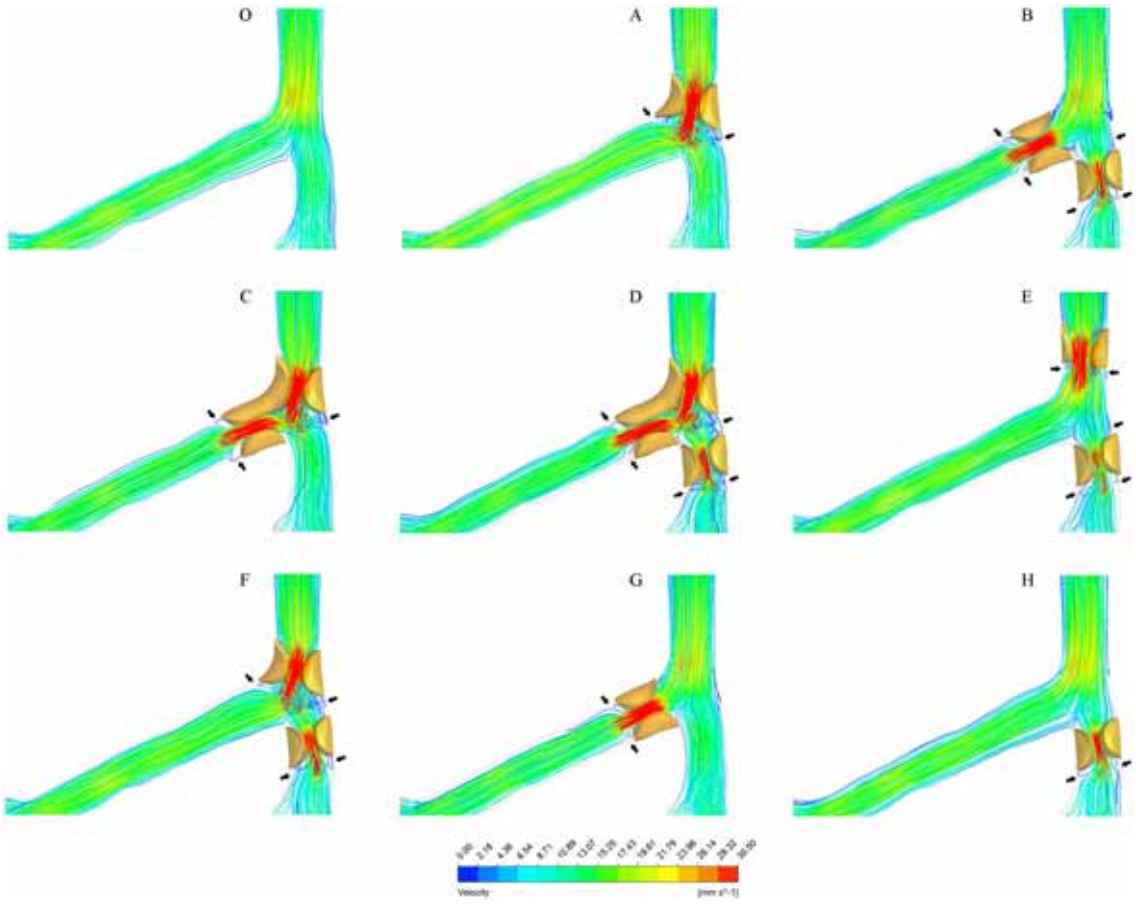

Figure 6. The velocity patterns inside left bifurcation at effective plaque locations with eight types of bifurcation plaque and normal condition during the diastolic phase (0.7 s).

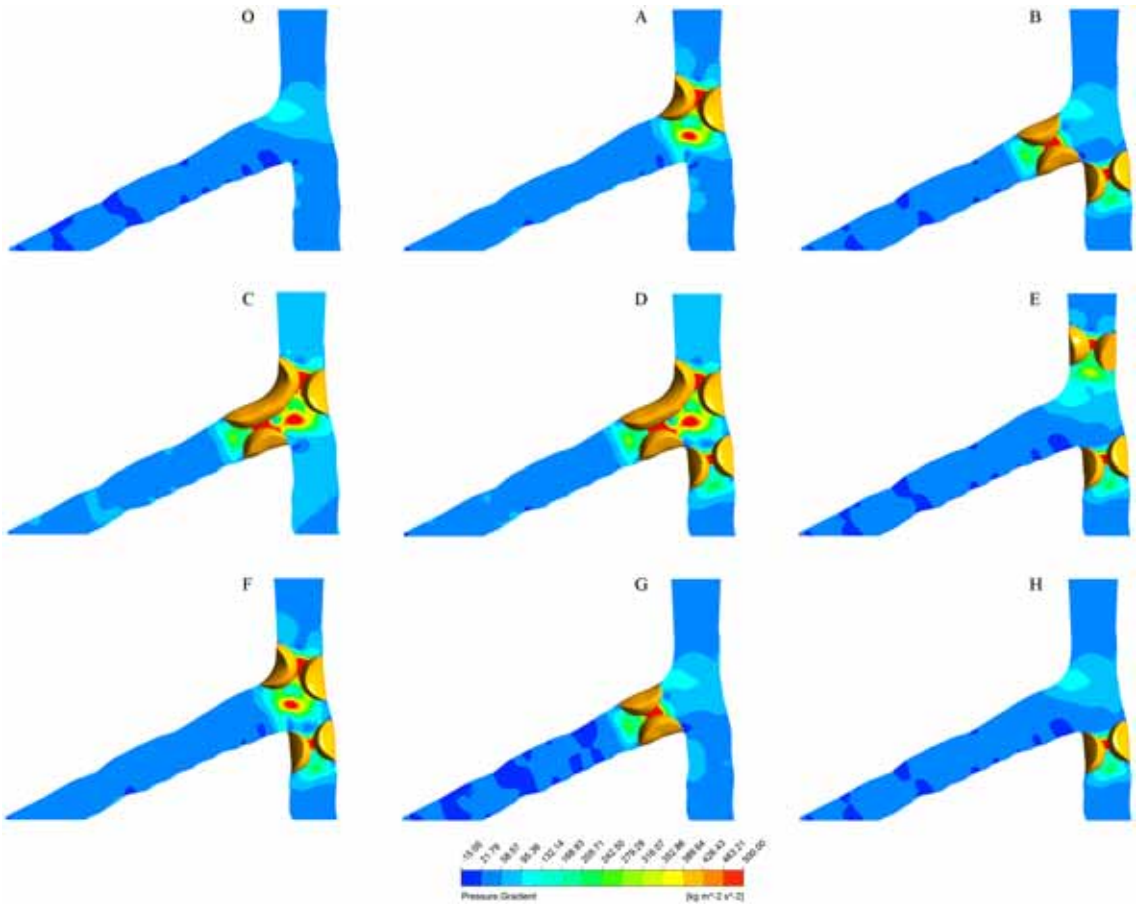

Figure 7. The pressure gradient patterns inside left bifurcation at effective plaque locations with eight types of bifurcation plaque and normal condition during the diastolic phase (0.7 s).

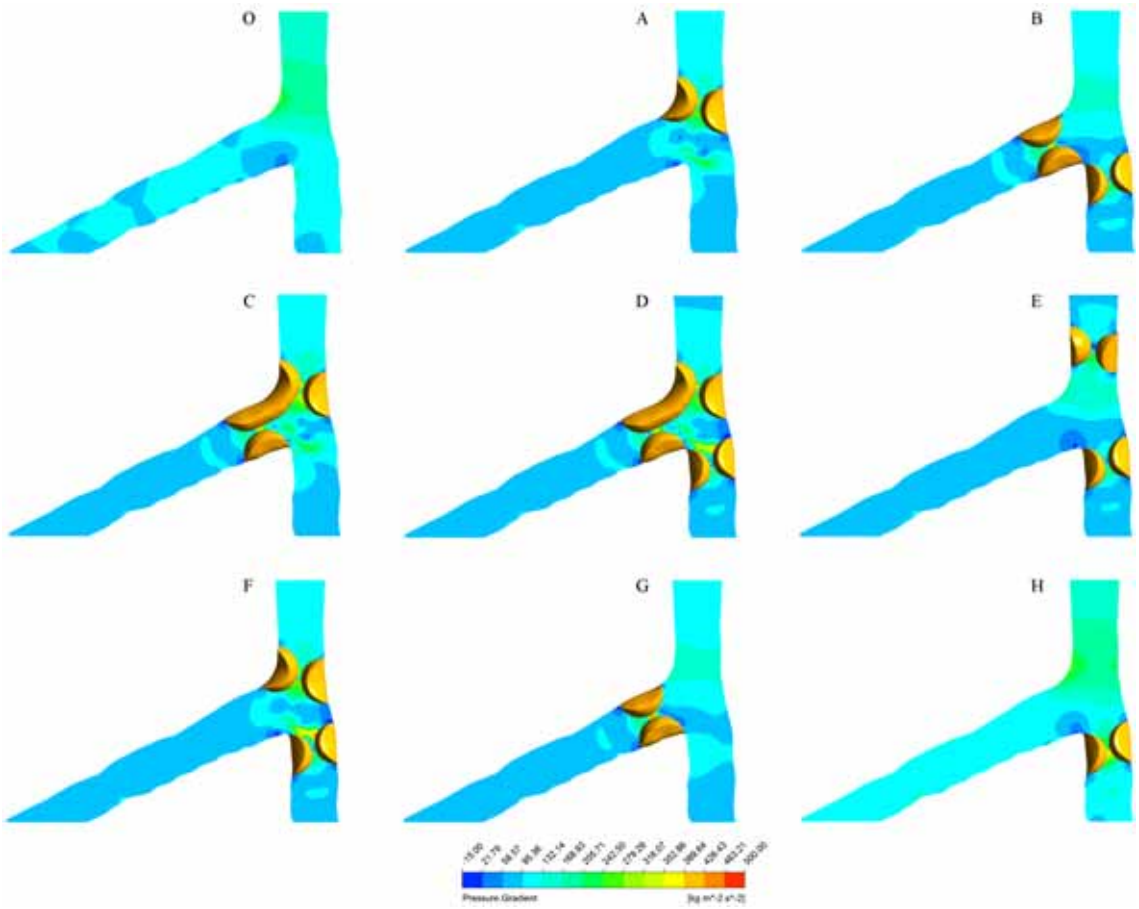

Figure 8. The pressure gradient patterns inside left bifurcation at effective plaque locations with eight types of bifurcation plaque and normal condition during the systolic phase (0.2 s).

Table 1. LCA geometry of mean diameters and lengths of major and side branches

Left coronary artery			Diameters (mm)	Lengths (mm)
LMS	Main branch	Inlet	4.599	29.441
LAD	Main branch		3.763	45.982
LCx	Main branch		3.585	62.303
LAD	Side branch 1	Outlet 1	0.548	124.301
	Side branch 2	Outlet 2	0.348	64.046
	Side branch 3	Outlet 3	0.609	38.452
LCx	Side branch 4	Outlet 4	0.666	104.231
	Side branch 5	Outlet 5	0.358	151.662
	Side branch 6	Outlet 6	0.714	81.386

LMS—left main stem, LAD—left anterior descending, LCx—left circumflex.

Table 2. Patient characteristics: multiple comparisons of major hemodynamic parameters at bifurcation plaques

Plaques-location vs. different types		Hemodynamic parameters (n=65530)					
		WSS		PSG		Velocity	
		mean±SD	*P*	mean±SD	*P*	mean±SD	*P*
A	B	0.064±0.069	1.000	248.077±296.079	0.083	0.0017±0.0016	0.069
	C	0.064±0.068	0.993	246.931±293.696	0.389	0.0016±0.0016	0.997
	D	0.068±0.071	<0.001*	256.960±308.596	<0.001*	0.0015±0.0015	<0.001*
	E	0.066±0.070	<0.05*	249.875±302.564	<0.05*	0.0015±0.0015	<0.001*
	F	0.065±0.069	1.000	246.277±293.437	0.685	0.0016±0.0016	1.000
	G	0.061±0.062	<0.001*	236.070±265.025	<0.001*	0.0016±0.0016	<0.001*
	H	0.068±0.066	<0.001*	255.301±280.550	<0.001*	0.0015±0.0015	<0.001*
B	A	0.064±0.069	1.000	243.480±292.989	0.830	0.0016±0.0016	0.069
	C	0.064±0.068	0.985	246.931±293.696	0.997	0.0016±0.0016	<0.05*
	D	0.068±0.071	<0.001*	256.960±308.596	<0.001*	0.0015±0.0015	<0.001*
	E	0.066±0.070	<0.05*	249.875±302.564	0.954	0.0015±0.0015	<0.001*
	F	0.065±0.069	1.000	246.277±293.437	0.946	0.0016±0.0016	<0.05*
	G	0.061±0.062	<0.001*	236.070±265.025	<0.001*	0.0016±0.0016	<0.001*
	H	0.068±0.066	<0.001*	255.301±280.550	<0.001*	0.0015±0.0015	<0.001*
C	A	0.064±0.069	0.993	243.480±292.989	0.389	0.0016±0.0016	0.997
	B	0.064±0.069	0.985	248.077±296.079	0.997	0.0017±0.0016	<0.05*
	D	0.068±0.071	<0.001*	256.960±308.596	<0.001*	0.0015±0.0015	<0.001*
	E	0.066±0.070	<0.001*	249.875±302.564	0.602	0.0015±0.0015	<0.001*
	F	0.065±0.069	0.937	246.277±293.437	1.000	0.0016±0.0016	0.999
	G	0.061±0.062	<0.001*	236.070±265.025	<0.001*	0.0016±0.0016	<0.001*
	H	0.068±0.066	<0.001*	255.301±280.550	<0.001*	0.0015±0.0015	<0.001*
D	A	0.064±0.069	<0.001*	243.480±292.989	<0.001*	0.0016±0.0016	<0.001*
	B	0.064±0.069	<0.001*	248.077±296.079	<0.001*	0.0017±0.0016	<0.001*
	C	0.064±0.068	<0.001*	246.931±293.696	<0.001*	0.0016±0.0016	<0.001*
	E	0.066±0.070	<0.001*	249.875±302.564	<0.001*	0.0015±0.0015	<0.001*
	F	0.065±0.069	<0.001*	246.277±293.437	<0.001*	0.0016±0.0016	<0.001*
	G	0.061±0.062	<0.001*	236.070±265.025	<0.001*	0.0016±0.0016	<0.001*
	H	0.068±0.066	0.687	255.301±280.550	0.970	0.0015±0.0015	0.924

E	A	0.064±0.069	<0.05*	243.480±292.989	<0.05*	0.0016±0.0016	<0.001*
	B	0.064±0.069	<0.05*	248.077±296.079	0.954	0.0017±0.0016	<0.001*
	C	0.064±0.068	<0.001*	246.931±293.696	0.602	0.0016±0.0016	<0.001*
	D	0.068±0.071	<0.001*	256.960±308.596	<0.001*	0.0015±0.0015	<0.001*
	F	0.065±0.069	<0.05*	246.277±293.437	0.315	0.0016±0.0016	<0.001*
	G	0.061±0.062	<0.001*	236.070±265.025	<0.001*	0.0016±0.0016	<0.001*
	H	0.068±0.066	<0.001*	255.301±280.550	<0.05*	0.0015±0.0015	<0.001*
F	A	0.064±0.069	1.000	243.480±292.989	0.685	0.0016±0.0016	1.000
	B	0.064±0.069	1.000	248.077±296.079	0.946	0.0017±0.0016	<0.05*
	C	0.064±0.068	0.937	246.931±293.696	1.000	0.0016±0.0016	0.999
	D	0.068±0.071	<0.001*	256.960±308.596	<0.001*	0.0015±0.0015	<0.001*
	E	0.066±0.070	<0.05*	249.875±302.564	0.315	0.0015±0.0015	<0.001*
	G	0.061±0.062	<0.001*	236.070±265.025	<0.001*	0.0016±0.0016	<0.001*
	H	0.068±0.066	<0.001*	255.301±280.550	<0.001*	0.0015±0.0015	<0.001*
G	A	0.064±0.069	<0.001*	243.480±292.989	<0.001*	0.0016±0.0016	<0.001*
	B	0.064±0.069	<0.001*	248.077±296.079	<0.001*	0.0017±0.0016	<0.001*
	C	0.064±0.068	<0.001*	246.931±293.696	<0.001*	0.0016±0.0016	<0.001*
	D	0.068±0.071	<0.001*	256.960±308.596	<0.001*	0.0015±0.0015	<0.001*
	E	0.066±0.070	<0.001*	249.875±302.564	<0.001*	0.0015±0.0015	<0.001*
	F	0.065±0.069	<0.001*	246.277±293.437	<0.001*	0.0016±0.0016	<0.001*
	H	0.068±0.066	<0.001*	255.301±280.550	<0.001*	0.0015±0.0015	<0.001*
H	A	0.064±0.069	<0.001*	243.480±292.989	<0.001*	0.0016±0.0016	<0.001*
	B	0.064±0.069	<0.001*	248.077±296.079	<0.001*	0.0017±0.0016	<0.001*
	C	0.064±0.068	<0.001*	246.931±293.696	<0.001*	0.0016±0.0016	<0.001*
	D	0.068±0.071	0.687	256.960±308.596	0.970	0.0015±0.0015	0.924
	E	0.066±0.070	<0.001*	249.875±302.564	<0.05*	0.0015±0.0015	<0.001*
	F	0.065±0.069	<0.001*	246.277±293.437	<0.001*	0.0016±0.0016	<0.001*
	G	0.061±0.062	<0.001*	236.070±265.025	<0.001*	0.0016±0.0016	<0.001*

WSS: Wall shear stress; PSG: Wall pressure gradient; *Significant comparison between stenotic types

Values given are mean±Standard deviation (SD) in following specific stenotic types

Table 3. Patient characteristics: multiple comparison of cross-sectional average velocity at effective plaques-locations

Left coronary artery		Velocity at coronary bifurcation with and without presence of plaques (mm s^-1)								
Physical location	Section	Normal	Type A	Type B	Type C	Type D	Type E	Type F	Type G	Type H
Systolic phase										
LMS	A	4.9426	4.7346	4.8702	4.9212	4.6690	4.7525	4.8360	4.9127	4.7060
	B	5.6617	5.3826	5.5377	5.6366	5.2824	✓ 7.7160	5.5047	5.6221	5.3358
	C	6.9447	✓ 6.8796	6.7661	✓ 7.2482	✓ 6.7422	✓✓ 6.9554	✓ 6.9750	7.0570	6.4041
	D	8.8754	✓✓ 11.0769	8.8526	✓✓ 11.7742	✓✓ 11.0441	✓ 9.0277	✓✓ 11.0614	8.9947	8.6107
	E	6.0109	✓ 9.5840	5.9581	✓ 10.5206	✓ 10.1077	6.6716	✓ 9.9472	5.9611	5.8277
LAD	F	3.9139	9.2165	✓ 5.3040	9.5973	✓ 9.7593	✓ 4.6824	✓ 9.7220	3.9451	✓ 4.4809
	G	*4.1282*	4.1619	✓✓ *13.6144*	4.5091	✓✓ *12.2903*	✓✓ *11.9853*	✓✓ *12.2602*	4.1659	✓✓ *11.4268*
	H	3.8786	3.7550	✓ 5.4653	4.0542	✓ 5.2002	✓ 5.0032	✓ 5.0925	3.9222	✓ 4.9604
	I	3.4298	3.3351	4.9486	3.5882	4.8004	4.6047	4.6186	3.4798	4.5760
	J	3.3243	3.2372	3.5046	3.4788	3.2357	3.0866	3.1712	3.3837	3.0490
LCx	K	5.2697	8.8070	✓ 7.3798	✓ 13.0383	✓ 13.0162	5.1861	8.8961	✓ 7.7061	5.2290
	L	*5.1833*	5.3797	✓✓ *18.8913*	✓✓ *17.8449*	✓✓ *18.0089*	5.0565	5.5283	✓✓ *19.8175*	5.1030
	M	5.4288	5.0420	✓ 6.9221	✓ 6.6866	✓ 6.7750	5.2883	5.1997	✓ 6.9535	5.3272
	N	5.3973	5.0474	6.4363	6.1765	6.3209	5.2554	5.2104	6.3951	5.2911
	O	5.5750	5.2203	5.3584	5.0966	5.1139	5.4229	5.3955	5.5061	5.4627
Diastolic phase										
LMS	A	10.7605	10.3331	10.7989	10.6249	10.4063	10.7016	10.4051	10.8429	10.5388
	B	12.1925	11.6741	12.2083	12.0520	11.7343	✓ 17.4703	11.7475	12.2851	11.8829
	C	13.9887	✓ 13.9348	14.0128	✓ 14.5393	✓ 14.0752	✓✓ 14.6522	✓ 13.9291	14.3221	13.4486
	D	19.0663	✓✓ 23.8734	19.1068	✓✓ 24.7323	✓✓ 23.9235	✓ 18.7828	✓✓ 23.7263	19.3828	18.6836
	E	12.9215	✓ 20.5599	12.9164	✓ 22.3226	✓ 22.0382	13.0396	✓ 20.9767	12.8872	12.7421
LAD	F	8.8536	8.6990	✓ 11.9847	9.3925	✓ 11.3902	✓ 11.2567	✓ 10.9066	9.1209	✓ 10.8257
	G	*9.3425*	8.9656	✓✓ *31.4238*	9.6121	✓✓ *29.1860*	✓✓ *29.2536*	✓✓ *28.1142*	9.6264	✓✓ *28.1677*
	H	8.6898	8.3352	✓ 12.0197	8.9617	✓ 11.4963	✓ 11.2067	✓ 11.0763	8.9665	✓ 10.9212
	I	7.6163	7.2964	8.5477	7.8501	8.0531	7.9518	7.6545	7.8757	7.7069
	J	7.4167	7.0881	7.6645	7.6504	7.2072	7.1358	6.8747	7.6955	6.9523

LCx	K	10.2367	10.6988	✓ 15.7602	✓ 24.4590	✓ 24.7782	10.3724	10.9462	✓ 15.9948	10.3025
	L	*10.3935*	9.8127	✓✓ *39.9110*	✓✓ *37.2152*	✓✓ *37.7786*	10.5364	10.0465	✓✓ *40.5723*	10.4525
	M	10.9170	10.3205	✓ 13.5612	✓ 12.9803	✓ 13.2232	11.0733	10.5727	✓ 13.6086	10.9742
	N	10.8520	10.2724	10.5810	9.9864	10.1203	10.9972	10.5300	10.6979	10.8916
	O	11.1789	10.5892	10.8860	10.3145	10.4139	11.3375	10.8601	11.0044	11.2293

LMS—left main stem, LAD—left anterior descending, LCx—left circumflex.
✓ — Plaques-intersection (PIN), ✓✓ — Exclusive plaques-intersection (EPIN)

Appendix II

Additional publications by the candidate relevant to the thesis but not forming part of it

Appendix I-B: Hemodynamic impacts of various types of stenosis in the left coronary bifurcation: A patient-specific analysis.

Hemodynamic impacts of various types of stenosis in the left coronary bifurcation: A patient-specific analysis

Thanapong Chaichana[1], Zhonghua Sun[1], James Jewkes[2]

1. Discipline of Medical Imaging, Department of Imaging and Applied Physics, Curtin University, Perth, Western Australia, Australia, 6845

2. Fluid Dynamics Research Group, Department of Mechanical Engineering, Curtin University, Perth, Western Australia, Australia, 6845

Corresponding author:

Dr Zhonghua Sun, Ph.D.

Associate Professor

Discipline of Medical Imaging, Department of Imaging and Applied Physics, Curtin University, GPO Box, U1987, Perth, Western Australia 6845, Australia

Tel: +61-8-9266 7509

Fax: +61-8-9266 2377

Email: z.sun@curtin.edu.au

Word count: 2,359

Abstract

This study investigates the hemodynamic changes to various types of coronary stenosis in the left bifurcation, based on a patient-specific analysis. Twenty two patients with left coronary artery disease were included in our study. All stenoses involving the left bifurcation were classified into four types, according to their locations: A) left circumflex (LCx) and left anterior descending (LAD), B) LCx only, C) left main stem only, and D) LAD only. Computational fluid dynamics (CFD) was performed to analyze the flow and wall shear stress (WSS) changes in all reconstructed left coronary geometries. Our results showed that the flow velocity and WSS were significantly increased at stenotic locations. High WSS was found at >70% lumen stenosis, which ranged from 2.5 Pa to 3.5 Pa. This study indicates that WSS plays an important role in providing information about the extent of coronary atherosclerosis in patients with significant stenosis in the left coronary artery branch.

Keywords: Atherosclerosis, coronary artery disease, hemodynamic, wall shear stress

1. Introduction

Hemodynamic parameters cannot be directly measured in vivo; accordingly, computational fluid dynamic analysis has become established as a method to predict hemodynamically induced shear stress in the coronary arteries. Low shear stress normally occurs at the bifurcated region due to the coronary angulation. Recently, wide angled bifurcations have been reported to lead to the development of atherosclerosis [1]. Studies using medical imaging techniques have revealed the distribution of coronary stenosis in the left main bifurcation, and evaluated the relationship between the bifurcation angle and development of coronary disease [2], [3]. It is generally believed that the left coronary artery geometry is more complicated than the right coronary artery since the left side consists of two large main branches forming an angle, with many side-branches [1]. Various configurations of bifurcation stenosis have been classified, that involve the left main coronary bifurcation; identification of the appropriate classification is a significant component in planning the appropriate treatment [4]. Bifurcation stenoses cause considerable lumen narrowing [4]. A stenosis of greater than 50% diameter results in significant flow changes to the coronary artery [5].

Early studies used computational fluid dynamics to analyze a >50% coronary stenosis distributed around the main bifurcation with promising results achieved [6], [7], [8]. Results showed the change of flow parameters at the bifurcated regions, and it produced some effects on the hemodynamic factors in coronary side-braches. Another study investigated the coronary blood flow under the diseased condition, with an assumed degree of stenosis [9], [10]. Despite the use of computer simulation in these studies to investigate the hemodynamic changes in coronary models, there have been no reports about the realistic bifurcation stenosis based on patient-specific

models. In this study, we aim to investigate the hemodynamic patterns and wall shear stress with detection and classification of the types of bifurcation stenosis based on a group of patients with suspected coronary artery disease. Research findings from this study could improve our understanding of hemodynamic effects of various stenosis distributions in the left coronary artery and the pathogenesis of coronary artery disease.

2. Material and Methods

2.1. Patient datasets

Twenty two patients suspected of coronary artery disease (CAD) were selected to represent the presence of stenosis at the left main coronary bifurcation. Patient's characteristics were shown in Table 1. Figure 1 shows an example patient, with a stenosis at the left main stem branch. All patients underwent coronary CT angiography, performed on a 64-slice CT scanner to allow the acquisition of high resolution cardiac images. CT volume data was used to reconstruct the actual 3D luminal models. Volume data post-processing was performed on a workstation equipped with Analyze 7.0 (Analyze Direct, Inc., Lexana, KS, USA). Image segmentation was used with a semi-automatic method with CT number thresholding, and scan-related artifacts and soft tissues were manually removed in some slices [11], [12]. The segmented 3D luminal models were created with an emphasis on the left main coronary bifurcation, which is composed of left main stem (LMS), left anterior descending (LAD), left circumflex (LCx), and its side branches. The 3D luminal models of twenty two patients were saved in 'STL format' for the generation of computational geometries. Blender version 2.48 (Blender Institute, Amsterdam, Netherlands) was used to reconstruct the 3D computational models. The twenty two geometries of arteries around the LMS, LAD and LCx were obtained from the

patient datasets with suspected CAD. The stenosis boundaries were kept in original from all anatomical structures that were shown on the CT images at left main bifurcation and its side-branches. The luminal surface geometries, consisting of stenosis boundaries, were converted into solid geometries and saved in 'STL format' for the meshing methodology.

2.2. Types of stenosis in the left coronary bifurcation

The coronary CT angiography images were used to classify the type of bifurcation stenosis at the left coronary artery in all patients [13]. These twenty two patients were classified according to the types of bifurcation stenosis: A) stenosis involving the ostium of the LCx and LAD branches; B) stenosis involving the ostium of the LCx branch; C) stenosis involving the LMS branch; D) stenosis involving the ostium of the LAD branch. The percentage of stenosis lumen was calculated based on measurements on CT images, as shown in Table 1. The diagram of stenosis classification of different types based on the patient datasets was shown in Figure 2.

2.3. Flow computation and solution

All realistic left coronary geometries were reconstructed with inclusion of the stenosis boundaries, referred to in Figure 2. The sample of four patients, with the different types of bifurcation stenoses in the left coronary artery is shown in Figure 3. Meshes were created for these geometries, with resolutions ranging from 9×10^5 to 9.8×10^5 cells. Mesh independence tests were performed for all coronary geometries. ANSYS ICEM CFD version 12 (ANSYS, Inc.) was used for the meshing process, with details having been described in previous studies [1], [14], [15]. Transient flow replicating systolic and diastolic phase at the left coronary artery was applied as an inflow boundary condition at LMS [16]. The outflow boundary condition was applied with the flow ratio through the side-branches at the LAD and LCx [17].

Murray's law [18] was used to define the flow relationship between inflow and outflow planes. Rheological parameters were applied, with a blood density of 1060 kg/m^3, blood viscosity of 0.0035 Pa s [19]. Blood flow was assumed to be laminar. The blood was assumed to be a Newtonian and incompressible fluid [19]. Blood vessels were assumed to be rigid, and a no-slip condition was applied at the walls [20]. The Navier-Stokes equations were solved using the ANSYS CFX version 12 (ANSYS, Inc.), on a Microsoft Windows 7 32-bit machine, 6 GB of RAM with a Xeon W3505 2.53 GHz CPU. Each timestep was converged to a residual target of less than 1×10^{-4}. ANSYS CFD-Post version 12 (ANSYS, Inc.) was used to calculate and visualize flow velocity and wall shear stress (WSS).

The WSS is a commonly used factor in hemodynamic analysis; endothelial cells have been shown to align themselves with the flow direction that corresponds to the local WSS. The coordinates of the wall surface elucidate the interaction of instantaneous WSS vectors and endothelial cells [21]. The WSS is defined as:

$$\mathrm{WSS} = \frac{1}{T}\int_0^T \left| \mu \frac{\partial v_t}{\partial_n} \right| dt \qquad (1)$$

where μ is blood viscosity, v_t is velocity vector near wall perpendicular to surface and n is distance to the wall surface, T is pulsatile period, dt is the time derivative of the local shear stress.

3. Results

The classification types of realistic bifurcation stenosis among twenty two patients were represented in Table 1. Figure 3 shows patients with these four types of stenosis. Ten patients had type D stenosis (LAD branch) and eight patients had stenosis type A (LAD and LCx branches). Three patients had stenosis type B (LCx branch) and remaining one patient had stenosis type C (LCx branch).

3.1. Hemodynamic patterns in the left coronary bifurcation

Flow patterns were calculated and compared in all types of bifurcation stenosis, as shown in Figure 4. The velocity contour levels ranged from 0 mm s-1 to 30.50 mm s-1 with 2.18 mm s-1 between levels. Figure 4A shows the bifurcation stenosis at the LCx and LAD, and this case revealed a type A stenosis. The high velocity surrounding the bifurcated location was found at the LCx and LAD, which ranged from 6.54 mm s-1 to 10.89 mm s-1 and 13.07 mm s-1 to 17.43 mm s-1, respectively. The type B stenosis was shown in Figure 4B, and a high velocity near the bifurcation was reached, from 8.71 mm s-1 to 13.07 mm s-1 at LCx branch. Figure 4C shows the stenosis involving the LMS branch (type C) and a high velocity was reached, ranging from 6.54 mm s-1 to 8.71 mm s-1, which is close to the bifurcation region. Type D stenosis represented patients who had stenosis at the LAD, and a high velocity close to the bifurcation ranging 17.43 mm s-1 to 19.61 mm s-1. In this analysis the velocity change was found to be high at the stenosis located near the bifurcation areas. The flow variation during diastolic phase was similar to the systolic phase, as the stenosis resulted in high velocity surrounding the bifurcation locations.

3.2. Wall shear stress in the left coronary bifurcation

Wall shear stress was calculated and compared in all patients with the various bifurcation stenoses, as shown in Table 2 and Figure 5. WSS distributions were mainly plotted to present the effects of lumen stenosis at left coronary bifurcations. Calculated WSS values during cardiac cycle ranged from 0 Pa to 3.50 Pa. Figure 5A shows the impact of stenosis at the LCx and LAD close to the bifurcation, representing patient stenosis in group 1. WSS variations increased at LCx and LAD

branches, ranging from 1.75 Pa to 2.0 Pa and 2.25 Pa to 2.5 Pa, respectively. Figure 5B demonstrates that the WSS increased at LCx ranging from 3.25 Pa to 3.5 Pa, which represented the type B stenosis. In addition, the stenosis at LMS had minor effects on WSS changes, which ranged from 0.75 Pa to 1.0 Pa near the bifurcation region, as shown in Figure 5C. Figure 5D shows stenosis located at LAD branch with WSS increased from 3.25 Pa to 3.5 Pa. In this situation, WSS change was found to increase at the stenotic areas in all patients. The WSS variation during systolic and diastolic phases was the same as WSS change, which increased depending on the types of stenosis in Figure 2 and the degree of lumen stenosis.

4. Discussion

This study investigated the flow change and WSS distribution in the left coronary, based on different types of stenosis from a group of patients presenting with coronary artery disease. The datasets used, consisted of reconstructions of the realistic left coronary geometries of 22 patients. Our results showed the various hemodynamic changes due to different types of stenosis, mainly due to the involvement of different left coronary branches. Thus, our study has potential value for improving the understanding of the impact of various types of bifurcation stenosis, and accordingly, the pathogenesis of coronary disease.

Coronary artery disease generally forms near the bifurcation, due to the blood vessel's inherent angulation and tortuosity, leading to low WSS [1], [2], [5]. Medical imaging techniques such as CT angiography provides excellent anatomical details of the coronary lumen changes, however, they are unable to provide hemodynamic factors such as WSS distribution and flow variation. Recent studies have used computational fluid analysis to overcome the limitations of imaging modalities by characterizing hemodynamic changes in the situation of coronary disease [6], [7],

[8], [9], [10]. Many studies reported in the literature have paid attention to the degree of stenosis and the effects of stenosis originating in left bifurcation to side-branches and subsequent hemodynamic changes [6], [7], [8], [9], [10]. There is very little research being conducted, correlating hemodynamic change with the various types of bifurcation stenosis in the left coronary artery.

This study focuses on two important factors: velocity and WSS, and the characterization of the flow patterns and WSS variation at stenosis locations in left main coronary bifurcation. The velocity was found to increase at stenotic locations in all types of bifurcation stenoses (as indicated with arrows in Figure 4). Factors that influence the velocity increase, include vessel diameter, bifurcation angle, vessel tortuosity, and length of the LMS branch [1], [6], [7], [8]. The patient demographics (Table 1) in this study showed that only one patient had insignificant stenosis belonging to type C, indicating a long LMS branch (Figure 4C). In contrast, the remaining 21 patients had very short LMS branch, thus, responsible for involvement of more left coronary branches (Figure 4A, B and D). Consequently, the length of LMS branch directly affected the flow field, leading to velocity changes in the left coronary artery, and this may be a factor that contributes to the coronary disease. Further studies focusing on the length of LMS in relation to the corresponding hemodynamic changes are needed to verify our results.

WSS was found to increase at the stenosis location in all patients due to the degree of narrowing of the lumen when compared to the WSS near bifurcations, as shown in Figure 5. The patient with a long LMS branch and a 30% stenosis displayed minor WSS change at the stenosis locations (arrows in Figure 5C), while other patients showed WSS to be high at locations close to the bifurcations (Figure 5A, B and D). WSS affects biological signals to mechanoreceptors in endothelial

cells, and it can affect gene expressions causing changes to the cellular functions of vessel walls [22], [23]. Low WSS was defined as < 1 Pa, intermediate WSS as >= 1 Pa to < 2.5 Pa, and high WSS as >= 2.5 Pa.[23,24] In this study, High WSS was found in vessel branches where a >70% stenosis was present, in a group of patients who had presented with high WSS at stenosis regions (Figure 5B and D, arrows pointed). This is in line with previous reports [22], [23], [24]. High WSS is also indicated as a contributor to the rupture and thrombosis of advanced atherosclerotic in human coronary artery [24], [25], [26]. Therefore, it could be assumed that patients having stenosis at LAD branch (Figure 5B) could lead to the plaque rupture.

Several limitations in this study should be addressed. Firstly, the walls of vessels were assumed to be rigid, a reasonable assumption in this case, supported by previous studies [20]. Secondly, the blood was assumed to be Newtonian, and this assumption is also supported by previous studies [6], [19]. Thirdly, the study population was restricted to a small number of patients that can only be classified into the four types of bifurcation stenosis at the left coronary artery. Therefore, future studies will use more patient's data, representing various types of actual stenosis, including all possible disease conditions in the left main coronary artery.

5. Conclusion

This study investigates the effects of stenosis on WSS and flow variation at bifurcated regions, and the patients' datasets were classified into the four types (A-D) of bifurcation stenosis. WSS and flow velocity was found to increase at different stenosis locations. WSS at >70% stenosis was significantly different from that observed at <30% of stenosis. Our results provide additional information about the hemodynamic effects of coronary stenosis when compared to medical imaging visualization, thus, improving the understanding of the hemodynamic

characterization of realistic bifurcation stenoses, although further studies based on a larger cohort are needed to confirm our results.

References

[1] Chaichana, T., Sun, Z., Jewkes, J., 2011. Computation of hemodynamics in the left coronary artery with variable angulations. Journal of Biomechanics 44(10), 1869-1878.

[2] Sun, Z., Cao, Y., 2011. Multislice CT angiography assessment of left coronary artery: Correlation between bifurcation angle and dimensions and development of coronary artery disease. European Journal of Radiology 79(2), e90-e95.

[3] Rodriguez-Granillo, G.A., Rosales, M.A., Degrossi, E., Durbano, I., Rodriguez, A.E., 2007. Multislice CT coronary angiography for the detection of burden, morphology and distribution of atherosclerotic plaque in the left main bifurcation. International Journal of Cardiovascular Imaging 23, 389-392.

[4] Topol, E.J., 2008. Textbook of interventional cardiology, 5th ed. Saunders Elsevier, Philadelphia, pp. 1075.

[5] Fuster, V., 1994. Lewis A. Conner memorial lecture. Mechanisms leading to myocardial infarction: insights from studies of vascular biology. Circulation 90(4), 2126-2146.

[6] Chaichana. T., Sun, Z., Jewkes, J., 2012. Computational fluid dynamics analysis of the effect of plaque in the left coronary artery. Computational and Mathematical Methods in Medicine 2012, 504367:1-9.

[7] Chaichana T, Sun Z, Jewkes J., 2012. Impact of plaques in the left coronary artery on wall shear stress and pressure gradient in coronary side branches. Computer Methods in Biomechanics and Biomedical Engineering, Epub ahead of print, 1-11. DOI: 10.1080/10255842.2012.671308.

[8] Chaichana, T., Sun, Z., Jewkes, J., 2012. Investigation of the haemodynamic environment of bifurcation plaques within the left coronary artery in realistic

patient models based on CT images. Australasian Physical & Engineering Sciences in Medicine 35(2), 321-326.

[9] Katritsis, D.G., Theodorakakos, A., Pantos, I., Andriotis, A., Efstathopoulos, E.P., Siontis, G., Karcanias, N., Redwood, S., Gavaises, M., 2010. Vortex formation and recirculation zones in left anterior descending artery stenosis: computational fluid dynamics analysis. Physics in Medicine and Biology 55(5), 1395-1411.

[10] Shanmugavelayudam, S.K., Rubenstein, D.A., Yin, W., 2010. Effect of geometrical assumptions on numerical modelling of coronary blood flow under normal and disease conditions. Journal of Biomechanical Engineering 132(6), 061004.

[11] Sun, Z., Winder, R.J., Kelly, B.E., Ellis, P.K., Kennedy, P.T., Hirst, D.G., 2004. Diagnostic value of CT virtual intravascular endoscopy in aortic stent grafting. Journal of Endovascular Therapy 11(1), 13-25.

[12] Sun, Z., Winder, R.J., Kelly, B.E., Ellis, P.K., Hirst, D.G., 2003. CT virtual intravascular endoscopy of abdominal aortic aneurysms treated with suprarenal endovascular stent grafting. Abdominal Imaging 28(4), 580-587.

[13] Sun, Z., Yvonne, A., Nadkarni, S., Roslyn, K., David, H., Lawrence-Brown, M., 2008. CT virtual intravascular endoscopy in the visualization of fenestrated endovascular grafts. Journal of Endovascular Therapy 15 (1), 42-51.

[14] Sun, Z., Chaichana, T., 2010. Fenestrated stent graft repair of abdominal aortic aneurysm: hemodynamic analysis of the effect of fenestrated stents on the renal arteries. Korean Journal of Radiology 11(1), 95-106.

[15] Sun, Z., Chaichana, T., 2009. Investigation of the hemodynamic effect of stent wires on renal arteries in patients with abdominal aortic aneurysms treated with

suprarenal stent-grafts. Cardiovascular and Interventional Radiology 32(4), 647-657.

[16] Berne, R.M., Levy, M.N., 2001. Cardiovascular physiology. Mosby, St Louis MI.

[17] van der Giessen, A.G., Groen, H.C., Doriot, P.A., de Feyter, P.J., van der Steen, A.F., van de Vosse, F.N., Wentzel, J.J., Gijsen, F.J., 2011. The influence of boundary conditions on wall shear stress distribution in patients specific coronary trees. Journal of Biomechanics 44(6), 1089-1095.

[18] Murray, C.D., 1926. The Physiological Principle of Minimum Work: I. The Vascular System and the Cost of Blood Volume. Proceeding of the National Academy of Science of the United States of America 12(3), 207-214.

[19] Johnston, B.M., Johnston, P.R., Corney, S., Kilpatrick, D., 2004. Non-Newtonian blood flow in human right coronary arteries: steady state simulations. Journal of Biomechanics 37(5), 709-720.

[20] Moore, J.E.Jr, Xu, C., Glagov, S., Zarins, C.K., Ku, DN., 1994. Fluid wall shear stress measurements in a model of the human abdominal aorta: oscillatory behavior and relationship to atherosclerosis. Atherosclerosis 110(2), 225-240.

[21] Kleinstreuer, C., Hyun, S., Buchanan, J.R. Jr., Longest, P.W., Archie, J.P. Jr., Truskey, G.A., 2001. Hemodynamic parameters and early intimal thickening in branching blood vessels. Critical Reviews in Biomedical Engineering 29(1), 1-64.

[22] Gibbons, G.H., Dzau, V.J., 1994. The emerging concept of vascular remodeling. The New England Journal of Medicine 330(20), 1421-1438.

[23] Malek, A.M., Alper, S.L., Izumo, S., 1999. Hemodynamic shear stress and its role in atherosclerosis. Journal of the American Medical Association 282 (21), 2035-2042.

[24] Samady, H., Eshtehardi, P., McDaniel, M.C., Suo, J., Dhawan, S.S., Maynard, C., Timmins, L.H., Quyyumi, A.A., Giddens, D.P., 2011. Coronary artery wall shear stress is associated with progression and transformation of atherosclerotic plaque and arterial remodeling in patients with coronary artery disease. Circulation 124: 779-788, 2011.

[25] Fukumoto, Y., Hiro, T., Fujii, T., Hashimoto, G., Fujimura, T., Yamada, J., Okamura, T., Matsuzaki, M., 2008. Localized elevation of shear stress is related to coronary plaque rupture: a 3-dimensional intravascular ultrasound study with in-vivo color mapping of shear stress distribution. Journal of the American College of Cardiology 51(6), 645-650.

[26] Gijsen, F.J., Wentzel, J.J., Thury, A., Lamers, B., Schuurbiers, J.C., Serruys, P.W., van der Steen, A.F., 2007. A new imaging technique to study 3-D plaque and shear stress distribution in human coronary artery bifurcations in vivo. Journal of Biomechanics 40(11), 2349-2357.

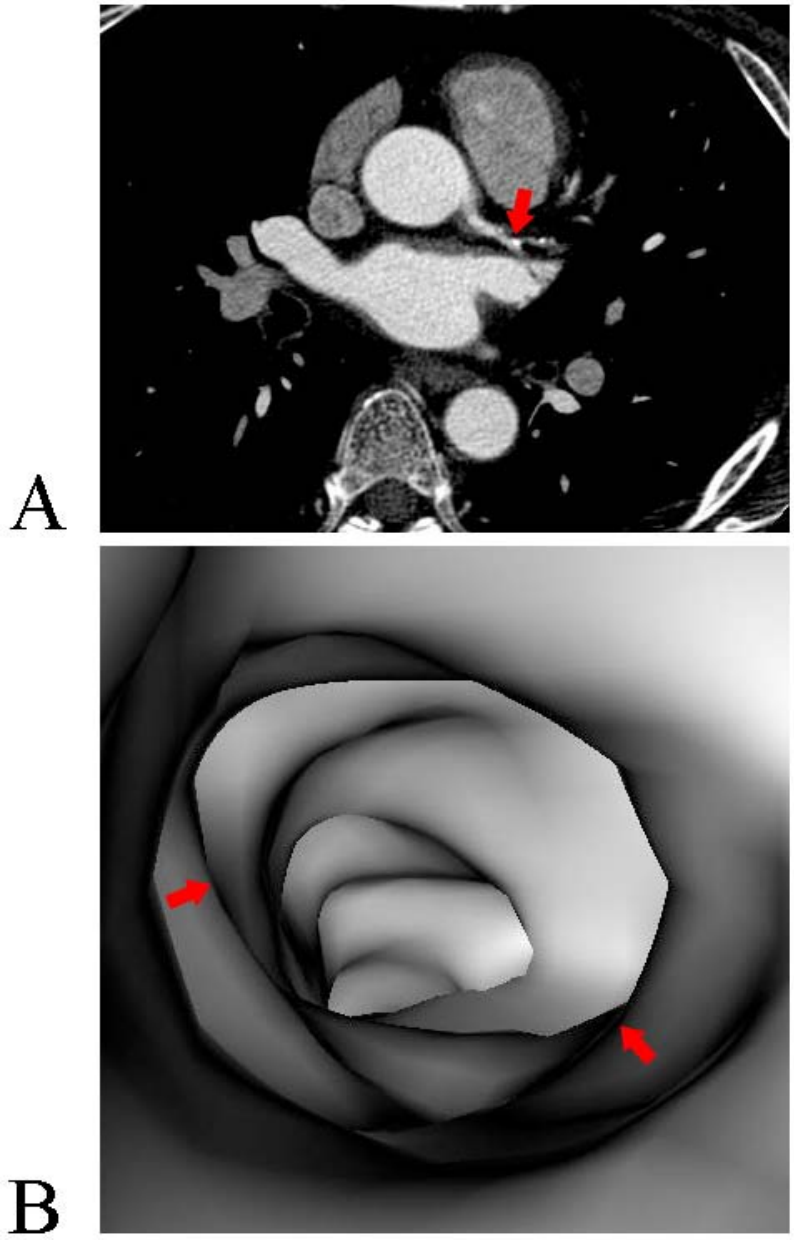

Figure 1. 2D medical imaging shows significant stenosis at left main stem due to calcified plaque, (arrow in A); corresponding virtual endoscopy confirms the lumen stenosis by demonstrating intravascular appearance (arrows in B).

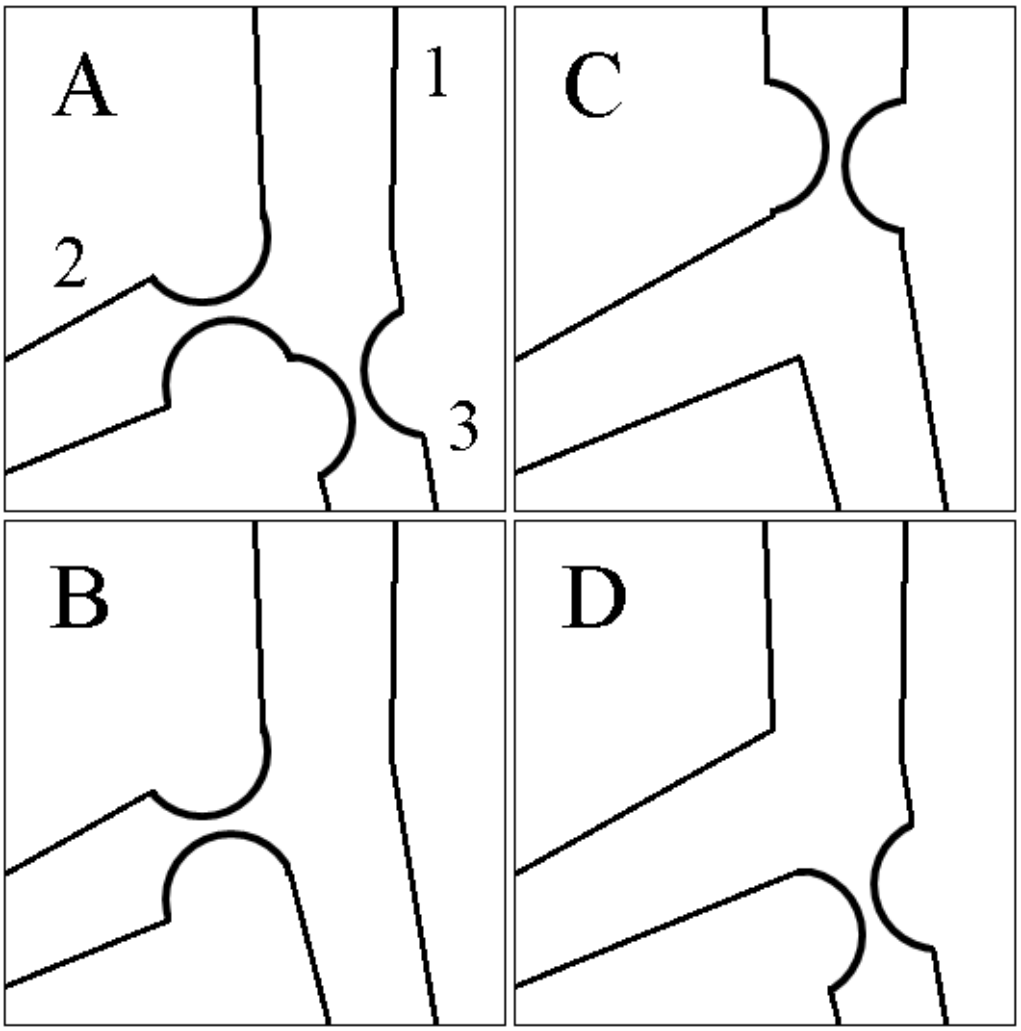

Figure 2. The diagram shows classification system of bifurcation stenosis in the left coronary artery with stenosis involving LAD and LCx (A), LCx (B), LMS (C), and LAD (D).

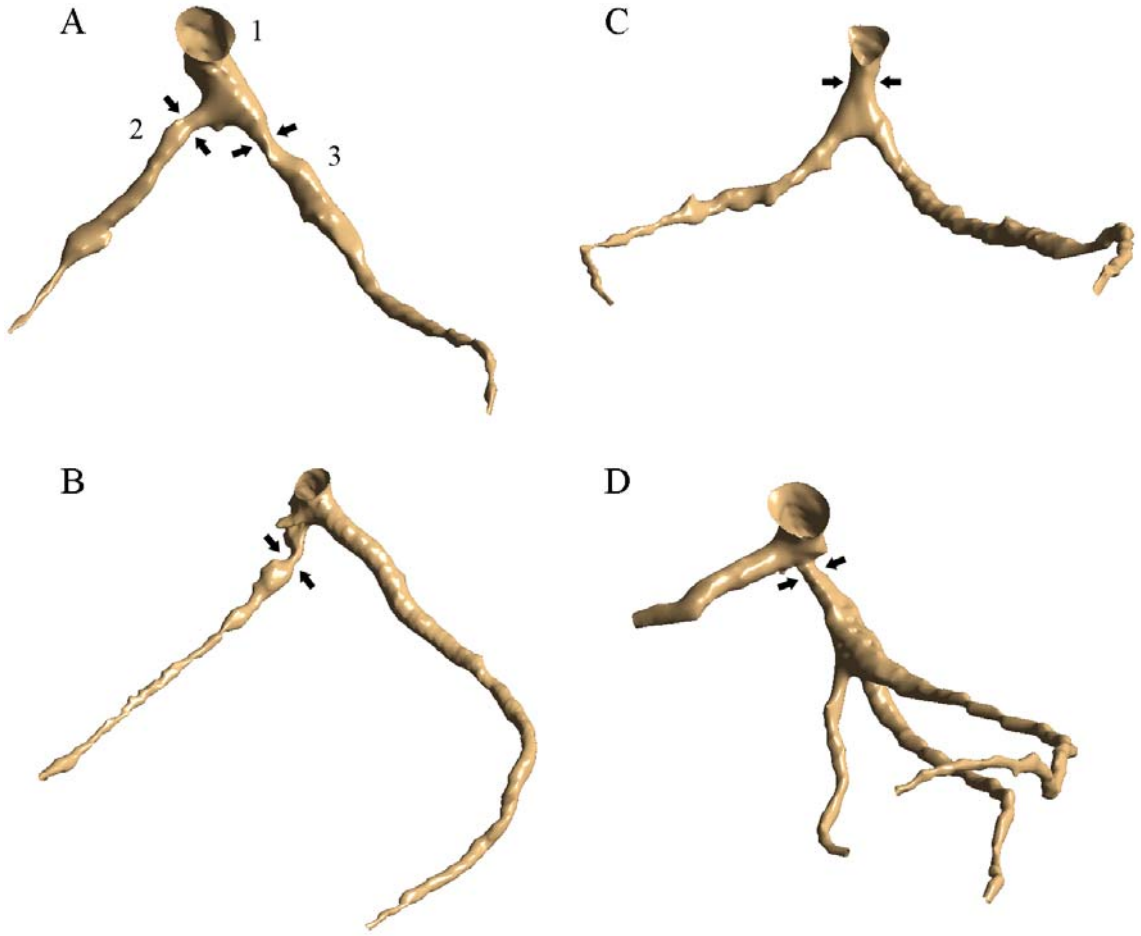

Figure 3. The selected geometries of realistic left coronary models with bifurcation stenosis based on the classification system in Figure 2, (A) stenosis type A in patient No. 1, (b) stenosis type B in patient No. 7, (c) stenosis type C in patient No. 16 and (d) stenosis type D in patient No. 10. Arrows reveal the stenosis locations.

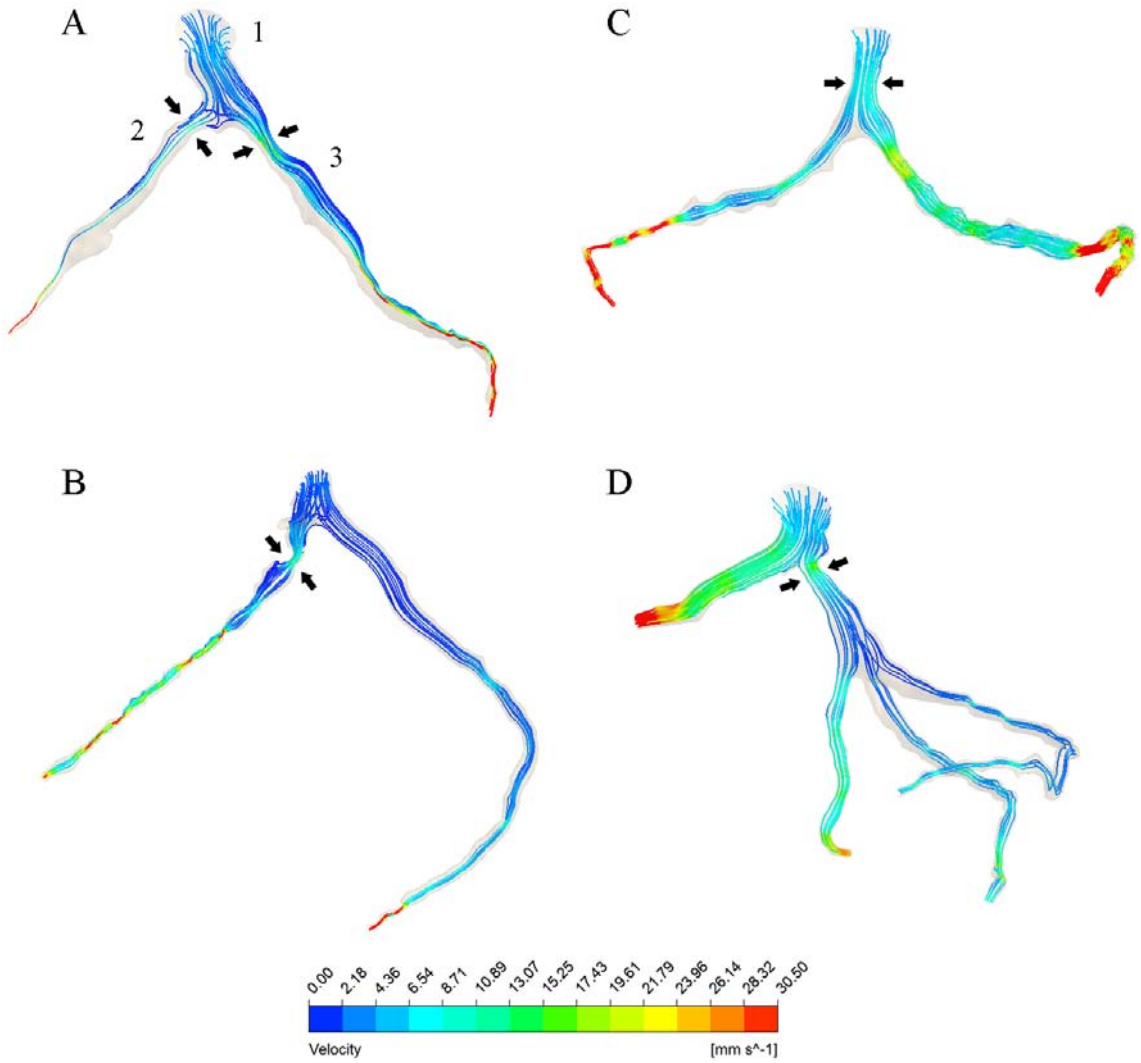

Figure 4. Flow patterns of velocity change surrounding bifurcation were reached at systolic of 0.2 s in patients who had (A) stenosis type A, (B) stenosis type B, (C) stenosis type C and (D) stenosis type D. Arrows identify the velocity to be high at stenosis positions near the bifurcations.

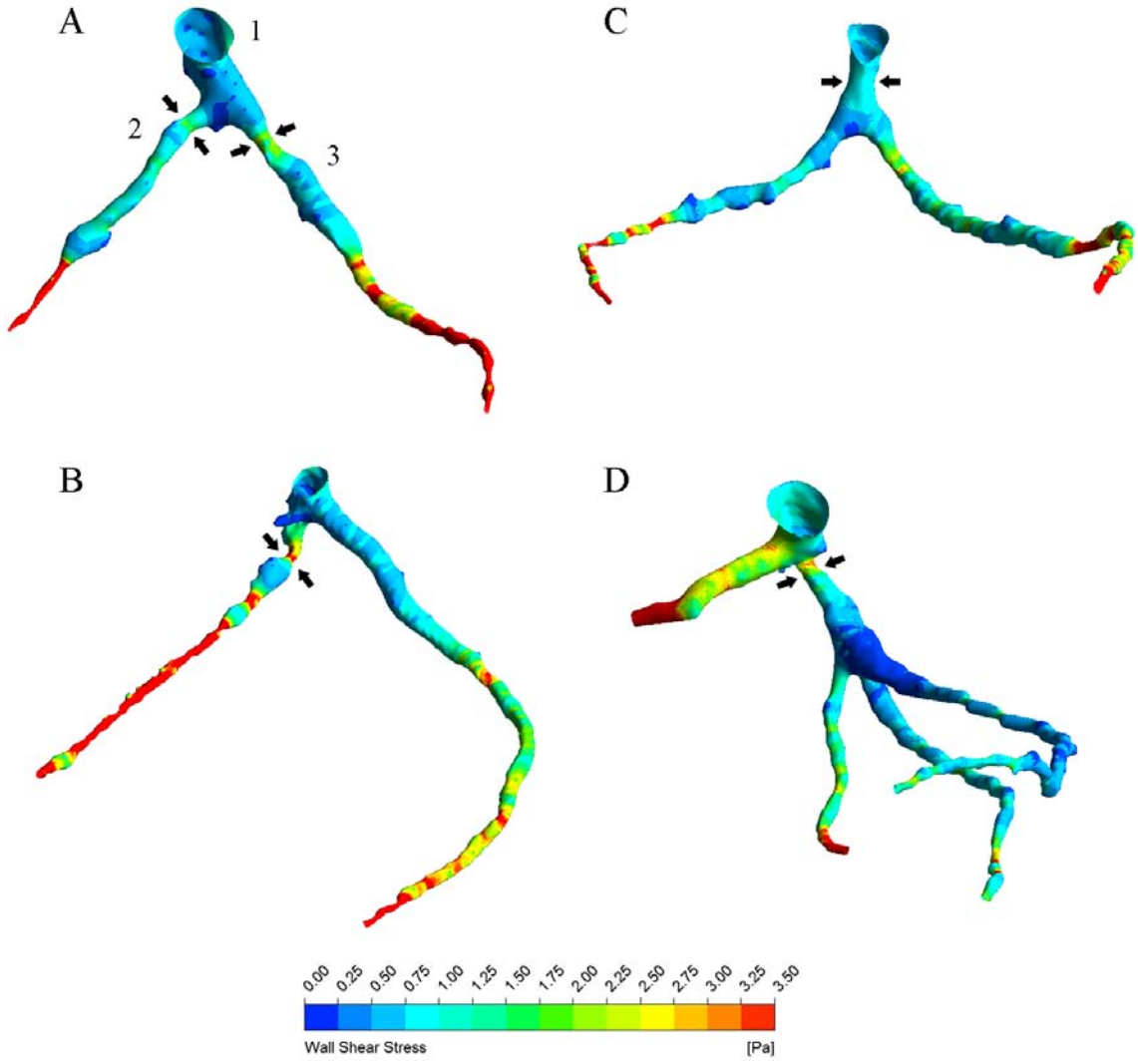

Figure 5. WSS distributions of WSS change surrounding bifurcation were reached at systolic of 0.2 s in patients who had (A) stenosis type A, (B) stenosis type B, (C) stenosis type C and (D) stenosis type D. Arrows identify the WSS to be high at stenosis positions nearby bifurcations.

Table 1. Patient characteristics: All patients with detection and classification of the types of stenosis at the left coronary bifurcations

No.	Age	Sex	Number of diseased vessels			Percent Stenosis	Types of stenosis			
			LMS	LAD	LCx		A	B	C	D
1	72	F	-	+	+	60	✓			
2	59	F	-	+	+	60	✓			
3	59	M	-	+	+	50	✓			
4	52	M	-	+	+	50	✓			
5	38	M	-	+	-	40				✓
6	53	F	-	+	-	60				✓
7	56	F	-	-	+	70		✓		
8	49	M	-	-	+	40		✓		
9	51	M	-	+	-	65				✓
10	69	M	-	+	-	70				✓
11	55	M	-	+	+	50	✓			
12	58	M	-	+	-	50				✓
13	56	M	-	-	+	50		✓		
14	42	M	-	+	+	30	✓			
15	56	F		+	-	50				✓
16	61	M	+	-	-	30			✓	
17	55	M	-	+	+	60	✓			
18	57	F	-	+	-	50				✓
19	43	F	-	+	-	40				✓
20	45	M	-	+	-	40				✓
21	47	M	+	+	-	40	✓			
22	47	M	-	+	-	50				✓

F—Female, M—Male, "+"—Plaques-Inclusion, "-"—Plaques-Exclusion
LMS—left main stem, LAD—left anterior descending, LCx—left circumflex

Table 2. Patient characteristics: All patients with correlation of WSS and stenosis lumen

No.	Type	WSS level (Pa)	
1	A	1.75 – 2.50	Intermediate
2	A	1.75 – 2.50	
3	A	1.75 – 2.50	
4	A	1.75 – 2.50	
5	D	1.50 – 1.75	
6	D	2.25 – 2.50	
7	B	3.25 – 3.50	High
8	B	1.50 – 1.75	Intermediate
9	D	2.25 – 2.50	
10	D	3.25 – 3.50	High
11	A	1.75 – 2.50	Intermediate
12	D	2.25 – 2.50	
13	B	2.25 – 2.50	
14	A	0.50 – 1.00	Low
15	D	2.25 – 2.50	Intermediate
16	C	0.75 – 1.00	Low
17	A	1.75 – 2.50	Intermediate
18	D	1.50 – 2.50	
19	D	1.50 – 1.75	
20	D	1.50 – 1.75	
21	A	1.50 – 2.25	
22	D	2.25 – 2.50	

Appendix III

Statements of Contributions of Others

Appendix III-A: "Statement of Contribution of Others" for "Chaichana, T., Sun, Z., Jewkes, J., 2011. Computation of hemodynamics in the left coronary artery with variable angulations. Journal of Biomechanics 44 (10), 1869–1878."

Statements of Contributions of Others for “Computation of hemodynamics in the left coronary artery with variable angulations”

1st May 2012

To Whom It May Concern

I, Dr. Zhonghua Sun, contributed by providing overall project supervision and technical advice and manuscript editing to the paper/publication entitled.

Chaichana, T., Sun, Z., Jewkes, J., 2011. Computation of hemodynamics in the left coronary artery with variable angulations. Journal of Biomechanics 44 (10), 1869–1878.

Undertaken with Thanapong Chaichana.

(Signature of Co-Author)

Zhonghua Sun

(Signature of First Author)

Thanapong Chaichana

Statements of Contributions of Others for “Computation of hemodynamics in the left coronary artery with variable angulations”

1st May 2012

To Whom It May Concern

I, Dr. James Jewkes, contributed by providing technical support and manuscript editing to the paper/publication entitled.

Chaichana, T., Sun, Z., Jewkes, J., 2011. Computation of hemodynamics in the left coronary artery with variable angulations. Journal of Biomechanics 44 (10), 1869–1878.

Undertaken with Thanapong Chaichana.

(Signature of Co-Author)

James Jewkes

(Signature of First Author)

Thanapong Chaichana

Appendix III-B: "Statement of Contribution of Others" for "Chaichana, T., Sun, Z., Jewkes, J., 2012. Computational fluid dynamics analysis of the effect of plaques in the left coronary artery. Computational and Mathematical Methods in Medicine 2012, 504367:1–9."

Statements of Contributions of Others for “Computational fluid dynamics analysis of the effect of plaques in the left coronary artery”

1st May 2012

To Whom It May Concern

I, Dr. Zhonghua Sun, contributed by providing overall project supervision and technical advice and manuscript editing to the paper/publication entitled.

Chaichana, T., Sun, Z., Jewkes, J., 2012. Computational fluid dynamics analysis of the effect of plaques in the left coronary artery. Computational and Mathematical Methods in Medicine 2012, 504367:1–9.

Undertaken with Thanapong Chaichana.

(Signature of Co-Author)

Zhonghua Sun

(Signature of First Author)

Thanapong Chaichana

Statements of Contributions of Others for “Computational fluid dynamics analysis of the effect of plaques in the left coronary artery”

1st May 2012

To Whom It May Concern

I, Dr. James Jewkes, contributed by providing technical support and manuscript editing to the paper/publication entitled.

Chaichana, T., Sun, Z., Jewkes, J., 2012. Computational fluid dynamics analysis of the effect of plaques in the left coronary artery. Computational and Mathematical Methods in Medicine 2012, 504367:1–9.

Undertaken with Thanapong Chaichana.

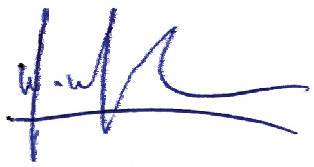

(Signature of Co-Author)

James Jewkes

(Signature of First Author)

Thanapong Chaichana

Appendix III-C: “Statement of Contribution of Others” for “Chaichana, T., Sun, Z., Jewkes, J., 2012. Impact of plaques in theleft coronary artery on wall shear stress and pressure gradient in coronary side branches. Computer Methods in Biomechanics and Biomedical Engineering, Epub a head of print, 1–11. doi:10.1080/10255842.2012.671308.”

Statements of Contributions of Others for “Impact of plaques in theleft coronary artery on wall shear stress and pressure gradient in coronary side branches”

1st May 2012

To Whom It May Concern

I, Dr. Zhonghua Sun, contributed by providing overall project supervision and technical advice and manuscript editing to the paper/publication entitled.

Chaichana, T., Sun, Z., Jewkes, J., 2012. Impact of plaques in theleft coronary artery on wall shear stress and pressure gradient in coronary side branches. Computer Methods in Biomechanics and Biomedical Engineering, Epub a head of print, 1–11. doi:10.1080/10255842.2012.671308.

Undertaken with Thanapong Chaichana.

(Signature of Co-Author)

Zhonghua Sun

(Signature of First Author)

Thanapong Chaichana

Statements of Contributions of Others for “Computation of hemodynamics in the left coronary artery with variable angulations”

1st May 2012

To Whom It May Concern

I, Dr. James Jewkes, contributed by providing technical support and manuscript editing to the paper/publication entitled.

Chaichana, T., Sun, Z., Jewkes, J., 2012. Impact of plaques in theleft coronary artery on wall shear stress and pressure gradient in coronary side branches. Computer Methods in Biomechanics and Biomedical Engineering, Epub a head of print, 1–11. doi:10.1080/10255842.2012.671308.

Undertaken with Thanapong Chaichana.

(Signature of Co-Author)

James Jewkes

(Signature of First Author)

Thanapong Chaichana

Appendix III-D: "Statement of Contribution of Others" for "Chaichana, T., Sun, Z., Jewkes, J., 2012. Investigation of the haemodynamic environment of bifurcation plaques within the left coronary artery in realistic patient models based on CT images. Australasian Physical & Engineering Sciences in Medicine 35 (2), 231–236."

Statements of Contributions of Others for "Investigation of the haemodynamic environment of bifurcation plaques within the left coronary artery in realistic patient models based on CT images"

1st May 2012

To Whom It May Concern

I, Dr. Zhonghua Sun, contributed by providing overall project supervision and technical advice and manuscript editing to the paper/publication entitled.

Chaichana, T., Sun, Z., Jewkes, J., 2012. Investigation of the haemodynamic environment of bifurcation plaques within the left coronary artery in realistic patient models based on CT images. Australasian Physical & Engineering Sciences in Medicine 35 (2), 231–236.

Undertaken with Thanapong Chaichana.

(Signature of Co-Author)

Zhonghua Sun

(Signature of First Author)

Thanapong Chaichana

Statements of Contributions of Others for "Investigation of the haemodynamic environment of bifurcation plaques within the left coronary artery in realistic patient models based on CT images"

1st May 2012

To Whom It May Concern

I, Dr. James Jewkes, contributed by providing technical support and manuscript editing to the paper/publication entitled.

Chaichana, T., Sun, Z., Jewkes, J., 2012. Investigation of the haemodynamic environment of bifurcation plaques within the left coronary artery in realistic patient models based on CT images. Australasian Physical & Engineering Sciences in Medicine 35 (2), 231–236.

Undertaken with Thanapong Chaichana.

(Signature of Co-Author)

James Jewkes

(Signature of First Author)

Thanapong Chaichana

Appendix IV

Copyright Forms

Appendix IV-A: Elsevier Journal Articles

Copyright information relating to;

Chaichana, T., Sun, Z., Jewkes, J., 2011. Computation of hemodynamics in the left coronary artery with variable angulations. Journal of Biomechanics 44 (10), 1869–1878.

ELSEVIER LICENSE
TERMS AND CONDITIONS

May 03, 2012

This is a License Agreement between Thanapong Chaichana ("You") and Elsevier ("Elsevier") provided by Copyright Clearance Center ("CCC"). The license consists of your order details, the terms and conditions provided by Elsevier, and the payment terms and conditions.

All payments must be made in full to CCC. For payment instructions, please see information listed at the bottom of this form.

Supplier	Elsevier Limited The Boulevard,Langford Lane Kidlington,Oxford,OX5 1GB,UK
Registered Company Number	1982084
Customer name	Thanapong Chaichana
Customer address	U1 24 Alexander Road Rivervale , WA 6103
License number	2901560617391
License date	May 03, 2012
Licensed content publisher	Elsevier
Licensed content publication	Journal of Biomechanics
Licensed content title	Computation of hemodynamics in the left coronary artery with variable angulations
Licensed content author	Thanapong Chaichana, Zhonghua Sun, James Jewkes
Licensed content date	7 July 2011
Licensed content volume number	44
Licensed content issue number	10
Number of pages	10
Start Page	1869
End Page	1878
Type of Use	reuse in a thesis/dissertation
Portion	full article
Format	both print and electronic
Are you the author of this Elsevier article?	Yes
Will you be translating?	No
Order reference number	None

Title of your thesis/dissertation	Haemodynamic Evaluation of Coronary Artery Plaques: Prediction of Coronary Atherosclerosis and Disease Progression
Expected completion date	Jun 2012
Estimated size (number of pages)	125
Elsevier VAT number	GB 494 6272 12
Permissions price	0.00 USD
VAT/Local Sales Tax	0.0 USD / 0.0 GBP
Total	0.00 USD
Terms and Conditions	

INTRODUCTION

1. The publisher for this copyrighted material is Elsevier. By clicking "accept" in connection with completing this licensing transaction, you agree that the following terms and conditions apply to this transaction (along with the Billing and Payment terms and conditions established by Copyright Clearance Center, Inc. ("CCC"), at the time that you opened your Rightslink account and that are available at any time at http://myaccount.copyright.com).

GENERAL TERMS

2. Elsevier hereby grants you permission to reproduce the aforementioned material subject to the terms and conditions indicated.

3. Acknowledgement: If any part of the material to be used (for example, figures) has appeared in our publication with credit or acknowledgement to another source, permission must also be sought from that source. If such permission is not obtained then that material may not be included in your publication/copies. Suitable acknowledgement to the source must be made, either as a footnote or in a reference list at the end of your publication, as follows: “Reprinted from Publication title, Vol /edition number, Author(s), Title of article / title of chapter, Pages No., Copyright (Year), with permission from Elsevier [OR APPLICABLE SOCIETY COPYRIGHT OWNER].” Also Lancet special credit - “Reprinted from The Lancet, Vol. number, Author(s), Title of article, Pages No., Copyright (Year), with permission from Elsevier.”

4. Reproduction of this material is confined to the purpose and/or media for which permission is hereby given.

5. Altering/Modifying Material: Not Permitted. However figures and illustrations may be altered/adapted minimally to serve your work. Any other abbreviations, additions, deletions and/or any other alterations shall be made only with prior written authorization of Elsevier Ltd. (Please contact Elsevier at permissions@elsevier.com).

6. If the permission fee for the requested use of our material is waived in this instance, please be advised that your future requests for Elsevier materials may attract a fee.

7. Reservation of Rights: Publisher reserves all rights not specifically granted in the combination of (i) the license details provided by you and accepted in the course of this licensing transaction, (ii) these terms and conditions and (iii) CCC's Billing and Payment terms and conditions.

8. License Contingent Upon Payment: While you may exercise the rights licensed immediately upon issuance of the license at the end of the licensing process for the transaction, provided that you have disclosed complete and accurate details of your proposed use, no license is finally effective unless and until full payment is received from you (either by publisher or by CCC) as provided in CCC's Billing and Payment terms and conditions. If full payment is not received on a timely basis, then any license preliminarily granted shall be deemed automatically revoked and shall be void as if never granted. Further, in the event that you breach any of these terms and conditions or any of CCC's Billing and Payment terms and conditions, the license is automatically revoked and shall be void as if never granted. Use of materials as described in a revoked license, as well as any use of the materials beyond the scope of an unrevoked license, may constitute copyright infringement and publisher reserves the right to take any and all action to protect its copyright in the materials.

9. Warranties: Publisher makes no representations or warranties with respect to the licensed material.

10. Indemnity: You hereby indemnify and agree to hold harmless publisher and CCC, and their respective officers, directors, employees and agents, from and against any and all claims arising out of your use of the licensed material other than as specifically authorized pursuant to this license.

11. No Transfer of License: This license is personal to you and may not be sublicensed, assigned, or transferred by you to any other person without publisher's written permission.

12. No Amendment Except in Writing: This license may not be amended except in a writing signed by both parties (or, in the case of publisher, by CCC on publisher's behalf).

13. Objection to Contrary Terms: Publisher hereby objects to any terms contained in any purchase order, acknowledgment, check endorsement or other writing prepared by you, which terms are inconsistent with these terms and conditions or CCC's Billing and Payment terms and conditions. These terms and conditions, together with CCC's Billing and Payment terms and conditions (which are incorporated herein), comprise the entire agreement between you and publisher (and CCC) concerning this licensing transaction. In the event of any conflict between your obligations established by these terms and conditions and those established by CCC's Billing and Payment terms and conditions, these terms and conditions shall control.

14. Revocation: Elsevier or Copyright Clearance Center may deny the permissions described in this License at their sole discretion, for any reason or no reason, with a full refund payable to you. Notice of such denial will be made using the contact information provided by you. Failure to receive such notice will not alter or invalidate the denial. In no event will Elsevier or Copyright Clearance Center be responsible or liable for any costs, expenses or damage incurred by you as a result of a denial of your permission request, other than a refund of the amount(s) paid by you to Elsevier and/or Copyright Clearance Center for denied permissions.

LIMITED LICENSE

The following terms and conditions apply only to specific license types:

15. **Translation**: This permission is granted for non-exclusive world **English** rights only unless your license was granted for translation rights. If you licensed translation rights you may only translate this content into the languages you requested. A professional translator must perform all translations and reproduce the content word for word preserving the integrity of the article. If this license is to re-use 1 or 2 figures then permission is granted for non-exclusive world rights in all languages.

16. **Website**: The following terms and conditions apply to electronic reserve and author websites:
Electronic reserve: If licensed material is to be posted to website, the web site is to be password-protected and made available only to bona fide students registered on a relevant course if:
This license was made in connection with a course,
This permission is granted for 1 year only. You may obtain a license for future website posting,
All content posted to the web site must maintain the copyright information line on the bottom of each image,
A hyper-text must be included to the Homepage of the journal from which you are licensing at http://www.sciencedirect.com/science/journal/xxxxx or the Elsevier homepage for books at http://www.elsevier.com, and
Central Storage: This license does not include permission for a scanned version of the material to be stored in a central repository such as that provided by Heron/XanEdu.

17. **Author website** for journals with the following additional clauses:
All content posted to the web site must maintain the copyright information line on the bottom of each image, and the permission granted is limited to the personal version of your paper. You are not allowed to download and post the published electronic version of your article (whether PDF or HTML, proof or final version), nor may you scan the printed edition to create an electronic version,

A hyper-text must be included to the Homepage of the journal from which you are licensing at http://www.sciencedirect.com/science/journal/xxxxx , As part of our normal production process, you will receive an e-mail notice when your article appears on Elsevier's online service ScienceDirect (www.sciencedirect.com). That e-mail will include the article's Digital Object Identifier (DOI). This number provides the electronic link to the published article and should be included in the posting of your personal version. We ask that you wait until you receive this e-mail and have the DOI to do any posting.
Central Storage: This license does not include permission for a scanned version of the material to be stored in a central repository such as that provided by Heron/XanEdu.

18. **Author website** for books with the following additional clauses:
Authors are permitted to place a brief summary of their work online only.
A hyper-text must be included to the Elsevier homepage at http://www.elsevier.com
All content posted to the web site must maintain the copyright information line on the bottom of each image
You are not allowed to download and post the published electronic version of your chapter, nor may you scan the printed edition to create an electronic version.
Central Storage: This license does not include permission for a scanned version of the material to be stored in a central repository such as that provided by Heron/XanEdu.

19. **Website** (regular and for author): A hyper-text must be included to the Homepage of the journal from which you are licensing at http://www.sciencedirect.com/science/journal/xxxxx. or for books to the Elsevier homepage at http://www.elsevier.com

20. **Thesis/Dissertation**: If your license is for use in a thesis/dissertation your thesis may be submitted to your institution in either print or electronic form. Should your thesis be published commercially, please reapply for permission. These requirements include permission for the Library and Archives of Canada to supply single copies, on demand, of the complete thesis and include permission for UMI to supply single copies, on demand, of the complete thesis. Should your thesis be published commercially, please reapply for permission.

21. **Other Conditions**:

v1.6

If you would like to pay for this license now, please remit this license along with your payment made payable to "COPYRIGHT CLEARANCE CENTER" otherwise you will be invoiced within 48 hours of the license date. Payment should be in the form of a check or money order referencing your account number and this invoice number RLNK500772986.
Once you receive your invoice for this order, you may pay your invoice by credit card.
Please follow instructions provided at that time.

Make Payment To:
Copyright Clearance Center
Dept 001
P.O. Box 843006
Boston, MA 02284-3006

For suggestions or comments regarding this order, contact RightsLink Customer Support: customercare@copyright.com or +1-877-622-5543 (toll free in the US) or +1-978-646-2777.

Gratis licenses (referencing $0 in the Total field) are free. Please retain this printable license for your reference. No payment is required.

Appendix IV-B: Hindawi Publishing Corporation Journals

Copyright information relating to;

Chaichana, T., Sun, Z., Jewkes, J., 2012. Computational fluid dynamics analysis of the effect of plaques in the left coronary artery. Computational and Mathematical Methods in Medicine 2012, 504367:1–9.

Appendix IV-C: Taylor & Francis Journals

Copyright information relating to;

Chaichana, T., Sun, Z., Jewkes, J., 2012. Impact of plaques in theleft coronary artery on wall shear stress and pressure gradient in coronary side branches. Computer Methods in Biomechanics and Biomedical Engineering, Epub a head of print, 1-11. doi:10.1080/10255842.2012.671308.

Taylor & Francis Journals

We are partnered with the Copyright Clearance Center to meet your licensing needs. You can now obtain permission to reuse our journal content quickly and easily directly from our website.

On any article page you can see a Reprints and permissions tab. This will give you the option to order reprints or request permissions for this article through the Copyright Clearance Center's RightsLink® service.

Once opened, RightsLink enables you to obtain instant price quotes, place orders, and track all of your licensing activity in realtime.

For questions about using RightsLink, please contact their Customer Care team via phone 877/622-5543 (toll free inside U.S. only) or 978/777-9929, or email customercare@copyright.com

Rightslink® by Copyright Clearance Center

RE: Request Help for Permission of the Article ID\# GCMB 671308 that has published in the Taylor & Francis Publisher [pfCase:411491, pfTicket:5496752]

16 May 2012 18:37

CustomerCare@copyright.com
18:37 (4 hours ago)

to me Venom 25 <venom25@gmail.com>

Dear Thanapong Chaichana,

Thank you for contacting Copyright Clearance Center's Rightslink service. Rightslink grants permission for the reuse of copyrighted materials on behalf of rightsholders who list their titles with us.

The message you see on the Rightslink order page informs you that if you are using the content in a thesis/dissertation, the permissions is automatically granted even if you do not place a Rightslink order.

However, should you decide to publish your thesis/dissertation as a book, then, Taylor & Francis requires that you place a permission request via Rightslink.

We hope this helps clear the confusion. Should you have any questions or require assistance, please feel free to contact us.

Sincerely,
Hanna

Please click here to participate in our online customer service survey.

Hanna Sta. Ines
Customer Service Representative
Copyright Clearance Center
222 Rosewood Drive
Danvers, MA 01923
+1.800.772.3350 Toll Free
+1.978.750.8400 Main
+1.978.646.8600 Fax

Click Here for Customer Service Live Chat

**Please include all prior email correspondence in your reply so that we may better serve you and provide you with a more timely response.

Appendix IV-D: Springer Journal Articles

Copyright information relating to;

Chaichana, T., Sun, Z., Jewkes, J., 2012. Investigation of the haemodynamic environment of bifurcation plaques within the left coronary artery in realistic patient models based on CT images. Australasian Physical & Engineering Sciences in Medicine 35 (2), 231-236.

SPRINGER LICENSE
TERMS AND CONDITIONS

May 15, 2012

This is a License Agreement between Thanapong Chaichana ("You") and Springer ("Springer") provided by Copyright Clearance Center ("CCC"). The license consists of your order details, the terms and conditions provided by Springer, and the payment terms and conditions.

All payments must be made in full to CCC. For payment instructions, please see information listed at the bottom of this form.

License Number	2910121471397
License date	May 15, 2012
Licensed content publisher	Springer
Licensed content publication	Australasian Physical and Engineering Science in Medicine
Licensed content title	Investigation of the haemodynamic environment of bifurcation plaques within the left coronary artery in realistic patient models based on CT images
Licensed content author	Thanapong Chaichana
Licensed content date	Jan 1, 2012
Type of Use	Thesis/Dissertation
Portion	Full text
Number of copies	None
Author of this Springer article	Yes and you are None
Order reference number	None
Title of your thesis / dissertation	Haemodynamic Evaluation of Coronary Artery Plaques: Prediction of Coronary Atherosclerosis and Disease Progression
Expected completion date	Jun 2012
Estimated size(pages)	125
Total	0.00 USD
Terms and Conditions	

Warranties: None
Example 1: Springer Science + Business Media makes no representations or warranties with respect to the licensed material.
Example 2: Springer Science + Business Media makes no representations or warranties with respect to the licensed material and adopts on its own behalf the limitations and disclaimers established by CCC on its behalf in its Billing and Payment terms and conditions for this licensing transaction.
Indemnity
You hereby indemnify and agree to hold harmless Springer Science + Business Media and CCC, and their respective officers, directors, employees and agents, from and against any and all claims arising out of your use of the licensed material other than as specifically authorized pursuant to this license.
No Transfer of License
This license is personal to you and may not be sublicensed, assigned, or transferred by you to any other person without Springer Science + Business Media's written permission.
No Amendment Except in Writing
This license may not be amended except in a writing signed by both parties (or, in the case of Springer Science + Business Media, by CCC on Springer Science + Business Media's behalf).
Objection to Contrary Terms
Springer Science + Business Media hereby objects to any terms contained in any purchase order, acknowledgment,
check endorsement or other writing prepared by you, which terms are inconsistent with these terms and conditions or CCC's Billing and Payment terms and conditions. These terms and conditions, together with CCC's Billing and Payment terms and conditions (which are incorporated herein), comprise the entire agreement between you and Springer Science + Business Media (and CCC) concerning this licensing transaction. In the event of any conflict between your obligations established by these terms and conditions and those established by CCC's Billing and
Payment terms and conditions, these terms and conditions shall control.
Jurisdiction
All disputes that may arise in connection with this present License, or the breach thereof, shall be settled exclusively by arbitration, to be held in The Netherlands, in accordance with Dutch law, and to be conducted under the Rules of the 'Netherlands Arbitrage Instituut' (Netherlands Institute of Arbitration). ***OR:***
All disputes that may arise in connection with this present License, or the breach thereof, shall be settled exclusively by arbitration, to be held in the Federal Republic of Germany, in accordance with German law.

Other terms and conditions:

v1.3

If you would like to pay for this license now, please remit this license along with your payment made payable to "COPYRIGHT CLEARANCE CENTER" otherwise you will be invoiced within 48 hours of the license date.
Payment should be in the form of a check or money order referencing your account number and this invoice number RLNK500779640.
Once you receive your invoice for this order, you may pay your invoice by credit card. Please follow instructions provided at that time.

Make Payment To:
Copyright Clearance Center
Dept 001
P.O. Box 843006
Boston, MA 02284-3006

For suggestions or comments regarding this order, contact RightsLink Customer Support: customercare@copyright.com or +1-877-622-5543 (toll free in the US) or +1-978-646-2777.

Gratis licenses (referencing $0 in the Total field) are free. Please retain this printable license for your reference. No payment is required.

Springer Journal Articles

Copyright information relating to;

Holzapfel, G.A., Gasser, T.C., Ogden, R.W., 2000. A new constitutive framework for arterial wall mechanics and comparative study of material models. Journal of Elasticity 61 (1-3), 1–48.

SPRINGER LICENSE
TERMS AND CONDITIONS

Jun 13, 2012

Order Completed

Thank you very much for your order.

This is a License Agreement between Thanapong Chaichana ("You") and Springer ("Springer"). The license consists of your order details, the terms and conditions provided by Springer, and thepayment terms and conditions.

Get the printable license.

License Number	2926970156315
License date	Jun 13, 2012
Licensed content publisher	Springer
Licensed content publication	Journal of Elasticity
Licensed content title	A New Constitutive Framework for Arterial Wall Mechanics and a Comparative Study of Material Models
Licensed content author	Gerhard A. Holzapfel
Licensed content date	Jan 1, 2000
Volume number	61
Issue number	1
Type of Use	Thesis/Dissertation
Portion	Figures
Author of this Springer article	No
Title of your thesis / dissertation	Haemodynamic Evaluation of Coronary Artery Plaques: Prediction of Coronary Atherosclerosis and Disease Progression
Expected completion date	Jun 2012
Estimated size (pages)	125
Total	0.00 USD

Appendix IV-E: JAMA Journal Articles

Copyright information relating to;

Parmet, S., 2004. Coronary Artery Disease. Journal of the American Medical Association 292 (20), 2540.

AMERICAN MEDICAL ASSOCIATION LICENSE
TERMS AND CONDITIONS

Jun 25, 2012

Order Completed

Thank you very much for your order.

This is a License Agreement between Thanapong Chaichana ("You") and American Medical Association ("American Medical Association"). The license consists of your order details, the terms and conditions provided by American Medical Association, and the payment terms and conditions.

Get the printable license.

License Number	2936000575982
License date	Jun 25, 2012
Licensed content publisher	American Medical Association
Licensed content publication	JAMA
Licensed content title	Coronary Artery Disease
Licensed content author	Parmet, Sharon, Glass, Tiffany J.
Licensed content date	Nov 24, 2004
Volume number	292
Issue number	20
Type of Use	Dissertation/Thesis
Requestor type	student
Format	print and electronic
Portion	figures/tables/images
Number of figures/tables/images	1
List of figures/tables/images	Coronary Artery Disease
Will you be translating?	no
Circulation/distribution	10
Distributing to	Worldwide
Order reference number	
Title of your thesis / dissertation	Haemodynamic Evaluation of Coronary Artery Plaques: Prediction of Coronary Atherosclerosis and Disease Progression
Expected completion date	Jun 2012
Billing Type	Credit Card
Credit card info	Master Card ending in 5317
Credit card expiration	09/2012
Total	40.00 USD

Appendix IV-F: Wolters Kluwer Health

Copyright information relating to;

Traub, O., Berk, B.C., 1998. Laminar Shear Stress: Mechanisms by Which Endothelial Cells Transduce an Atheroprotective Force. Arteriosclerosis, Thrombosis, and Vascular Biology 18, 677–685.

WOLTERS KLUWER HEALTH LICENSE
TERMS AND CONDITIONS

Jun 25, 2012

Order Completed

Thank you very much for your order.

This is a License Agreement between Thanapong Chaichana ("You") and Wolters Kluwer Health ("Wolters Kluwer Health"). The license consists of your order details, the terms and conditions provided by Wolters Kluwer Health, and the payment terms and conditions.

Get the printable license.

License Number	2935970976533
License date	Jun 25, 2012
Licensed content publisher	Wolters Kluwer Health
Licensed content publication	ATVB
Licensed content title	Laminar Shear Stress: Mechanisms by Which Endothelial Cells Transduce an Atheroprotective Force
Licensed content author	Oren Traub, Bradford C. Berk
Licensed content date	May 1, 1998
Volume number	18
Issue Number	5
Type of Use	Dissertation/Thesis
Requestor type	Individual
Title of your thesis / dissertation	Haemodynamic Evaluation of Coronary Artery Plaques: Prediction of Coronary Atherosclerosis and Disease Progression
Expected completion date	Jun 2012
Estimated size (pages)	125
Total	0.00 USD

Bibliography

Anderson, H.V., Roubin, G.S., Leimgruber, P.P., Cox, W.R., Douglas, J.S., Jr, King, S.B., 3rd, Gruentzig, A.R., 1986. Measurement of transstenotic pressure gradient during percutaneous transluminal coronary angioplasty. Circulation 73 (6), 1223–1230.

Asakura, T., Karino, T., 1990. Flow patterns and spatial distribution of atherosclerotic lesions in human coronary arteries. Circulation Research 66, 1045–1066.

Australian Institute of Health and Welfare, 2011. Cardiovascular disease: Australian facts 2011, Cat. no. CVD 53. Canberra: AIHW.

Australian Institute of Health and Welfare, 2010. Cardiovascular disease mortality Trends at different ages, Cat. no. CVD 47. Canberra: AIHW.

Australian Institute of Health and Welfare, 2006. The tenth biennial health report of the Australian Institute of Health and Welfare, Cat. no. AUS 73. Canberra: AIHW.

Ballyk, P.D., Steinman, D.A., Ethier, C.R., 1994. Simulation of non-newtonial blood flow in an end-to-side anastomosis. Biorheology 31 (5), 565–586.

Berne, R.M., Levy, M.N., 2001. Cardiovascular physiology. Mosby, St Louis (MI), 230-231.

Bluestein, D., Alemu, Y., Avrahami, I., Gharib, M., Dumont, K., Ricotta, J.J., Einav, S., 2008. Influence of microcalcifications on vulnerable plaque mechanics using FSI modelling. Journal of Biomechanics 41 (5), 1111–1118.

Borghi, A., Wood, N.B., Mohiaddin, R.H., Xu, X.Y., 2008. Fluid–solid interaction simulation of flow and stress pattern in thoracoabdominal aneurysms: a patient-specific study. Journal of Fluids and Structures 24, 270–280.

Boutsianis, E., Dave, H., Frauenfelder, T., Poulikakos, D., Wildermuth, S., Turina, M., Ventikos, Y., Zund, G., 2004. Computational simulation of intracoronary flow based on real coronary geometry. European Journal of Cardio-thoracic Surgery 26 (2), 248–256.

Caro, C.G., Fitz-Gerald, J.M., Schroter, R.C., 1971a. Proposal of a shear dependent mass transfer mechanism for atherogenesis. Clinical Science 40 (2), 5P.

Caro, C.G., Fitz-Gerald, J.M., Schroter, R.C., 1971b. Atheroma and arterial wall shear: Observation, correlation and proposal of a shear dependent mass transfer mechanism for atherogenesis. Proceedings of the Royal Society B: Biological Sciences 177 (46), 109–159.

Chaichana, T., Sun, Z., Jewkes, J., 2012. Impact of plaques in the left coronary artery on wall shear stress and pressure gradient in coronary side branches. Computer Methods in Biomechanics and Biomedical Engineering. doi:10.1080/10255842.2012.671308

Chaichana, T., Sun, Z., Jewkes, J., 2012. Investigation of the haemodynamic environment of bifurcation plaques within the left coronary artery in realistic patient models based on CT images. Australasian Physical & Engineering Sciences in Medicine 35 (2), 231-236.

Chaichana, T., Sun, Z., Jewkes, J., 2012. Computational fluid dynamics analysis of the effect of plaques in the left coronary artery. Computational and Mathematical Methods in Medicine 2012, 504367:1-9.

Chaichana, T., Sun, Z., Jewkes J., 2011. Computation of hemodynamics in the left coronary artery with variable angulations. Journal of Biomechanics 44 (10), 1869–1878.

Chandran, K.B., Wahle, A., Vigmostad, S.C., Olszewski, M.E., Rossen, J.D., Sonka, M., 2006. Coronary arteries: imaging, reconstruction, and fluid dynamic analysis. Critical Reviews in Biomedical Engineering 34 (1), 23–103.

Cheng, L.C., Robertson, J.M., Clark, M.E., 1973. Numerical Calculations of plane oscillatory non-uniform flow – II. Parametric study of pressure gradient and frequency with square wall obstacles. Journal of Biomechanics 6 (5), 521–538.

Cheruvu, P.K., Finn, A.V., Gardner, C., Caplan, J., Goldstein, J., Stone, G.W., Virmani, R., Muller, J.E., 2011. Frequency and distribution of thin-cap fibroatheroma and ruptured plaques in human coronary arteries: a pathologic study. Journal of the American College of Cardiology 50, 940–949.

Chervu, A., Moore, W.S., 1990. An overview of intimal hyperplasia, Surgery Gynecology Obstetrics 171 (5), 433–447.

Chien, S., 2007. Mechanotransduction and endothelial cell homeostasis: the wisdom of the cell. American Journal of Physiology—Heart and Circulatory Physiology 292 (3), H1209–H1224.

Cho, G.Y., Lee, C.W., Hong, M.K., Kim, J.J., Park, S.W., Park, S.J., 2001. Effects of stent desing on side branch occlusion after coronary stent placement. Catheterization and Cardiovascular Interventions 52 (1), 18–23.

DeBakey, M.E., Lawrie, G.M., Glaeser, D.H., 1985. Patterns of atherosclerosis and their surgical significance. Annals of Surgery 201 (2), 115–131.

De Hart, J., Baaijens, F.P., Peters, G.W., Schreurs, P.J., 2003a. A computational fluid-structure interaction analysis of a fiber-reinforced stentless aortic valve. Journal of Biomechanics 36 (5), 699–712.

De Hart, J., Peters, G.W., Schreurs, P.J., Baaijens, F.P., 2003b. A three-dimensional computational analysis of fluid–structure interaction in the aortic valve. Journal of Biomechanics 36 (1), 103–112.

Diletti, R., Onuma, Y., Farooq, V., Gomez-Lara, J., Brugaletta, S., van Geuns, R.J., Regar, E., de Bruyne, B., Dudek, D., Thuesen, L., Chevalier, B., McClean, D., Windecker, S., Whitbourn, R., Smits, P., Koolen, J., Meredith, I., Li, D., Veldhof, S., Rapoza, R., Garcia-Garcia, H.M., Ormiston, J.A., Serruys. P.W., 2011. 6-Month clinical outcomes following implantation of the bioresorbable everolimus-eluting vascular scaffold in vessels smaller or larger than 2.5 mm. Journal of the American College of Cardiology 58, 258–264.

Enderle, J.D., Bronzino, J.D. 2011. Introduction to biomedical engineering, third. Academic Press, London 1–5.

Farmakis, T.M., Soulis, J.V., Giannoglou, G.D., Zioupos. G.J., Louridas. G.E., 2004. Wall shear stress gradient topography in the normal left coronary arterial tree: possible implications for atherogenesis. Current Medical Research & Opinion 20 (5), 587–596.

Feuchtner, G.M., Cury, R.C., Jodocy, D., Friedrich, G.J., Blumenthal, R.S., Budoff, M.J., Nasir, K., 2011. Differences in coronary plaques composition by noninvasive computed tomography in individuals with and without obstructive coronary artery disease. Atherosclerosis 215, 90–95.

Fishman, E.K., 2005. Multidetector-row computed tomography to detect coronary artery disease: the importance of heart rate. European Heart Journal Supplements 7 (suppl G), G4–G12.

Frauenfelder, T., Lotfey, M., Boehm, T., Wildermuth, S., 2006. Computational fluid dynamics: hemodynamic changes in abdominal aortic aneurysm after stent-graft implantation. CardioVascular and Interventional Radiology 29 (4), 613–623.

Friedman, M.H., Ding, Z., 1998. Variability of the planarity of the human aortic bifurcation. Medical Engineering & Physics 20 (6), 469–472.

Fry, D.L., 1969. Certain histological and chemical responses of the vascular interface to acutely induced mechanical stress in the aorta of the dog. Circulation Research 24 (1), 93–108.

Fry, D.L., 1968. Acute vascular endothelial changes associated with increased blood velocity gradients. Circulation Research 22 (2), 165–197.

Fukumoto, Y., Hiro, T., Fujii, T., Hashimoto, G., Fujimura, T., Yamada, J., Okamura, T., Matsuzaki, M., 2008. Localized elevation of shear stress is related to coronary plaque rupture: a 3-dimensional intravascular ultrasound study with in-vivo color mapping of shear stress distribution. Journal of the American College of Cardiology 51 (6), 645-650.

Fung, Y.C., 1997. Biomechanics: circulation, 2nd ed. Springer-Verlag, New York.

Fung, Y.C., 1993. Biomechanics: mechanical properties of living tissues, second. Springer-Verlag, New York 1–5.

Fuster, V., 1994. Lewis A. Conner memorial lecture. Mechanisms leading to myocardial infarction: insights from studies of vascular biology. Circulation 90, 2126–2146.

Gao, H., Long, Q., Das, S.K., Sadat, U., Graves, M., Gillard, J.H., Li, Z. 2011. Stress analysis of carotid atheroma in transient ischemic attack patient: Evidence for extreme stress-induced plaque rupture. Annals of Biomedical Engineering 39 (8), 2203–2212.

Gao, H., Long, Q., Graves, M., Gillard, J.H., Li, Z. 2009. Carotid arterial plaque stress analysis using fluid-structure interactive simulation based on *in-vivo* magnetic resonance images of four patients. Journal of Biomechanics 42 (10), 1416–1423.

Gao, H., Long, Q., 2008. Effects of varied lipid core volume and fibrous cap thickness on stress distribution in carotid arterial plaques. Journal of Biomechanics 41 (14), 3053–3059.

Garcia, D., Pibarot, P., Louis-Gilles, D., 2005. Analytical modeling of the instantaneous pressure gradient across the aortic valve. Journal of Biomechanics 38 (6), 1303-1311.

Garcia, D., Kadem, L., Savéry, D., Pibarot, P., Durand, L.G., 2006. Analytical modeling of the instantaneous maximal transvalvular pressure gradient in aortic stenosis. Journal of Biomechanics 39 (16), 3036–3044.

Giannoglou, G.D., Soulis, J.V., Farmakis, T.M., Giannakoulas, G.A., Parcharidis, G.E., Louridas, G.E., 2005. Wall pressure gradient in normal left coronary artery tree. Medical Engineering & Physics 27 (6), 455–564.

Giannoglou, G.D., Soulis, J.V., Farmakis, T.M., Farmakis, D.M., Louridas, G.E., 2002. Haemodynamic factors and the important role of local low static pressure in coronary wall thickening. International Journal of Cardiology 86 (1), 27–40.

Gibbons, G.H., Dzau, V.J., 1994. The emerging concept of vascular remodeling. The New England Journal of Medicine 330 (20), 1421-1438.

Gijsen, F.J., Wentzel, J.J., Thury, A., Lamers, B., Schuurbiers, J.C., Serruys, P.W., van der Steen, A.F., 2007. A new imaging technique to study 3-D plaque and shear stress distribution in human coronary artery bifurcations in vivo. Journal of Biomechanics 40 (11), 2349–2357.

Glagov, S., Weisenberg, E., Zarins, C.K., Stankunavicius, R., Kolettis, G.J., 1987. Compensatory enlargement of human atherosclerotic coronary arteries. New England Journal of Medicine 316 (22), 1372–1375.

Grayburn, P.A., Willard, J.E., Haagen, D.R., Brickner, M.E., Alvarez, L.G., Eichhorn, E.J., 1992. Measurement of coronary flow using high-frequency intravascular ultrasound imaging and pulsed Doppler velocimetry: in vitro feasibility studies. Journal of the American Society of Echocardiography 5 (1), 5–12.

Gziut, A.I., 2006. Comparative analysis of atherosclerotic plaque distribution in the left main coronary artery and proximal segments of left anterior descending and left circumflex arteries in patients qualified for percutaneous coronary angioplasty. Annales Academiae Medicae Stetinensis 52 (2), 51–62.

Hachamovitch, R., Berman, D.S., Shaw, L.J., Kiat, H., Cohen, I., Cabico, J.A., Friedman, J., Diamond, G.A., 1998. Incremental prognostic value of myocardial perfusion single photon emission computed tomography for the prediction of cardiac death: differential stratification for risk of cardiac death and myocardial infarction. Circulation 97 (6), 535–543.

Han, S.H., Puma, J., Garcı´a-Garcı´a, H.M., Nasu, K., Margolis, P., Leon, M.B., Lerman, A., 2010. Tissue characterisation of atherosclerotic plaque in coronary artery bifurcations: an intravascular ultrasound radiofrequency data analysis in humans. EuroIntervention. 6 (3), 313–320.

Hart, J.D., 1997. Nonparametic smoothing and lack-of-fit tests, 1st ed. Springer-Verlag, New York.

He, X., Ku, N.D., 1996. Pulsatile flow in the human left coronary artery bifurcation: average conditions. Journal of Biomechanical Engineering 118 (1), 74–82.

He, X., Ku, D.N., 1995. Flow in T-bifurcations: effect of the sharpness of the flow divider. Biorheology 32 (4), 447–458.

Hingorani, A., Ascher, E., Marks, N., 2007. Preprocedural imaging: New options to reduce need for contrast angiography. Seminars in vascular surgery 20 (1), 15–28.

Holzapfel, G.A., Gasser, T.C., Ogden, R.W., 2000. A new constitutive framework for arterial wall mechanics and comparative study of material models. Journal of Elasticity 61 (1-3), 1–48.

Imoto, K., Hiro, T., Fujii, T., Murashige, A., Fukumoto, Y., Hashimoto, G., Okamura, T., Yamada, J., Mori, K., Matsuzaki, M., 2005. Longitudinal structural determinants of atherosclerotic plaque vulnerability : A computational analysis of stress distribution using vessel models and three-dimensional intravascular ultrasound imaging. Journal of the American College of Cardiology 46 (8), 1507–1515.

Jeong, W.W., Rhee, K., 2009. Effects of surface geometry and non-newtonian viscosity on the flow field in arterial stenoses. Journal of Mechanical Science and Technology 23 (9), 2424–2433.

Johnston, B.M., Johnston, P.R., Corney, S., Kilpatrick, D., 2006. Non-Newtonian blood flow in human right coronary arteries: Transient simulations. Journal of Biomechanics 39 (1), 1116–1128.

Johnston, B.M., Johnston, P.R., Corney, S., Kilpatrick, D., 2004. Non-Newtonian blood flow in human right coronary arteries: steady state simulations. Journal of Biomechanics 37 (5), 709–720.

Jung, J., Lyczkowski, R.W., Panchal, C.B., Hassanein, A., 2006. Multiphase hemodynamic simulation of pulsatile flow in a coronary artery. Journal of Biomechanics 39 (11), 2064–2073.

Katritsis, D.G., Theodorakakos, A., Pantos, I., Andriotis, A., Efstathopoulos, E.P., Siontis, G., Karcanias, N., Redwood, S., Gavaises, M., 2010. Vortex formation and recirculation zones in left anterior descending artery stenosis: computational fluid dynamics analysis. Physics in Medicine and Biology 55 (5), 1395–1411.

Katritsis, D., Kaiktsis, L., Chaniotis, A., Pantos, J., Efstathopoulos, E.P., Marmarelis, V., 2007a. Wall shear stress: theoretical considerations and methods of measurement. Progress in Cardiovascular Diseases 49 (5), 307–329.

Katritsis, D.G., Pantos, J., Efstathopoulos, E., 2007b. Hemodynamic factors and atheromatic plaque rupture in the coronary arteries: from vulnerable plaque to vulnerable coronary segment. Coronary Artery Disease 18, 229–237.

Kimura, B.J., Russo, R.J., Bhargava, V., McDaniel, M.B., Peterson, K.L., DeMaria, A.N. 1996. Atheroma morphology and distribution in proximal left anterior descending coronary artery: in vivo observations. Journal of the American College of Cardiology 27, 825–831.

Kleinstreuer, C., Hyun, S., Buchanan, J.R., Longest, P.W., Archie, J.P., Truskey, J.P., 2001. Hemodynamic parameters and early intimal thickening in branching blood vessels. Critical Reviews in Biomedical Engineering 29 (1), 1–64.

Ku, D.N., 1997. Blood flow in arteries. Annual Review of Fluid Mechanics 29, 399–434.

Ku, D.N., Giddens, D.P., Zarins, C.K., Glagov, S., 1985. Pulsatile flow and atherosclerosis in the human carotid bifurcation. Positive correlation between plaque location and low oscillating shear stress. Arteriosclerosis 5 (3), 293–302.

Koskinas, K.C., Chatzizisis, Y.S., Antoniadis, A.P., Giannoglou, G.D., 2012. Role of Endothelial Shear Stress in Stent Restenosis and Thrombosis: Pathophysiologic Mechanisms and Implications for Clinical Translation. Journal of the American College of Cardiology 59 (15), 1337–1349.

LaDisa, J.F. Jr., Olson, L.E., Guler, I., Hettrick, D.A., Kersten, J.R., Warltier, D.C., Pagel, P.S., 2004. Circumferential vascular deformation after stent implantation alters wall shear stress evaluated with time-dependent 3D computational fluid dynamics models. Journal of Applied Physiology 98, 947–957.

Lantz, J., Renner, J., Karlsson, M., 2011. Wall shear stress in a subject specific human aorta – Influence of fluid-structure interaction. International Journal of Applied Mechanics 3 (4), 759–778.

Lee, B., 2011. Computational fluid dyanamics in cardiovascular disease. Korea Circulation Journal 41 (8), 423–430.

Lehoux, S., 2006. Redox signalling in vascular responses to shear and stretch. Cardiovascular Research 71 (2), 269–279.

Lei, M., Giddens, D.P., Jones, S.A., Loth, F., Bassiouny, H., 2001. Pulsatile flow in an end-to-side vascular graft model: comparison of computations with experimental data. Journal of Biomechanical Engineering 23, 80–87.

Lei, M., Kleinstreuer, C.,Truskey, G.A., 1996. A focal stress gradient-dependent mass transfer mechanism for atherogenesis in branching arteries. Medical Engineering and Physics 18 (4), 326–332.

Lim, M.J., Kern, M.J., 2005. Utility of coronary physiologic hemodynamics for bifurcation, aorto-ostial, and ostial branch stenoses to guide treatment decisions. Catheterization and Cardiovascular Interventions 65 (4), 461–468.

Lou, Z., Yang, W.J., 1993. A computer simulation of the non-Newtonian blood flow at theaortic bifurcation. Journal of Biomechanics 26, 37–49.

Mahesh, M., 2002. Search for isotropic resolution in CT from conventional through multiple-row detector. Radiographics 22 (4), 949–962.

Malek, A.M., Alper, S.L., Izumo, S., 1999. Hemodynamic shear stress and its role in atherosclerosis. Journal of American Medical Association 282 (21), 2035–2042.

Milnor, W., 1989. Hemodynamics. Williams & Wilkins, Baltimore.

Montenegro, M.R., Eggen, D.A., 1968. Topography of atherosclerosis in the coronary arteries. Laboratory Investigation 18, 586–593.

Moore, J.E., Jr., Xu, C., Glagov, S., Zarins, C.K., Ku, D.N., 1994. Fluid wall shear stress measurements in a model of the human abdominal aorta: oscillatory behavior and relationship to atherosclerosis. Atherosclerosis 110 (2), 225–240.

Morbiducci, U., Ponzini, R., Nobili, M., Massai, D., Montevecchi, F.M., Bluestein, D., Redaelli, A., 2009. Blood damage safety of prosthetic heart valves. Shear-induced platelet activation and local flow dynamics: A fluid–structure interaction approach. Journal of Biomechanics 42 (12), 1952–1960.

Murray, C.D., 1926. The physiological principle of minimum work: I. The vascular system and the cost of blood volume. Proceedings of the National Academy of Sciences of the United States of America 12 (3), 207–214.

Myers, J.G., Moore, J.A., Ojha, M., Johnston, K.W., Ethier, C.R., 2001. Factors influencing blood flow patterns in the human right coronary artery. Annals of Biomedical Engineering 29 (2), 109–120.

Nichols, W., O'Rourke, M., 2005. McDonald's blood flow in arteries. Hodder Arnold, London, 326–327.

Nieman, K., Oudkerk, M., Rensing, B.J., van Ooijen, P., Munne, A., van Geuns, R.J., de Feyter, P.J., 2001. Coronary angiography with multi-slice computed tomography. Lancet 357 (9256), 599–603.

Nordgaard, H., Swillens, A., Nordhaug, D., Kirkeby-Garstad, I., Loo, D., Vitale, N., Segers, P., Haaverstad, R., Lovstakken, L., 2010. Impact of competitive flow on wall shear stress in coronary surgery: computational fluiddynamics of a LIMA–LAD model. Cardiovascular Research 88 (3), 512–519.

Noto, T.J. Jr, Johnson, L.W., Krone, R., Weaver, W.F., Clark, D.A., Kramer, J.R. Jr, Vetrovec, G.W., 1991. Cardiac catheterization 1990: a report of the registry of the Society for Cardiac Angiography and Interventions. (SCA&I). Catheterization and Cardiovascular Diagnosis 24 (2), 75–83.

Ojha, M., 1993. Spatial and temporal variations of wall shear stress within an end- to-side arterial anastomosis model. Journal of Biomechanics 26, 1377–1388.

Pantos, J., Efstathopoulos, E., Katritsis, D.G., 2007. Vascula wall shear stress in clinical practice. Current Vascular Pharmacology 5, 113–119.

Parmet, S., 2004. Coronary Artery Disease. Journal of the American Medical Association 292 (20), 2540.

Pedley, T.J., 1980. The Fluid Mechanics of Large Blood Vessels. Cambridge university press, Cambridge, 30–31.

Perktold, K., Hofer, M., Rappitsch, G., Loew, M., Kuban, B.D., Friedman, M.H., 1998. Validated computation of physiologic flow in a realistic coronary artery branch. Journal of Biomechanics 31 (3), 217–228.

Pflederer, T., Ludwig, J., Ropers, D., Daniel, W.G., Achenbach, S., 2006. Measurement of coronary artery bifurcation angles by multidetector computed tomography. Investigative Radiology 41 (11), 793–798.

Phillips, T.L., 2002. 50 years of radiation research: Medicine. Radiation research 158 (4), 389–417.

Qi, Y.X., Qu, M.J., Long, D.K., Liu, B.,Yao, Q.P., Chien, S., Jiang, Z.L., 2008. Rho-GDP dissociation inhibitor alpha downregulated by low shear stress promotes vascular smooth muscle cell migration and apoptosis: a proteomic analysis. Cardiovascular Research 80 (1), 114–122.

Rajabi-Jaghargh, E., Kolli, K.K., Back, L.H., Banerjee, R.K., 2011. Effect of guidewire on contribution of loss due to momentum change and viscous loss to the translesional pressure drop across coronary artery stenosis: an analytical approach. Biomedical Engineering Online 10, 51.

Reig, J., Petit, M., 2004. Main trunk of the left coronary artery: anatomic study of the parameters of clinical interest. Clinical Anatomy 17, 6–13.

Rodriguez-Granillo, G.A., Rosales, M.A., Degrossi, E., Durbano, I., Rodriguez, A.E., 2007. Multislice CT coronary angiography for the detection of burden, morphology and distribution of atherosclerotic plaque in the left main bifurcation. International Journal of Cardiovascular Imaging 23, 389-392.

Rushmer, R.F., 1976. Cardiovascular dynamics. WB Saunders, Philadelphia.

Rybicki, F.J., Melchionna, S., Mitsouras, D., Coskun, A.U., Whitmore, A.G., Steigner, M., Nallamshetty, L., Welt, F.G., Bernaschi, M., Borkin, M., Sircar, J., Kaxiras, E., Succi, S., Stone, P.H., Feldman, C.L, 2009. Prediction of coronary artery plaque progression and potential rupture from 320-detector row prospectively ECG-gated single heart beat CT angiography: Lattice Boltzmann evaluation ofendothelial shear stress. International Journal of Cardiovascular Imaging 25, 289–299.

Sabbah, H.N., Khaja, F., Hawkins, E.T., Brymer, J.F., McFarland, T.M., van der Bel-Kahn, J., Doerger, P.T., Stein, P.D., 1986. Relation of atherosclerosis to arterial wall shear in the left anterior descending coronary of man. American Heart Journal 112 (3), 453–458.

Samady, H., Eshtehardi, P., McDaniel, M.C., Suo, J., Dhawan, S.S., Maynard, C., Timmins, L.H., Quyyumi, A.A., Giddens, D.P., 2011. Coronary artery wall shear stress is associated with progression and transformation of atherosclerotic plaque and arterial remodeling in patients with coronary artery disease. Circulation 124, 779–788.

Schroeder, A., Falk, E., 1995. Vulnerable and dangerous coronary plaques. Atherosclerosis Supplements, S141–S149.

Sequeira, A., Artoli, A.M., Silva-Herdade, A.S., Saldanha, C., 2009. Leukocytes dynamics in microcirculation under shear-thinning blood flow. Computers and Mathematics with Applications 58, 1035–1044.

Shanmugavelayudam, S.K., Rubenstein, D.A., Yin, W., 2010. Effect of geometrical assumptions on numerical modelling of coronary blood flow under normal and disease conditions. Journal of Biomechanical Engineering 132, 061004.

Sharan, M., Popel, A.S., 2001. A two-phase model for flow of blood in narrow tubes with increased effective viscosity near the wall. Biorheology 38, 415–428.

Slager, C.J., Wentzel, J.J., Gijsen, F.J.H., Thury, A., van der Wal, A.C., Schaar, J.A., Serruys, P.W., 2004. The role of shear stress in the destabilization of vulnerable plaques and related therapeutic implications. Nature Clinical Practice Cardiovascular Medicine 2, 456–464.

Smith, S., 1997. The scientist and engineer's guide to digital signal processing. California Technical Publishing, California, 255–256.

Sommer, T., Hackenbroch, M., Hofer, U., Schmiedel, A., Willinek, W.A., Flacke, S., Gieseke, J., Träber, F., Fimmers, R., Litt, H., Schild, H., 2005. Coronary MR angiography at 3.0 T versus that at 1.5 T: initial results in patients suspected of having coronary artery disease. Radiology 234 (3), 718–25.

Soulis, J.V., Farmakis, T.M., Giannoglou, G.D., Louridas, G.E., 2006. Wall shear stress in normal left coronary artery tree. Journal of Biomechanics 39 (4), 742–749.

Speelman, L., Akyildiz, A.C., den Adel, B., Wentzel, J.J., van der Steen, A.F.W., Virmani, R., vander Weerd, L., Jukema, J.W., Poelmann, R.E., van Brummelen, E.H., Gijsen, F.J.H., 2011. Initial stress in biomechanical models of atherosclerotic plaques. Journal of Biomechanics 44 (13), 2376–82.

Sun, Z., Cao, Y., 2011. Multislice CT angiography assessment of left coronary artery: correlation between bifurcation angle and dimensions and development of coronary artery disease. European Journal of Radiology 79 (2), e90–e95.

Sun Z., Cao Y., Li H., 2011. Multislice CT angiography in the diagnosis of coronary artery disease. Journal of Geriatric Cardiology 8 (2), 104–113.

Sun, Z., Chaichana, T., 2010. Fenestrated stent graft repair of abdominal aortic aneurysm: hemodynamic analysis of the effect of fenestrated stents on the renal arteries. Korean Journal of Radiology 11 (1), 95–106.

Sun, Z., Chaichana, T., 2009. Investigation of the hemodynamic effect of stent wires on renal arteries in patients with abdominal aortic aneurysms treated with suprarenal stentgrafts. CardioVascular and Intervention al Radiology 32 (4), 647–657.

Sun, Z., Dimpudus, F.J., Nugroho, J., Adipranoto, J.D., 2010. CT virtual intravascular endoscopy assessment of coronary artery plaques: a preliminary study. European Journal of Radiology 75 (1), e112–e119.

Sun, Z., Lin, C.H., Davidson, R., Dong, C., Liao, Y., 2008. Diagnostic value of 64-slice CT angiography in coronary artery disease: a systematic review. European Journal of Radiology 67, 78–84.

Sun, Z., Mwilpatayi, B., Chaichana, T., Ng, C., 2009. Hemodynamic effect of calcified plaque on blood flow in carotid artery disease: a preliminary study. Proceedings of IEEE Bioinformatics and Biomedical Engineering 1, 1–4.

Sun, Z., Ng, K.H., 2010. Multislice CT angiography in cardiac imaging. Part II: clinical applications in coronary artery disease. Singapore Medical Journal 51 (4), 282–289.

Sun, Z., Winder, R.J., Kelly, B.E., Ellis, P.K., Hirst, D.G., 2003. CT virtual intravascular endoscopy of abdominal aortic aneurysms treated with suprarenal endovascular stent grafting. Abdominal Imaging 28 (4), 580–587.

Sun, Z., Winder, R.J., Kelly, B.E., Ellis, P.K., Kennedy, P.T., Hirst, D.G., 2004. Diagnostic value of CT virtual intravascular endoscopy in aortic stent grafting. Journal of Endovascular Therapy 11 (1), 13–25.

Sun, Z., Yvonne, A., Nadkarni, S., Roslyn, K., David, H., Lawrence-Brown, M., 2008. CT virtual intravascular endoscopy in the visualization of fenestrated endovascular grafts. Journal of Endovascular Therapy 15 (1), 42-51.

Sung, H.W., Yu, P.S., Hsu, C.H., Hsu, J.C., 1997. Can cardiac catheterization accurately assess the severity of aortic stenosis? An in vitro pulsatile flow study. Annals of Biomedical Engineering 25 (5), 896–905.

Takuro, T., Souki, L., Shuichi, H., Kouichi, T., Daisuke, K., Keisuke, K., Hitoshi, T., Toshihiro, T., Masaaki, M., Ryuichiro, A., Yutaka, O., Chuwa, T., 2007. Limitation of angiography to identify the culprit plaque in acute myocardial infarction with coronary total occlusion: Utility of coronary plaque temperature measurement to identify the culprit plaque. Journal of the American College of Cardiology 50 (23), 2197–2203.

Tang, T.D., Giddens, D.P., Zarins, C.K., Glagov, S., 1990. Velocity profile and wall shear measurements in a model human coronary artery. ASME Advanced Biomedical Engineering 17, 261–263.

Tarbell, J.M., 2010. Shear stress and the endothelial transport barrier. Cardiovascular Research 87 (2), 320–330.

Thubrikar, M.J., Robicsek, F., 1995. Pressure-induced arterial wall stress and atherosclerosis. Annals of Thoracic Surgery 59 (6), 1594–1603.

Topol, E.J., 2008. Textbook of interventional cardiology, fifth. Saunders Elsevier, Philadelphia, 1075.

Torii, R., Keegan, J., Dowsey, A., Wood, N., Yang, G.Z., Firmin, D., Hughes, A., Thom, S., Xu. X.Y., 2008. A CFD study on coronary artery haemodynamics with dynamic vessel motion based on MR images. Journal of Biomechanics 41 (Suppl 1), S212.

Townsend, D.W., 2008. Dual-modality imaging: Combining anatomy and function. Journal of nuclear medicine 49 (6), 938–955.

Traub, O., Berk, B.C., 1998. Laminar Shear Stress: Mechanisms by Which Endothelial Cells Transduce an Atheroprotective Force. Arteriosclerosis, Thrombosis, and Vascular Biology 18 (5), 677–685.

Tse, K.M., Chiu, P., Lee, H.P., Ho, P., 2011. Investigation of hemodynamics in the development of dissecting aneurysm within patient-specific dissecting aneurismal aortas using computational fluid dynamics (CFD) simulations. Journal of Biomechanics 44 (5), 827–836.

Tu, J., Yeoh, G.H., Liu, C., 2008. Computational fluid dynamics: A practical approach. Butterworth-Heinemann: Elsevier, Burlington (MA).

van der Giessen, A.G., Groen, H.C., Doriot, P.A., de Feyter, P.J., van der Steen, A.F., van de Vosse, F.N., Wentzel, J.J., Gijsen, F.J., 2011. The influence of boundary conditions on wall shear stress distribution in patients specific coronary trees. Journal of Biomechanics 44 (6), 1089–1095.

VanderLaan, P.A., Reardon, C.A., Getz, G.S., 2004. Site specificity of therosclerosis: site-selective responses to atherosclerotic modulators. Arteriosclerosis Thrombosis and Vascular Biology 24, 12–22.

van Zanten, G.H., de Graaf, S., Slootweg, P.J., Heijnen, H.F., Connolly, T.M., de Groot, P.G., Sixma, J.J., 1994. Increased platelet deposition on atherosclerotic coronary arteries. Journal of Clinical Investigation 93 (2), 615–632.

Versluis, A., Bank, A.J., Douglas, W.H., 2006. Fatigue and plaque rupture in myocardial infarction. Journal of Biomechanics 39 (2), 339–347.

Vilahur, G., Padro, T., Badimon, L., 2011. Atherosclerosis and thrombosis: insights from large animal models. Journal of Biomedicine and Biotechnology 2011, 907575.

Wellnhofer, E., Osman, J., Kertzscher, U., Affeld, K., Fleck, E., Goubergrits, L., 2010. Flow simulation studies in coronary arteries—impact of side-branches. Atherosclerosis 213 (2), 475–481.

White, C.R., Haidekker, M., Bao, X., Frangos, J.A., 2001. Temporal gradients in shear, but not spatial gradients, stimulate endothelial cell proliferation. Circulation 103, 250–2513.

World medical association declaration of Helsinki, 1997. Recommendations guiding physicians in biomedical research involving human subjects. Cardiovascular Research 35, 2–3.

Zarins, C.K., Giddens, D.P., Bharadvaj, B.K., Sottiurai, V.S., Mabon, R.F., Glagov, S., 1983. Carotid bifurcation atherosclerosis. Quantitative correlation of plaque localization with flow velocity profiles and wall shear stress. Circulation Research 53, 502–514.

Zheng, Y., Fujioka, H., Grotberg, J.C., Grotberg, J.B., 2006. Effects of inertia and gravity on liquid plug splitting at a bifurcation. Journal of Biomechanical Engineering 128, 707–716.

.....
Thanapong Chaichana

5th August 2012